1-1-2012

Seismic Response of Ground-Supported Circular Concrete Tanks

Ahmed Hafez
Ryerson University

Seismic Response of Ground-Supported Circular Concrete Tanks

By

Ahmed Hafez

A Dissertation

presented to Ryerson University

in partial fulfillment of the

requirements for the degree of

Doctor of Philosophy

in the Program of

Civil Engineering

Toronto, Ontario, Canada, 2012

AUTHOR'S DECLARATION

AUTHOR'S DECLARATION FOR ELECTRONIC SUBMISSION OF A DISSERTATION

I hereby declare that I am the sole author of this dissertation. This is a true copy of the dissertation, including any required final revisions, as accepted by my examiners.

I authorize Ryerson University to lend this dissertation to other institutions or individuals for the purpose of scholarly research

I further authorize Ryerson University to reproduce this dissertation by photocopying or by other means, in total or in part, at the request of other institutions or individuals for the purpose of scholarly research.

I understand that my dissertation may be made electronically available to the public.

Ahmed Hafez

Seismic Response of Ground-Supported Circular Concrete Tanks

Ahmed Hafez, Doctor of Philosophy, 2012

Department of Civil Engineering

Ryerson University

ABSTRACT

This study is focused on the nonlinear behavior of ground-supported open top circular concrete tanks under the effect of seismic loads. The tank support conditions are considered in this study where both flexible and nonflexible supports are investigated. A comparison between the behavior of reinforced concrete (RC) and prestressed concrete (PC) tanks is undertaken for flexible base condition. The finite element (FE) method is used to study the nonlinear response of circular tanks under dynamic time-history and push-over analysis. Furthermore, the response modification factors (R) included in current practice are evaluated based on the results of nonlinear dynamic and push-over analysis. Several tank configurations with different aspect ratios, construction method, and base conditions are used in this study to attain reliable results and to validate the R-values. The behavior of circular RC tanks under shrinkage effect is also investigated. Moreover, an innovative approach is presented in this study for flexile base tanks in order to further reduce the seismic response of these structures by using passive energy dissipation systems such as fluid viscose dampers (FVD). The results of this study show

that higher R-values could be applied to fixed base tanks as compared to hinged base tanks. Also, shallower concrete tanks can be assigned higher R-values as compared to tall tanks. The results of this study show that the type of construction affects the tanks ductility. PC tanks show lower ductility as compared to RC tanks. Furthermore, this study shows that the flexible base tanks with seismic cables do not dissipate the seismic forces, as expected, due to the elastic behavior of the seismic cables. Based on the results of the FE analysis, it is shown that, using FVD reduces the tank response under seismic loads. The use of FVD improves the tank serviceability by reducing the concrete cracking. It is concluded that flexible based tanks equipped with FVD can be used as an economically feasible system in high seismic zones.

ACKNOWLEDGMENTS

I would like to express my sincere gratitude to my research supervisor Dr. Reza Kianoush, and co-supervisor Dr. Homayoun Abrishami.

I am heartily thankful to my supervisor, Dr. Reza Kianoush, whose encouragement, guidance and support from the initial to the final level of my research has enabled me to develop an understanding of the subject.

I offer my regards and blessings to all of those who supported me in any respect during the completion of this study.

I am deeply and forever indebted to my mother, Mrs. Amal Taher, and to the soul of my father Mr. Hafez Mohamed for their unconditional love, encouragement and support throughout my entire life.

My deepest gratitude goes to my dear wife, Mrs. Mona Elkhadem, and my lovely kids, Mohamed, Maryam, and Sayf for their love, support and understanding.

Finally, all praises and thanks are to God, the lord of mankind and all that exists for his help, guidance and support.

TABLE OF CONTENTS

AUTHOR'S DECLARATION **II**

ABSTRACT **iii**

ACKNOWLEDGMENTS **v**

TABLE OF CONTENTS **vi**

LIST OF TABLES **xii**

LIST OF FIGURES **xiv**

LIST OF APPENDICES **xxi**

LIST OF SYMBOLS **xxii**

CHAPTER 1 **1**

INTRODUCTION 1

1.1 General 1

1.2 Research Significance 2

1.3 Objectives, Assumptions, and Limitations 3

1.4 Outline of Thesis 4

CHAPTER 2 **8**

LITERATURE REVIEW 8

2.1 General 8

2.2 Ground-supported tank classifications 8

2.3 Seismic damage to LCS 13

2.3.1 Damage to steel tanks 14

2.3.2 Damage to concrete LCS 17

2.4 Previous research studies on seismic response of LCS 17

2.5 Response Modification Factor 24

2.6 Cracking of concrete 31

2.7 Characteristics of concrete model 34

2.8 Passive energy dissipation systems 36

2.9 Applicable codes and standards for LCS 42

CHAPTER 3 **46**

EFFECT OF TANK PARAMETERS ON SEISMIC RESPONSE 46

3.1 General 46
3.2 Tank behavior under seismic loads 47
3.3 ACI 350.3 design requirements and code background 48
3.4 Effect of tank dimensions on hydrodynamic forces 51
3.5 Finite element implementation 56
3.5.1 Tank configuration and design parameters 57
3.5.2 Computer model and FE analysis 58
3.5.3 Model verification 60
3.5.4 Results of FE analysis 63
3.6 Comparison between the results of FE analysis and closed-form solution 68
3.7 Comparison between results of fixed, hinged, and free base tanks 71
3.8 Summary 73
CHAPTER 4 **74**
PROPERTIES AND FINITE ELEMENT MODELING OF MATERIALS 74
4.1 General 74
4.2 Finite element program ABAQUS/CAE 74
4.2.1 Selection of finite element analysis technique 74
4.2.2 Conditional stability and time increment in the explicit method 77
4.3 Material properties 79
4.3.1 Concrete Model 79
4.3.2 Smeared cracking 79
4.3.3 Brittle cracking 79
4.3.4 Concrete damaged plasticity (CDP) 80
4.3.4.1 Behavior of concrete in tension 80
4.3.4.2 Behavior of concrete in compression 82
4.3.4.3 Behavior of concrete under cyclic loading 83

4.3.5 Stress–strain relationship in concrete 85

4.3.6 Reinforcement 87

4.3.7 Prestressing Tendons 89

4.3.8 Elastomeric bearing pad 90

CHAPTER 5 **92**

EFFECT OF SHRINKAGE ON CRACKING 92

5.1 General 92

5.2 Concrete shrinkage 93

5.3 Member restraints 93

5.4 Principal of minimum reinforcement and theory of shrinkage cracking 94

5.5 Degree of restraint 101

5.6 Computer model and finite element analysis 104

5.6.1 Tank configuration and design parameters 105

5.6.2 Finite element model 106

5.6.3 Material properties 108

5.6.5 Loads 109

5.7 Results of analysis 109

5.7.1 Free base condition and model verification 110

5.7.2 Hinged base condition 115

5.7.3 Fixed base condition 116

5.7.4 Sensitivity study 118

5.8 Summary 120

CHAPTER 6 **121**

NONLINEAR BEHAVIOR OF GROUND-SUPPORTED CIRCULAR TANKS UNDER PUSH-OVER ANALYSIS 121

6.1 General 121

6.2 Tank configuration and design parameters 121

6.3 Finite element analysis 126
6.4 Results of push-over FE analysis 126
6.4.1 Mesh sensitivity study 128
6.4.2 Hinged base condition 129
6.4.3 Fixed base condition 139
6.4.4 Free base condition 148
6.4.5 Discussion of the results 149
6.5 Summary 155
CHAPTER 7 **156**
NONLINEAR BEHAVIOR UNDER TIME-HISTORY ANALYSIS 156
7.1 General 156
7.2 Tank configuration and design parameters 157
7.2.1 Nonflexible base tanks 160
7.2.2 Anchored flexible base tanks 161
7.3 Computer model and finite element analysis 166
7.3.1 Geometry 166
7.3.2 Material properties 167
7.3.3 Damping 168
7.3.4 Boundary conditions and flexible support 169
7.3.5 Loads 171
7.3.5.1 Prestressing 171
7.3.5.2 Earthquake ground forces 172
7.3.5.3 Gravity load 179
7.3.5.4 Hydrostatic load 179
7.3.5.5 Mass 180

7.3.5.6 Shear resistance for anchored flexible base tanks 183
7.4 Results of time-history FE analysis 184
7.4.1 Model verification 184
7.4.2 Sensitivity study 189
7.4.3 Comparison between the results of FE analysis and current practice 190
7.4.4 R-values based on the results of time-history FE analysis 193
7.4.5 Discussion of the results 201
7.4.6 Comparison between results of push-over and time-history FE analysis 205
7.5 Summary 206
CHAPTER 8 **209**
APPLICATION OF PASSIVE ENERGY DISSIPATION SYSTEM 209
8.1 General 209
8.2 Application of passive energy dissipation system 209
8.2.1 Fluid viscous dampers 210
8.2.2 Tank configuration and design parameters 213
8.3 Computer model and FE analysis 214
8.4 Results of time-history FE analysis 215
8.4.1 Internal forces 216
8.4.2 Base shear and deflection 217
8.5 Summary 222
CHAPTER 9 **223**
SUMMARY, CONCLUSIONS, AND RECOMMENDATIONS 223
9.1 Summary 223
9.2 Conclusions 224
9.3 Recommendations for future research 226
APPENDIX A.1 228
DESIGN OF GROUND-SUPPORTED NONFLEXIBLE-BASE CIRCULAR TANK

APPENDIX A.2 242
DESIGN OF GROUND-SUPPORTED ANCHORED FLEXIBLE-BASE CIRCULAR TANK
APPENDIX A.3 253
EFFECT OF RECTANGULAR TANK DIMENSIONS ON HYDRODYNAMIC FORCES
APPENDIX A.4 259
TAYLOR DEVICES INC. FLUID VISCOUS DAMPERS DATASHEET
APPENDIX B.1 261
INPUT FILES OF COMPUTER MODELS – PUSH-OVER ANALYSIS
APPENDIX B.2 268
INPUT FILES OF COMPUTER MODELS – TIME-HISTORY ANALYSIS
REFERENCES 294

LIST OF TABLES

Table 2.1 - Response modification factor R (ACI 350.3-06 2006) 30

Table 3.1 – Reaction force in the radial direction at tank base under uniform pressure .. 61

Table 4.1 - Comparison between ABAQUS/Standard and ABAQUS/Explicit (Dassault Systèmes Simulia Corp. 2008)..... 76

Table 5.1 – Tanks dimensions and reinforcement 106

Table 6.1 - Tank dimensions and reinforcement 125

Table 6.2 – Summary of response modification factor results for Case 1 151

Table 6.3 – Summary of response modification factor results for Case 5 152

Table 7.1 – Earthquake hydrodynamic forces 159

Table 7.2 – Earthquake hydrodynamic bending moments on the entire tank..... 160

Table 7.3 - Tank dimensions and reinforcement – Fixed and hinged base..... 164

Table 7.4 - Tank dimensions and reinforcement – Anchored flexible base 165

Table 7.5 - Tank prestressing and seismic cable details – Anchored flexible base 165

Table7.6 – Ground motions properties 176

Table 7.7 – Computer model verification – Tank 2H 187

Table 7.8 – Comparison between results of nonlinear time-history FE analysis and current practice – Nonflexible base conditions..... 191

Table 7.9 – Comparison between results of nonlinear time-history FE analysis and current practice – Anchored flexible base condition 192

Table 7.10 – Summary of R_i-values based on results of FE analysis 196

Table A.1.1 – Design hydrodynamic and hydrostatic pressures at (θ) =0 deg – Hinged and Fixed Base…….....233

Table A.2.1 – Design hydrodynamic and hydrostatic pressures at (θ) =0 deg – Anchored, Flexible-Base…….....248

LIST OF FIGURES

Figure 2.1 – Ground-supported tank support connections; (a) Nonflexible fixed base, (b) Nonflexible hinged base, (c) Flexible base (ACI 350.3-06) 10

Figure 2.2 – Anchored flexible base ; (a) Details of seismic cables, (b) Distribution of base shear - Membrane shear transfer at the base of circular tanks 12

Figure 2.3 – Typical wall section of cast-in-place tank; (a) Horizontally-prestressed, (b) Horizontally and Vertically-prestressed (ACI 373R-97 and ACI 372R-03) 13

Figure 2.4 – Damages to Steel LCS; (a) Elephant-foot buckling, (b) Sloshing damage to the upper shell of the tank (Malhorta et al. 2000) 16

Figure 2.5 – Housner's model 18

Figure 2.6 – Inelastic force-deformation curve (FEMA 450, 2003) 26

Figure 2.7 – Factors affecting overstrength (FEMA 450, 2003) 27

Figure 2.8 – Ductility factor comparison (ATC-19 1995) 29

Figure 2.9 – Typical cross section of fluid viscous damper 38

Figure 2.10 – Recorded values of peak force versus peak velocity for a range of ambient temperature levels (Symans and Constantinou 1998) 39

Figure 2.11– Force-velocity relationship of viscous dampers (Hwang 2005) 40

Figure 3.1– Liquid-containing tank rigidly supported on the ground; (a) Fluid motion in tank, (b) Dynamic model, (c) Dynamic equilibrium of horizontal forces 48

Figure 3.2 – Effect of circular tank dimensions on hydrodynamic forces, T_w = 400 mm, Zone 4, (a) Impulsive force, (b) Convective force 52

Figure 3.3 – Effect of circular tank dimensions on Earthquake/Hydrostatic force ratios, D=10m, T_w = 400mm, (a) Base shear, (b) Base moments 53

Figure 3.4 – Effect of circular tank dimensions on sloshing height, (a) Water depth, D=30m T_w = 400 mm (b) Tank diameter, H_L = 6m, T_w = 400 mm 54

Figure 3.5 – Effect of circular tank dimensions on seismic forces HL = 6.0m, Zone 4, (a) Hydrodynamic forces, (b) Bending moments 55

Figure 3.6 – Hydrodynamic pressure distribution in circular tanks; (a) Cosine pressure distribution, (b) Uniform pressure distribution 56

Figure 3.7 – Vertical distribution of hydrodynamic pressure (adapted from Fig R5.3.3 – ACI350.3-06) 57

Figure 3.8 – Design hydrodynamic and hydrostatic pressures at (θ) = 0 deg..... 58

Figure 3.9 – FE model of circular tank; (a) Full Tank, (b) ½ Tank, (c) Axi- symmetric . 60

Figure 3.10 – Radial deflection under uniform pressure 62

Figure 3.11 – Hoop stress under uniform pressure 62

Figure 3.12 – Bending stresses in vertical direction under uniform pressure..... 63

Figure 3.13 – Radial deflection; (a) Hinged base, (b) Fixed base 65

Figure 3.14 – Hoops stress; (a) Hinged base, (b) Fixed base 66

Figure 3.15 – Bending stress; (a) Hinged base, (b) Fixed base 67

Figure 3.16 – Hoop force in tank wall; (a) Hinged base, (b) Fixed base..... 70

Figure 3.17 – Bending moment in tank wall; (a) Hinged base, (b) Fixed base 71

Figure 3.18 – Total seismic hoop force in tank wall..... 72

Figure 3.19 – Percentage of total hoop force in tank wall relative to free base condition 72

Figure 4.1 - Cost versus model size in using the explicit and implicit methods (Dassault Systèmes Simulia Corp. 2008)..... 77

Figure 4.2 – Response of concrete to uniaxial loading in tension 81

Figure 4.3 - Response of concrete to uniaxial loading in compression 82

Figure 4.4 - Uniaxial load cycle (tension–compression–tension) assuming $w_t = 0$ and $w_c = 1$ (default values) for the stiffness recovery (Dassault Systèmes Simulia Corp. 2008).... 84

Figure 4.5 - Stress-strain curve for concrete - Modified Hognested..... 86

Figure 4.6 - Stress-strain curve for reinforcement - Elastic-Plastic 88

Figure 4.7 - Stress–strain curve for steel in cyclic loading illustrating the Bauschinger effect (Kent et al. 1973) 88

Figure 4.8 - Stress-strain curve for prestressing tendons 89

Figure 4.9 - Values of Tangential or Slope Static Moduli for Rubber in Shear (Handbook of Molded and Extruded Rubber, Good Year, second edition, 1959) 91

Figure 5.1 – Shrinkage cracking after first crack; (a) Crack pattern, (b) Concrete stresses, (c) Reinforcement stresses 97

Figure 5.2 – Final shrinkage cracking; (a) Cracks pattern, (b) Concrete stresses, (c) Reinforcement stresses 100

Figure 5.3 – Finite element model for Tank 3F - ABAQUS/CAE 107

Figure 5.4 – Strain and stress distribution for Tank 2FR; (a) Total Horizontal strain, (b) Horizontal restraint strain, (c) Stress in horizontal rebars, (d) Hoop stress in concrete . 112

Figure 5.5 – Maximum hoop stress in concrete; (a) Tank 1H, (b) Tank 2H, (c) Tank 3H 116

Figure 5.6 – Maximum hoop stress in concrete; (a) Tank 1F, (b) Tank 2F, (c) Tank 3F 118

Figure 5.7 – Sensitivity study – Maximum hoop stress in concrete - Tank 2F 119

Figure 5.8 – Maximum hoop stress in concrete for ε_{sh} -120 x 10^{-6} - Tank 2F 119

Figure 6.1 – Mesh sensitivity study – Load-deflection response for Tank 1H-1 129

Figure 6.2 - Load-deflection response – Tank 1H-1 130

Figure 6.3 - Load-deflection response – Tank 1H-4 131

Figure 6.4 - Load-deflection response – Tank 1H-5 131

Figure 6.5 - Load-deflection response – Tank 2H-1 133

Figure 6.6 - Load-deflection response – Tank 2H-2 133

Figure 6.7 - Load-deflection response – Tank 2H-3 134

Figure 6.8 - Load-deflection response – Tank 2H-4 134
Figure 6.9 - Load-deflection response – Tank 2H-5 135
Figure 6.10 - Load-deflection response – Tank 3H-1 136
Figure 6.11 - Load-deflection response – Tank 3H-2 137
Figure 6.12 - Load-deflection response – Tank 3H-3 137
Figure 6.13 - Load-deflection response – Tank 3H-4 138
Figure 6.14 - Load-deflection response – Tank 3H-5 138
Figure 6.15 - Load-deflection response – Tank 1F-1 140
Figure 6.16 - Load-deflection response – Tank 1F-4 140
Figure 6.17 - Load-deflection response – Tank 1F-5 141
Figure 6.18 - Load-deflection response – Tank 2F-1 142
Figure 6.19 - Load-deflection response – Tank 2F-2 143
Figure 6.20 - Load-deflection response – Tank 2F-3 143
Figure 6.21 - Load-deflection response – Tank 2F-4 144
Figure 6.22 - Load-deflection response – Tank 2F-5 144
Figure 6.23 - Load-deflection response – Tank 3F-1 146
Figure 6.24 - Load-deflection response – Tank 3F-2 146
Figure 6.25 - Load-deflection response – Tank 3F-3 147
Figure 6.26 - Load-deflection response – Tank 3F-4 147
Figure 6.27 - Load-deflection response – Tank 3F-5 148
Figure 6.28 - Load-deflection response – Tank 2FR-1 149
Figure 6.29 – Effect of tank dimensions on response modification factor – Case 1 151
Figure 6.30 – Effect of tank dimensions on response modification factor – Case 5 152
Figure 6.31 – Effect of tank reinforcement on R_i-values; (a) Hinged, (b) Fixed 153

Figure 6.32 – Effect of tank reinforcement on R_μ-values; (a) Hinged, (b) Fixed..... 154

Figure 7.1 – Finite element model for Tank 2FL - ABAQUS/CAE..... 167

Figure 7.2 – Flexible support model..... 170

Figure 7.3 – Scaled earthquake record (horizontal component); (a) El-Centro, (b) Northridge,..... 175

Figure 7.4 – Time-history of base shear response for Tank 1H; (a) El-Centro, (b) Northridge,..... 178

Figure 7.5 – Percentage of peak base shear relative to El-Centro ground motion..... 178

Figure 7.6 – Hydrostatic pressure; (a) Vertical distribution, (b) Horizontal distribution (tank circumference)..... 180

Figure 7.7 – Time-history of base shear response for Tank 1H - El-Centro 183

Figure 7.8 – Comparison between FE time-history and current practice – Tank 2H; (a) Hoop force, (b) Bending moment..... 188

Figure 7.9 – Mesh sensitivity study - Tank 1H; (a) Hoop forces, (b) Bending moments190

Figure 7.10 – Effect of R_i-values on stress in reinforcement; (a) Tank 1, (b) Tank 2, (c) Tank 3 196

Figure 7.11 – Tank response under time-history analysis – Tank 1FL-PC 197

Figure 7.12 – Effect of R-values on crack width; (a) Tank 1, (b) Tank 2, (c) Tank 3.... 201

Figure 7.13 – Effect of tank dimensions and support conditions on R-values 202

Figure 7.14 – Effect of tank dimensions and support conditions on dynamic base shear 202

Figure 7.15 – Effect of tank dimensions and support conditions on the ratio between nonlinear and linear dynamic base shear 204

Figure 7.16 – Effect of tank dimensions and support conditions on R-values - PC flexible base 205

Figure 7.17 – Comparison between R-values based on push-over and time-history analysis..... 206

Figure 8.1 – Fluid viscous damper detail and dimensions; (a) Front view, (b) Side view 211

Figure 8.2 – Fluid viscous damper connection detail; (a) Section, (b) Plan..... 212

Figure 8.3 – Fluid viscous dampers layout – Plan view 213

Figure 8.4 – Flexible support and damper model; (a) 3-D view, (b) Radial direction ... 215

Figure 8.5 – Effect of damping coefficient on hoop forces - Tank 2FL..... 217

Figure 8.6 – Effect of tank dimensions and damping coefficient on base shear 218

Figure 8.7 – Effect of damping coefficient on base shear –Tank 2FL 220

Figure 8.8 – Effect of damping constant on response modification factor – Tank 2FL. 220

Figure 8.9 – Effect of tank dimensions and damping constant on response modification factor 221

Figure 8.10 – Effect of damping coefficient on base deflection –Tank 2FL..... 221

Figure A.1.1 – Design hydrodynamic and hydrostatic pressures at (θ) =0 deg – Hinged and Fixed Base…….....233

Figure A.1.2 – Design hydrodynamic and hydrostatic hoop forces at (θ) =0 deg – Hinged Base.....…….....234

Figure A.1.3 – Design hydrodynamic and hydrostatic bending moment at (θ) =0 deg – Hinged Base…….....234

Figure A.2.1 – Design hydrodynamic and hydrostatic pressures at (θ) =0 deg – Anchored, Flexible-Base…….....248

Figure A.3.1 - Effect of rectangular tank dimensions on hydrodynamic forces B = 40 m and Zone 4, (a) Impulsive force, (b) Convective force….....255

Figure A.3.2 - Effect of rectangular tank height on Earthquake/Hydrostatic force ratio B=20m, L=20m, (a) Base shear, (b) Base moments…….....256

Figure A.3.3- Effect of rectangular tank dimensions on sloshing height, (a) Water depth B=20m, L=60m, (b) Tank length parallel to the earthquake force B=20m, HL=6m…..257

Figure A.3.4 - Effect of rectangular tank dimensions on seismic forces B=40m, H_L=6.0m, Zone 4, (a) Hydrodynamic forces, (b) Bending moments…….....258

LIST OF APPENDICES

APPENDIX A.1 – Design of ground-supported nonflexible-base circular tank…….228

APPENDIX A.2 – Design of ground-supported anchored flexible-base circular tank...242

APPENDIX A.3 – Effect of rectangular tank dimensions on hydrodynamic forces…...253

APPENDIX A.4 – Taylor devises inc. Fluid viscous damper datasheet…….....259

APPENDIX B.1 – Input file of computer model – Push-over analysis…….....261

APPENDIX B.2 – Input files of computer models – Time-history analysis…….....268

LIST OF SYMBOLS

Ac	Area of concrete section
API	American Petroleum Institute
As max	Maximum are of reinforcement to eliminate compression (brittle) failure.
As min	Minimum area of reinforcement specified by ACI350-06 for shrinkage and temperature
As	Area of reinforcement
ASCE	American Society of Civil Engineers
A_t	Effective concrete area in uniform tension (mm^2)
Axi	Axisymmetric elements
C/C	Center to center
Cosine	Cosine distribution of seismic force
D	Inside diameter of circular tank, significant duration of earthquake, and linear deformation of rubber pad
d_b	Rebar diameter
E(D)	Total energy input during time D
E_c	Modulus of elasticity of concrete
E_{ce}	Effective modulus of elasticity of concrete given as
EF	Each face
EQ	Actual earthquake pressure at tank base based on ACI 350 (R included)
EQmax	Maximum value of earthquake forces at polar coordinate angle (θ) = 0 deg
E_s	Modulus of elasticity of steel
f'c	specified compressive strength of concrete
$f_{c,a}$	Actual stress in concrete
$f_{c,r}$	Stress in concrete if the member is fully restrained
f_{cr}	Final tensile strength of concrete
f_{cr}	Cracking failure stress of concrete
FE	Finite element

f_{pu}	Specified tensile strength of prestressing strands
f_s	Stress in reinforcement
FT	Full tank
FVD	Fluid viscous damper
f_y	yield strength of reinforcement
G_p	Shear modules of elastomeric bearing pad
G_p	The shear module of elastomeric bearing pad
HEF	Horizontal each face
H_L	Liquid/Water depth
HS	Hydrostatic water pressure at tank base
H_w	Wall depth
IF	Inside face
K_L	The linear spring rate of the rubber pad
K_R	Degree of restraint
K_t	The stiffness of the anchored flexible support in the tangential direction
Lc	The length of the RUBATEX Sleeve plus the embedded length
LCS	liquid-containing structures
L_p	Length of elastomeric bearing pad
M	Minimum number of cracks
M2	Bending moment in cylindrical wall
M_b	Bending moment on the entire tank cross section just above the base of the tank wall
M_c	Bending moment on the entire tank cross section just above the base of the tank wall due to the convective force
MCE	Maximum considered earthquake
M_i	Total impulsive mass
M_i	Bending moment on the entire tank cross section just above the base of the tank wall due to the impulsive force P_i
m_{res}	The mass resultant calculated as the sum of individual masses m_i at the different each nodes along the $\theta = 0$ meridian

M_w	Bending moment on the entire tank cross section just above the base of the tank wall due to the wall inertia force
N	Hoop Force
N_{cr}	The force required to cause cracking in concrete
N_{cr1}	Restraining force after first crack
n	The ratio of the modulus of elasticity of the reinforcement to the modulus of elasticity of concrete
n_e	The ratio of the modulus of elasticity of the reinforcement to the effective modulus of elasticity of concrete
NL	Nonlinear load-deflection response of the tank wall
OF	Outside face
P_a	Power index
PC	Prestressed concrete
P_c Cosine	Cosine distribution of convective force
P_c Max "Axi"	Maximum value of convective force at $\theta = 0$ deg that is used for axisymmetric elements.
P_c Max	Uniform distribution of convective force using maximum value at $\theta = 0$ deg.
P_c	Convective force
PCA	Closed form solution using Portland cement association handbook
P_{cr}	Pressure at which cracking of concrete is initiated
P_e	Effective circumferential prestressing force (after long term losses)
PGA	Peak ground acceleration
PGV	Peak ground velocity
P_i Cosine	Cosine distribution of impulsive force
P_i Max	Maximum value of impulsive force at $\theta = 0$ deg.
P_i	Impulsive force
P_i	Initial circumferential prestressing force
P_{yH}	Pressure at which yield of horizontal bars is initiated
P_{yV}	Pressure at which yield of vertical bars is initiated
P_w	lateral inertia force of accelerating wall

R	Response modification factor, and tank radius
RC	Reinforced concrete
R_c	Convective response modification factor
R_i	Impulsive response modification factor
R_R	Redundancy factor
R_s	Strength factor
R_μ	Ductility factor
S	Spacing between reinforcement and spacing between cracks
S_1	Mapped maximum considered earthquake 5% damped spectral response acceleration; parameter at a period of 1 second, expressed as a fraction of acceleration due to gravity g
S11	Hoop stress
S22	Stresses in the vertical direction
S_c	Spacing between the seismic cables
SDOF	Single degree of freedom
S_p	Spacing of elastomeric bearing pad
S_s	Mapped maximum considered earthquake 5% damped spectral response acceleration parameter short periods, expressed as a fraction of acceleration due to gravity g
T	Rubber pad thickness, and tank natural period
T_0	Time at the beginning of the strong shaking phase
T_c	Natural period of the first convective mode of sloshing
T_i	Fundamental period of oscillation of the tank plus the impulsive component of contents
t_p	Thickness of elastomeric bearing pad
T_w	Wall thickness
U1	Radial deflection of the tank wall
U_{max}	Maximum radial deflection, displacement corresponding to the limiting state response
USA	United State of America
V	Total Horizontal base shear

V_0	Base shear at maximum displacement
$V_{ACI350.3}$	Base shear base shear due to impulsive and lateral inertia force of accelerating wall
V_d	Design base shear (FEMA 450)
V_E	Elastic base shear
VEF	Vertical each face
$V_{El\text{-}Centro}$	Absolute maximum value of peak base shear to impulsive and lateral inertia force of accelerating wall from time-history analysis due to El-Centro horizontal record
VIF	Vertical inside face
V_{max}	Maximum peak base shear due to impulsive and lateral inertia force of accelerating wall from time-history analysis
V_{min}	Minimum peak base shear due to impulsive and lateral inertia force of accelerating wall from time-history analysis
VOF	Vertical outside face
Vs	Design base shear (ATC-19)
Vy	Base shear at yield - Yielded strength
w_c	Crack width
w_i	The natural frequency at mode i
w_p	Width of elastomeric bearing pad
α_c	Thermal expansion coefficient of concrete
α_R	Rayleigh damping factor for mass proportional damping
α_s	Thermal expansion coefficient of reinforcement
α_{spt}	Thermal expansion coefficient of prestressing tendons
β_R	Rayleigh damping factor for stiffness proportional damping
θ	Polar coordinate angle
$\Omega 0$	Structural overstrength factor
Ω_D	Design overstrength factor
Ω_M	Material overstrength factor
$\varepsilon_{restraint}$	Restraint strain in concrete
ε_s	Strain in reinforcement

Ψ_s	Crack spacing factor
Ω_S	System overstrength factor
ε_{sh}	Final shrinkage strain
$\varepsilon_{shrinkage}$	Shrinkage strain
ε_{total}	Total strain in concrete
ϕ	Final creep coefficient of concrete
ζ_i	Critical damping
ν_c	Poisson's ratio of concrete
ν_{pt}	Poisson's ratio of prestressing tendons
ν_s	Poisson's ratio of reinforcement
ρ	Reinforcement ratio
ρ_{min}	Minimum required reinforcement ratio
σ_{av}	Average stress in concrete given as
σ_{c1},	Stress in concrete after first crack
σ_{cst1}	Compressive stress in reinforcement after first crack
σ_e	Effective stresses in prestressing tendons
σ_i	Initial stresses in prestressing tendons
σ_{st1}	Tensile stress in reinforcement after first crack
ε_y	Yield strain
ϕ	Strength reduction factor
μ	Displacement ductility ratio
Δf_s	Net stress in prestressing tendons (MPa)
$\sum O$	Sum of perimeters of all effective bars crossing section on tension side (mm)

CHAPTER 1
INTRODUCTION

1.1 General

Liquid-containing structures (LCS) are important components in the commercial and industrial applications as they are used for storage water and other products such as oil and gas. Therefore, storage tanks can be considered as the lifeline of the industrial facilities. They are critical elements in the municipal water supply and fire fighting systems, and are used extensively for storage and/or processing of a variety of liquids and liquid-like materials, including oil, liquefied natural gas, chemical fluids, and wastes of different forms.

Conventionally RC tanks have been used extensively for municipal and industrial facilities for several decades. There are many types of storage tanks depending on the structure type, geometry, construction material, support condition, etc. Ground-supported tanks can be classified according to tank configuration (rectangular or circular), wall support condition (flexible and nonflexible base connections), and method of construction (RC) or (PC) (ACI 350.3-06 2006).

Many tanks, particularly the cylindrical ones, have been made of steel. However, concrete tanks including the cylindrical ones are becoming more popular. This is due to improved service life and durability and also due to numerous observed failures of steel tanks during past earthquakes.

The design of liquid-containing structures (LCS) requires that attention be given not only to strength, but also to serviceability requirements. Hence, concrete tanks may be used to store contaminated or hazardous materials, while leakage of such materials can cause damage to the environment with associated costs more than the damage caused by earthquake itself. Furthermore, the functionality of LCS is very important after the occurrence of an earthquake to meet the emergency requirements. Therefore, concrete storage tanks should be designed to meet the serviceability limits such as leakage in addition to the strength requirements.

A properly designed tank must be able to withstand the applied loads with limited crack widths to prevent leakage. The goal of providing a structurally sound tank that will not leak is achieved

by providing proper amount and distribution of reinforcement, proper spacing and detailing of construction joints, and use of quality concrete placed by proper construction practices. RC walls of circular tanks are subjected to shrinkage and temperature effects. As a result, appropriate amount of reinforcement is necessary to reduce the amount of cracking.

As numbers and sizes of the liquid-containing structures have increased over the years, so have their importance and the need for a better understanding of their behavior in order to formulate rational and efficient methods for their analysis and design. This need has been particularly pressing for developing systems that can withstand the applied loads including earthquakes and other dynamic excitations. Even though, some studies were performed on the response of the tanks subjected to ground shaking, very little attention has been given to the nonlinear response and the level of available ductility for the ground-supported concrete circular tanks. As LCS are unique in their behavior under seismic loads, there are some debates about the basis on recommended values of the response modification factors (R) included in the current standards. The R-values have a significant effect on the seismic forces considered in the design and accordingly the required concrete dimensions and the amount of reinforcement. Hence, considering the large number and size of concrete liquid storage tanks any safe reduction in the dimensions, wall thickness and reinforcement can result in economical benefits.

This study is focused on the nonlinear behavior of ground-supported circular reinforced concrete tanks under the effect of seismic loads. The nonlinear response of ground-supported circular tanks using push-over and time-history analysis is investigated. The values of response modification factors included in the current design codes and standards are evaluated.

1.2 Research Significance

This research study provides information on the nonlinear behavior of circular tanks in terms of strength, stiffness, load-deformation response, and also the possible failure modes, based on the analytical investigations. The results of this research contribute significantly to the understanding of the behavior of ground-supported RC circular tanks with the aim to improve the design codes for such structures.

Considering the environmental consequences of wide spread tank failure, which could occur in an earthquake event, proves that the use of appropriate R values in design is important. This study aims at investigating the validity if current R-values used in design.

Currently, there is no rational on the R-values specified in the current codes and standards of ground-supported RC and PC circular tanks. This research study will contribute to the need of the industry by estimating R-values, which is a major factor in calculating the design earthquake forces. This study includes investigating the effects of tank characteristics, such as tank aspect ratio, construction methods, and support conditions on R-values.

In this study, an innovative design approach is introduced in order to reduce tank response under seismic loads. A new design technique is proposed by means of using passive energy dissipation system such as fluid viscous dampers in the radial direction of circular tanks.

1.3 Objectives, Assumptions, and Limitations

The primary focus of this research is to study the nonlinear behavior of ground-supported concrete circular tanks under earthquake loads. To examine such behavior, nonlinear finite element models are developed in order to simulate the tank behavior under push-over and time-history analysis. The finite element models of this study are then used for a parametric study to investigate the influence of tank characteristics on the response modification factor, R.

The main objectives of this research are summarised as follows:

1) To understand the effect of tank dimensions on hydrodynamic forces
2) To investigate shrinkage effect on concrete cracking and internal stresses of circular tanks
3) To simulate the nonlinear behavior of concrete circular tanks under push-over and time-history dynamic loading using finite element techniques
4) To understand the nonlinear behavior of ground-supported RC and PC circular tanks under seismic loads
5) To investigate and assess the current values of the response modification factor for ground-supported circular tanks

6) To investigate the system characteristics and the factors affecting the response modification factor of ground-supported concrete circular tanks such as tank dimensions, method of construction (RC and PC), and wall support condition (fixed, hinged, and flexible base connections)
7) To examine an innovative technique for seismic response reduction in ground-supported tanks. In this technique, a passive energy dissipation system, in the form of fluid viscous dampers, in the radial direction of the tank at the base is used

The assumptions and limitations for this study are summarized as follows:

1) The tanks are assumed to be anchored to rigid ground such that no sliding or uplift may occur. Thus, the soil-structure interaction effect is not considered
2) Only open top concrete circular ground-supported tanks are considered in this study
3) Only tanks with diameter/water depth ratios between 4 to 13 are considered in this study
4) In the FE analysis, only the effect of horizontal ground motion in considered
5) The fluid is assumed to be incompressible and inviscid
6) In FE analysis, only the impulsive component of the fluid is considered
7) The response modification factor for convective component of the accelerating liquid is not investigated in this study
8) The fluid-structure interaction is not considered in this study

1.4 Outline of Thesis

This thesis consists of nine chapters. A brief description of the contents of each chapter is described as follows:

Chapter 1 presents a brief introduction on the liquid-containing structures, research significance, scope and objective of this study.

Chapter 2 presents a literature review on response modification factor including a historical review about evolution of this factor. Also, the details of the response modification factor

components such as the overstrength and factor ductility factor are also presented. This chapter also discusses the tanks behavior under seismic loads, and previous research studies on the seismic behavior of liquid-containing structures including the mathematical models proposed for description of the behavior of these structures, codes design requirements, fluid viscous dampers, concrete cracking and nonlinear behavior of circular tanks.

Chapter 3 provides a detailed outline of tank behavior under seismic loads, ACI 350.3-06 (2006) design requirements, code background (ACI 350.3-01 2001), and the effect of circular tank dimensions on hydrodynamic forces. This chapter also addresses the use of uniform pressure distribution based on the maximum pressure obtained from cosine distribution versus the use of the actual cosine distribution of seismic forces. This chapter investigates the validity of using the approximation of uniform distributed load (using axisymmetric elements) instead of the actual cosine distribution (using shell elements). Also, this chapter presents a comparison between analytical and closed-form solutions.

Chapter 4 explains the nonlinear properties of the construction materials including concrete, steel reinforcement and elastomeric bearing pad. Also, this chapter describes various modelling features of ABAQUS/CAE software.

Chapter 5 addresses the cracking and shrinkage effect on concrete strength of circular tanks. The concrete shrinkage including theory of shrinkage cracking, shrinkage and temperature reinforcement, member restraints, degree of restraint, and degree of restraint caused by reinforcement are discussed. This chapter presents the results of nonlinear FE analysis that are carried out in order to investigate the effect of shrinkage on concrete tensile stress of RC circular tanks for free, hinged, and fixed base conditions.

Chapter 6 examines the nonlinear Behavior of ground-supported circular liquid-containing concrete structures under push-over analysis. Nonlinear FE analysis is carried out to investigate the nonlinear behavior of fixed, hinged and free based RC circular tanks under seismic loading. The nonlinear push-over FE analysis is performed using axisymmetric elements. This chapter describes in detail the FE model developed to predict the nonlinear behavior of above-ground

circular tanks under push-over analysis. The results of FE analysis are presented. A parametric study is carried out in order to investigate the effect of different parameters, such as reinforcement ratios and tank relative dimensions, on tank response. The results of this parametric study are presented in this chapter. Also, the results of the nonlinear FE pushover analysis are used to calculate the response modification factor for each case to verify the recommended values by current practice.

Chapter 7 outlines the details of the nonlinear FE model developed to predict the behavior of the above ground circular tanks under dynamic loading (time-history analysis). This chapter discusses the results of a parametric study carried out on ground-supported RC and PC circular tanks using nonlinear FE technique. A wide range of tank sizes, support conditions (flexible and nonflexible), and construction methods (RC and PC) are considered in this study. The results of the FE analysis are presented; the results of FE analysis are used to calculate R-values, and the validity of the R-values specified in the current practice is addressed. Also, this chapter discusses the design considerations of the circular tanks including support conditions, tank relative dimensions, tank reinforcement, and prestressing.

Chapter 8 presents a new innovative design technique to reduce the seismic response of tanks by using FVD system for flexible base circular tanks. Nonlinear FE time-history analysis is performed in order to investigate the effect of using FVD on the results. The RC and PC concrete circular tanks with a wide range of relative dimensions are considered in this chapter. The effect of damping constant on the results of FE analysis is also investigated.

Chapter 9 presents the main conclusions of the study along with some recommendations and suggestions for future work on response modification factor and nonlinear behavior of reinforced concrete circular tanks.

The thesis ends with a list of references and two appendices. The first appendix provides detailed calculations for design of circular tank and the calculations of earthquake design loads and load distribution in accordance to ACI30.3-06 (2006) and ACI350-06 (2006). The effect of

rectangular tank dimensions on hydrodynamic forces is also included in the first appendix. The input text command files for tanks used in this study are given in the second appendix.

CHAPTER 2
LITERATURE REVIEW

2.1 General

This chapter provides a literature review on the dynamic behavior including aspects of ground shaking response of liquid-containing structures (LCS). The different types of tank supports and construction types are explained. In addition, the earthquake damage to LCS and research studies on observation and identification of causes of damage and failure for LCS are discussed in this chapter. This chapter provides also literature review on the response modification factor, R, for circular tanks. The significant contributions made by previous research studies on LCS and effect of cracking on concrete are also highlighted. Furthermore, the applications of passive energy dissipation systems and the effect of using such systems on the seismic response by providing an alternative source of energy dissipation system are also presented. An overview on existing codes, standards, and guidelines used in the design of LCS and passive energy dissipation systems is provided.

2.2 Ground-supported tank classifications

Ground supported tanks including on-grade and below grade structures can be classified according to the following characteristics (ACI 350.3-06, 2006):

- Tank configuration (rectangular or circular)
- Wall support condition (nonflexible base connections: fixed and hinged, or flexible base connections)
- Method of construction (reinforced concrete (RC) or prestressed concrete(PC))

It should be noted that, the most general type of LCS is upright rectangular and circular tanks. This study focuses on on-grade open top circular tanks for fixed, hinged, and anchored flexible base conditions. Reinforced and prestressed concrete construction methods are considered in this research study. It should be noted that the use of prestressed concrete is only considered for circular tanks with flexible base. Figure 2.1 show the support conditions and details for nonflexible (fixed and hinged) and flexible base connections.

Figures 2.1 (a) and (b) show the base configurations for two types of fixed base and two types of hinged base tanks, respectively. For fixed base support, no movement or rotation are allowed at the wall base. The bending moment at tank base is resisted by vertical reinforcement connecting tanks base and tank wall where the vertical reinforcement extends across the joint. However, for fixed base connection with closure strip, no vertical reinforcement extends between the base and the wall. Thus, the wall is not connected directly to foundation in order to overcome the shrinkage. In this case, the fixity between the wall and tank base is provided through the closure strip. For hinged base support, no bending moment is transmitted between the tank wall and base in which rotation is allowed. In addition, for fixed and hinged base tanks, the earthquake base shear is transmitted partially by membrane (tangential shear) and the rest by radial shear that cause vertical bending.

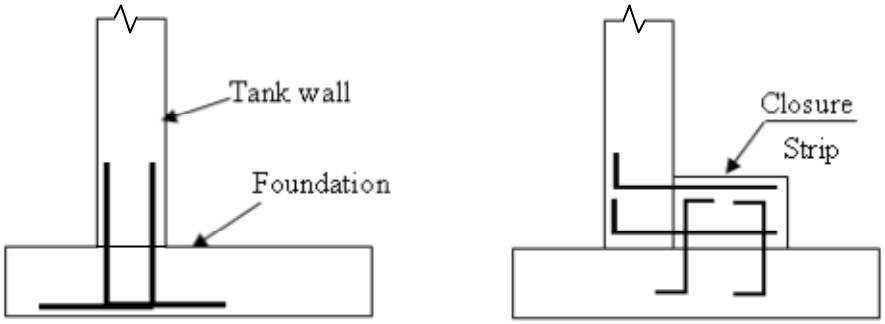

(a)

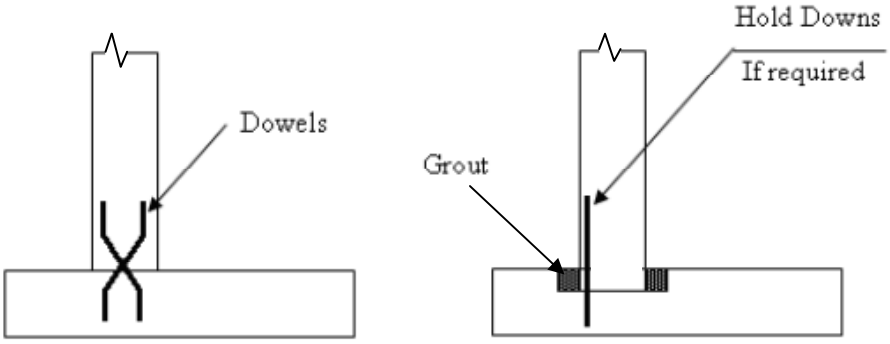

(b)

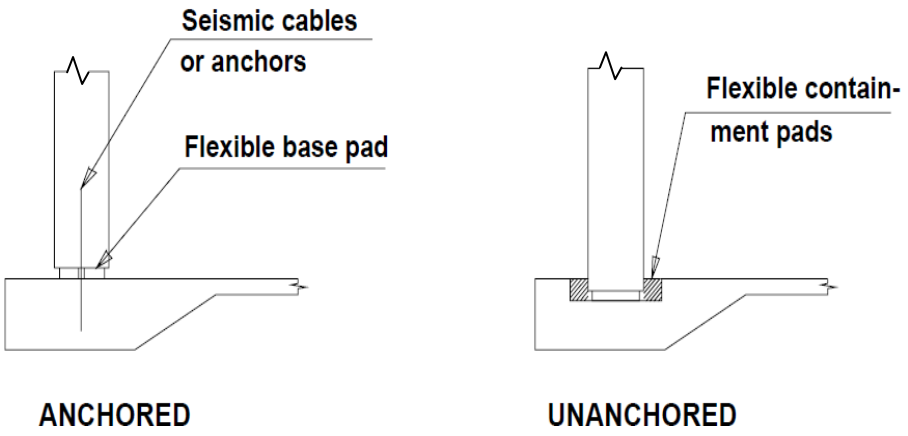

(c)

Figure 2.1 – Ground-supported tank support connections; (a) Nonflexible fixed base, (b) Nonflexible hinged base, (c) Flexible base (ACI 350.3-06)

*Water-stop, wall, footing reinforcement, and prestressing tendons are not shown for clarity

The flexible base supports are used for prestressed circular tanks (ACI 350.3-06 2006). For unanchored, flexible-base tanks, it is assumed that the base shear is transmitted by friction only. If friction between the wall base and footing, or between the wall base and bearing pads, is insufficient to resist earthquake shear, some form of mechanical restraint may be required. For anchored, flexible-base tanks, it is assumed that the entire base shear is transmitted by membrane (tangential) shear. The anchored, flexible-base support consists of seismic cables connecting the wall and the footing, as well as elastomeric bearing pads. The main mechanism for transferring the base shear from the wall to the foundation is the tangential resistance offered by a system of "seismic cables" connection the wall to the perimeter footing. Figure 2.2 (a) shows a typical detail of the seismic cables. Typically the cables are 15 mm diameter, 7-wire high-strength strands. Each cable is embedded partially in the footing and partially in the wall and is inclined at 45° from the horizontal in a direction tangent to the wall. When the unbalanced horizontal force, such as seismic force, acts on the tank, the cables parallel to the force offer the maximum resistance, while the base cables normal to the direction of that force offer little or no resistance. This cable resistance is in the form of cable tension that prevents the displacement of the wall relative to the footing. The resistance offered by cables varies according to the cosine of the

angle as shown in Figure 2.2 (b). In view of the fact that the seismic force can act in any direction, also, the direction of seismic force changes during a seismic event. The cable inclination alternates so that for every cable that is in tension there is a cable in compression, and hence "inactive", but ready to resist the horizontal force when it reverses direction. Furthermore, elastomeric bearing pads may add stiffness to the flexible base supports.

The concept of the "seismic cables" as an earthquake load-resisting mechanism was confirmed in the late 1950's by tests conducted by John A. Blume and Associates, with guidance by Professor G. Housner (Housner, G. W. 1963)

The maximum force per acting seismic cable (F_{max}) can be calculated using the following equations (ACI 350.3-06 2006):

$$F_{max} = 2\,(q_o S) \tag{2-1}$$

$$q_{max} = q_o = \frac{V}{\pi R} \tag{2-2}$$

where,

q_{max} and q_o are the maximum shear force per unit length

q_r is shear force per unit length at angle θ

R is the tank radius

S is the spacing between seismic cables

V is the total base shear

Furthermore, for circular tanks with flexible base, only PC is allowed to be used (ACI 350.3-06 2006). As shown in Figure 2.3, the crack control and watertightness of such tanks is achieved by using circumferential prestressing, together with vertical prestressed reinforcement near the center of the wall, or non-prestressed vertical reinforcement near each face of the wall.

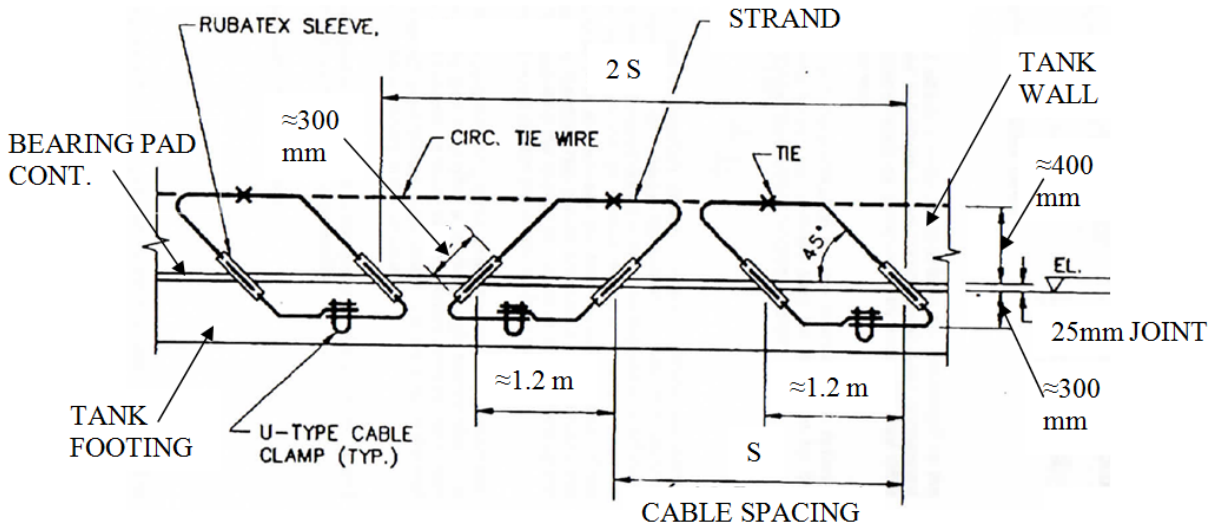

(a)

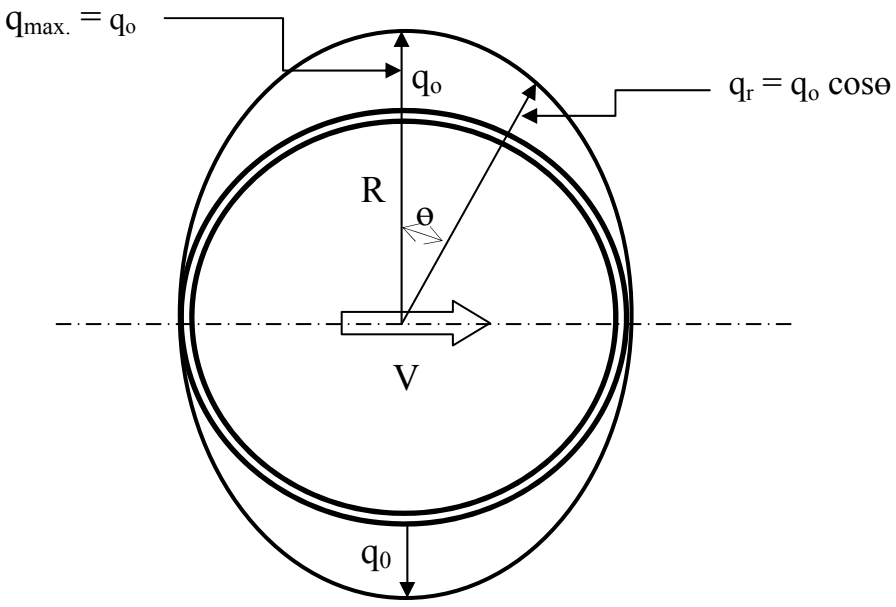

(b)

Figure 2.2 – Anchored flexible base ; (a) Details of seismic cables, (b) Distribution of base shear - Membrane shear transfer at the base of circular tanks

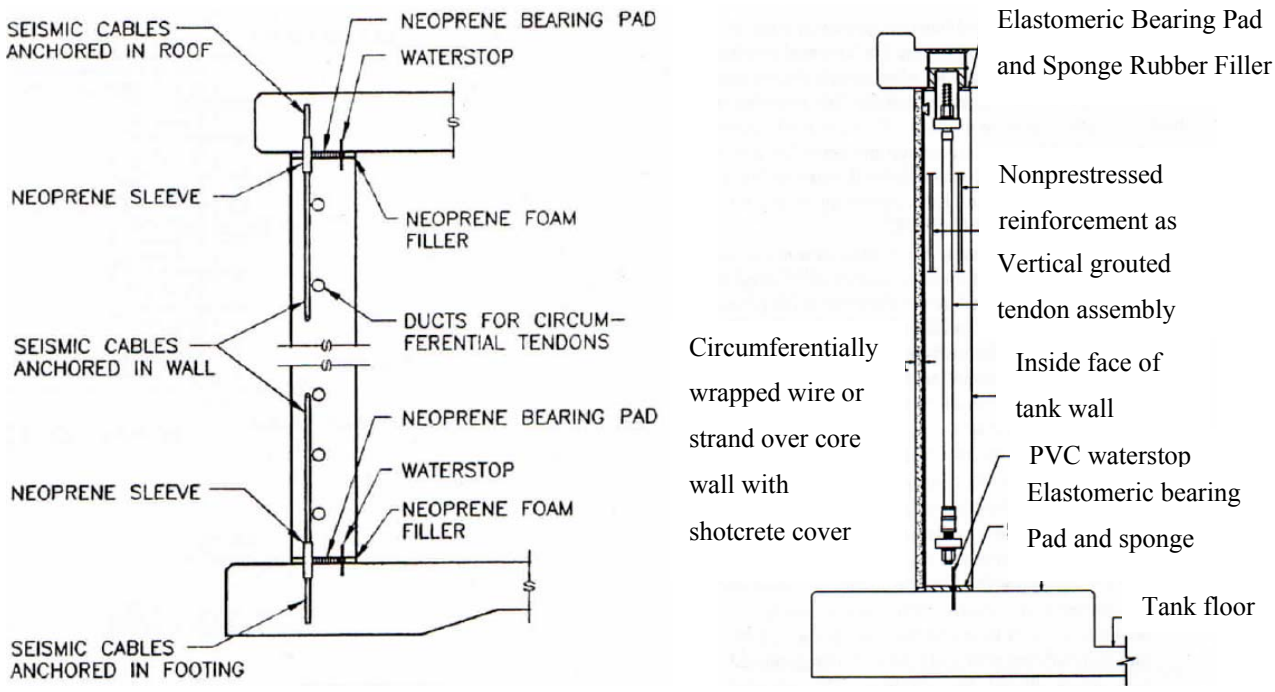

(a) (b)

Figure 2.3 – Typical wall section of cast-in-place tank; (a) Horizontally-prestressed, (b) Horizontally and Vertically-prestressed (ACI 373R-97 and ACI 372R-03)

2.3 Seismic damage to LCS

There are many reports on damage to LCS tanks due to seismic events. It was reported that there were heavy damages to both concrete and steel LCS during the strong seismic events of 1933 Long Beach, 1952 Kern County, 1964 Alaska, 1964 Niigata, 1966 Parkfield, 1971 San Fernando, 1978 Miyagi prefecture, 1979 Imperial County, 1983 Coalinga, 1994 Northridge and 1999 Kocaeli earthquakes (Rinne (1967), Shibata (1974), Kono (1980), Rai (2002), and Sezen and Whittaker (2006)). It should be noted that the damage to steel LCS may be different from the damage to concrete LCS under the effect of seismic loads.

The main causes of the damage to steel LCS are due to elephant-foot buckling around the base, anchorage system failure, and sloshing damage to the roof and upper shell of the tank. The main causes of damage to concrete LCS are mainly due to deformations, cracks, and leakage in the

tank wall. Furthermore, damage to LCS due to earthquakes is an evident that these structures are subjected to relatively large hydrodynamic forces during seismic events in addition to the hydrostatic loads.

The damage to LCS can be categorized as follows (Moslemi 2011):

1. Buckling of the shell caused by excessive axial compression of the shell structure due to exerted overturning moment (elephant-foot buckling)
2. Deformation, cracks and leakage inside shell
3. Damage to the roof or the upper shell of the tank, due to sloshing of the upper portion of the contained liquid in tanks with insufficient free board provided between the liquid free surface and the roof
4. Spillover of the stored liquid
5. Failure of piping and other accessories connected to the tank because of the relative movement of the flexible shell
6. Damage to the supporting structure in elevated tanks
7. Damage to the anchor bolts and the foundation system
8. Failure of supporting soil due to over-stressing

However, failure mechanism of liquid storage tanks depends on different parameters such as construction material, tank configuration, tank type, and support conditions. In addition, the significance of preventing damage to LCS has led to extensive research study carried out on the dynamic behavior of LCS. These studies, indeed, resulted in a better understanding and knowledge of LCS under seismic loads.

2.3.1 Damage to steel tanks

Many catastrophic failures of steel LCS tanks took place over the years such as the failure of the steel molasses tank in Boston Massachusetts, USA in 1919 (Puleo 2003). The tank was around 27 m diameter and 15 m in height. The explosion of the large tank, which was filled to the top, killed 12 and injured 150 people. The failure was due to poor design and construction where the steel wall was too thin to resist repeated loads from the contents. However, the increase in the

internal pressure due to the development of carbon dioxide as a result of fermentation occurring inside the tank is considered to have a contribution to the failure. The tank had only been filled to capacity eight times since it was built a few years before, putting the walls under an intermittent cyclical load (Sadjadi 2009).

During and after the Turkey Earthquake in 1999 several tank failures accrued. This includes, the air release of 200 metric tons of hazardous anhydrous ammonia; the leakage of 6500 metric tons of toxic acrylonitrile from ruptured tanks; the spill of 50 metric tons of diesel fuel from a broken fuel loading arm, liquid petroleum gas leakages, and oil spills at oil refinery, and the enormous fires are clear signs of damages that can occur as a result of storage tank failure. The environmental damage due to this earthquake has caused animal deaths and has affected the vegetation within 200 meters of the tanks (Steinberg and Cruz 2004).

Due to 1964 Niigata Earthquake in Japan (Watanabe 1966), a friction and impact between the roof and sidewall of the storage tank led to sparking which caused a fire that burned for more than 14 days consuming around 122 million liters of oil. It was found that, the seal material between the roof and the sidewall was metallic, and it was the seal that led to sparking when it scraped against the side wall. These sparks ignited the petroleum vapours contained inside the tank, which led to a major fire.

The 1994 Northridge earthquake caused extensive damage to major facilities in the Los Angeles area. In the San Fernando Valley area, the earthquake caused damage to five steel LCS. Much of the observed damage was related to uplift of the tanks during the earthquake. All of the damaged tanks showed signs of buckling in the tank walls. The roofs of several tanks also collapsed due to the impact of the sloshing water waves. In addition, the earthquake caused damage to many liquid storage tanks in the power generating plant. Two steel tanks shifted 100 mm from their original positions, even though the tanks had been anchored to a reinforced concrete ring foundation by 50.8 mm diameter steel anchor bolts. Another two fire-fighting water storage tanks were also damaged, losing their water contents. One of the fire-fighting tanks was a bolted steel tank unanchored at the base. The other was a welded steel tank with a very strong anchorage system. The bolted tank wall failed in an elephant-foot buckling around the base,

where the welded tank anchoring system prevented the damage to the welded tank wall (Lund 1996).

As indicated before, the most common damage to steel LCS is due to elephant-foot buckling, where the lower part of the side shell bulged all along the perimeter. This buckling type damage generally happens due to the excessive overturning moment generated during the seismic event.
It should be noted that, full base anchorage is not always a possible or economical alternative. Therefore, many tanks are either unanchored or partially anchored at their bases. If the tank is not rigidly anchored to the ground, the generated overturning moment due to earthquake may be large enough to result in lift-off of the tank base. As the tank base falls back down after lift-off, high compressive stresses are generated in the wall near the base leading to elephant-foot wall buckling. This mode of damage is more common in steel tanks since they are generally more flexible than concrete tanks. Some studies show that base-lift-off in tanks having flexible soil foundations does not cause high axial compressive in the tank wall. As a result, unanchored tanks flexibly supported at their base are less susceptible to elephant-foot buckling mode, but are more susceptible to uneven settlement of the foundation (Malhotra 1995) and (Malhotra 1997). Figure 2.4 shows some of the common damages to steel LCS.

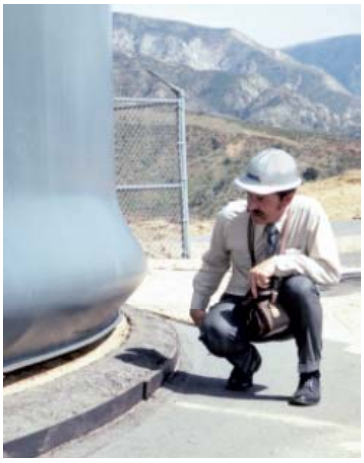

(a)

(b)

Figure 2.4 – Damages to Steel LCS; (a) Elephant-foot buckling, (b) Sloshing damage to the upper shell of the tank (Malhorta et al. 2000)

2.3.2 Damage to concrete LCS

During previous earthquakes, concrete LCS have been subjected to damages. As reported in the 1971 San Fernando earthquake, an underground water reservoir was subjected to an estimated inertial force of forty percent of ground acceleration (g) and suffered severe damages including the collapse of a wall (Jennings 1971). During the south-central Illinois earthquake in 1968, pre-existing hairline cracks in 15.8 m diameter circular reinforced concrete (RC) ground-supported tank opened, sending a 15.2 m jet of water into the adjacent parking area. The 3.6 m high and 300 mm thick tank wall was bound with five 20 mm bands that probably prevented the complete failure of the tank (Gordon et al. 1970).

Anshel (1999) has reported heavy damage to cylindrical buried concrete tanks due to the 1995 Kobe earthquake. During the 1971 San Fernando earthquake, an underground concrete tank was severely damaged in the form of the collapse of the wall (Jennings 1971).

As indicated before, deformation, cracking and leakage are the most common forms of damage in concrete tanks. Stresses caused by large hydrodynamic pressures together with the additional stresses resulted from the large inertial mass of concrete may cause cracks, leakage and ultimately tank failure.

2.4 Previous research studies on seismic response of LCS

The dynamic response of LCS has been studied by many researchers, theoretically and experimentally. The hydrodynamics of liquids were initially considered for rigid tanks resting on rigid foundations. Extensive study on the dynamic behavior of LCS started in the late 1940's. Jacobsen (1949) calculated the effective hydrodynamic masses and mass moments for the fluid inside a cylindrical tank under horizontal translation of the tank base. Jacobsen and Ayre (1951) also studied the effect of ground motions on cylindrical storage tanks. In their study, four tanks, from 150 mm to 1200 mm in diameter, were subjected simultaneously to lateral ground motions of simplified type. The data included samples of the wave envelopes, photographic studies of the wave formation, maximum wave heights and the locations of these maxima, and the fluid damping coefficients.

Moreover, Housner (1963) introduced an analytical model that is widely used for circular and rectangular rigid tanks, in his proposal, the hydrodynamic pressures were classified into impulsive and convective components as shown in Figure 2.5. Fluid was also assumed to be incompressible, and the tank walls were assumed to be rigid. It was shown that a part of the liquid moves in long-period sloshing motion, while the rest moves rigidly with the tank wall which is known as the impulsive liquid component. Therefore, the impulsive part experiences the same acceleration as the ground and contributes predominantly to the base shear and overturning moment. Housner's theory was considered as a guideline for most seismic designs involved LCS. However, failures of liquid storage tanks during past earthquakes suggested that Housner's theory may not be as accurate and conservative as expected. It should be noted that, even though much research is performed on the seismic response, yet, many current standards and guides such as ACI 350.3-06 and ACI 371R-08 have adopted Housner's method with some modifications which were the results of subsequent studies by other researchers for seismic design of liquid storage tanks. However, as Housner's method is not capable of accounting for the effect of the tank wall flexibility. Therefore, as an approximate method ACI 350.3-06 accounts for wall flexibility by determining the oscillating water mass components from the rigid tank solution and only using the amplified pseudo acceleration corresponding to the fundamental natural frequency of the system instead of the ground acceleration. This approximation may be inaccurate for liquid depth/tank radius ratio (H/R) greater than one (Veletsos and Kumar 1984).

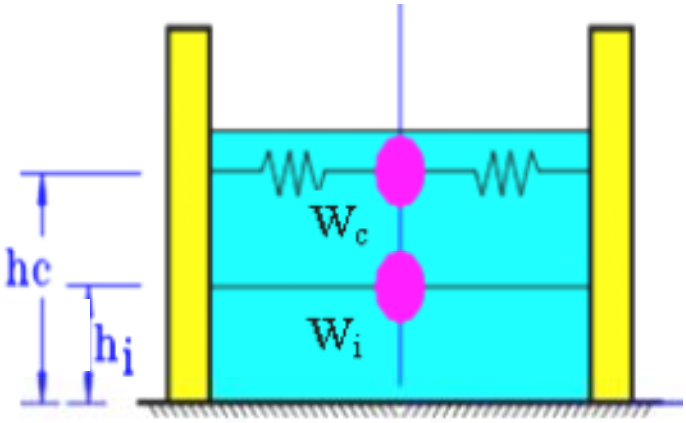

Figure 2.5 – Housner's model

The first finite element method for evaluating the seismic response of flexible tanks was proposed by Edward (1969). The hydrodynamic effects of fluid were taken into account as an added mass matrix in the equation of motion of the coupled fluid-tank system (Ma et al. 1982). Arya et al. (1971) studied the dynamic characteristics of fixed base liquid containers. Virtual mass due to the liquid was considered while sloshing effect was ignored. The first experimental tests of the seismic response of a large scale thin shell LCS were conducted by Clough and Clough (1977), and Clough and Niwa (1979). The experiment results indicated that the hydrodynamic pressures had much larger values than those obtained based on Housner's analytical model. The difference in pressures was considered as a result of the tank wall flexibility. Haroun (1984) presented a detailed analytical method for rectangular tanks where the hydrodynamic pressures were calculated using classical potential flow approach assuming a rigid wall boundary condition. Veletsos and Yang (1974) analyzed the earthquake response of a circular liquid storage tank, assuming the tank as a cantilever beam and considering a deformed shape of the tank system. The tank system including fluid was considered as a single degree of freedom system for the tank lateral displacement at the free surface level. The fluid inertial effect was considered using the added mass approach in which part of fluid mass is added to the structural mass of the tank; thus, only the impulsive component was included in their study. Yang (1976) found that for circular tanks with realistic flexibility, the impulsive forces are considerably higher than those in a rigid wall. Epstein (1976) used Housner's model to produce design curves for calculating the overturning moment due to hydrodynamic pressures in both rectangular and cylindrical storage tanks. Clough (1977) tested different specimens of broad cylindrical tanks on a shaking table at the University of California, Berkeley. The results showed that the circumferential and axial wave modes of the shell theory were strongly excited by seismic loads. Niwa (1978) conducted experimental tests on a scaled model of a ground-supported, thin-shell, cylindrical liquid storage tank to assess the applicability of current seismic design practice to such liquid storage tanks. Hunt and Priestley (1978) studied the dynamic behavior of inviscid fluid contained in horizontally accelerated circular and rectangular tanks and developed mathematical equations describing the fluid motion. Comparisons of predicted and measured free-surface displacements of a model circular tank subjected to both sinusoidal and seismic accelerations on a shaking table showed an agreement between theoretical and

experimental results. The solutions for seismic accelerations in one horizontal direction were then generalized to include acceleration components in all three coordinate directions.

Balendra (1979) presented a finite element analysis of an annular cylindrical tank with an axisymmetric elastic dome. The fluid inside the tank was considered as inviscid and incompressible, where the fluid sloshing was neglected. Clough et al. (1979) conducted experimental studies on the seismic response of ground-supported, thin shell, cylindrical liquid storage tanks using the shaking table at University of California at Berkeley. Several models fabricated from sheet aluminum were subjected to simulated ground acceleration record that was scaled to 0.5g. Shih and Babcock (1980) conducted experimental evaluation of tank buckling under the effects of ground motion and confirmed the important role of the fundamental mode in tank failures. Haroun and Housner (1981) showed that the flexibility of the tank wall may cause the impulsive liquid to experience accelerations that are several times greater than the peak ground acceleration. They also conducted vibration tests on full-scaled liquid storage tanks (Housner and Haroun 1979). Manos and Clough (1982) compared the static and dynamic lateral load responses of a ground-supported circular liquid storage tank model. A rigid and a flexible foundation were studied. It was found that the rotational uplift mechanism was accentuated by the static excitation as compared with that produced by the dynamic input, particularly for the soft foundation material. Veletsos (1984) considered the effect of the wall flexibility on the magnitude and distribution of the hydrodynamic pressures and associated tank forces in circular tanks. It was assumed that the tank-fluid system behaved like a single degree of freedom system, and the base shear and moment were evaluated for several prescribed modes of vibration.

Haroun (1984) evaluated the dynamic response of rectangular concrete liquid storage tanks using the classical potential flow approach assuming a rigid wall boundary condition. The fluid was assumed to be homogeneous, incompressible and inviscid. The tank was assumed to be subjected to the simultaneous action of horizontal and vertical components of earthquake. Bending moments developed in the walls of rectangular liquid-filled tanks due to seismic excitation at their base were calculated. As a result of this study, theoretical equations to evaluate the internal moments in the tank wall were derived, and numerical values of moment coefficients to be used in seismic design of rectangular tanks were tabulated. Haroun and Tayel (1985) employed the

finite element technique for investigating the dynamic behavior of cylindrical liquid storage tanks having elastic wall and being subjected to vertical seismic excitations. The proposed method was based on the superposition analysis technique using the axisymmetrical free vibration modes of the tank-liquid system. The axial and radial components of the wall displacement together with the resulting stresses were calculated. In obtaining the dynamic response of the tanks, effect of liquid sloshing was ignored.

The changes in the impulsive response in tanks, supported on flexible foundations through rigid base mats, were studied by Veletsos and Tang (1990). They concluded that the base translation and rocking resulted in longer impulsive periods and larger effective damping. Park et al. (1992) studied the dynamic behavior of concrete rectangular tanks considering both impulsive and convective components and using boundary element modeling for the fluid motion and finite element modeling for the solid walls. The time-history analysis method was used to obtain the dynamic response of liquid storage tanks subjected to earthquakes.

Kim et al. (1996) studied the dynamic behavior of a 3-D flexible rectangular fluid filled isotropic container using Rayleigh-Ritz method ignoring the effects of sloshing and considering only the walls perpendicular to the direction of the ground motion. Koh et al. (1998) presented a coupled boundary element method-finite element method to analyze three-dimensional rectangular storage tanks subjected to horizontal ground excitation. The tank was modeled using the finite element method and the fluid domain using the indirect boundary element method. Chen and Kianoush (2005) developed a procedure called the sequential method for computing hydrodynamic pressures in two-dimensional rectangular tanks in which the effect of flexibility of the tank wall was taken into account. The dynamic behavior of rectangular containers under vertical seismic excitations was also investigated later by Kianoush and Chen (2006) in a two-dimensional space. It was concluded that the vertical ground excitation could cause significant seismic response in rectangular concrete tanks and therefore, such effect should be considered in the design. Another approach for seismic analysis of rectangular liquid storage tanks in the time domain taking into account the effects of both impulsive and convective components was introduced by Kianoush et al. (2006). The method was able to solve the coupled liquid-filled tank problem in three-dimensional space.

Virella et al. (2006) studied the fundamental impulsive modes of vibration of cylindrical tank-liquid systems anchored to the foundation under horizontal motion. The analyses were performed using a general purpose finite element (FE) program, and the influence of the hydrostatic pressure and the self-weight on the natural periods and modes was considered. The roof and walls are represented with shell elements, and the liquid was modeled using two techniques: the added mass formulation and acoustic finite elements. In this study, the effect of the geometry on the fundamental modes for the tank-liquid systems was investigated using eigenvalue and harmonic response analyses. The results of this study indicated that similar fundamental periods and mode shapes were found from these two approaches. Also, the results from the added mass formulation and acoustic finite elements techniques were found to be very similar.

Masoudi et al. (2006) investigated the failure mechanism and seismic response of elevated concrete tanks with shaft and frame staging (supporting system). The study was performed in order to verify the current code-based seismic design methodology. A computer model was developed to determine the Response Modification Factors (R) of the shaft and frame staging elevated tanks. Linear and nonlinear time-history analyses were performed on the model for nine different earthquake records. Masoudi also studied the effects of multi component earthquakes, fluid-structure interaction and P-Δ on the inelastic behavior of tanks. The results of this study indicated that, a large length of staging may enter inelastic range and multi plastic hinges may be formed, which has a significant influence on the ductility demands during an earthquake. Therefore, they concluded that, using just one hinge at the bottom of the staging and considering hinges only on the lower levels of the frame supporting system is not a reliable method for estimating the ductility demands. They also concluded that, fluid-structure interaction can lead to a strong or weak performance of the structure in the inelastic range depending on the frequency content of the earthquake acceleration. Because there are significant differences between the results of the linear and nonlinear analyses in the interacting and non-interacting models, they suggested considering the effect of fluid- structure interaction in the analysis and design. It was also found that, the P-Δ effect can be very significant in the nonlinear analysis of elevated tanks. The calculated R factor for the elevated tank in this research was less than three.

Sadjadi (2009) aimed to evaluate evaluation of the leakage behavior of ground supported open top rectangular RC tanks under the effect of cyclic loading. Full-scale specimens representing a cantilever wall were designed and constructed to simulate the leakage through the most critical region of the tank wall. A steel water pressure chamber was installed at the wall foundation connection to simulate the effect of the water pressure for the induced cracks at the critical location of the tank wall. Cyclic loading was applied on the top of the wall while the critical region of the wall was subjected to pressurized water. Different variables such as the thickness of the wall and the configuration of the shear key were investigated. In order to assess the viability of the application of the FE analysis to the investigation of the cyclic behavior of the RC rectangular tanks, analytical studies using FE software were also performed. It was found that, FE analysis results correlated well with the experimental observations. The effect of R factor on the design loads was also included in this study. The ductility and overstrength factors were investigated and determined for the case of rectangular reinforced concrete LCS considering the leakage as the limit state. This study was limited to rectangular tanks in which the wall dimensions promote a one-way behavior. In this study, it was found that the cracking at both faces of the wall is necessary for leakage to occur. Furthermore, it was concluded that, it may be appropriate to assume that leakage occurs soon after the yielding of the reinforcement. It was also indicated that, under cyclic loading the crack opening may start as the load is increased. However, when the load direction is reversed and the part of section containing the crack experience compressive stress/strain, the crack closes and the compression block is able to prevent the leakage. In this study, the response modification factor was considered as a product of overstrength and ductility components. The overstrength component was calculated as 1.29, and the ductility component was assumed as unity. Accordingly, the response modification factor for the impulsive component, Ri, was calculated to be equal to 1.7 for wall heights of 3, 4, and 5 m, and equal to 2 for wall heights of 6 through 10 m.

Ghaemmaghami et al. (2010) investigated the seismic response of concrete rectangular and cylindrical liquid containing tanks in three-dimensional space. The tank supports were assumed to be rigid. Both impulsive and sloshing seismic force components were included in the analyses. The tank models were analyzed in the time domain under the horizontal and vertical components of a real earthquake record. Fluid-structure interaction effects were taken into account

incorporating wall flexibility. The study indicated that the effect of vertical excitation on the seismic response of the liquid tanks could be significant when considered separately; however, it was not as significant when the horizontal earthquake component was included, simultaneously, with the vertical component.

Moslemi (2011) evaluated, using finite element method, the seismic response of concrete ground-supported cylindrical and liquid-filled elevated tanks supported on concrete shaft. He examined the effects of liquid sloshing, tank wall flexibility, vertical ground acceleration, tank aspect ratio, base fixity, and earthquake frequency content on the dynamic behavior of the tanks. The adequacy of current practice in seismic analysis and design of LCS was also investigated. Moslemi proposed two different strategies to reduce the seismic response of elevated tanks. In the first strategy, the inclined cone angle of the lower portion of the vessel increased, while in the second strategy the supporting shaft structure is isolated either from the ground, or the vessel mounted on top. It was found that, the effects of the tank wall flexibility, vertical ground acceleration, base fixity, and earthquake frequency content have a significant effect on the dynamic behavior of LCS. This study showed that increasing the cone angle of the vessel can result in a significant reduction in seismically induced forces of the tank. This study, also, concluded that the application of passive control devices to conical elevated tanks offers a substantial benefit for the earthquake-resistant design of such structures.

2.5 Response Modification Factor

Response modification factors were first proposed by the Applied Technology Council (ATC) in the ATC-3-06 report published in 1978. The National Earthquake Hazards Reduction Program (NEHRP) provisions, first published in 1985, are based on the seismic design set forth in ATC-9-06. Similar factors, modified to reflect the allowable stress design approach, were adopted in Uniform Building Code (UBC) in 1988 (ATC-19 1995).

Some studies have been performed to determine appropriate values for response modification factor (R) of concrete shaft and frame staging (supporting system) elevated concrete tanks (Masoudi 2006), which behave in a ductile manner and fail in flexural mode instead of shear mode. Other studies have been performed in order to investigate R values for ground-supported

rectangular tanks (Sadjadi 2009). However, the upright circular tanks (the most general type of liquid-containing structures) that are supported by a rigid foundation with the same shape of the tank cross-section have not been examined until now.

Response modification factor, R, essentially represents the ratio of the forces that would develop under the specified ground motion if the structure had an entirely linearly elastic response to the prescribed design forces. The structure is to be designed so that the level of significant yield exceeds the prescribed design force.

The factor R is expressed by the Equation 2-3, where V_E and V_S are the elastic and the design base shear, respectively. As shown in Figure 2.6, the system ductility reduction factor (R_d) is defined as the ratio between elastic base shear (V_E) and fully yielded strength (V_y) as shown in Equation 2-4 (Newmark and Hall, 1982). Then it is clear that the response modification factor, R, is the product of the ductility reduction factor (R_d) and structural overstrength factor (Ω_0) as shown in Equation 2-5.

$$R = V_E/V_S \tag{2-3}$$

$$R_d = V_E/V_y \tag{2-4}$$

$$R = R_d\,\Omega_0 \tag{2-5}$$

As shown in Figure 2.7, the structural overstrength factor (Ω_0) consists of three components (BSSC 2003) namely the design overstrength, material overstrength, and system overstrength. The design overstrength (Ω_D) is the difference between the lateral base shear force at which the first significant yield of the structure will occur and the minimum specified force given by minimum elastic seismic force. To some extent, this is system dependent. This portion of the overstrength coefficient could be as low as 1.0 for optimum design.

The material overstrength (Ω_M) results from the fact that the design values used to proportion the elements of a structure are specified by the provisions to be conservative lower bound estimates

of the actual probable strengths of the structural materials and their effective strengths in the as-constructed condition. Code requirements for reinforced concrete have historically used a factor of 1.25 to account for the ratio of mean to specified strength and effects of some strain hardening. Considering a typical strength reduction factor (Ø) of 0.9, this would indicate that the material overstrength for systems constructed of these materials would be on the order of 1.25/0.9, or 1.4 (FEMA 450, 2003).

The system overstrength (Ω_S) is the ratio of the ultimate lateral force the structure is capable of resisting to the actual force at which first significant yield occurs. For structures with no redundancy, the system overstrength factor would be 1.0.

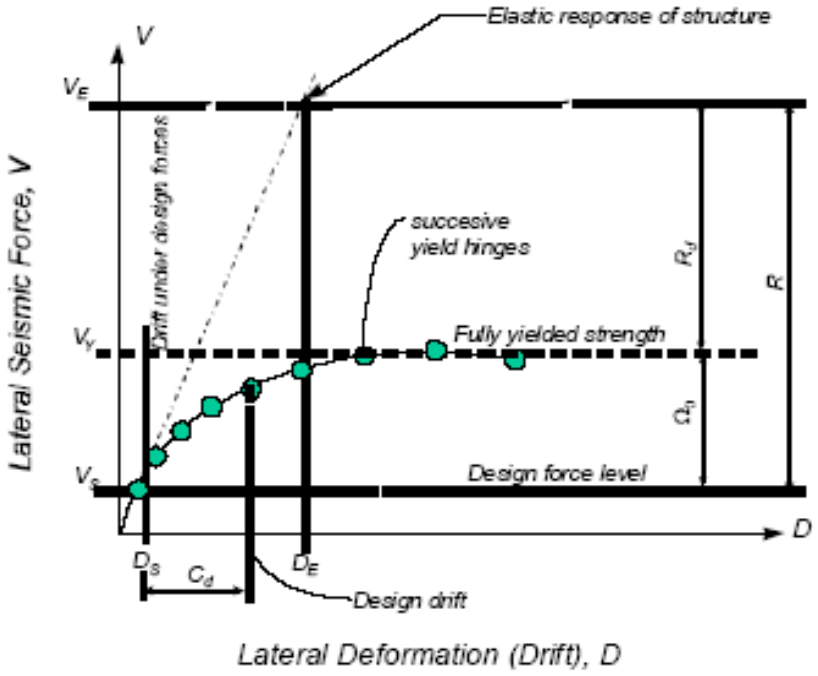

Figure 2.6 – Inelastic force-deformation curve (FEMA 450, 2003)

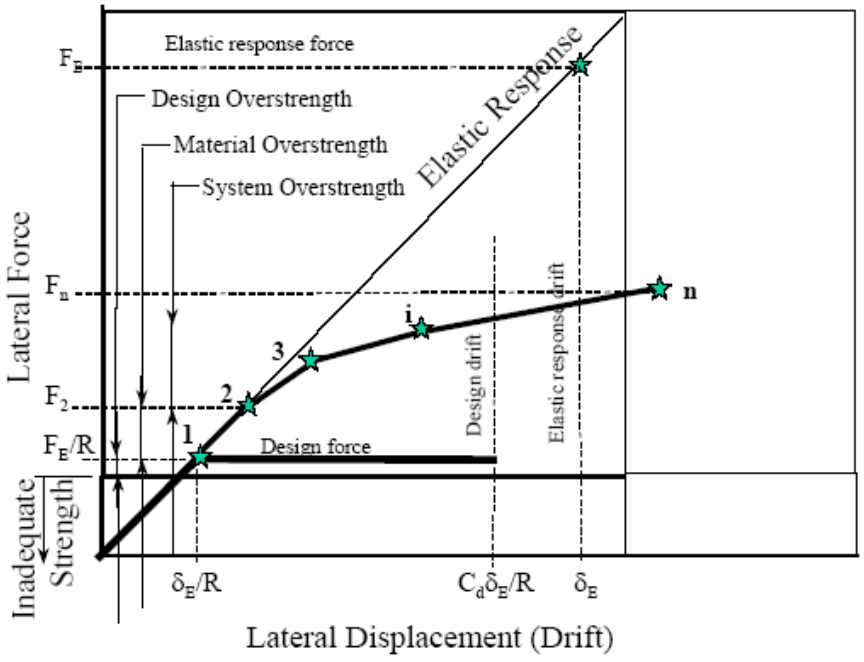

Figure 2.7 – Factors affecting overstrength (FEMA 450, 2003)

Further research ((ATC-19 1995) and Freeman 1990)) has been completed since the first formulation for response modification factor (R) was proposed. Equation 2-6 shows a formulation expresses R as product of three factors; strength factor, ductility factor, and redundancy factor.

$$R = R_s R_\mu R_R \tag{2-6}$$

Overstrength factor (R_s) as shown in Equation 2-7 is the ratio between the base shear at maximum displacement, which is the displacement corresponding to the limiting state response (V_0), and the design base shear (V_d).

$$R_s = V_0/V_d \tag{2-7}$$

Ductility factor (R_μ) depends on the ductility ratios (μ). The ductility ratio is normally expressed in terms of the displacement ductility ratio. The displacement ductility ratio (μ) is defined as the

ratio between the drift capacity and the yield drift, where the drift capacity is, the smaller of the maximum drift specified by code and the system ultimate displacement.

The relationship between displacement ductility and ductility factor using approaches developed by (Krawinkler and Nasser 1992), and (Miranda and Bertero 1994) have been used in this study.

Krawinkler and Nasser (1992), referred to as (K and N), developed a R_μ-μ-T relationship as shown in Equations 2-8 and 2-9 of singe degree of freedom (SDOF) systems on rock or stiff soil sites considering the effect of the natural period of the structure (T) on R_μ. They used the results of statistical study based on 15 western United States ground motion records from earthquakes ranging in magnitude from 5.7 to 7.7. They assumed damping equal to 5 percent of critical, their equation is:

$$R_\mu = [c(\mu - 1) + 1]^{1/c} \quad (2\text{-}8)$$

$$c(T, \alpha) = \frac{T^a}{1 + T^a} + \frac{b}{T} \quad (2\text{-}9)$$

Parameters (a) and (b) were obtained from different strain-hardening ratios. For α equal to 0% corresponding to elastic-plastic system (which is used in this study), a and b are equal to 1.00 and 0.42 respectively

Miranda and Bertero (1994), referred to as (M and B), summarized and reworked the R_μ-μ-T relationships developed by many researchers including (Newmark and Hall 1982), and (Krawinkler and Nasser 1992) to develop general R_μ-μ-T equations for rock, alluvium, and soft soil sites. R_μ can be calculated using Equations 2-10, where the parameter Φ is calculated using Equations 2-11, and 2-12 for rock and alluvium sites, respectively. It should be noted that, their equation for rock sites has been used in this study. The Miranda and Betrero equations were developed using 124 ground motions recorded on a wide range of soil conditions, and assumed five percent damped bilinear SDOF systems undergoing displacement ductility ratio (μ) between 2 and 6.

$$R_{\mu}=\frac{(\mu-1)}{\Phi+1}+1 \tag{2-10}$$

$$\Phi = 1+\frac{1}{10T-\mu T}-\frac{1}{2T}e^{-1.5(\ln(T)-0.6)^2} \tag{2-11}$$

$$\Phi = 1+\frac{1}{12T-\mu T}-\frac{2}{5T}e^{-2(\ln(T)-0.2)^2} \tag{2-12}$$

A comparison of the Krawinkler and Nasser and Miranda and Bertero the R_{μ}-μ-T relationships for rock and alluvium sites (ATC-19 1995) is shown in Figure 2.8. As shown in this figure, the differences between these two relationships are relatively small; thus, it can be ignored for engineering purposes.

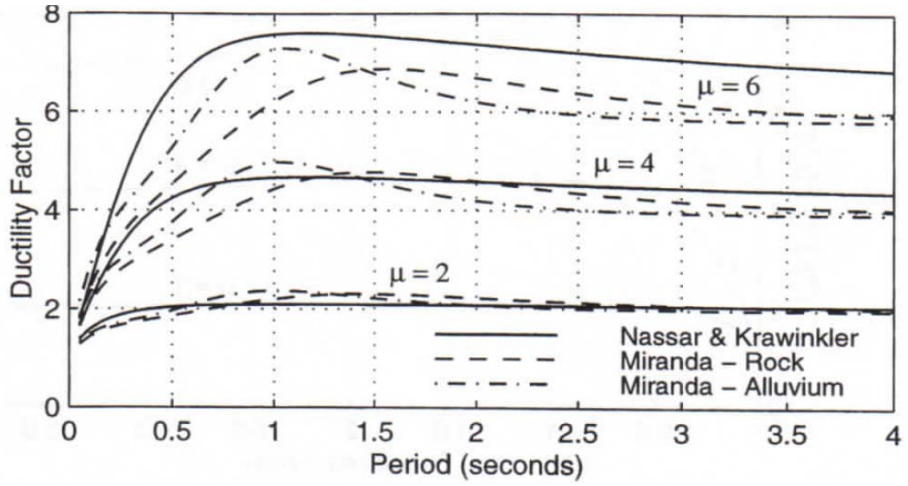

Figure 2.8 – Ductility factor comparison (ATC-19 1995)

Furthermore, a redundant seismic framing system should be composed of multiple resisting elements. For tanks, only the tank wall will resist the lateral pressure of hydrostatic and hydrodynamic forces. Therefore, the redundancy factor (R_R) will be considered equal to one. In addition, damping is the general term often used to characterize energy dissipation in structural element, irrespective of whether the energy is dissipated by hysteretic behavior or viscous damping. Based on uniform building code (UBC 1994) the damping factor corresponding to five percent viscous damping (of critical damping) is one.

For the design of LCS, response into nonlinear range should be limited in order to control concrete cracking. As a result, R in LCS is mainly attributed to overstrength and not so much to ductility. For LCS, the response modification factors for impulsive component (R_i) reduce the elastic response in order to account for the structure's ductility, energy-dissipating properties, and redundancy (ACI 350.3-06 2006). However, R for LCS is assigned lower values in design codes in comparison with building structures to reduce cracking.

It should be noted that, for LCS the values of the natural period of the first convective mode of sloshing (T_c) are located in high period range, typically more than four seconds. In this period range, no reduction in seismic force occurs. As a result, R_c is assigned a value of one in the current practice. Also, in ACI 350.3-06 (2006), R_i is assigned different values based on the type of LCS. In this study, only anchored flexible base and nonflexible base (fixed and hinged) tanks are investigated. In the current practice, R_i is assigned a higher value for anchored flexible base tanks. This is based on the assumption that flexible tanks are free to move at the base, and therefore, can dissipate more energy than non-flexible base tanks. In this study, the validity of this assumption is investigated. The values of R_c and R_i according to ACI 350.3-06 (2006) are presented in Table 2.1.

Table 2.1 - Response modification factor R (ACI 350.3-06 2006)

Type of structure	**R_i**		**R_c**
	On or above grade	**Buried***	
(a) Anchored, flexible-base tanks	3.25	3.25	1.0
(b) Fixed or hinged-base tanks	2.0	3.0	1.0
(c) Unanchored, contained, or uncontained tanks	1.5	2.0	1.0
(d) Pedestal-mounted tanks	2.0	----	1.0
* Buried tank is defined as a tank whose maximum water surface at rest is at or below ground level. For partially buried tanks, the R_i value may be linearly interpolated between that shown for tanks on grade, and for buried tanks			

2.6 Cracking of concrete

Considering that the concrete is relatively weak and brittle in tension, cracks will be developed when the concrete members are subjected to significant tensile stresses. Reinforcement and prestressing steel can be used to resist the tensile stresses and to reduce the concrete cracking. A report by ACI Committee 224 (ACI 224.2R-92 2004) covers cracking of concrete members in direct tensions, where a separate report (ACI 224R-01 2008) covers control of cracking in concrete members in general with only brief reference to tension cracking. Therefore, ACI 224.2R-92 (2004) was used to calculate concrete cracks in this study since the main forces affecting the circular tank design are the hoop forces

According to ACI224.2R-92 (2004), as a result of the formation of cracks in member that is under direct tension, a new stress pattern develops between the cracks. The formation of additional primary cracks continues as the stress increases until the average crack spacing is approximately twice the cover thickness as measured to the center of reinforcing bars. The expected value of the maximum crack spacing is about twice that of the average crack spacing (Broms and Lutz 1965).

Based on ACI224.2R-92 (2004), the maximum crack width may be estimated by multiplying the maximum crack spacing (4 times concrete cover) at high steel stress by the average strain in the reinforcement. When tensile members with more than one reinforcing bar are considered, the actual concrete cover is not the most appropriate variable for calculating the maximum crack width. Instead, an effective concrete cover (t_e) is used, where t_e is defined as a function of the reinforcement spacing and the concrete cover measured to the center of the reinforcement. According to Broms and Lutz (1965), the t_e in mm can be calculated from Equation 2-13, where the maximum tensile crack width (w_{max}) can be calculated from Equation 2.14 as follows:

$$t_e = \sqrt{1 + \left(\frac{s}{4\, d_c}\right)^2} \qquad (2\text{-}13)$$

$$w_{max} = 4\, \varepsilon_s\, t_e \qquad (2\text{-}14)$$

By substituting t_e from Equation 2.13 in Equation 2-14, w_{max} (mm) for tensile cracking can be calculated from Equation 2-15:

$$w_{max} = 0.10\, f_s \sqrt[3]{d_c\, A}\, x10^{-3}\, x\, 0.145 \qquad (2\text{-}15)$$

where,

d_c = distance from the center of bar to extreme tension fiber (mm)

s = bar spacing (mm)

A = area of concrete symmetric width reinforcing steel divided by number of bars (mm^2)

f_s = the reinforcement stress (MPa)

ε_s = the reinforcement strain

The cracking behavior of reinforced concrete members in axial tension is similar to that of flexural members, except that the maximum crack width is larger than that predicted by expressions for flexural members. The reason for the large crack width in members under direct tension is probably the resultant restraint imposed by the compression zone of flexural members (ACI 224R-01 2008).

For flexural members, there is a large variability in the maximum crack width. The maximum flexural crack width can be calculated using Equation 2-16 (ACI 224.2R-92 2004) and (ACI 224R-01 2008):

$$w_{max} = 0.076\beta\, f_s \sqrt[3]{d_c\, A}\, x10^{-3}\, x0.145 \qquad (2\text{-}16)$$

In which β is the ratio of distance between neutral axis and tension face to distance between neutral axis and centroid of reinforcing steel, $\beta \approx 1.2$. Accordingly, the coefficient 0.076β in

Equation 2.16 becomes 0.091, therefore, for the same section and steel stress, the maximum tensile crack width is about 10% wider than the maximum flexural crack (ACI 224.2R-92 2004).

Further studies were carried out in order estimate the cracking in LCS (Kianoush et al. 2006), in which the crack widths were calculated based on Froschs' approach (1999). This study was based on 200 bar spacing and 50 mm concrete cover. Accordingly, the crack width (w_c) for flexural cracking was calculated using Equation 2-17 as follows:

$$w_c = 112\ \Psi_s\ \varepsilon_s \qquad (2\text{-}17)$$

where,

ε_s is strain in reinforcement

w_c is the crack width

(Ψ_s) is the crack spacing factor

Crack spacing factor (Ψ_s) of 1.0 was recommended when this equation is used in combination with finite element analysis (Kianoush et al. 2008). Also, it was recorded that the crack spacing factor (Ψ_s) of 1.0 is appropriate for liquid-containing structures where increased amounts of reinforcement are used, resulting in relatively small cracks.

By using ε_s = yield strain(ε_y) = 0.002

w_c = 112x1.0x0.002 = 0.224 mm < 0.25mm which is the crack width limit for normal environmental exposure (ACI 350-06 2006). Accordingly, the tank response at yield is considered to be appropriate regarding leakage.

However, Froschs' approach (Frosch, 1999) can be reliable for flexural cracking (vertical bars), yet, for the horizontal bars that are under direct tension, this approach may not be appropriate. A report by ACI 224R-01 (2008) limits the allowable crack width to 0.1 mm in water-retaining

structures. Furthermore, due to the fact that the earthquake load is a transit load, the self-healing phenomenon of concrete by means of water permeability will help to seal the crakes. Studies on concrete specimens under direct tension (Edvardsen 1999) indicated that cracks with initial effective width of 0.2 mm can be completely sealed after seven weeks of water exposure. Another study by Ziari and Kianoush (2009a) on concrete leakage and cracking under direct tension concluded that tension cracks as wide as 0.25 mm, which is the crack limit for normal environmental exposure according to ACI350-06 (2006), can partially remediate itself through the self-healing process when it is exposed to flow of water, and width of crack is kept constant under steady tensile load. In this study, the effective concrete cover (t_e) and the maximum tensile crack width (w_{max}) are calculated according (ACI 224.2R-92 2004).

The main reason for crack control is to minimize the crack widths. In the past, tolerable crack widths have been related to exposure conditions (ACI 224R-01 2008). However, at least in terms of protecting reinforcement from corrosion, the effect of surface crack width appears to be relatively less significant than believed previously (ACI 224.2R-92 2004). For severe exposures, it is preferable to provide a greater thickness of concrete cover even though this will lead to wider surface cracks. The serviceability requirements for liquid-containing structures (ACI 350R 2006) may require narrower crack widths such as 0.2 mm. Furthermore, since crack width is related to tensile stress in reinforcement, cracks attributed to transit load such as seismic force, which is only applied for short periods, may not be as serious as cracks due to sustained load, while the cracks due to live load may be expected to close or at least decrease in width upon removal of such transit load.

2.7 Characteristics of concrete model

In this section, the characteristics of concrete model in FE analysis are presented in order choose the appropriate FE model for concrete including the nonlinear properties. A study was performed by Ziaolhagh (2008) in order to investigate the appropriate nonlinear FE model of concrete. A wall with length/height ratio of one with a wall height (H) of 1.0 m was analyzed using smeared cracking and brittle cracking model. The behavior of concrete was investigated under concrete shrinkage. The reinforcement ratio of the wall was chosen to be 0.5% in both horizontal and

vertical directions. In their analysis, the concrete wall was modeled using quadratic 50 mm x 50 mm shell elements with 4 integration points and reinforcement was modeled as a steel layer embedded in the mid thickness of the shell elements.

It was found that, the analysis of the wall modeled using smeared cracking model aborted at nearly 60% of shrinkage strain and the program was unable to complete the analysis because of diverging from the solution. However, in the analysis, the program completed the analysis of the wall modeled with brittle cracking model and the total amount of shrinkage strain was applied to the wall.

According to the material properties used in that study, the cracking failure stress of concrete (f_t) was 2.7 MPa. The tensile stress of concrete modeled with smeared cracking model exceeded the failure stress. However, the maximum tensile stress of concrete modeled with brittle cracking model was slightly less than the failure stress. In addition, after concrete cracks, the tensile stress of concrete declines to zero at approximately 95% of shrinkage strain and remains zero to the end of analysis which is in compliance with the tension stiffening defined for concrete.

Also, as indicated by Ziaolhagh (2008), the smeared cracking model for concrete in ABAQUS applies Von Mises failure criterion to detect cracking in concrete. However, Von Mises failure criterion is most applicable to ductile materials. In this criterion, plastic yield initiates when the Von Mises stress reaches the initial yield stress in uniaxial tension. Then, the Von Mises stress is used to predict failure by ductile tearing. The failure of concrete in tension is dominated by crack propagation, which depends on the maximum principal stress and Von Mises failure criterion, is not appropriate in such type of failure. While the brittle cracking model for concrete in ABAQUS applies the maximum principal stress to detect crack initiation. This model is considered functional in the restrained shrinkage problems as the concrete compressive stresses are expected to remain low and within the elastic range of material behavior.

As a result, Ziaolhagh (2008) concluded based on the comparison between the behavior of concrete modeled with smeared cracking and brittle cracking that, the brittle cracking model

simulates more accurately the behavior of reinforced concrete walls subjected to restrained shrinkage.

2.8 Passive energy dissipation systems

Damping is one of many different methods that have been proposed for allowing a structure to achieve optimal performance when it is subjected to seismic, wind storm, blast or other types of transient shock and vibration disturbances. Conventional methods would resist or dissipate the effects of such forces by means of strength, flexibility, and deformability. The level of damping in a conventional elastic structure is very low, and hence the amount of energy dissipated during transient disturbances is also very low. During strong motions, such as earthquakes, conventional structures usually deform well beyond their elastic limits and eventually fail or collapse. Therefore, most of the energy dissipated is absorbed by the structure itself through localized damage as it fails. The concept of supplemental dampers added to a structure assumes that much of the energy input to the structure from a transient load will be absorbed, not by the structure itself, but rather by supplemental damping elements.

The energy dissipation and seismic isolation systems are used to enhance the performance of structures by reducing damaging deformations in structural and nonstructural components, as well as, reducing acceleration response to minimize related damage. The seismic damage can be reduced by providing an alternate source of energy dissipation systems which can be achieved by utilizing a supplemental (or added) damping system.

The change in damping and frequency with accumulated damage was experimentally investigated as part of 1981/1982 US-JAPAN project (Charney and Bertero 1982). The test was performed on 1/5-scale concrete building model tested at UC Berkeley. It was found that the increase in the mass of the model resulted in a reduction in both the natural frequency, and damping ratio. Moreover, the natural frequencies and damping ratios were measured using free vibration tests performed subsequent to seismic loading tests. With peak ground acceleration near zero, the natural frequency and damping ratio corresponds to elastic response. As the seismic load increased, the concrete frame was damaged, and the dynamic properties changed. The natural frequency decreased due to a loss in lateral stiffness while the effective damping

ratio increased due to accumulated damage in the form of concrete cracking and loss of bond to reinforcement.

As a result of the previous studies, also, in order to avoid damages due to earthquakes, an alternate source of energy dissipation, such as fluid viscous dampers, should be provided.

The passive energy dissipation systems for seismic applications have been under development for a number of years with a rapid increase in implementations starting in the mid-1990s. The principal function of a passive energy dissipation system is to reduce the inelastic energy dissipation demand on the framing system of a structure (Constantinou and Symans 1993b; Whittaker et al. 1993). The passive energy dissipation systems can be classified as follows:

- Velocity-dependent systems such as fluid viscous or viscoelastic solid dampers. The velocity-dependent systems consist of dampers with force output depends on the rate of change of the displacement (velocity). The fluid viscous dampers (FVD) are the most commonly used system for energy dissipation. They are exclusively velocity-dependent; therefore, they do not add additional stiffness to a structure. The viscoelastic solid dampers exhibit both velocity and displacement-dependence.
- Displacement-Dependent Systems such as metallic yielding or friction dampers. These systems always add stiffness to structure. The displacement-dependent systems consist of dampers with force output depends on the displacement, not the rate of change of the displacement. Moreover, the force output of displacement-dependent dampers generally depends on both the displacement and the sign of the velocity.
- Other systems such as re-centering devices (shape-memory alloys, etc.) and vibration absorbers (tuned mass dampers), these systems are available but not commonly used.

As shown in Figure 2.9, a fluid viscous damper (FVD) consists of a hollow cylinder filled with a fluid. As the damper piston rod and piston head are stroked, fluid is forced to flow through orifices either around or through the piston head. The fluid flows at high velocities, resulting in the development of friction and thus heat. The heat is dissipated harmlessly to the environment. Interestingly, although the damper is called a viscous fluid damper, the fluid typically has a

relatively low viscosity. The term viscous fluid damper comes from the macroscopic behavior of the damper which is essentially the same as an ideal viscous dashpot (i.e., the force output is directly related to the velocity).

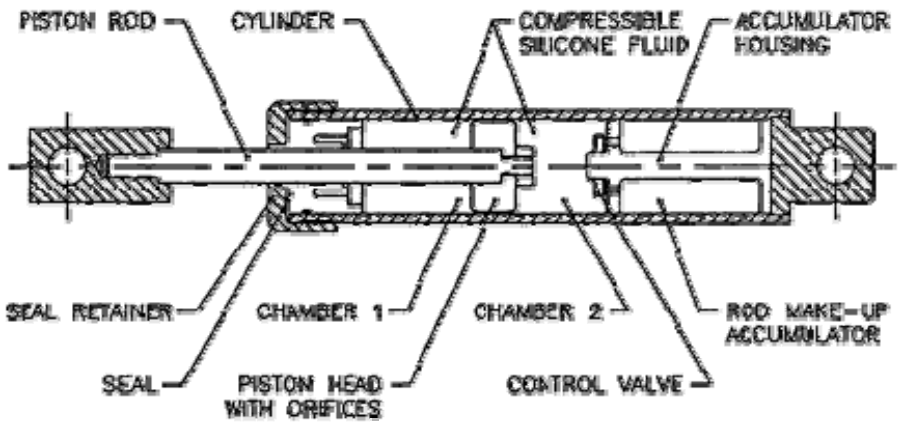

Figure 2.9 – Typical cross section of fluid viscous damper

Constantinou and Symans (1992) investigated the dependence of damping coefficient on temperature for a typical fluid damper. A 8.9 kN (2 Kips) capacity "single-ended" damper was tested, it was found that due to a special design of the orifices within the piston head that allows for temperature compensation, the damping coefficient has a relatively minor dependence on the ambient temperature. However, the temperature-dependence is much stronger for viscoelastic solid dampers.

Another study by Symans and Constantinou (1998) was also performed to investigate the effect of temperature on damping constant (C). Figure 2.10 shows the peak force for each test plotted against the imposed peak velocity. In this figure, the experimental results were fitted with slope equal to C. It was found that for room temperature (24^o C) and above, the behavior was essentially linear, however, as the temperature drops, the experimental results deviated from linearity at lower velocities. The experimental results indicated also, that the damper exhibited a stable behavior under a wide range of temperatures. It was also found for temperatures between 0^o C and 50^o C the damping constant was reduced by a factor less than two. They also indicated that, by assuming the dampers are anchored at a temperature about 24^o C, variation of

temperature of range 0° C and 50° C will result in variations of a damping ratio of 44% to 25%. That if a design calls for a damping ratio of 20%, this will alter the damping ratio in the range of 15% to 29%. Therefore, it was concluded the temperature change has a small effect on the results over wide range temperatures. The effect of temperature on damper behavior is excluded from this study.

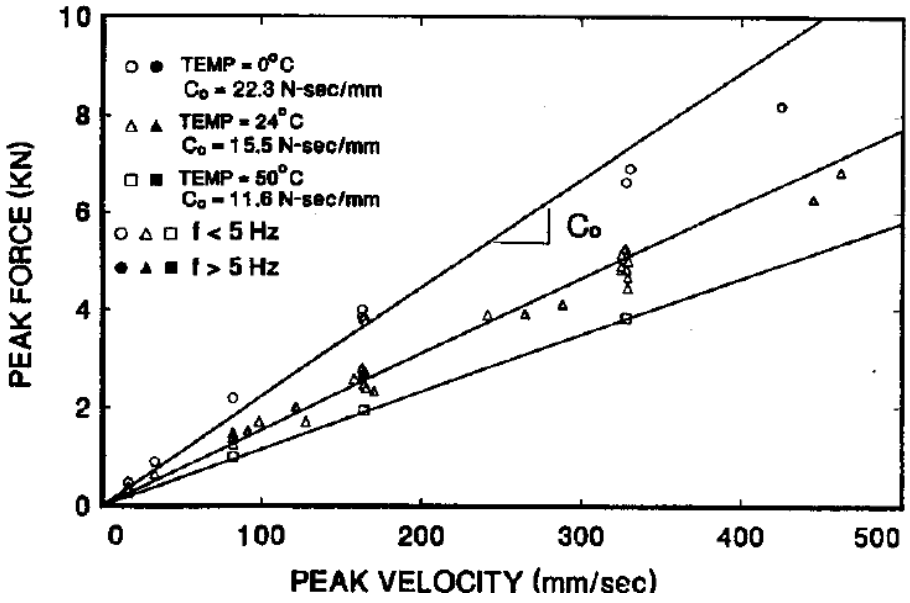

Figure 2.10 – Recorded values of peak force versus peak velocity for a range of ambient temperature levels (Symans and Constantinou 1998)

Generally, a simple dashpot can be used to model dampers that exhibit viscosity and little or no elasticity. This model employs a Newtonian dashpot in which the force is proportional to the velocity. The proportionality constant is the damping coefficient. In a viscous damping model, the output of the damper is calculated using Equation 2.18 as follows:

$$F_{damper} = CV^{\alpha} \tag{2-18}$$

where,

C = damping constant

V = velocity

α = velocity exponent

Generally for viscose dampers the velocity exponent should be: $0.3 \leq \alpha \leq 1.0$. It should be noted that, once performance requirements have been satisfied using linear damping ($\alpha = 1.0$), further refinement can be evaluated with lower velocity exponents. The effect of the damping velocity exponent has been investigated by (Hwang 2005) where linear and nonlinear dampers have been examined. It should be noted that dampers with α greater than one have not been seen in the practical applications.

The damper with α equal to one is called a linear viscous damper, where damper with α smaller than one is called nonlinear viscous damper which are effective for minimizing the high velocity shocks. Figure 2.11 shows the efficiency of the nonlinear damper in minimizing the high velocity shocks. However, for the purpose of this study, only first iteration for linear dampers with α equal to one is considered in the analysis, considering that, the tank behavior may be further improved by using nonlinear dampers.

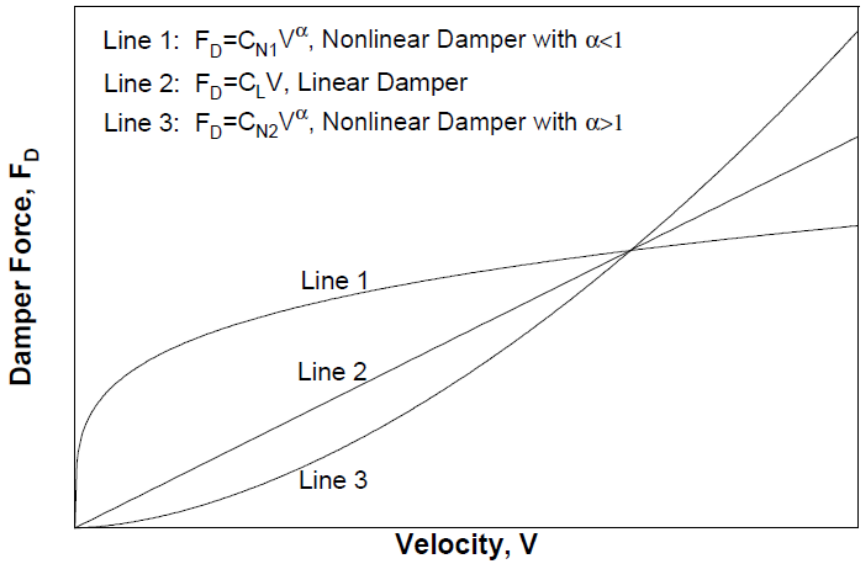

Figure 2.11– Force-velocity relationship of viscous dampers (Hwang 2005)

As indicated before the FVD is the most commonly used system for energy dissipation. However, there are advantages and disadvantages of using such systems, which can be summarized as follows:

Advantages:

- High reliability
- High force and displacement capacity
- Force limited when velocity exponent < 1.0
- Available through several manufacturers
- No added stiffness at lower frequencies
- Damping force (possibly) out of phase with structure elastic forces
- Moderate temperature dependency
- May be able to use linear analysis

Disadvantages:

- Additional cost may be added, however, cost saving due to reduction in design seismic force may have more effect on the total project cost in some cases
- Not force limited (particularly when exponent = 1.0)
- Necessity for nonlinear analysis in most practical cases (as it has been shown that it is generally not possible to add enough damping to eliminate all inelastic response)

Today, hundreds of major structures such as high rise buildings and bridges are using fluid viscous dampers as a primary design element to enhance the structure response. Damper sizes being used range from as little as 5 tonnes force to more than 900 tonnes force, with deflections as low as 5 mm and as high as 1.5 meters. Therefore, the use of supplemental fluid viscous dampers can be one of the main solutions for seismic resisting systems.

Recently, damping systems have been specified for application to buildings with a wide variety of structural configurations. The growth in application of damping systems in buildings has been steady to the extent that there are now numerous applications (Soong and Spencer 2002). Given

that, two examples are provided below for relatively recent applications to buildings for seismic protection (Symans et al. 2008):

- Hotel Stockton, Stockton, Calif.: This historic 13,470 m2, six-story nonductile reinforced concrete structure was built in 1910 and renovated in 2004. The renovation included a seismic retrofit wherein a combination of 16 nonlinear viscous fluid dampers and four viscoelastic fluid dampers were employed within diagonal bracing at the first story level to mitigate a weak soft story and a torsional irregularity.
- Torre Mayor Tower, Mexico City, Mexico: Construction of this 57-story steel and reinforced concrete office hotel tower with 77,000 m2 of column-free office space was completed in 2003. The tower is currently the tallest building in Latin America. The superstructure consists of a rectangular tower with a curved facade, the tower consisting of steel framing encased in concrete for approximately the lower half of the building and primarily steel framing for the upper half. The final design employs nonlinear fluid viscous dampers located in the trussed core (72 dampers with 2,670-kN capacity) and along the two faces of the building (24 dampers with 5,340-kN capacity).

In this study, a velocity-dependent system is introduced for flexible base tanks in order to dissipate the seismic force; and therefore, improve the response under the effect of earthquakes.

2.9 Applicable codes and standards for LCS

A brief overview of the available codes and standards for seismic design of LCS is presented in this section. This overview concentrates mainly on the codes and standards that are used in North America. The International Building Code, IBC (2011) provides a comprehensive and detailed method for seismic force calculation for LCS; however, this code is mostly used in United State of America (USA). The ASCE -10 (2010) standard is referred to for seismic design of common liquid storage tanks. In ASCE 7-10, the ground motion is defined as a response spectrum corresponding to the Maximum Considered Earthquake (MCE) for earthquake with a 2% probability of exceedance in a 50-year period (equivalent to a recurrence interval of approximately 2500 years).

Currently, there are no direct guidelines for structural design of environmental structures in Canadian design codes and standards. Yet, many other codes and standards are available such as ACI 350.3-06 (2006), New Zealand Standard NZS 3106 (2010), European Eurocode-8 (2006), and British Standard BS 8007 (1987). However, ACI 350.3-06 is the most comprehensive and widely used standard for seismic design of LCS.

Current revision of the Code (ACI 350.3-06 2006) is based on the ultimate strength design method, where an equivalent mechanical model based on the Housner's method (Housner 1963) has been implemented; thus, the resultant seismic forces calculated.

Furthermore, two standards intended for the design of prestressed concrete liquid storage tanks were published by the American Water Work Association (AWWA); AWWA D110 (1995), and AWWA D115 (1995). The guidelines regarding the design of welded steel liquid storage containers were provided in AWWA D100 (2005). In addition, for circular tanks where prestressing is used, guidelines for design and construction of circular wire-and strand-wrapped prestressed-concrete structure ACI 372R-00 (2000), and guidelines for design and construction of circular prestressed concrete structures with circumferential tendons ACI 373R-97 (1997) can be used.

The American Petroleum Institute (API) published two standards; API 650 (1998), and API 620 (1998) for the design of tanks used in the petroleum industry.

American Society of Civil Engineers (ASCE) provided two publications including useful guidelines regarding the seismic design of storage tanks used in the nuclear industry; ASCE 4-98 (1998), and ASCE 58 (1980). Tanks used in the nuclear industry should meet more stringent design requirements compared to those used in other industries because of the potential hazard of radioactive materials to public safety.

Most of the standards including ACI 350.3-06, AWWA D100, AWWA DUO, and API 650 have implemented the Housner's mathematical model (Housner 1963) with some modifications for determining the seismic forces associated with the accelerated contained liquid. In NZS 3106

(2010), the model proposed by Veletsos and Yang (1977) is used for seismic analysis of rigid tanks while the model developed by Haroun and Housner (1981) is used for deformable liquid storage tanks. In Eurocode-8 (2006), the dynamic analysis of rigid circular tanks is performed using Veletsos and Yang's model (1977). Models developed by Veletsos and Kumar (1984) and Haroun and Housner (1981) together with the approach proposed by Malhotra et al. (2000) are used for dynamic analysis of flexible circular tanks.

Guidelines for the implementation of energy dissipation or damping devices in new buildings were first proposed by the Structural Engineers Association of Northern California (SEAONC) to provide guidance to structural engineers, building officials, and regulators who were tasked with implementing such devices in building frames (Whittaker et al. 1993). These guidelines were prepared in response to the increased interest shown in damping devices following widespread damage to building frames in the 1989 Loma Prieta earthquake in Northern California and the emergence of vendors of damping hardware (Symans et al. 2008). In the mid 1990s, the Federal Emergency Management Agency (FEMA) funded the development of guidelines for the seismic rehabilitation of buildings (Kircher 1999). Four new methods of seismic analysis and evaluation were presented in the National Earthquake Hazards Reduction Program (NEHRP) Guidelines for the Seismic Rehabilitation of Buildings; FEMA Reports 273 and 274 (ATC 1997a, b): linear static procedure, linear dynamic procedure, nonlinear static procedure, and nonlinear dynamic procedure. All four methods were displacement based, and all directly or indirectly made use of displacement-related information for component checking.

With regard to structures incorporating passive energy dissipation devices, the basic principles to be followed included: spatial distribution of dampers at each story and on each side of building, redundancy of dampers (at least two dampers along the same line of action), for maximum considered earthquake, dampers and their connections to be designed to avoid failure i.e., not the weak link in the system, and members that transmit damper forces to foundation designed to remain elastic (Symans et al. 2008).

The 2003 NEHRP Recommended Provisions were reformatted and included in the 2005 edition of the ASCE/SIE 7-05 Standard entitled “Minimum design loads for buildings and other

structures" (ASCE 2005). The earthquake load provisions in the ASCE/SEI 7-05 standard are substantially adopted by reference in the 2006 International Code Council (ICC 2006) and the Building Construction and Safety Code (NFPA 2006).

CHAPTER 3
EFFECT OF TANK PARAMETERS ON SEISMIC RESPONSE

3.1 General

This chapter provides an overview of the aspects of ground shaking response for circular tanks, and presents information and concepts in which the critical hydrodynamic effects for such systems may affect the design of these structures. The study presented in this chapter is limited to the response of above ground tanks that are anchored at the base.

This chapter presents a brief overview of the basic concepts involved in the seismic analysis of liquid-containing structures (LCS) along with an outline of the basic theory that underlines the computation of earthquake-induced forces. This chapter also discusses the specific elastic deign response spectrum adopted by ACI 350.3 (2001 and 2006). The correlation between the classical equations and the lateral seismic force equations contained in ACI 350.3 (2001 and 2006) is presented. Also, the effect of vertical and horizontal distribution of hydrodynamic forces on the wall of circular tanks is discussed.

The effect of various parameters on the response of LCS is presented. With the aid of several design parameters, the behavior of LCS in terms of impulsive and convective forces, base shear and bending moment ratios and other design parameters is investigated. It should be noted that, for the purpose of comparison and for the sake of better understanding of the tank Behavior, the study presented in this chapter is performed in accordance with ACI 350.3-01 (2001). In this case, the response of the tank is presented and compared for different seismic zones. However, the detailed seismic force calculations in accordance with ACI 350.3-06 (2006) are included in Appendices A.1 and A.2.

Furthermore, the study presented in this chapter investigates the accuracy of using axi-symmetric elements to model circular tanks. For this reason, the results of linear FE analysis of tank model using axi-symmetric are compared with the results of the same tank model using shell elements.

3.2 Tank behavior under seismic loads

The most general liquid-containing system examined is the upright rectangular or circular tanks that are supported through a rigid foundation with the same shape of the tank cross-section. The study presented in this chapter is based on concrete LCS filled with homogeneous liquid that is incompressible and inviscid. The tank walls are considered to be of constant thickness and connected to its base so that no sliding or uplift may occur.

Most of the design codes such as ACI 350.3 (2006) code assume an equivalent static model for calculating the resultant seismic forces acting on the ground-based fluid container with rigid walls. In this model as indicated in Figure 3.1, the equivalent mass of the impulsive component of the stored liquid W_i represents the resultant effect of the impulsive seismic pressure on the tank walls. The equivalent mass of the convective component of the stored liquid, W_c represents the resultant of the sloshing fluid pressures. In the model, it is assumed that W_i acts rigidly with the tank walls at an equivalent height h_i above the tank bottom that corresponds to the location of the resultant impulsive force P_i. The impulsive pressure are generated by the seismic accelerations of the tank walls so that the force P_i is evenly divided into a pressure on the wall accelerating into the fluid, and a suction on the wall accelerating away from the fluid. During an earthquake, the force P_i changes direction several times per seconds, corresponding to the change in the direction of the base acceleration. W_c is the equivalent mass of the oscillating fluid that produces the convective pressures on the tank walls with resultant force P_c, which acts at an equivalent height of h_c above the tank bottom. In the model, it is assumed that W_c is flexibly connected to the tank walls that produce a period of vibration corresponding to the period of fluid sloshing. The sloshing pressures on the tank walls result from the fluid motion associated with the wave oscillation. The period of oscillation of sloshing depends upon the ratio of fluid depth to tank diameter and is usually several seconds. The forces P_i and P_c exert overturning moments at the base of the tank wall.

The forces P_i and P_c act independently and simultaneously on the tank. The force P_i (and its associated pressures) primarily acts to stress the tank wall, whereas P_c acts primarily to uplift the tank wall. The vertical vibrations of the ground are also transmitted to fluid, thus producing

pressures that act on the tank walls. They act to increase or decrease the hoop stresses in the case of the circular tanks.

The pressure and the forces on a cylindrical tank are similar to, but not the same as, those acting on a rectangular tank. The rapid fluctuation of the force P_i means that the bending moments and the stresses in the tank wall also vary rapidly. It is worth noting that the damping of sloshing water is small, approximately 0.5 % to 1% of the critical damping.

The sloshing increases or decreases the fluid pressure on the wall. Normally, this effect is smaller than the impulsive effect, but if there is not sufficient dead load, the tank will tend to uplift.

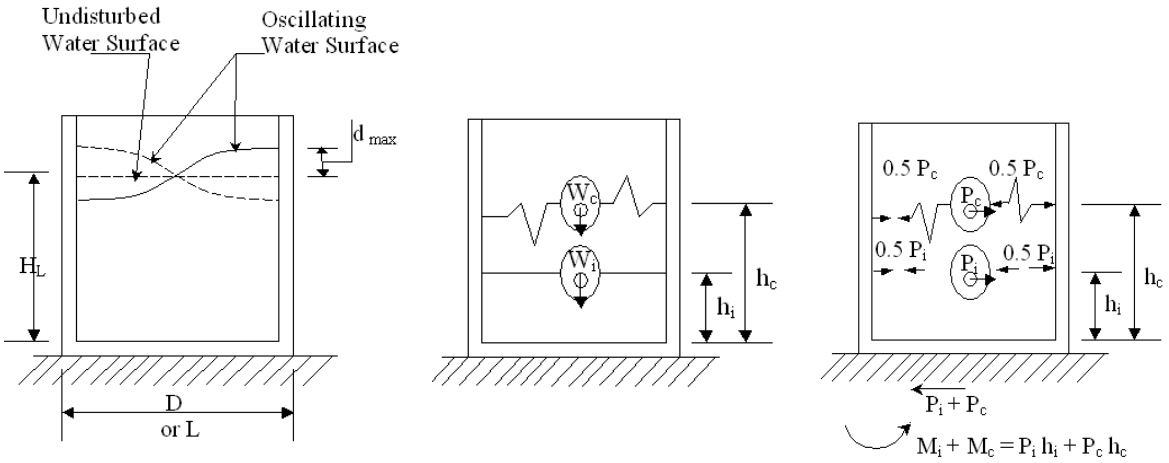

(a) (b) (c)

Figure 3.1– Liquid-containing tank rigidly supported on the ground; (a) Fluid motion in tank, (b) Dynamic model, (c) Dynamic equilibrium of horizontal forces

3.3 ACI 350.3 design requirements and code background

According to ACI 350.3 (2001 and 2006) the walls, floors, and the roof of liquid-containing structures should be designed to withstand the effect of both the design horizontal acceleration

and the design vertical acceleration combined with the effect of the applicable static loads. With regards to the horizontal acceleration, the design could take into account the effects of the transfer of the forces between the wall and the footing, and between the wall and the roof, and the dynamic pressure acting on the wall above the base.

The effects of maximum horizontal and vertical acceleration should be combined by the square root of the sum of the squares (SRSS) method. The walls of LCS should be designed for the following dynamic forces in addition to the static pressures (ACI 350.3-01 2001):

Lateral inertia force of the accelerating wall,

$$P_w = ZSIC_i \varepsilon W_w/R_{wi} \quad (3\text{-}1)$$

Lateral inertia force of the accelerating roof,

$$P_r = ZSIC_i \varepsilon W_r/R_{wi} \quad (3\text{-}2)$$

Hydrodynamic impulsive pressure from the contained liquid,

$$P_i = ZSIC_i W_i/R_{wi} \quad (3\text{-}3)$$

Hydrodynamic convective pressure from the contained liquid,

$$P_C = ZSIC_c W_c/R_{wc} \quad (3\text{-}4)$$

As indicated before, the tank shall be also designed for the effects of vertical acceleration. In the absence of a site-specific response spectrum, the ratio of the vertical to the horizontal acceleration shall not be less than 2/3. The hydrostatic load q_{hy} from the tank contents, at level y above the base, shall be multiplied by the spectral acceleration $Ü_v$ to account for the effect of the vertical acceleration. The resultant hydrodynamic pressure P_{vy} shall be computed as follows:

The effect of the vertical acceleration,

$$P_{vy} = \ddot{U}_v q_{hy} \qquad (3\text{-}5)$$

The general equation for total shear normally encountered in the earthquake-design, in building codes, is modified in Equations 3-1 to 3-4 by replacing the term W with four effective masses: The effective mass of the tank wall - εW_w, the effective mass of the tank roof - εW_r, the impulsive component of the liquid mass W_i, and the impulsive component of the liquid mass Wc.

The effective mass coefficient ε represents the ratio of the equivalent dynamic mass of the tank shell to its actual total mass. Because the impulsive and the convective component are not in phase with each other, normal practice is to combine them using SRSS method.

Also, the general equation for base shear is modified by the soil profile coefficient S. The imposed ground motion is represented by an elastic response spectrum that is either derived from an actual earthquake record for the site, or is constructed by analogy to sites with known soil and seismic characteristics. The product ZC defines the profile of the response spectrum. Factor Z represents the maximum effective peak ground acceleration for the site, while C is a period-dependent spectral-amplification factor. In Equations 3-1 to 3-4, the factor C is represented by C_i and C_c, corresponding to the response of the impulsive and convective components, respectively. The factor I represents the importance factor and provides a means for the engineer to increase the factor of safety for some categories of structures.

The response modification factors R_{wc} and R_{wi} reduce the elastic response spectrum S to account for the structure's ductility, energy-dissipating properties, and redundancy. The term $ZISC/R_w$ represents the resulting inelastic response spectrum.

As indicated in Equation 3-5, the tank should be designed for the effects of vertical acceleration. In the absence of a site-specific response spectrum, the ratio of the vertical to the horizontal acceleration should not be less than 2/3.

Where site-specific elastic response spectra are used, the force calculated based on the Equations 3-1 to 3-4 should be modified by substituting A_i, corresponding to T_i, for ZSC_i, and A_c, corresponding to T_c, for ZSC_c, and equation 3-5 should be modified by substituting A_v, corresponding to T_v, for ZSC_v. The symbols A_c, A_i, and A_v represent the spectral acceleration, expressed as a fraction of the acceleration due to gravity, g, from site-specific response spectrum. Also, the computed forces shall not be less than 80% of those obtained by using the Equations 3-1 to 3-5. The peak ground acceleration (PGA) corresponding to Seismic Zones 1, 2a, 3 and 4 are 0.075g, 0.15g, 0.3g and 0.4g, respectively, where g is the acceleration due to gravity (9.807 m/s^2).

In ACI 350.3 (2001 and 2006), the vertical distribution, per unit length of wall height, of the dynamic forces acting perpendicular to the plane of the wall are calculated based on a linear force distribution along the wall height.

The detailed calculations of hydrodynamic forces according to ACI 350.3-06 (2006) are included in Appendices A.1 and A.2.

3.4 Effect of tank dimensions on hydrodynamic forces

This study is carried out to investigate the effect of the different parameters on the response of circular tanks based on ACI 350.3 (2001) Code requirements for the purpose of comparison. Three different water heights, H_L, of 3m, 6m and 9m are used. The diameters of the tanks are assumed as 10m and 30m. The thicknesses of the tank walls are assumed to be 400mm.

Figure 3.2 shows the effect of the tank diameter (D) on the hydrodynamic forces for different tank heights. The hydrodynamic forces are divided by the tank height for a better comparison. For the same depth of stored liquid, the effect of the tank diameter on the impulsive force is relatively small in general because by increasing the total mass of the stored liquid W_L, the rate of the ratio between the equivalent mass of the impulsive component to the total mass of the stored liquid W_i/W_L decreases which equalizes the total effect. It should be noted that, for the impulsive force, the tank diameter is more significant for taller tanks as compared to shallower tanks.

At the same time for the same depth of stored liquid, the tank diameter has a major effect on the convective force, because the rate of both the ratio between the equivalent mass of the convective component to the total mass of the stored liquid W_c/W_L and the total mass of the stored liquid W_L increase as diameter D increases.

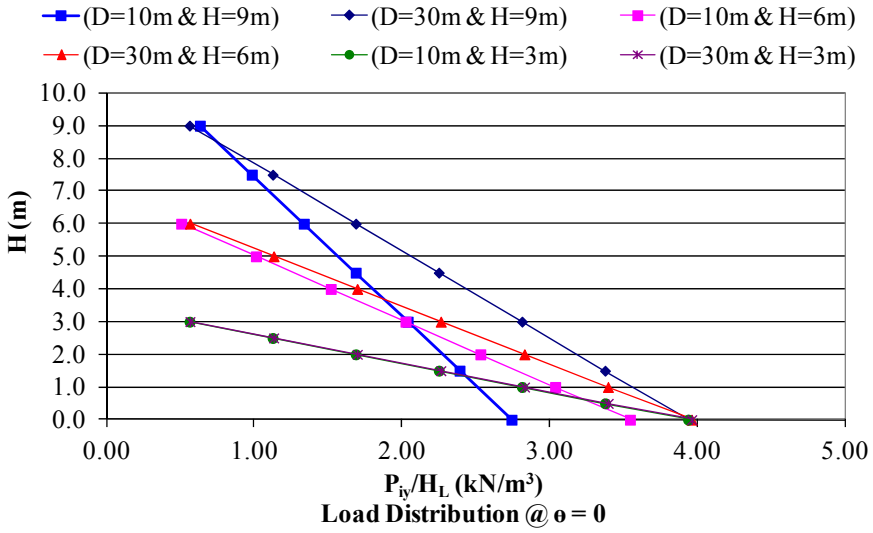

(a)

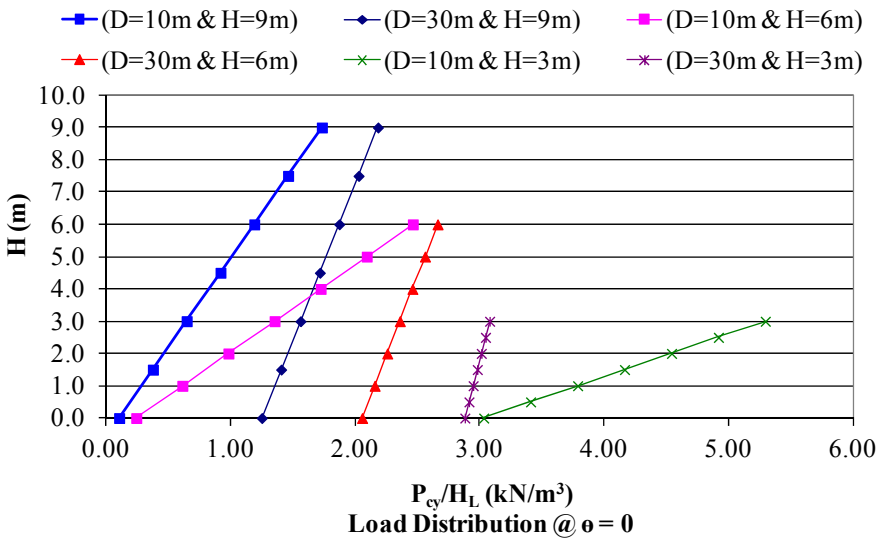

(b)

Figure 3.2 – Effect of circular tank dimensions on hydrodynamic forces, T_w = 400 mm, Zone 4, (a) Impulsive force, (b) Convective force

Figure 3.3 shows the effect of tank height on earthquake/hydrostatic force (V_{EQ}/V_S) and bending moment (M_{EQ}/M_S) ratios for different seismic zones. Figures 3.3 (a) and (b) show that base shear and base moment ratios are linearly proportion to the seismic zone factor. Also, as the tank height increases the ratios decrease proportionally.

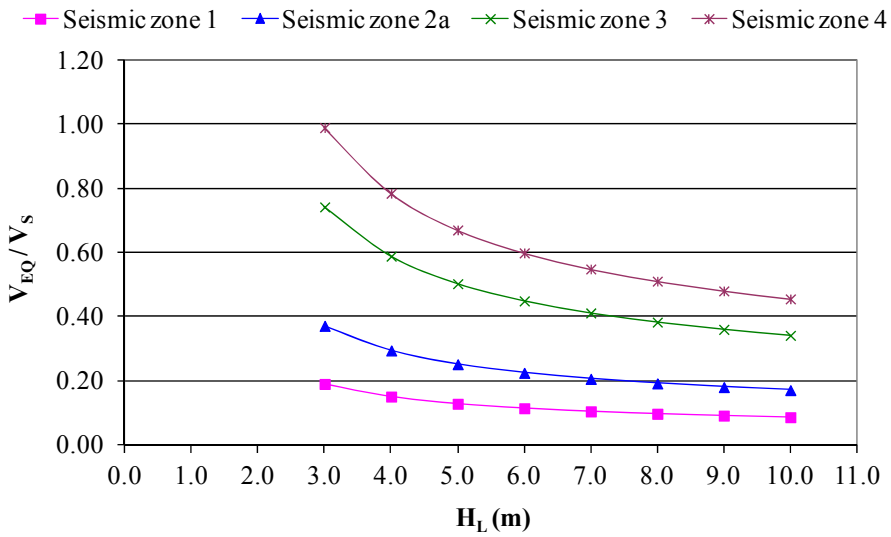

(a)

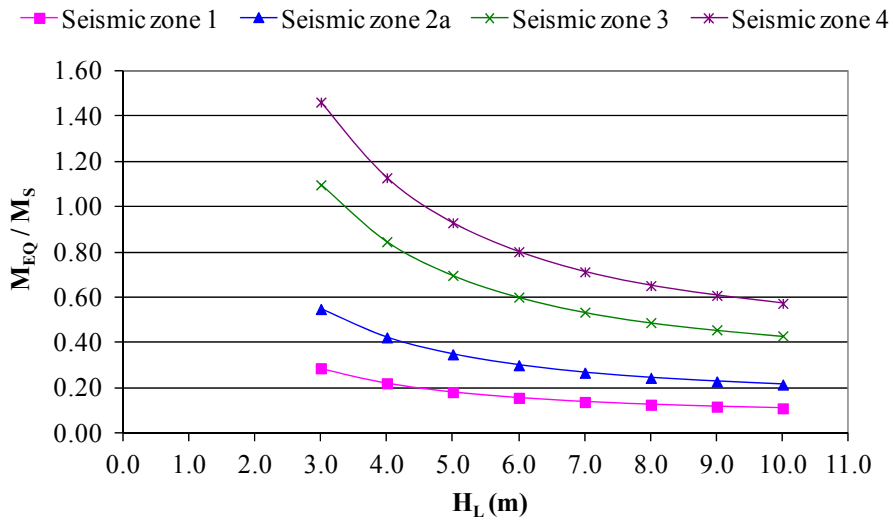

(b)

Figure 3.3 – Effect of circular tank dimensions on Earthquake/Hydrostatic force ratios, D=10m, T_w = 400mm, (a) Base shear, (b) Base moments

Figure 3.4 shows that the freeboard (sloshing height) is directly proportional to the seismic zone factor and to the depth of stored liquid. Also, the freeboard is inversely proportional to the tank diameter.

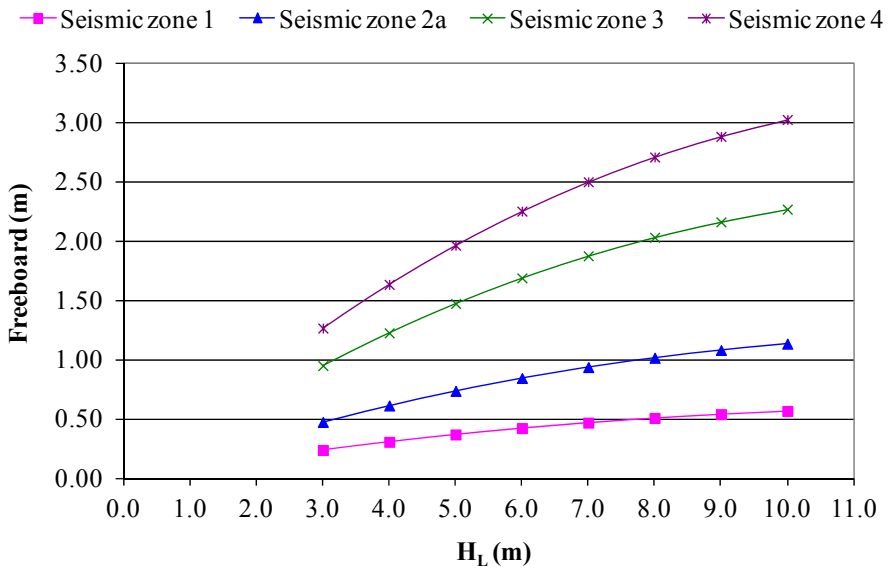

(a)

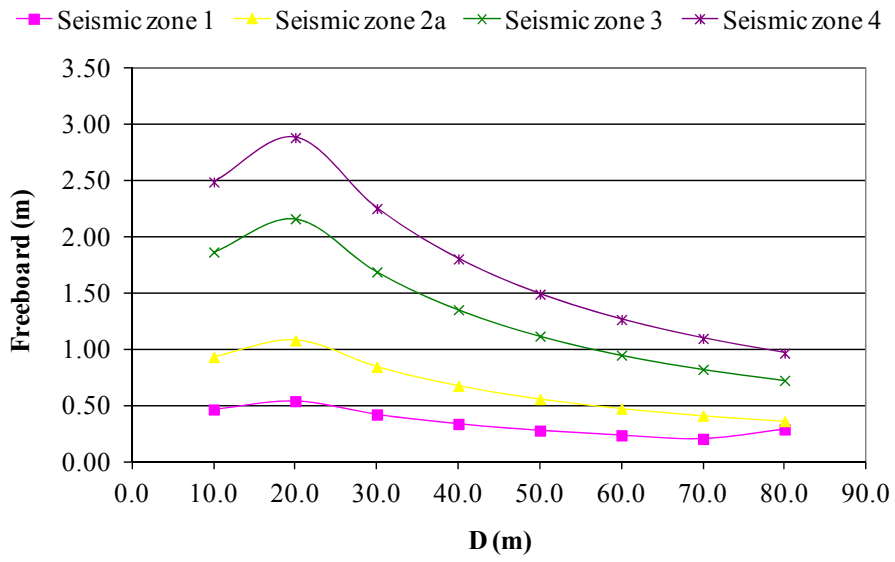

(b)

Figure 3.4 – Effect of circular tank dimensions on sloshing height, (a) Water depth, D=30m T_w = 400 mm (b) Tank diameter, H_L = 6m, T_w = 400 mm

Figure 3.5 shows the effect of the tank diameter on seismic forces. It is clear that all the components of the earthquake forces, as well as the bending moment, are directly proportional to the tank diameter. However, the changing rates of the different components are not the same.

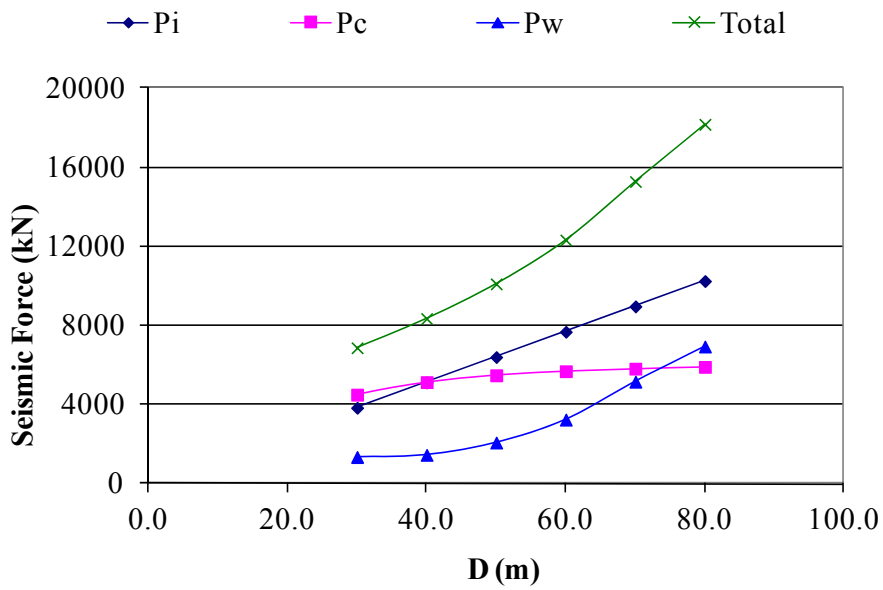

(a)

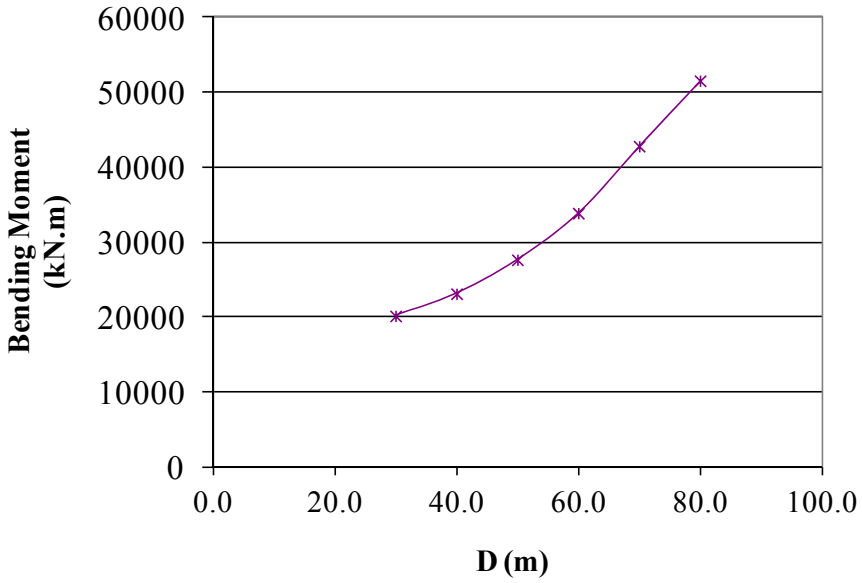

(b)

Figure 3.5 – Effect of circular tank dimensions on seismic forces HL = 6.0m, Zone 4, (a) Hydrodynamic forces, (b) Bending moments

It should be noted that the effect of rectangular tank dimensions on hydrodynamic forces is included in Appendix A.3.

3.5 Finite element implementation

Under actual condition, the distribution of seismic forces on circular tank circumferential is based on cosine distribution as shown in Figure 3.6 (a). This study investigates using axi-symmetric elements in order to perform FE analysis for circular tanks. The use of axi-symmetric elements is much simpler than the corresponding shell elements. However, to use axi-symmetric elements, a cosine distribution of hydrodynamic forces is not possible; and therefore, a uniform pressure distribution around tank circumference should be considered. FE analysis is carried out in order to verify the use of uniform pressure distribution based on the maximum pressure obtained from cosine distribution as shown Figure 3.6 (b). For this reason, FE analysis is performed on entire tank models, using shell elements, under both cosine pressure distribution as well as uniform pressure distribution. In order to verify the results, a comparison of FE results, for the maximum response values, for axi-symmetric model and shell element models (uniform and cosine pressure distributions) is performed.

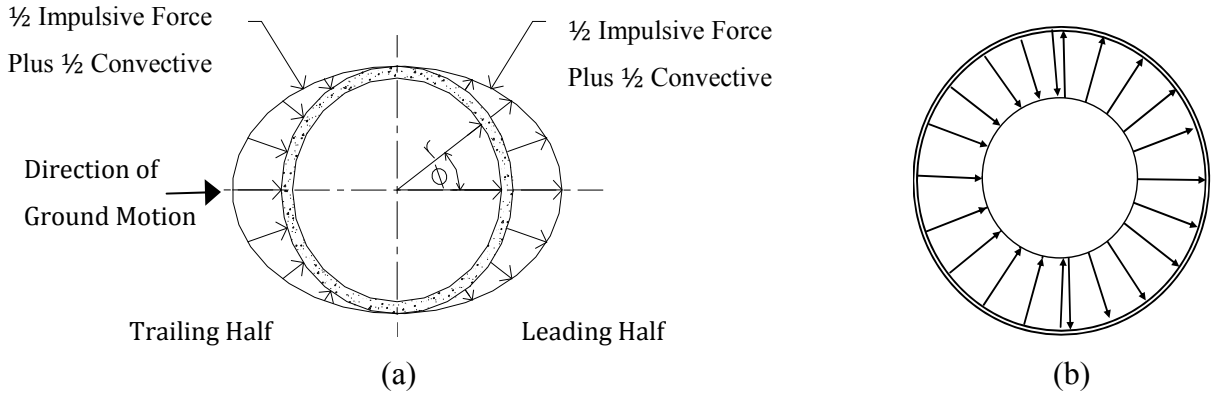

Figure 3.6 – Hydrodynamic pressure distribution in circular tanks; (a) Cosine pressure distribution, (b) Uniform pressure distribution

3.5.1 Tank configuration and design parameters

In this study FE analysis is performed for a 3-D model of ground-supported open top circular tank with a diameter of (D) = 61m, water depth (H_L) = 6.1 m, wall height (H_w) = 7.3 m, and wall thickness of (t_w) =400 mm. Both hinged and fixed base conditions are considered in this study.

The nonlinear behavior of tank material is not considered in this study. For the purpose of analysis and design, the specified compressive strength of concrete (f'_c) and yield strength of reinforcement (f_y) are considered 28 MPa and 400 MPa, respectively. The modulus of elasticity of concrete (E_c) and reinforcement (E_s) are taken as 26000 MPa and 200000 MPa, respectively.

The hydrodynamic forces are calculated based on ACI 350.3-06 (2006) representing a high seismic zone having S_s= 150% and S_1= 60%, where S_s is the mapped maximum considered earthquake 5% damped spectral response acceleration parameter at short periods, expressed as a fraction of acceleration due to gravity g, and S_1 is the mapped maximum considered earthquake 5% damped spectral response acceleration; parameter at a period of 1 second, expressed as a fraction of acceleration due to gravity g.

The vertical distribution of hydrodynamic pressure along the tank wall is considered linear (linear approximation) as adopted by ACI 350.3-06 (2006) as shown in Figure 3.7. The design hydrodynamic and hydrostatic pressures are shown in Figure 3.8. In the Figure, HS refers to hydrostatic pressure.

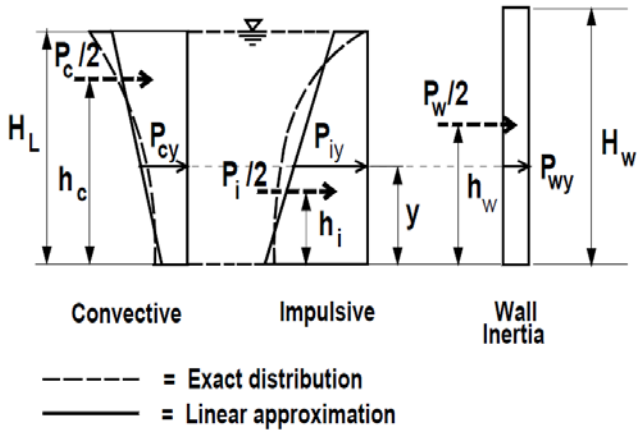

Figure 3.7 – Vertical distribution of hydrodynamic pressure (adapted from Fig R5.3.3 – ACI350.3-06)

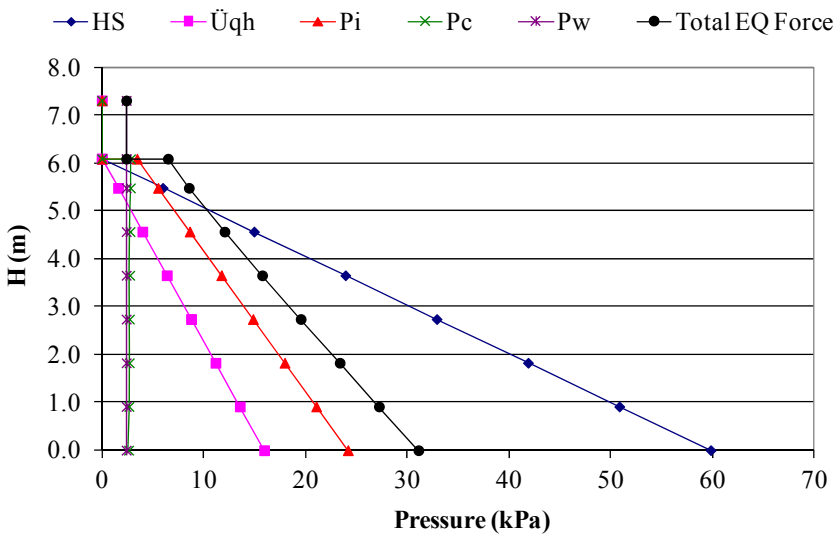

Figure 3.8 – Design hydrodynamic and hydrostatic pressures at (θ) = 0 deg

3.5.2 Computer model and FE analysis

The FE analysis is conducted using ABAQUS/CAE Version 6.8.3. Using the interactive and graphical technique the computer model is created using ABAQUS/CAE. Material properties, loads, and boundary conditions are assigned to the geometry. FE analysis is carried out on the circular tank described in the previous section. The tank is modeled using shell elements and axi-symmetric elements. In this study, static analysis is performed where the nonlinearity of construction materials is not considered. Both impulsive (P_i) and convective (P_c) pressures are included separately in the FE analysis. As discussed before, the impulsive pressure is defined as the pressure generated by the seismic accelerations of the tank walls and the lower portion of liquid inside the tank, where the convective pressure is the sloshing fluid pressure.

Three different FE models are considered in this study as follows:

- Full Tank (FT): The entire tank is modeled using 0.9mx0.9m (total of 1680 elements) four-node quadrilateral shell elements, referred to as “Full Tank - FT” model as shown in Figure 3.9 (a).

- ½ Tank (½ T): Half of the tank is modeled using 0.9mx0.9m (total of 840 elements) four-node quadrilateral shell elements, referred to as "½ Tank - ½ T" model as shown in Figure 3.9 (b). This model is used for model verification only.

- Axi-symmetric (AXI): The entire tank is modeled using axi-symmetric elements (total of 8 elements along the wall height), referred to as "Axi-sym" as shown in Figure 3.9 (c).

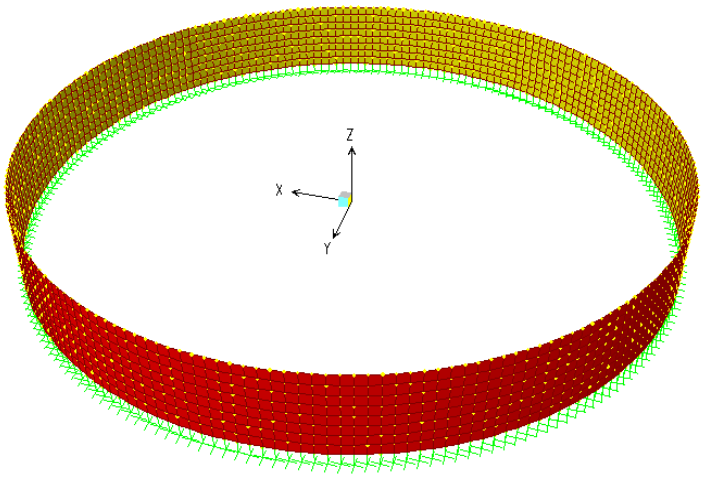

(a)

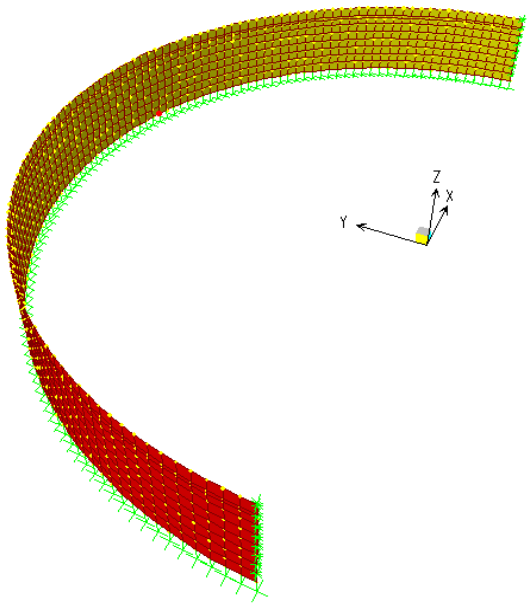

(b)

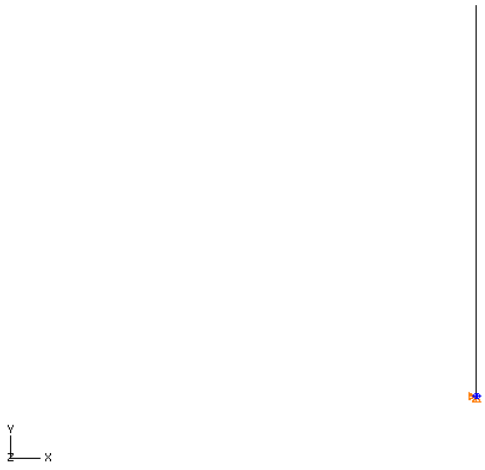

(c)

Figure 3.9 – FE model of circular tank; (a) Full Tank, (b) ½ Tank, (c) Axi- symmetric

In the FE analysis performed in this study, the hydrodynamic pressures are modeled using two methods around tank circumferential. In the first method, the hydrodynamic pressures are modeled using cosine distribution of the seismic load based on ACI350.3-6 (2006) as shown in Figure 3.6 (a), referred to as (Cosine). In the second method, the maximum value of earthquake forces at polar coordinate angle (θ) = 0 deg is applied to the entire tank as shown in Figure 3.6 (b), referred to as uniform distribution load (EQmax). The hydrodynamic pressure is considered linear along the tank wall in the vertical direction according to ACI-350.3-05 (2006) as shown in Figures 3.8 for both cosine (Cosine) and uniform load distribution (EQmax). Both impulsive (P_i) and convective (P_c) pressures are considered independently. For Axi- symmetric model, a cosine force distribution is not possible; therefore, only the uniform pressure distribution is used.

3.5.3 Model verification

In order to verify the FE model that is used in this study, FE analysis is performed for Models 1, 2, and 3 for fixed base condition using two FE computer programs, SAP2000 (CSI 2008) and ABAQUS/CAE (Dassault Systèmes Simulia Corp. 2008). Three different FE models are considered in this verification for fixed base condition (total of six models).

Since the objective of this study is to verify that the tank is modeled correctly using ABAQUS/CAE, this verification is performed under the effect of uniform pressure of 1.4 kPa acting in the positive radial direction.

As shown in Table 3.1, the reaction force in the radial direction (R1) at the tank base are very similar for all models with the maximum difference in results of 1.7 % for AXI model (axisymmetric elements) compared to FT model, which indicates that the tank models using SAP2000 and ABAQUS are compatible.

Table 3.1 – Reaction force in the radial direction at tank base under uniform pressure

R1 (kN/m)		R1 (kN/m)		R1 (kN/m)	
SAP2000 FT	ABAQUS FT	SAP2000 1/2T	ABAQUS 1/2T	SAP2000 AXI	ABAQUS AXI
11.4	11.3	11.4	11.3	11.5	11.4

As shown in Figure 3.10, the radial deflection (U1) at different height of the tank wall are identical for Models 1 and 2, (Full tank and Half Tank), for both of the computer programs (SAP2000 and ABAQUS). Therefore, modeling half of the tank will be more efficient in terms of reducing the number of equations to be solved. The maximum difference of the wall radial deflection between SAP2000 and ABAQUS for Models 1 and 2 is 7.7% at the top of the wall. This difference is inversely proportional with the height. The average of the differences in the results for U1 is about 4%. However, the results of Model 3 “Axi-sym” using ABAQUS and SAP000 are the same.

Figure 3.11 shows the hoop stresses (S11) for Models 1, 2 and 3. The maximum difference of the hoop stresses between SAP2000 and ABAQUS for Models 1 and 2 is 7.7% at the top of the wall with an average difference of 4%. Similarly, for both computer programs, the hoop stresses at different height of the wall are identical for Models 1 and 2 (Full tank and Half Tank).

As shown in Figure 3.12, the bending stresses in the vertical direction (S22) are almost identical for Models 1, 2 and 3 using SAP2000 and ABAQUS, which indicates that using Models 1, 2 or 3

with either program (SAP2000 or ABAQUS) will result in reliable FE results for the parameters under consideration.

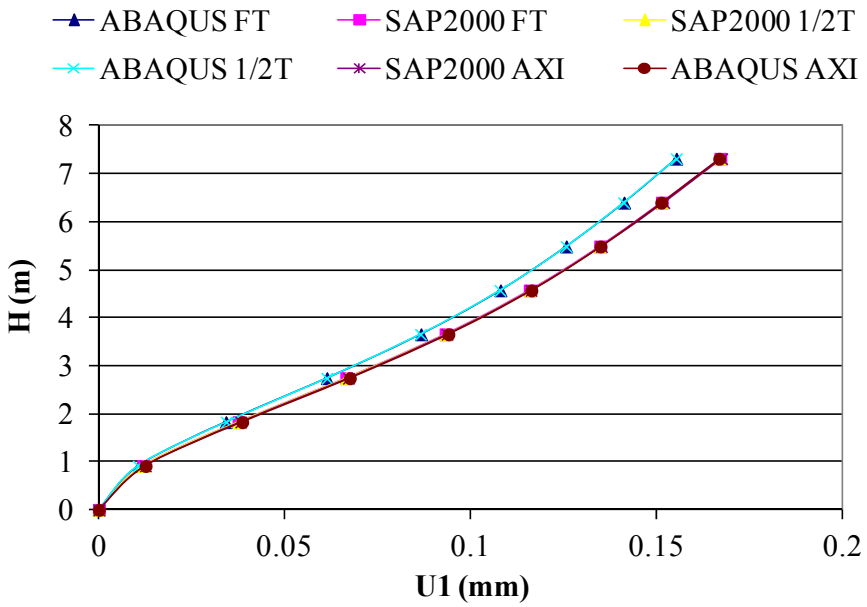

Figure 3.10 – Radial deflection under uniform pressure

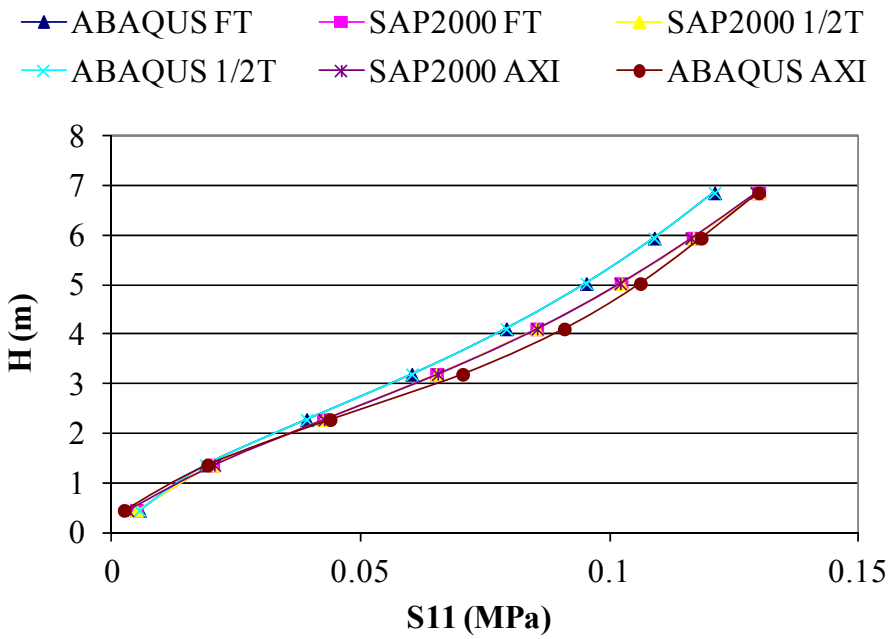

Figure 3.11 – Hoop stress under uniform pressure

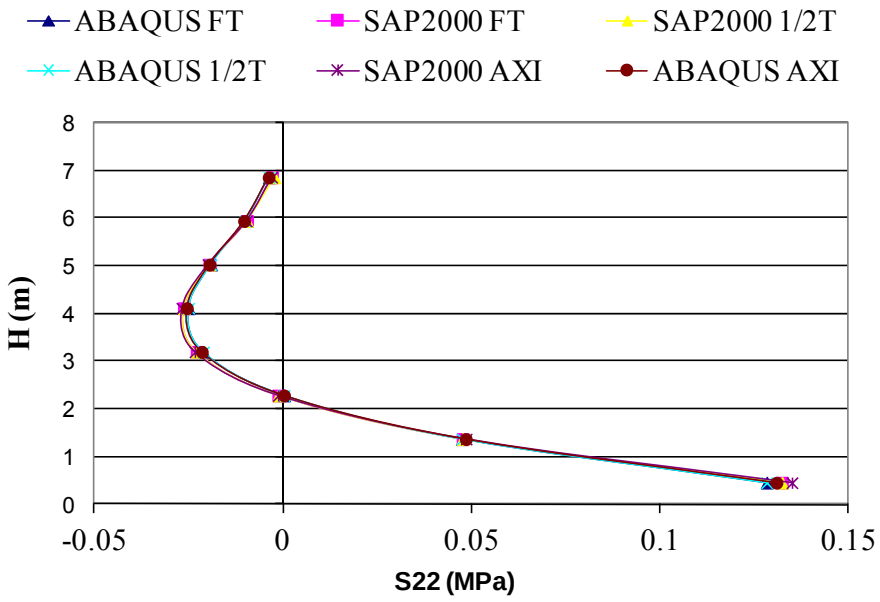

Figure 3.12 – Bending stresses in vertical direction under uniform pressure

3.5.4 Results of FE analysis

The results of FE analysis for different tank models under the effect of hydrodynamic forces are presented in this section. However, the results of ½ Tank (½T) model are identical to the results of Full Tank (FT) model. Therefore, only the results of FT and Axi- symmetric (AXI) models are presented. For FT model the hydrodynamic forces are modeled using the cosine and uniform pressure distributions around the tank circumferential as described before. The results of FE analysis for these two models are referred to as Cosine and Max, respectively.

The results of FE analysis for FT model are referred to as (Pi Max), (Pi Cosine), (Pc Max), and (Pc Cosine), for uniform impulsive, cosine impulsive, uniform convective, and cosine convective, respectively.

The results of FE analysis for Axi- symmetric (AXI) model are referred to as (Pi Max ”Axi”), and (Pc Max ”Axi”) for impulsive (P_i) and convective (P_c) forces, respectively.

As shown in Figure 3.13, for both convective (P_c) and impulsive (P_i) forces, the radial deformations (U1) are very similar in general for cosine and uniformly distributed loads. For

impulsive force, the maximum value of U1 for FT model using cosine distribution of seismic force (Pi Cosine) are 2% and 5% higher than using uniformly distributed load (Pi Max) for hinged and fixed base tanks, respectively. The reason for the differences is that, for Pi Max the total resultant force near polar angles $\theta = 90$ and 270 deg. (see Figure 3.6 (a)), increase the radial deformation of the tank wall in the direction normal to the seismic force. Therefore, the tank wall near polar angle $\theta = 0$ deg. will be pulled back under uniform load (Pi Max), which is more than the case for cosine distribution (Pi Cosine). However, the difference between the results is considered to be small. Furthermore, the results of FE analysis show that, the maximum value of U1 for FT model are very similar to the results of AXI model for fixed and hinged base tanks. The maximum differences between the results of AXI model (Pi Max "Axi") and FT model using cosine load distribution (Pi Cosine) are around 5% and 10% for hinged and fixed base tanks, respectively. Also, the results of FE analysis for convective force are very similar for Pc Cosine, PC Max and PC Max "Axi" with maximum differences of 9% and 6% for hinged and fixed base tanks, respectively. Therefore, it is appropriate to use the approximation of uniform distributed load instead of the actual cosine distribution for maximum response.

As shown in Figure 3.14, for hoop stresses (S11), the maximum difference in the results between cosine (Pi and Pc Cosine) and uniform (Pi and Pc Max) load distributions using FT model, is around 3 % for hinged and fixed base conditions. This is contrary to the effect on radial deformations in which the hoop stresses due to uniform load distribution (Pi and Pc Max) resulted in higher stresses than the cosine distribution (Pi and Pc Cosine). The small increase in the stresses due to uniform load distribution is expected due to the increase of the total hoop force around the entire tank circumference. The maximum values of hoop stresses S11 for "Axi-sym" model are around 10% and 6% higher than those for FT model for impulsive and convective forces, respectively. However, the differences in stresses between FT and Axi-sym models two models are considered acceptable reasonable for the design purposes.

The results for the stresses in the vertical direction (S22) are shown in Figure 3.15. For FT model, the maximum difference in stresses between cosine (Pi and Pc Cosine) and uniform (Pi and Pc Max) load distributions is less than 2% for fixed and hinged base conditions. Also, the

difference between the results of “Axi-sym” model and the FT model is around 9%, which is considered acceptable for design application.

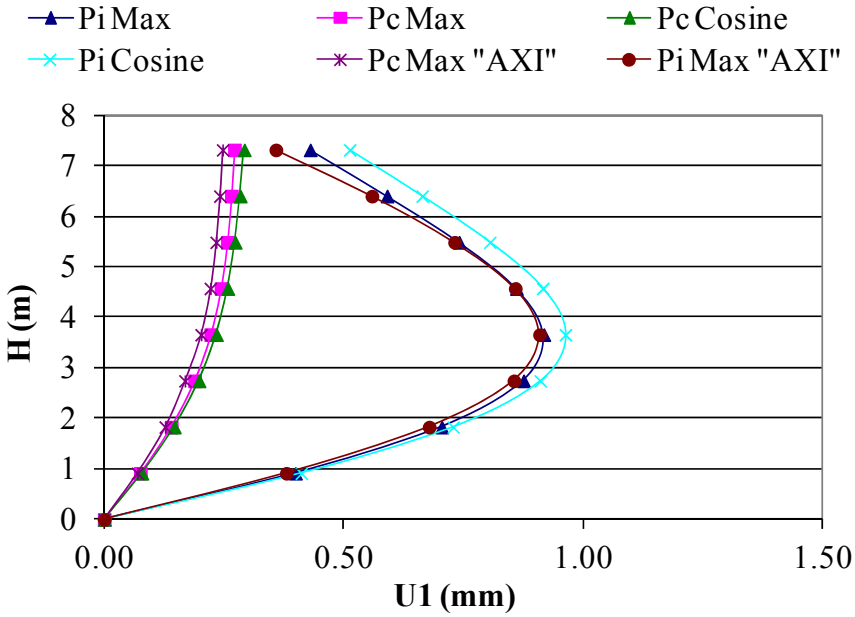

(a)

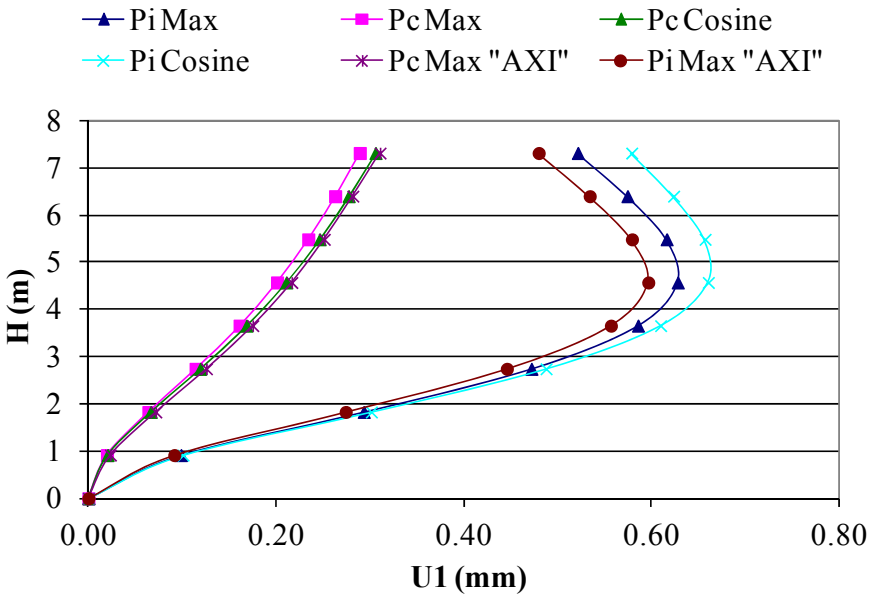

(b)

Figure 3.13 – Radial deflection; (a) Hinged base, (b) Fixed base

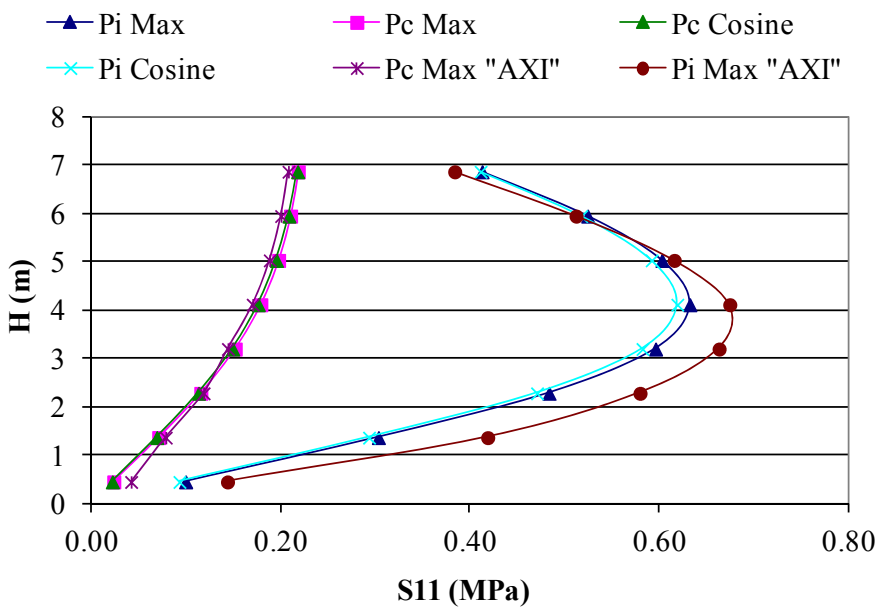

(a)

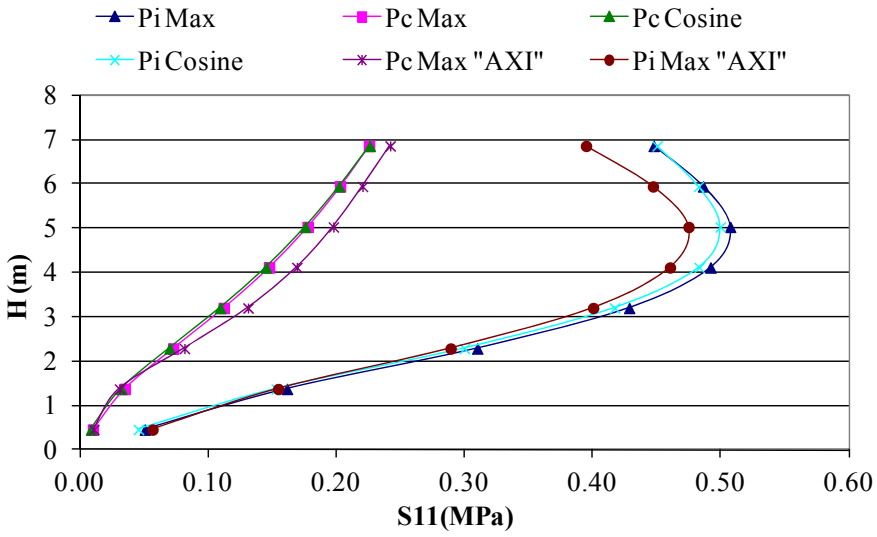

(b)

Figure 3.14 – Hoops stress; (a) Hinged base, (b) Fixed base

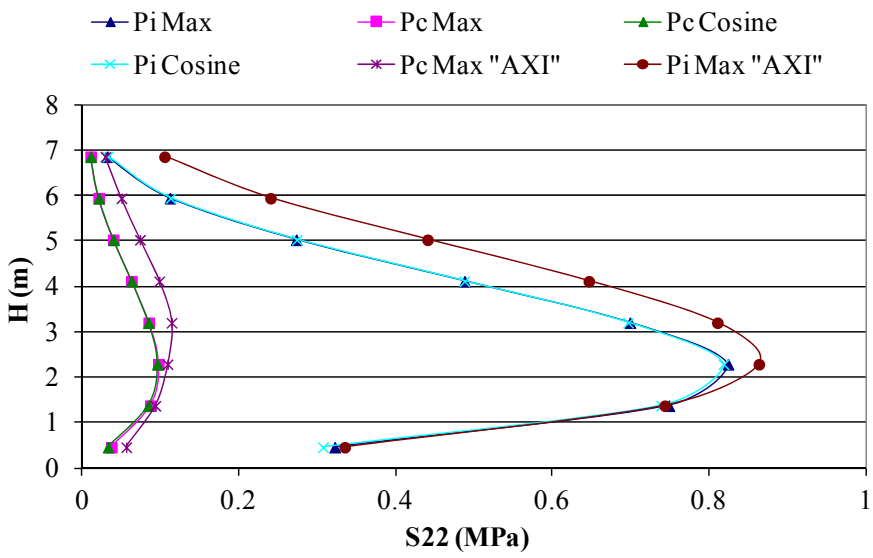

(a)

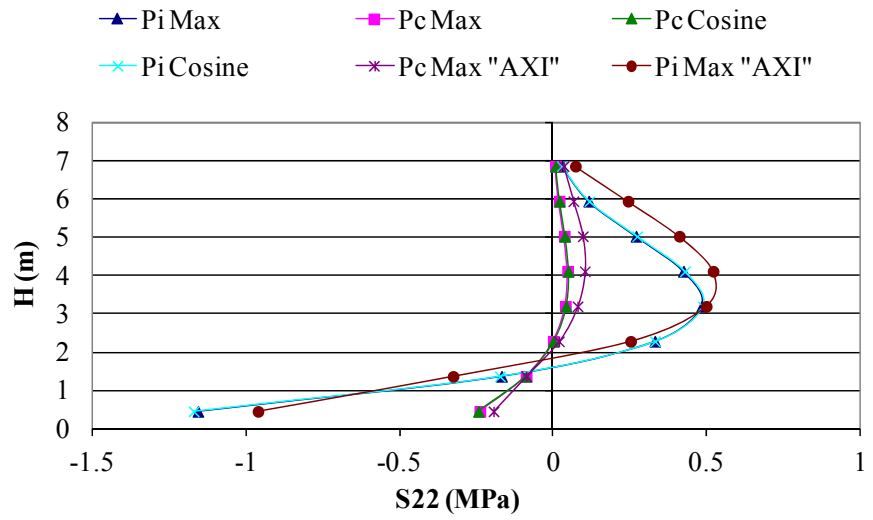

(b)

Figure 3.15 – Bending stress; (a) Hinged base, (b) Fixed base

Based on the results of this study, it is appropriate to use the approximation of uniform distributed load instead of the actual cosine distribution for maximum response. Therefore, Axi-sym model can be used to model circular tanks with a reasonable level of accuracy for analysis and design application.

3.6 Comparison between the results of FE analysis and closed-form solution

In this study, a comparison is made between the results of FE analysis and closed-form solution under the effect of seismic forces. This study is performed in order to further verify the results of FE analysis. The same tank as described in Section 3.5 is considered for this comparison. For FE analysis, the entire tank is modeled where FT model as described before is used. Both hydrostatic and seismic forces are considered in this study.

The results of FE analysis are compared with those of closed-form solution using PCA method (PCA 1992) in the form of tables. In this study, both fixed and hinged base conditions are considered.

For FE analysis, the hydrodynamic forces are modeled using the actual cosine distribution (Cosine). The FE analysis is performed using computer program SAP2000. For closed-form solution, the cosine distribution of hydrodynamic forces is not possible; therefore, the maximum value of earthquake forces at polar coordinate angle (θ) = 0 deg is considered in the calculations. It should be noted that the tables in PCA Handbook (PCA 1992) for tanks assume the tank height is the same as the water depth. The computer model is adjusted, accordingly, to eliminate the shell elements above the water level where the water height (H_W) is considered to be the same as that of the wall height (H_L).

For the hinged base condition, Figure 3.16 (a) shows that the maximum hoop forces calculated based on the closed-form solution are 1% and 8% higher than the results of FE analysis for hydrostatic and earthquake forces, respectively. The maximum values of the hoop forces based on closed-form solution and FE analysis occur almost at the same location.

Similarly, for the fixed base condition, as shown in Figure 3.16 (b) the maximum hoop forces calculated based on the closed-form solution are 2.8% and 1% less than FE analysis for hydrostatic and seismic forces respectively. Also, the maximum values for the hoop forces occur at the same location.

The results of the closed-form solution are very similar to FE analysis when H_L equals to H_w. Therefore, closed-form solution can be used to estimate the design forces for cases where the wall height is close to the water height. It should be noted that, for closed-form solution, the maximum value of earthquake forces at polar coordinate angle (θ) = 0 should be used.

For hinged base condition, Figure 3.17 (a) shows that the bending moment in the tank wall based on the closed-form solution are 5% and 9% more than the FE analysis for hydrostatic and earthquake forces, respectively. Also, they occur at the same location near the mid height of the tank wall.

Similarly, for fixed base condition, as shown in Figure 3.17 (b) the bending moment in the tank wall based on the closed-form solution are 1.5% and 2.5% less than those of the FE analysis for hydrostatic and earthquake forces, respectively. Also, both values occur at the same location near the mid height of the tank wall.

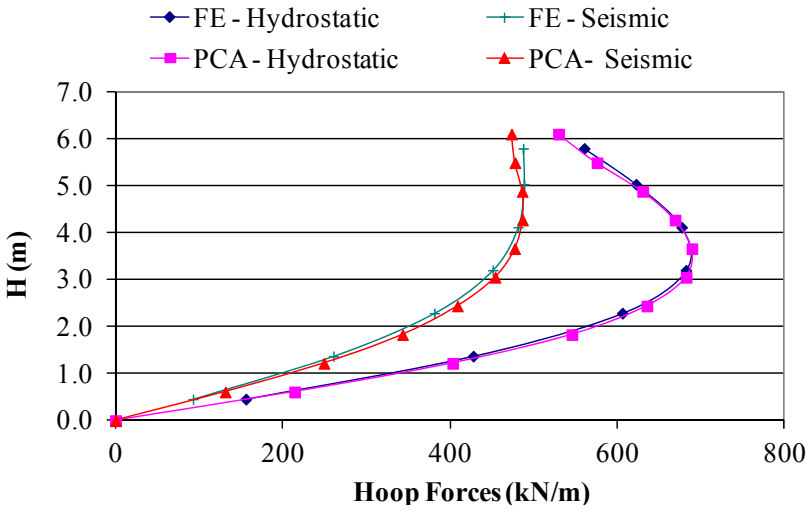

(a)

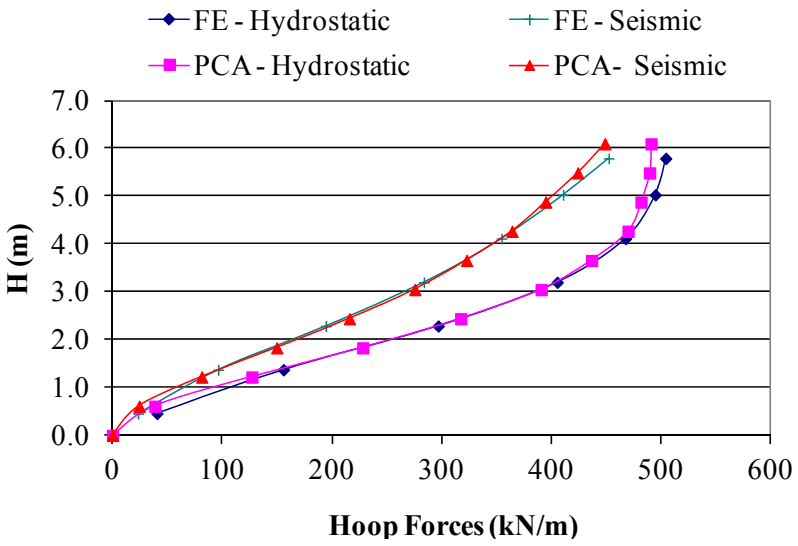

(b)

Figure 3.16 – Hoop force in tank wall; (a) Hinged base, (b) Fixed base

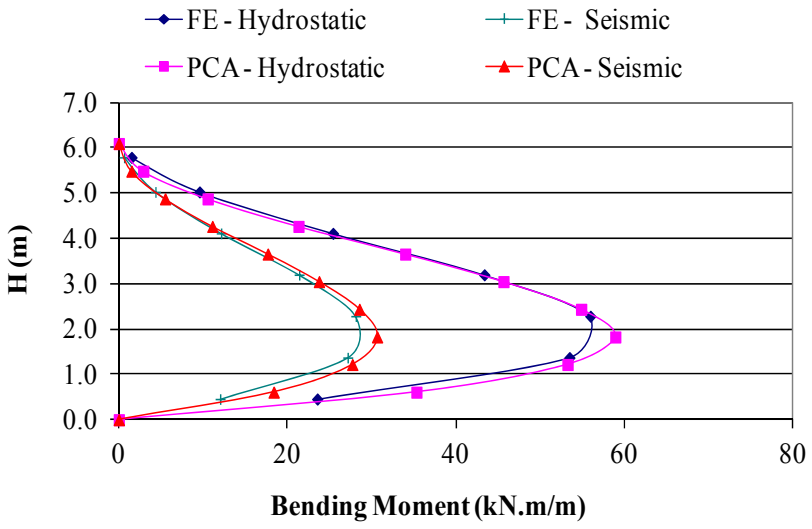

(a)

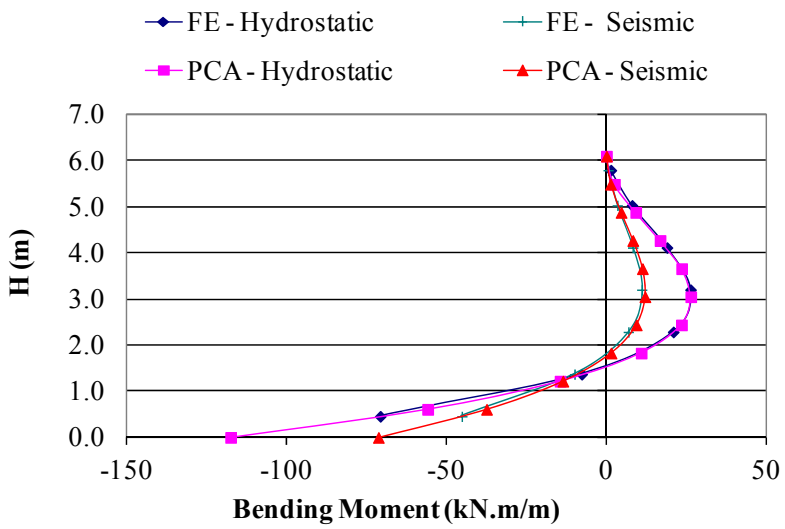

(b)

Figure 3.17 – Bending moment in tank wall; (a) Hinged base, (b) Fixed base

3.7 Comparison between results of fixed, hinged, and free base tanks

This study is undertaken in order to investigate the effect of tank support conditions on the internal hoop force in the tank wall and base shear. In this study, FE analysis is performed for Model 1 where Fixed, Hinged, Free base conditions are considered. The seismic force is modeled using the actual cosine distribution (Cosine) of the seismic load based on ACI350.3-06 (2006). The FE analysis is performed using SAP2000. Hydrostatic force is not considered in this comparison.

The results of FE analysis as shown in Figures 3.18 and 3.19 indicate that, 48% and 64% of the total seismic hoop forces are transferred to the tank base by diaphragm action for hinged and fixed base conditions, respectively. No force is transferred to the tank base in case of the free base tank. It should be noted that the fixed and hinged base tanks are designed for R_i = 2.0 and free base tanks for R_i = 3.25 based on ACI 350.3 (2006). It should also be noted that, for tanks with fixed and hinged base conditions, the tank walls need to be designed for additional forces due to bending moments in the cylindrical wall in the vertical direction.

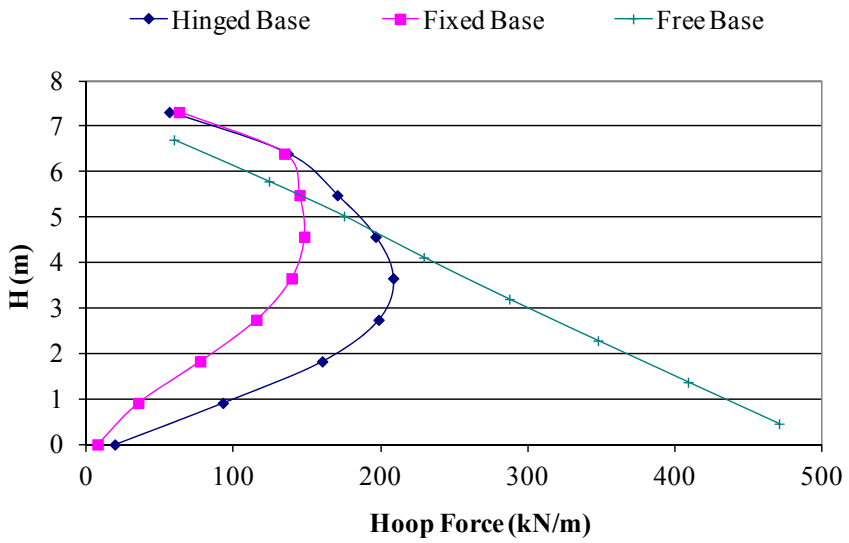

Figure 3.18 – Total seismic hoop force in tank wall

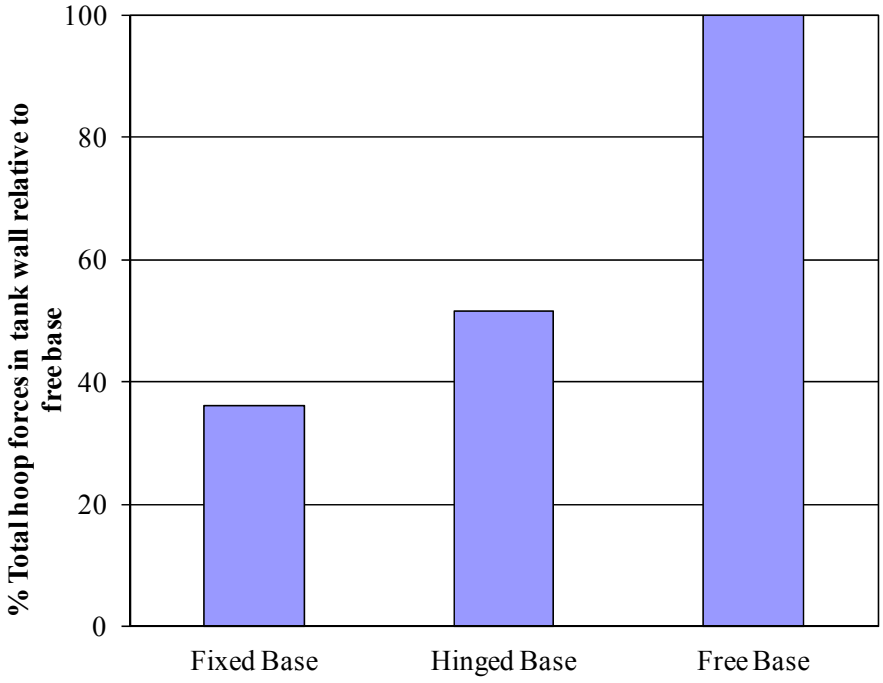

Figure 3.19 – Percentage of total hoop force in tank wall relative to free base condition

3.8 Summary

The study included in this chapter is prepared based on the American Concrete Institute Codes for the Design of Liquid-Containing Concrete Structures ACI 350.3 (2001, 2006).

This study presents the response of circular tanks subjected to ground motions. The sensitivity of their response to variations in the governing parameters is investigated using ACI Codes (2001, 2006). The effect of uniform versus cosine pressure distribution is also investigated.

For hinged and fixed base tanks, the tank response including radial deformation (U1), hoop stresses (S11), and bending stresses in the vertical direction (S22), are very similar for cosine and uniform load distribution. Also, the results of FE analysis for modeling the entire tank using shell elements are very similar to the results of axisymmetric elements model. Therefore, it is appropriate to use the approximation of uniform distributed load and axisymmetric elements instead of the actual cosine distribution by modeling the entire tank using shell elements for maximum response.

It should be noted that the elements at polar coordinate angle (θ) = 0 deg. are subjected to maximum values of the stresses and deformations for the actual cosine distribution of the applied earthquake force. Considering that the earthquake force can be generated in any direction, the elements located at the maximum load value will govern the design. Consequently, for the purpose of the design, the maximum value of earthquake forces at polar coordinate angle (θ) = 0 can be used instead of the actual cosine distribution.

Also, it is found that, most of the hoop force is transferred by diaphragm action at the tank base for fixed and hinged base tanks. Therefore, anchoring the tank wall to the base instead of using a free base is recommended.

CHAPTER 4
PROPERTIES AND FINITE ELEMENT MODELING OF MATERIALS

4.1 General

FE modeling of RC members is performed to develop numerical models for the nonlinear behavior of circular tanks. In this chapter, the nonlinear properties of the construction materials (Concrete, Steel reinforcement, Prestressing tendons, and Elastomeric bearing pad) are discussed. Also, this chapter describes various modelling features of ABAQUS/CAE (Dassault Systèmes Simulia Corp. 2008).

For RC modeling, the steel stresses/strain can be determined by concrete section analysis, which may be a time consuming approach for the actual structure under different types of loadings. Due to a complex interaction between the various components of real structures, their dynamic characteristics cannot be identified solely from dynamic tests of scale models. Moreover, the cost of such tests for large specimens is substantial. Historically these difficulties have been overcome by static tests on components and reduced scale subassemblages of structures under cyclic load reversals. Results from these tests are then used in the development of hysteretic models that permits the extrapolation of the available test data to other cases and to the dynamic response of the complete structures (Taucer 1991).

4.2 Finite element program ABAQUS/CAE

The FE analysis is conducted using ABAQUS/CAE Version 6.8.3. ABAQUS/CAE provides an interactive and graphical technique and allows a model to be created easily by producing the geometry into mesh able regions. Material properties, loads, and boundary conditions can be assigned to the geometry. ABAQUS/CAE has easy interface and it is suitable for simulation of nonlinear engineering problems, also, its visualization module is an efficient option to interpret the results.

4.2.1 Selection of finite element analysis technique

ABAQUS/CAE consists of two main analysis products; a) ABAQUS/Standard and b) ABAQUS/Explicit. ABAQUS/Standard is typically used for general–purpose analysis problems

where a system of equations is solved implicitly at each solution increment. It can solve a wide range of linear and nonlinear problems involving the static, dynamic, thermal, and electrical response of components. In the implicit method, equilibrium is achieved through an iterative procedure.

On the other hand, ABAQUS/Explicit is used for special–purpose analyses which use an explicit dynamic finite element formulation. It uses central difference method to integrate the equations of motion explicitly through time. The explicit time integration method uses the kinematic conditions at one increment to calculate the kinematic conditions at the next increment. It is suitable for modeling brief, transient dynamic events, such as impact problems, and is also very efficient for nonlinear problems involving. The explicit method requires many small time increments. Since there are no simultaneous equations to solve, each increment is inexpensive. Table 4.1 shows the difference between ABAQUS/Standard and ABAQUS/Explicit. This table is excerpted from the ABAQUS documentations (Dassault Systèmes Simulia Corp., 2008).

For analyzing a nonlinear problem with a large number of degrees of freedoms (DOFs), using ABAQUS/Explicit is recommended since, for each iteration, ABAQUS/Standard requires a solution of a large set of linear equations through iteration process. On the other hand, ABAQUS/Explicit determines the solution without iterating by explicitly advancing the kinematic state from the previous increment. Although, for a large number of the DOFs, the analysis may require a large number of time increments using the explicit method, the analysis can be more efficient in ABAQUS/Explicit compared to ABAQUS/Standard. The explicit method has great cost savings over the implicit method as the model size increases. Figure 5.1 shows the variation of the computational cost versus number of DOF for ABAQUS/Explicit and ABAQUS/Standard. The relation between the computational costs by increasing the number of DOF in ABAQUS/Explicit is almost linear.

Table 4.1 - Comparison between ABAQUS/Standard and ABAQUS/Explicit (Dassault Systèmes Simulia Corp. 2008)

Parameter	ABAQUS/Standard	ABAQUS/Explicit
Element library	Offers an extensive element library	Offers an extensive library of elements well suited for explicit analyses. The elements available are a subset of those available in ABAQUS/Standard
Analysis procedures	General and linear perturbation procedures are available	General procedures are available
Material models	Offers a wide range of material models	Similar to those available in ABAQUS/Standard; a notable difference is that failure material models are allowed
Contact formulation	Has a robust capability for solving contact problems	Has a robust contact functionality that readily solves even the most complex contact simulations
Solution technique	Uses a stiffness-based solution technique that is unconditionally stable	Uses an explicit integration solution technique that is conditionally stable
Disk space and memory	Due to the large numbers of iterations possible in an increment, disk space and memory usage can be large	Disk space and memory usage is typically much smaller than that for ABAQUS/Standard

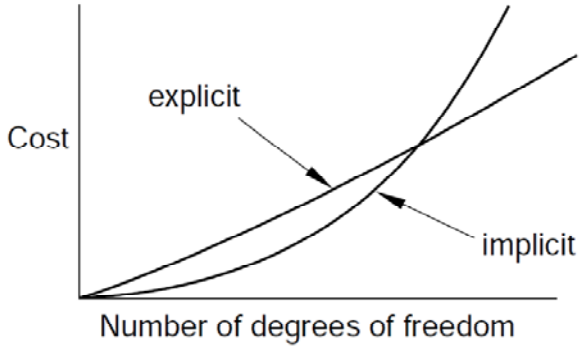

Figure 4.1 - Cost versus model size in using the explicit and implicit methods (Dassault Systèmes Simulia Corp. 2008)

Therefore, The ABAQUS/Explicit was used for the following reasons:

- Concrete degradation can cause severe convergence difficulties in ABAQUS/Standard (implicit) analysis program but in the ABAQUS/Explicit can perform well,
- Reduce the computational cost (time) for the composite wall model,

4.2.2 Conditional stability and time increment in the explicit method

The maximum time increment is a critical factor for performance and stability of the ABAQUS/Explicit. If the time increment is larger than a specified value, a numerical instability may happen. The maximum time increment used by the ABAQUS/Explicit solver has a great effect on reliability and accuracy of the results. The material properties and the finite element mesh size can change the critical time increment. The wave speed depends on both density and stiffness of the material. The higher material density results in a reduction of the wave speed and an increase in the critical time increment. On the other hand, the higher material stiffness results in an increase of the wave speed and a reduction in the critical time increment. The wave speed is constant for a specific material when the analysis is in the linear portion and, and therefore the critical time depends only on the smallest element size in the finite element mesh.

ABAQUS/Explicit automatically controls the time increment size throughout the analysis to maintain stability. ABAQUS/Explicit calculates the stable time increment based on the highest

frequency in the model which can be estimated by individual elements in the model. Based on the element–by–element estimate, the stability time limit (Δt_{stable}) can be defined using the shortest element length (L_e) and the wave speed of the material (C_d) (Dassault Systèmes Simulia Corp., 2008):

$$\Delta t_{stable} = \frac{L_e}{C_d} \tag{4-1}$$

The wave speed is a property of the material. For a linear elastic material with a Poisson's ratio of zero, the wave speed can be derived from the following equation:

$$C_d = \sqrt{\frac{E}{\rho}} \tag{4-2}$$

where E is Young's modulus and ρ is the mass density.

In a nonlinear material, such as a metal with plasticity or concrete, the wave speed changes as the material yields and stiffness of the material changes. In the nonlinear portion of the analysis, the modulus of elasticity decreases which reduces the wave speed and increases the critical time increment. ABAQUS/Explicit monitors the effective wave speeds in the model throughout the analysis, and the current material state in each element is used for stability estimates.

The shortest element dimension has a direct effect on the stability time limit (Equation 4-2), and it is recommended to keep the element size as large as possible. On the other hand, for accurate analyses a fine mesh is needed. The best approach for meshing a FE Model is to have a mesh which is as uniform as possible. Also, to make a balance in the mesh size in order not to compromise the analysis accuracy or having very small stable time limit.

4.3 Material properties

4.3.1 Concrete Model

There are three different models to simulate the concrete behavior in ABAQUS/CAE Version 6.8.3; the smeared cracking model, brittle cracking model and the concrete damaged plasticity model (Dassault Systèmes Simulia Corp. 2008).

4.3.2 Smeared cracking

This model is intended for applications in which the concrete is subjected to essentially monotonic straining at low confining pressures, where a material point exhibits either tensile cracking or compressive crushing. Therefore, this model was used in the push-over analyses in this study. In this model, cracking is assumed to be the most important aspect of the behavior and the representation of cracking and postcracking anisotropic behavior dominates the modeling. Because this model is intended for application where the problems involve relatively monotonic straining, no attempt is made to include prediction of cyclic response or of the reduction in the elastic stiffness caused by inelastic straining under predominantly compressive stress.

When concrete is loaded in compression, it initially performs elastically. As the stress increases, non-recoverable (inelastic) strain occurs and the response of the material softens. After the material reaches the ultimate stress, it loses strength until it can no longer carry any stress. However, in reality, if the load is removed after inelastic straining has occurred, the unloading response is softer than the initial elastic response and the elasticity is damaged. This effect is ignored in the model, since it is assumed that the applications involve primarily monotonic straining, with only occasional, minor unloading.

4.3.3 Brittle cracking

This model is intended for applications in which the concrete behavior is dominated by tensile cracking, and compressive failure is not important. The compressive behavior is assumed to be always linear elastic. The crack formation criterion states that a crack forms when the maximum principal tensile stress exceeds the tensile strength of the brittle material. As soon as the criterion for crack formation has been met, it is assumed that a first crack has formed. Cracking is irrecoverable in the sense that, once a crack has occurred at a point, it remains throughout the

rest of the calculations. However, crack closing and reopening may take place along the directions normal to the crack surfaces.

4.3.4 Concrete damaged plasticity (CDP)

The Concrete Damage Plasticity (CDP) model (Lubliner et al. 1989, Lee et al. 1998, and Li et al. 2005) is the most comprehensive model. The CDP is a continuum, plasticity-based damage model for concrete. It assumes two concrete failure mechanisms: tensile cracking and compressive crushing of the material, and that the uniaxial tensile and compressive response of concrete is characterized by damaged plasticity. The CDP model in ABAQUS/CAE is designed for applications in which concrete is subjected to monotonic, cyclic, and/or dynamic loading under low confining pressures for all types of structures (beams, trusses, shells, and solids). The model uses concepts of isotropic damaged elasticity in combination with isotropic tensile and compressive plasticity to represent the inelastic behavior of concrete. Also, the stiffness recovery effects during cyclic load reversals can be controlled by the user. Therefore, this model is used in the nonlinear dynamic analyses of the tanks.

This chapter presents the concrete behavior in tension, compression and cyclic loading which is mostly excerpted from the ABAQUS documentations (Dassault Systèmes Simulia Corp. 2008).

4.3.4.1 Behavior of concrete in tension

As shown in Figure 4.2, the concrete behavior in uniaxial loading in tension. The stress-strain response follows a linear elastic relationship until the failure stress (σt0). Beyond the failure stress, there will be a softening stress-strain response. When the concrete specimen is unloaded from any point on the strain softening branch of the stress-strain curve, the unloading response is weakened, and the elastic stiffness of the material is degraded or damaged. The degradation of the elastic stiffness is characterized by damage variable in tension (dt), which can take the value from zero, representing the undamaged material, to one, representing the total loss of strength.

The cracking strain $\left(\tilde{\varepsilon}_t^{ck}\right)$ is defined as the total strain (ε_t) minus the elastic strain corresponding to the undamaged material; which is:

$$\tilde{\varepsilon}_t^{ck} = \varepsilon_t - \sigma_t/E_0 \tag{4-3}$$

where σ_t is tensile stress and E_0 is the initial elastic stiffness of the concrete. Tension stiffening data are given in terms of the cracking strain, $\tilde{\varepsilon}_t^{ck}$. The unloading data are provided to ABAQUS in terms of tensile damage curves (d_t versus $\tilde{\varepsilon}_t^{ck}$). ABAQUS automatically converts the cracking strain values to plastic strain values $\left(\tilde{\varepsilon}_t^{pl}\right)$ using the following relationship:

$$\tilde{\varepsilon}_t^{pl} = \tilde{\varepsilon}_t^{ck} - \frac{d_t}{(1-d_t)}\frac{\sigma_t}{E_0} \tag{4-4}$$

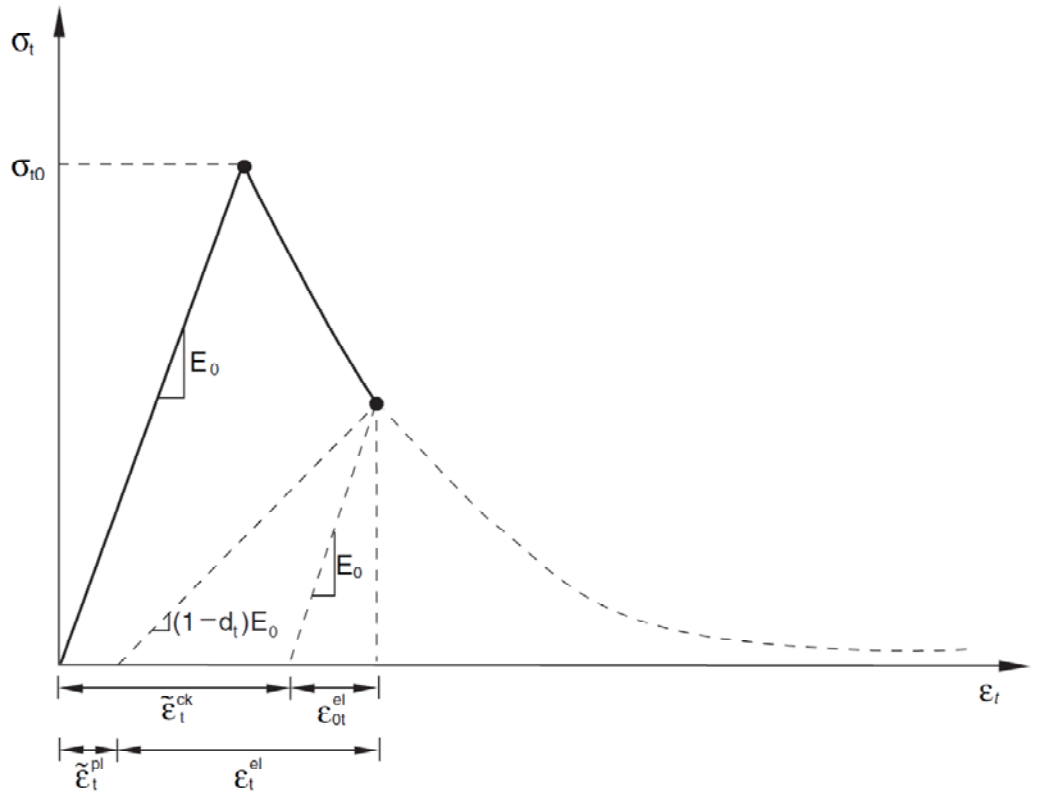

Figure 4.2 – Response of concrete to uniaxial loading in tension
(Dassault Systèmes Simulia Corp. 2008)

4.3.4.2 Behavior of concrete in compression

Figure 4.3 shows the concrete behavior in uniaxial loading in compression. Under uniaxial compression, the response is linear until the value of initial yield, σ_{c0} is reached. In the plastic regime, the response is typically characterized by stress hardening followed by strain softening beyond the ultimate stress, σ_{cu}.

When the concrete specimen is unloaded from any point on the strain softening branch of the stress-strain curves, the unloading response is weakened and the elastic stiffness of the material is degraded or damaged. The degradation of the elastic stiffness is characterized by damage variable, d_c, which can take values from zero, representing the undamaged material, to one, representing the total loss of strength.

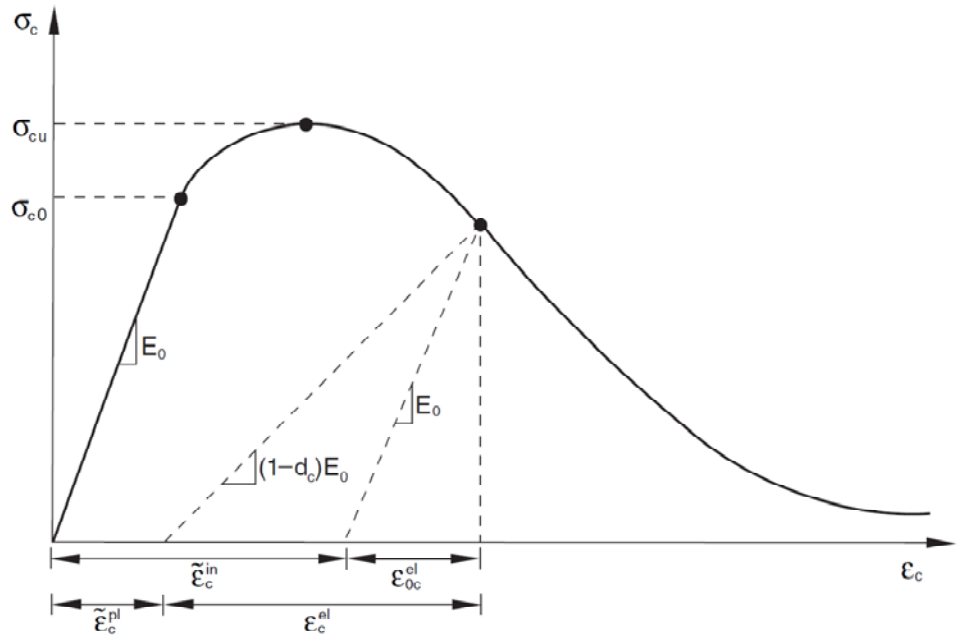

Figure 4.3 - Response of concrete to uniaxial loading in compression
(Dassault Systèmes Simulia Corp. 2008)

Compressive stress data is provided as a tabular function of inelastic or crushing strain $\left(\tilde{\varepsilon}_c^{in}\right)$. Positive (absolute) values should be given for the compressive stress and strain. The stress-strain curve can be defined beyond the ultimate stress, into the strain-softening regime.

Hardening data are given in terms of an inelastic strain, $\tilde{\varepsilon}_c^{in}$, instead of plastic strain, $\tilde{\varepsilon}_c^{pl}$. The compressive inelastic strain is defined as the total strain minus the elastic strain corresponding to the undamaged material,

$$\tilde{\varepsilon}_c^{in} = \varepsilon_c - \sigma_c/E_0 \tag{4-5}$$

Where E_0 is the initial elastic stiffness of the concrete. Unloading data are provided to ABAQUS in terms of compressive damage curves (d_c versus $\tilde{\varepsilon}_c^{in}$). ABAQUS automatically converts the inelastic strain values to plastic strain values $\left(\tilde{\varepsilon}_c^{pl}\right)$ using the following relationship:

$$\tilde{\varepsilon}_c^{pl} = \tilde{\varepsilon}_c^{in} - \frac{d_c}{(1-d_c)}\frac{\sigma_c}{E_0} \tag{4-6}$$

4.3.4.3 Behavior of concrete under cyclic loading

The degradation mechanisms of concrete under uniaxial cyclic loading are quite complex, involving the opening and closing of previously formed micro-cracks and also their interaction. It is observed experimentally that there is some recovery of the elastic stiffness as the load changes sign during a uniaxial cyclic test. The stiffness recovery effect is an important aspect of the concrete behavior under cyclic loading. The effect is usually more obvious as the load changes from tension to compression, causing tensile cracks to close, which results in the recovery of the compressive stiffness.

The concrete damaged plasticity model assumes that the reduction of the elastic modulus is given in terms of a scalar degradation variable (*d)* as:

$$E = (1-d)E_0 \tag{4-7}$$

The degradation or damage variable in the strain-softening part can be calculated from the following equations (Jankowiak et al. 2005):

$$d_c = \frac{\sigma_{cu} - \sigma_c}{\sigma_{cu}} \tag{4-8}$$

where d_c is damage variable in compression, σ_{cu} is ultimate compressive stress (Fig. 4.4) and σ_c is compressive stress.

and

$$d_t = \frac{\sigma_{t0} - \sigma_t}{\sigma_{t0}} \tag{4-9}$$

where d_t is damage variable in tension, σ_{t0} is tensile stress at failure (Figure 4.3) and σ_t is compressive stress.

The effect of stiffness recovery in compression (w_c) and in tension (w_t) on the behavior of the concrete material is shown in Figure 4.4. The value of w_c and w_t are between zero and one, and they control the recovery of the compressive and tensile stiffness upon load reversal. ABAQUS allows direct user specification of the stiffness recovery factors w_c and w_t.

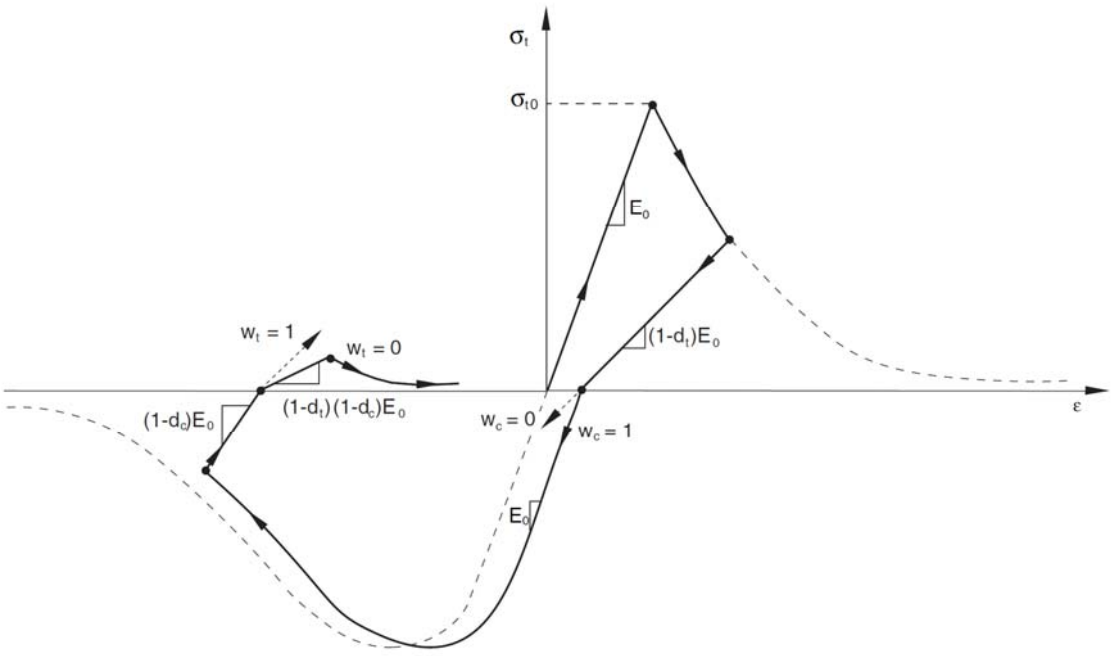

Figure 4.4 - Uniaxial load cycle (tension–compression–tension) assuming $w_t = 0$ and $w_c = 1$ (default values) for the stiffness recovery (Dassault Systèmes Simulia Corp. 2008)

The experimental observation in most quasi–brittle materials, including concrete, shows that the compressive stiffness is recovered upon crack closure as the load changes from tension to compression. On the other hand, the tensile stiffness is not recovered as the load changes from compression to tension once crushing micro–cracks have developed. This behavior, which corresponds to $w_t = 0$ and $w_c = 1$, is the default used by ABAQUS. If $w_c = 1$, the material fully recovers the compressive stiffness which in this case is the initial undamaged stiffness ($E = E_0$). If $w_c = 0$, there is no stiffness recovery. Intermediate values of w_c result in partial recovery of the compressive stiffness. In the composite wall model, the default values for stiffness recovery ($w_t = 0$ and $w_c = 1$) are used.

4.3.5 Stress–strain relationship in concrete

The stresses in concrete shell of the circular tanks are bending and bending plus axial stresses. Therefore, the Modified Hognestad method (MacGregor 1997) is used as analytical approximation for the compressive stress-strain curve for concrete as shown in Figure 4.5. The modulus of elasticity of concrete (E_c) is taken as 26000 MPa. Generally, the stress-strain curves of concrete rise to maximum stress, reached at a strain of between 0.0015 and 0,0025, followed by descending branch. The shape of the curve results from the gradual formation of the microcracks within the structure of the concrete. Furthermore, the length of the descending branch of the curve strongly affected by the test condition. Frequently, an axially loaded concrete test cylinder will fail explosively at the point of maximum stress. This will occur in axially flexible testing machine if the strain energy released by the testing machine as the load drops exceeds the energy that the specimen can absorb. In a member loaded in bending, or bending plus axial load, the descending branch will exist since the stress drops in the most highly strain fibers, other less highly strain fiber can resist the load, thus delaying the failure of the highly strained fibers. The modulus of elasticity of concrete (Ec) has been calculated based on ACI 350 (2006) for the normal-weight concrete with normal density of 2300 Kg/m^3 as:

$$E_c = 57{,}000\,(f'_c)^{1/2}/145 \qquad (4\text{-}10)$$

In Modified Hognestad model, the value of compressive concrete stress (f_c) is a function of concrete strain (ε_c), which can be derived from the following Equation:

$$\frac{f_c}{f''_c} = \frac{2\varepsilon_c}{\varepsilon_0} - \left(\frac{\varepsilon_c}{\varepsilon_0}\right)^2 \qquad (4\text{-}11)$$

where:

f'_c = ultimate compressive strength of concrete

$f''_c = 0.9f'_c$

E_c = initial tangent concrete modulus of elasticity as shown in Equation 4-10

ε_0 = strain when f_c reaches f'_c, $\varepsilon_0 = 1.8\frac{f''_c}{E_c}$

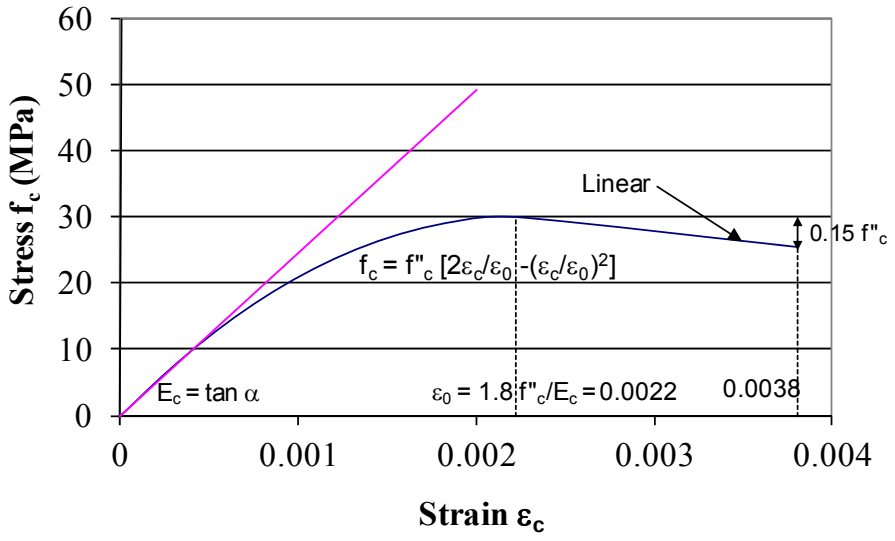

Figure 4.5 - Stress-strain curve for concrete - Modified Hognested

For concrete under tension, the modulus of elasticity of concrete (E_c) is also taken as 26000 MPa. A reasonable starting point, for relatively heavily reinforced concrete modeled with a fairly detailed mesh, is to assume that the strain softening after failure reduces the stress linearly to zero at a total strain of about 10 times the strain at failure. The tensile strain at failure in normal

concretes is typically 10^{-4}, which suggests that tension stiffening that reduces the stress to zero at a total strain of about 10^{-3} is reasonable. However, this value is considered as 0.005 in the FE dynamic analysis due to the effect of strain rate loading on tensile stress-strain curve of concrete. The strain rate is the time duration of the loading processes, which describes the rapidness of deformation processes.

Other parameters of the CDP model in the absence of the required information were taken as the default values in the ABAQUS (Sadjadi 2009).

4.3.6 Reinforcement

The analytical approximation to the tension and compression stress-strain curve for reinforcement is modeled using elastic-plastic curve for grade 400 reinforcing bars with yield strength (f_y) equals to 400 MPa, and maximum strain at ultimate load, which equals to 0.1 as shown in Figure 4.6.

For cyclic loading, two kinematic hardening models are provided in ABAQUS to model the cyclic loading of metals. The first one, the linear kinematic model, approximates the hardening behavior with a constant rate of hardening using two pairs of data (the yield stress at zero plastic strain and a yield stress at a finite plastic strain value). The second model, the nonlinear isotropic/kinematic (combined) model, gives better predictions but requires more detailed calibration. Linear kinematic hardening model is used to model the behavior of metals subjected to cyclic loading. The linear kinematic hardening model is selected by specifying the "Plastic", and "Hardening = Kinematic" option. The linear kinematic hardening component takes the Bauschinger effect into consideration (Driver et al. 1998). Bauschinger effect is characterized by a reduced yield stress upon load reversal after plastic deformation has occurred during the initial loading as shown in Figure 4.7. This phenomenon decreases with continued cycling.

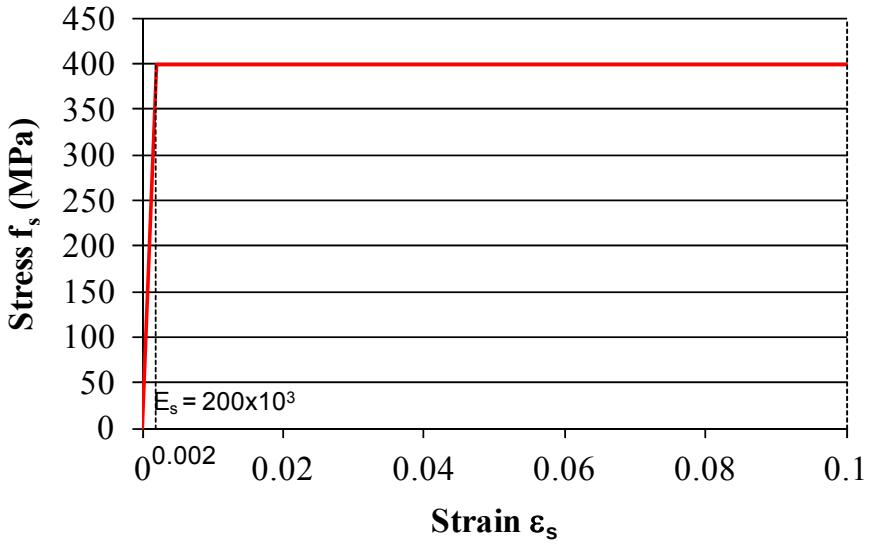

Figure 4.6 - Stress-strain curve for reinforcement - Elastic-Plastic

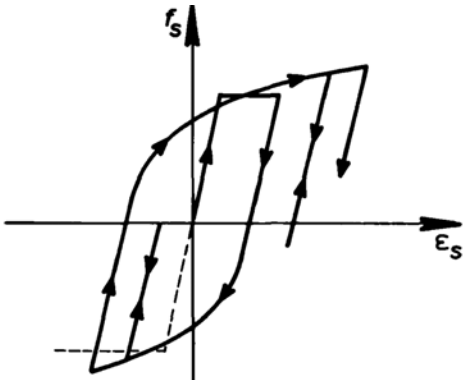

Figure 4.7 - Stress–strain curve for steel in cyclic loading illustrating the Bauschinger effect (Kent et al. 1973)

It should be noted that the inelastic material properties must be input into ABAQUS in the form of true (Cauchy) stress (σ_{true}) and true (logarithmic) strain (ε_{true}), which can be calculated from the engineering stress (σ_{eng}) and engineering strain (ε_{eng}) using the following equations (Lubliner 1990):

$$\sigma_{true} = \sigma_{eng}(1 + \varepsilon_{eng}) \quad (4\text{-}12)$$

and,

$$\varepsilon_{true} = \ln(1 + \varepsilon_{eng}) \quad (4\text{-}13)$$

4.3.7 Prestressing Tendons

The design requirements for prestressing tendons are specified in CSA Standards A23.3 (2010) and A23.1(2010) including the minimum specified yield strength, and the minimum ultimate tensile strength. In this study, seven-wire strands grade CSA G279 are used for prestressing steel.

It should be noted that, the steel grades for tendons depend on the minimum tensile strength (f_{pu}) which is 1860 MPa for grade CSA G279, and the yield strength (f_y) is 1581 MPa. Furthermore, the elastic modulus of non-prestresses tendons (E_s) is required to be detriment by test or supplied by manufacturer according to CSA Standard A23.3 (2010). Where typical values will range from 190,000 to 200,000 MPA, E_s for prestressing steel is taken as 200,000 MPa in this study. Figure 4.8 shows the stress-strain curve for the used prestressing tendons.

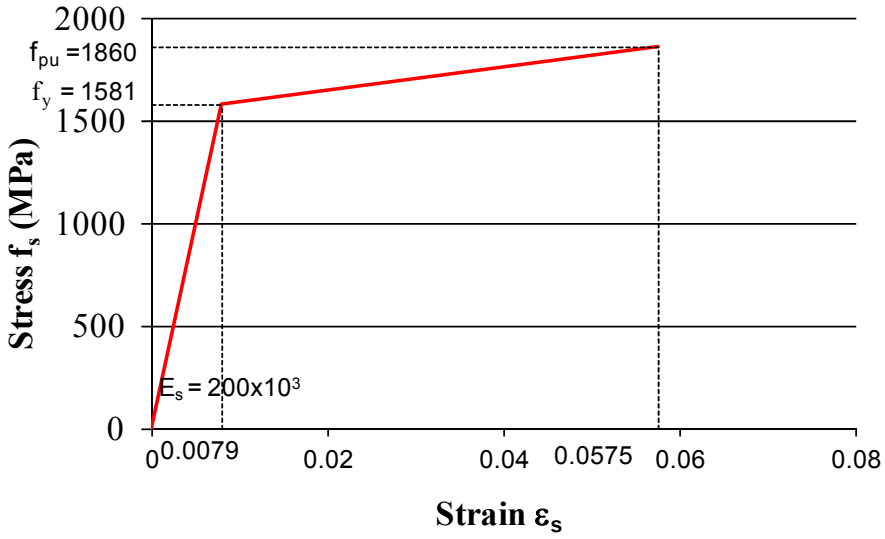

Figure 4.8 - Stress-strain curve for prestressing tendons

4.3.8 Elastomeric bearing pad

The most common type of elastomeric pads is 40H which was used for the flexible based tank bearing pads. The shear module of elastomeric bearing pad (G_p, referred to as S in Figure 4.9) is taken 0.345 MPa (50 psi) for type 40H according to Figure 4.9 where the values of shear modulus for different types of rubber are shown. The shear strain is defined as the ratio of the linear deformation (d) to the rubber thickness (t). Typically the thickness of the elastomeric bearing pad (t) between the tank wall and the base is 25 mm where the bearing pad is continuous. In this case, the rubber pad is deformed under shear between the tank wall and the base.

Hence, the mathematical analysis of rubber in shear is based on an element rectangular parallelogram. For all equations (d) and (t) are set up as differential quantities, and an expression is developed for deflection which can be integrated with respect to dt. Accordingly, the slope of the shear curve was assumed to be constant for the purpose of deriving the spring rate equation. However, the variation of the shear curve slope can be taken into account during the design stage if necessary. The spring rate of the rubber pad (K_L) is considered linear within the allowable lateral deformation (d), which can be calculated using the following equation:

$$K_L = \frac{G_p A}{t} \tag{4-14}$$

where A is the area of the shear plane

It should be noted that, the deformation of the elastomeric bearing pad is controlled by the seismic cables which connect the tank wall and base.

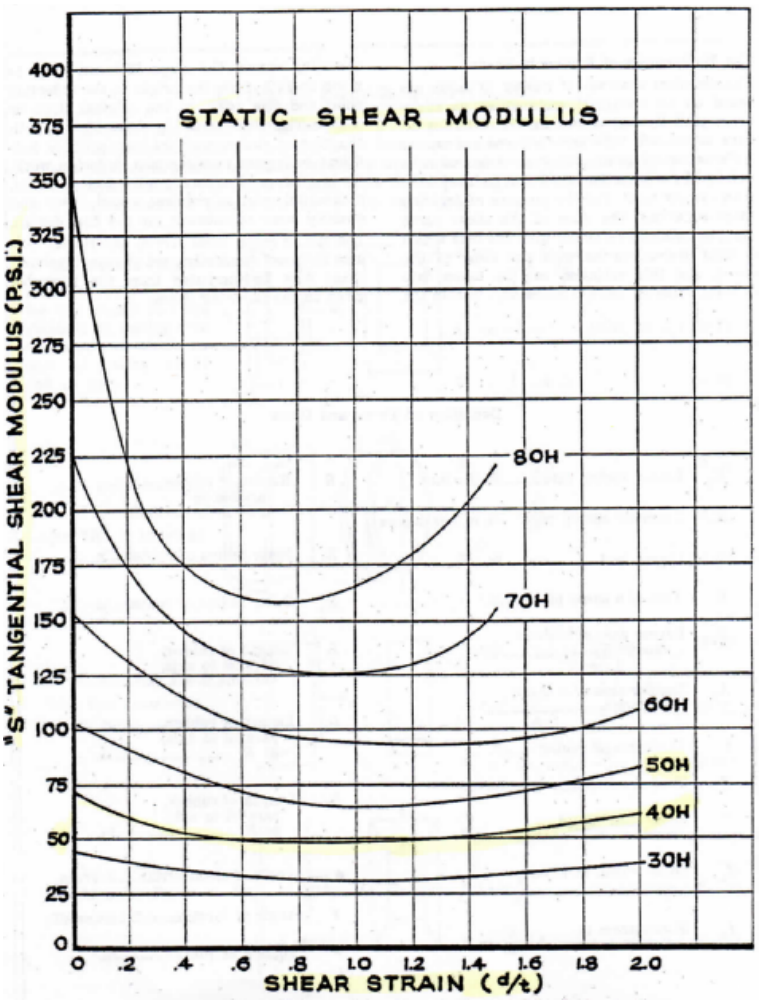

Figure 4.9 - Values of Tangential or Slope Static Moduli for Rubber in Shear (Handbook of Molded and Extruded Rubber, Good Year, second edition, 1959)

CHAPTER 5
EFFECT OF SHRINKAGE ON CRACKING

5.1 General

Concrete members start to crack as the tensile stress exceeds the tensile strength of concrete. Cracks in concrete may lead to severability problems such as leakage which, accordingly will result in corroded reinforcement that may jeopardise the structural strength and integrity. It should be noted that shrinkage is one of the main causes for cracking in concrete, especially in large concrete members such as walls when shrinkage movement is prevented.

Typically, the foundations of concrete tanks are constructed before the walls. Therefore, the tank wall will have different shrinkage movement than the foundation. For tanks with hinged and fixed base conditions, the relative movement between the wall and the base is prevented because the wall and base are rigidly connected. Hence, this restraint induces tensile stresses in concrete and may cause cracking in the wall.

Cracking due to the volumetric change can be minimized by providing the proper curing at the early age of concrete. The effect of shrinkage can also be controlled by providing movement joints within or between the concrete members since these joints allow members to move freely. However, these joints may cause serviceability and maintenance problems, and also, they may affect the design and the cost associated with tank construction.

Minimum area of reinforcement is typically specified by design codes in order to accommodate the shrinkage and temperature effects. However, the minimum reinforcement will not prevent shrinkage cracking; instead, it will control the size and the number of cracks. This study investigates the effect of shrinkage on cracking in ground-supported, open top, RC circular tanks with free, hinged, and fixed base conditions.

5.2 Concrete shrinkage

Shrinkage of concrete is defined as the reduction in the concrete volume. There are different types of shrinkage in a concrete member as defined in (ACI 224R-01 2008) such as drying shrinkage and carbonation shrinkage.

Drying shrinkage is caused by the loss of water in concrete mixture due to evaporation of water in capillary pores in the hardened concrete. Drying shrinkage along with changes in moisture content are an inherent characteristic of hydraulic-cement paste in concrete (ACI 224R-01 2008).

Carbonation shrinkage results from the chemical effects of carbon dioxide in the atmosphere on the products of hydration. From the reaction of carbon dioxide and hydration products, calcium carbonate will form and absorbs water available in capillary pores. However, in high-quality concrete with low porosity, carbonation shrinkage is of minor concern in the overall shrinkage of the structure because carbon dioxide does not penetrate much into the surface of the concrete member (ACI 224R-01 2008).

Shrinkage of concrete develops slowly over time and makes it difficult to obtain an accurate prediction from short-term laboratory tests. In general, a coefficient variation of 20% is used in predicting long-term shrinkage of concrete. A typical value for the final shrinkage strain of concrete in most structures is 600×10^{-6} mm/mm (ACI 224R-01 2008).

However, if the concrete members are restrained, shrinkage will result in concrete cracking and tensile stress will develop in concrete members accordingly.

5.3 Member restraints

All concrete members are relatively restrained either by member supports or certain components of the members such as embedded parts or reinforcement. Preventing any volumetric changes in the form of movement restraints will induce internal tensile or compressive stresses in concrete members as a result of contraction or expansion. However, the main concern is the restraint conditions induce tensile stresses in concrete which may lead to cracking in concrete.

The degree of restraint is the ratio of actual stress in concrete resulting from volume change to the stress that would result if concrete is completely restrained (ACI 207.2R-07 2007).

Alternatively, the degree of restraint is the ratio of strain of concrete caused by restraint to the strain that would occur if concrete is not restrained (ACI 207.2R-07 2007). Generally, there are two types of restraint for the concrete members; internal and external restraint.

Internal restraint is due to the non-uniform volumetric change over on a cross section within a concrete member. This restraint takes place within large concrete members such as walls and slabs. In this case, the interior temperature of concrete is greater than surface temperature, or drying shrinkage is different from outside to inside of the member.

The external restraint arises when fresh concrete is placed against old (hardened) concrete or any other material such as steel plates or reinforcement. Therefore, the tank wall movement at tank base will be restrained by the foundation which is constructed in advance. Hence, the degree of restraint decreases considerably away from the restraint location (tank foundation). It should be noted that the contact surface between new and old concrete in consecutive lifts of the tank wall are considered as external restraint to some degree. Also, the external restraint depends on the relative dimensions, strength, and modulus of elasticity of concrete and restraining material. However, in this study, the tank walls are assumed to be placed at one time.

5.4 Principal of minimum reinforcement and theory of shrinkage cracking

In reinforced concrete members, all the cracking force is transferred to the member reinforcement that crosses the crack. As the concrete shrinkage takes place, the concrete contracts, while the restraints prevent movement of the member at the restrained locations.

Considering that the force required to cause cracking in concrete, N_{cr}, is given by

$$N_{cr} = A_c f_{cr} \quad (5\text{-}1)$$

where,

A_c is the area of concrete section
f_{cr} is the cracking failure stress of concrete

The strength of the member reinforcement is specified by $A_s f_y$ where, A_s is the area of reinforcement and f_y is the yield stress of the reinforcement.

In order to prevent yielding of reinforcement on the first crack, and therefore spread cracks in the concrete member, the following condition should be satisfied:

$$A_s f_y > A_c f_{cr} \tag{5-2}$$

By substituting $\rho_{min} = \frac{A_s}{A_c}$ in equation 5–2 and rearranging

$$\rho_{min} > \frac{f_{cr}}{f_y} \tag{5-3}$$

where,
ρ_{min} is the minimum required reinforcement ratio for shrinkage and temperature

This provides the principles of the minimum reinforcement ratio required to control cracking. However, the actual equation incorporates some factors taking account for different types of loading, non-uniform distribution of stresses within the concrete section, and exposure conditions (Ziaolhagh 2008).

Furthermore, the mechanism of direct tension cracking in reinforced concrete members has been developed by Gilbert (1992) as a rational approach for the determination of the number and spacing of cracks and the average crack width in a fully restrained member and subjected to an axial restraining force caused by shrinkage. It should be noted that, this method is used to calculate the stresses in reinforcement of circular tank in order to verify the results of FE analysis in this Chapter.

A reinforced concrete member in considered to be restrained at both ends and subjected to shrinkage strain. As concrete shrinks, an axial restraining force, N, equal to $A_c f_t$ starts to develop with time, where f_t is the tensile stress in concrete.

As shown in Figure 5-1, when the stress in concrete at a specific location reaches the tensile strength of concrete, the first crack starts to develop; then, the restraining force reduces, while the stress in concrete away from the crack location is less than the tensile strength of concrete. At crack location, the entire restraining force is carried by reinforcement and the stress in concrete is zero.

In the region adjacent to the crack, the concrete and steel stresses vary considerably. The reinforcement is in tension at crack location and is in compression in the region away from the crack. The tensile stress in reinforcement at the first crack, σ_{st1}, drops gradually to the compressive stress, σ_{sc1}, over the distance z away from the crack. The stress in concrete is zero at the first crack location and decreases gradually to the compressive stress, σ_{c1}, over the distance z away from the crack. An approximation of z is given as:

$$z = \frac{d_b}{10\rho} \qquad (5\text{-}4)$$

where;
d_b is the bar diameter
ρ is the reinforcement ratio

This expression was proposed earlier by Favre (1983) for a member containing deformed bars or welded wire mesh.

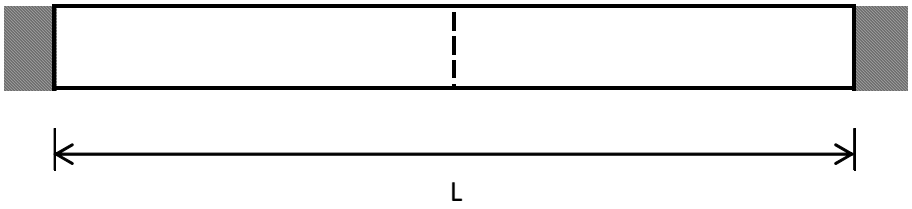

(a)

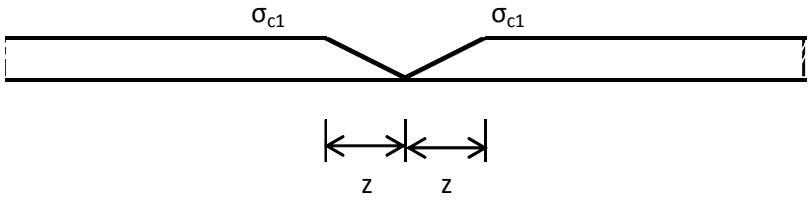

(b)

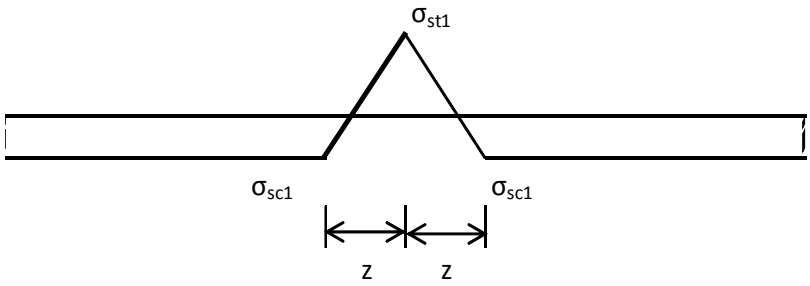

(c)

Figure 5.1 – Shrinkage cracking after first crack; (a) Crack pattern, (b) Concrete stresses, (c) Reinforcement stresses

Applying compatibility and equilibrium equations, Gilbert (1992) derived expressions for the restraining force N_{cr1}, stress in concrete σ_{c1}, tensile stress in reinforcement σ_{st1}, and compressive stress in reinforcement σ_{cst1} immediately after the first crack.

$$N_{cr1} = \frac{n\rho f_{cr1} A_c}{C_1 + n\rho(1 + c_1)} \quad (5\text{-}5)$$

$$\sigma_{c1} = \frac{N_{cr1}(1 + c_1)}{A_c} \quad (5\text{-}6)$$

$$\sigma_{st1} = \frac{N_{cr1}}{A_s} \quad (5\text{-}7)$$

$$\sigma_{sc1} = C_1 \sigma_{st1} \quad (5\text{-}8)$$

where;

$$C_1 = \frac{2z}{(3L - 2z)} \quad (5\text{-}9)$$

n is the ratio of the modulus of elasticity of reinforcement to concrete
f_{cr1} is the tensile strength of concrete at the time of first cracking
A_s is the area of reinforcement
L is the total length of the member

As the shrinkage continue, the restraining force and stress in the concrete member away from the crack location increase. The second crack takes place when the tensile capacity of concrete at that location is exceeded. Additional cracks may occur as the shrinkage strain continues to increase with time. Accordingly, as new cracks develop, the stiffness of the concrete member reduces, the amount of shrinkage strain required to form new cracks increases. Eventually, the

process continues until the final crack pattern is developed. The factors affecting the number of cracks and the average crack width are the aspect ratio of the member, reinforcement ratio, bond stress between concrete and steel, shrinkage strain, and concrete properties (Gilbert 1992).

The generic final crack pattern is shown in Figure 5-2. The final tensile stress in reinforcement at crack, σ_{st}, decreases gradually to the final compressive stress in the reinforcement, σ_{sc}, over the distance z away from the crack as described earlier in this chapter. Also, the stress in concrete is zero at crack location and increases gradually to the final stress, σ_{ci}, over the distance z away from the crack which is assumed to remain the same as the case for the first cracking. The second assumption is that the final cracks are equally distributed along the member length. Therefore, the minimum number of cracks m, is equal the member length, L, divided by crack spacing, s.

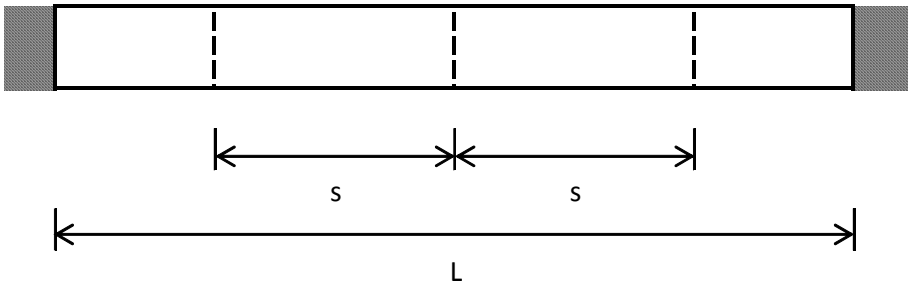

(a)

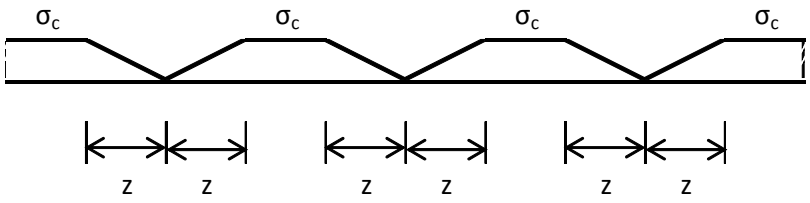

(b)

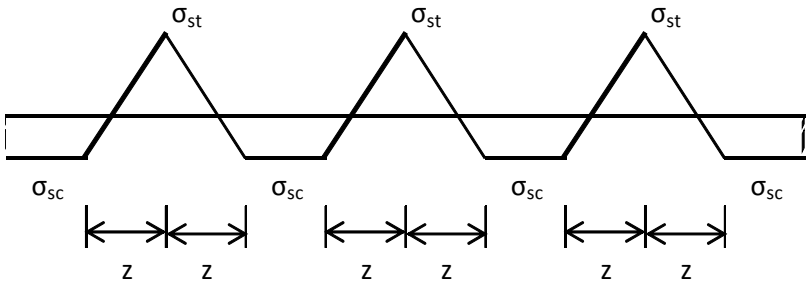

(c)

Figure 5.2 – Final shrinkage cracking; (a) Cracks pattern, (b) Concrete stresses, (c) Reinforcement stresses

Applying compatibility and equilibrium equations, Gilbert (1992) developed the following relationships for the final restraining force N_{cr}, final stress in concrete σ_c, final tensile stress in reinforcement σ_{st}, final compressive stress in steel σ_{sc}, crack spacing s, and average crack width w:

$$N_{cr1} = \frac{n_e A_s}{C_2} (\sigma_{av} + \varepsilon_{sh} E_{ce}) \quad (5\text{-}10)$$

$$\sigma_{st} = \frac{N_{cr}}{A_s} \quad (5\text{-}11)$$

$$\sigma_{sc} = - C_2 \sigma_{st} \quad (5\text{-}12)$$

$$\sigma_c = \frac{N_{cr} - \sigma_{sc} A_s}{A_c} \quad (5\text{-}13)$$

$$S = \frac{2z(1 + C_3)}{3C_3} \quad (5\text{-}14)$$

$$w = -\left[\frac{\sigma_c}{E_{ce}} (s - z) + \varepsilon_{sh} s\right] \quad (5\text{-}15)$$

where,

$$C_2 = \frac{2z}{3s - 2z} \tag{5-16}$$

$$C_3 = \frac{-n_e\rho\,(\sigma_{av} + \varepsilon_{sh}\,E_{ce})}{n_e\rho(\sigma_{av} + \varepsilon_{sh}\,E_{ce}) + f_{cr}} \tag{5-17}$$

n_e is the ratio of the modulus of elasticity of the reinforcement to the effective modulus of elasticity of concrete

E_{ce} is the effective modulus of elasticity of concrete given as:

$$E_{ce} = \frac{E_c}{1 + \phi} \tag{5-18}$$

ϕ is the final creep coefficient of concrete (2.5)

E_c is the modulus of elasticity of concrete

σ_{av} is the average stress in concrete given as:

$$\sigma_{av} = \frac{(\sigma_{c1} + f_{cr})}{2} \tag{5-19}$$

f_{cr} is the final tensile strength of concrete

ε_{sh} is the final shrinkage strain (-600×10^{-6})

5.5 Degree of restraint

In concrete members, the connections between concrete members and other parts of the structure, such as foundations, provide restraint to shrinkage which may cause the concrete to crack. The degree of restraint is the ratio of the actual stresses in the concrete resulting from volume change to the stress that would result if the concrete was completely restrained (ACI 207.2R-07 2007). Therefore, the degree of restraint is:

$$K_R = \frac{f_{c,a}}{f_{c,r}} \quad (5\text{-}20)$$

where,

K_R is the degree of restraint

$f_{c,a}$ is the actual stress in concrete

$f_{c,r}$ is the stress in concrete if the member is fully restrained

Therefore, the total strain in the concrete member that is subjected to shrinkage is the summation of the shrinkage strain and the strain caused by the restraint due to the parts connected to this member.

$$\varepsilon_{total} = \varepsilon_{shrinkage} + \varepsilon_{restraint} \quad (5\text{-}22)$$

where,

ε_{total} is the total strain in concrete

$\varepsilon_{shrinkage}$ is the shrinkage strain

$\varepsilon_{restraint}$ is the restraint strain in concrete

The restraint strain in concrete is in the opposite direction of shrinkage strain. Therefore, tensile stresses develop in concrete. For uncracked concrete section, the actual stress in concrete, $f_{c,a}$, is

$$f_{c,a} = E_c \, \varepsilon_{restraint} = E_c \, (\varepsilon_{total} - \varepsilon_{shrinkage}) \quad (5\text{-}23)$$

When the concrete member is fully restrained, the total strain is equal to zero. Therefore, the stress in concrete, f_{cr}, is

$$f_{cr} = E_c \varepsilon_{restraint} = E_c \, (- \varepsilon_{shrinkage}) \quad (5\text{-}24)$$

By substituting Equation 5-23 in Equation 5-24 the degree of restraint, K_R, can be expressed alternatively as

$$K_R = -\frac{\varepsilon_{total} - \varepsilon_{shrinkage}}{\varepsilon_{shrinkage}} = -\frac{\varepsilon_{restraint}}{\varepsilon_{shrinkage}} \quad (5\text{-}25)$$

In addition, bonded reinforcement in reinforced concrete members provides restraint to shrinkage. As concrete shrinks, compressive stresses develop in the reinforcement, and the reinforcement imposes an equal and opposite tensile force on the concrete.

When a reinforced concrete member is subjected to shrinkage, the total strain in the concrete will be caused by shrinkage and restraint from reinforcement. Due to the bond between concrete and reinforcement, the total strain in concrete is the same as the total strain in the reinforcement. Therefore,

$$\varepsilon_s = \varepsilon_{total} = \varepsilon_{shrinkage} + \varepsilon_{restraint} \quad (5\text{-}26)$$

$$\varepsilon_s = \frac{f_s}{E_s} \quad (5\text{-}27)$$

$$\varepsilon_{restraint} = \frac{f_c}{E_c} \quad (5\text{-}28)$$

Accordingly,

$$\varepsilon_{shrinkage} = \varepsilon_s - \varepsilon_{restraint} = \frac{f_s}{E_s} - \frac{f_c}{E_c} \quad (5\text{-}29)$$

where,
ε_s is the strain in reinforcement
f_s is the stress in reinforcement
E_s is the modulus of elasticity of steel

When reinforced concrete member is subjected to shrinkage, the concrete will be under tension due to restraint caused by reinforcement and the reinforcement is under compression, therefore,

$$f_c A_c = - f_s A_s \tag{5-30}$$

$$f_s = -\frac{f_c}{\rho} \tag{5-31}$$

$$\varepsilon_{shrinkage} = \varepsilon_s - \varepsilon_{restraint} = \frac{f_s}{E_s} - \frac{f_c}{E_c} = -\frac{f_c}{E_c}\left(1 + \frac{1}{n\rho}\right) \tag{5-32}$$

where $\rho = \frac{A_s}{A_c}$ and $E_s = nE_c$

By substituting $\varepsilon_{restraint}$ and $\varepsilon_{shrinkage}$ from Equations 5-28 and 5-32, respectively, in Equation 5-25 the degree of restraint caused by reinforcement is

$$K_R = \frac{1}{1 + \frac{1}{n\rho}} \tag{5-33}$$

5.6 Computer model and finite element analysis

The FE analysis is performed using ABAQUS (ABAQUS/CEA 2008) version 6.8.3 using the interactive and graphical technique. Material properties, loads and boundary conditions are assigned to the geometry. In this study, FE analysis is performed in order to investigate the effect of concrete shrinkage on stresses in concrete and steel reinforcement. The results of analysis under shrinkage effect would indicate the level of cracking in the tank walls prior to seismic effect. The results of this study will be used as a precondition when the tanks are analyzed under seismic loading, which are discussed in the subsequent chapters. For this purpose, three circular ground-supported tanks having different aspect ratios (diameter/height ratios) are modeled using 3-D FE technique. Furthermore, the nonlinear behavior of concrete and steel reinforcement is considered. The concrete shrinkage is applied to the FE model in the form of thermal contraction load. Moreover, in the analysis, the tank walls are assumed to be rigidly anchored to the base. As a result, no sliding may occur. However, for tanks with free base, movement is allowed in the radial direction.

For all tank configurations, design loads are calculated based on ACI 350.3-06 (2006), and the tank walls are designed accordingly. However, for the purpose of comparison the thicknesses of the walls are considered to be the same for all tanks. The dimensions, design procedure, and other properties of the tanks are fully explained in the following subsections.

5.6.1 Tank configuration and design parameters

The tank diameter (D) is considered to be 40 m. Various water depths (H_L) are considered in the analysis with H_L equal to 3 m, 6 m and 9 m corresponding to wall heights (H_w) equal to 3.25m, 6.5m and 9.6m, respectively. These tanks are referred to as Tanks 1, 2 and 3, respectively. For the purpose of direct comparison, the wall thickness (t_w) is assumed to be 400 mm for all cases. The effect of tank support conditions is also considered in this study. Therefore, hinged, fixed and free support conditions are investigated. Hinged, fixed and free supports are referred to as H, F and FR, respectively. The hinged and fixed base conditions are considered for Tanks 1, 2 and 3. In addition, in order to investigate the effect of the base restraint on the results, the free base condition (no restraint in radial direction) is considered for Tank 2 only. It should be noted that, the FE results for Tank 2FR is used for model verifications as described later in this chapter.

In this study, the tanks are designed according to ACI 350-06 (2006) for the combined effect of hydrostatic and hydrodynamic loads. The hydrodynamic forces are calculated representing high seismic zone having S_s = 150% and S_1 = 60%. The tanks are designed to safely resist the load combinations including hydrostatic and hydrodynamic loads according to ACI 350-06 (2006): thus, all strength and serviceability requirements are satisfied. For all tanks, the wall reinforcement is considered to be uniform along the tank height, in which the design is performed based on maximum forces along the tank wall. The detailed design information such as support condition, water depth, wall height, size of reinforcement, and spacing between bars for Tanks 1, 2, and 3 are shown in Table 5.1.

Table 5.1 – Tanks dimensions and reinforcement

				Horizontal Bars, Inside and Outside		Vertical Bars, Inside Face		Vertical Bars, Outside Face	
Tank No.	Base condition	Water Depth H_L(m)	Wall Height H_w (m)	Bar Size	Spacing (mm)	Bar Size	Spacing (mm)	Bar Size	Spacing (mm)
1H	Hinged	3.00	3.25	20M	250	20M	250	20M	250
2H	Hinged	6.00	6.50	20M	220	20M	250	20M	250
3H	Hinged	9.00	9.60	25M	200	20M	250	20M	250
1F	Fixed	3.00	3.25	20M	250	20M	250	20M	250
2F	Fixed	6.00	6.50	20M	250	20M	200	20M	250
3F	Fixed	9.00	9.60	25M	240	25M	170	20M	250
2FR	Free	6.00	6.50	20M	220	20M	250	20M	250

5.6.2 Finite element model

The computer program ABAQUS (ABAQUS/CEA 2008) is used in performing the analysis using shell elements. Both linear and nonlinear behavior of construction material, concrete and reinforcement, are considered in the analysis.

Since the wall thickness is significantly smaller than the wall height and tank diameter, using shell elements to model the tank wall is considered appropriate. In this case, the element thickness is defined through the section property definition. The entire tank is modeled using four-node quadrilateral shell elements. The conventional shell elements that are used in the analysis have three displacement and three rotational degrees of freedom at each joint. The number of elements along the wall height is considered as four, seven, and ten elements for Tanks 1, 2 and 3, respectively. A typical tank model is shown in Figure 5.3 which represents Tank 3F.

Along the water height (H_w), the tank wall is divided equally into 1.0 meter long elements, where the number of elements along the wall up to the water height is considered three, six, and nine

elements for Tanks 1, 2 and 3, respectively. One additional element is considered above the water level, thus the length of the very top element above water level is considered to be equal to the tank freeboard which is equal to 0.25m, 0.5m and 0.6m for Tanks 1, 2 and 3, respectively. In order to maintain the aspect ratio close to one, each tank circumference is divided into 128 equal elements where the element size along the tank circumference is around 1 m. Accordingly, the total number of elements for Tanks 1, 2 and 3 are 512, 896 and 1280, respectively. However, mesh sensitivity study is carried on in order to investigate the effect of the element size on the results of FE analysis. The results of sensitivity study will be discussed in detail later in this chapter. The tank supports are defined by applying boundary conditions that restrain the movements or rotations in the desire directions.

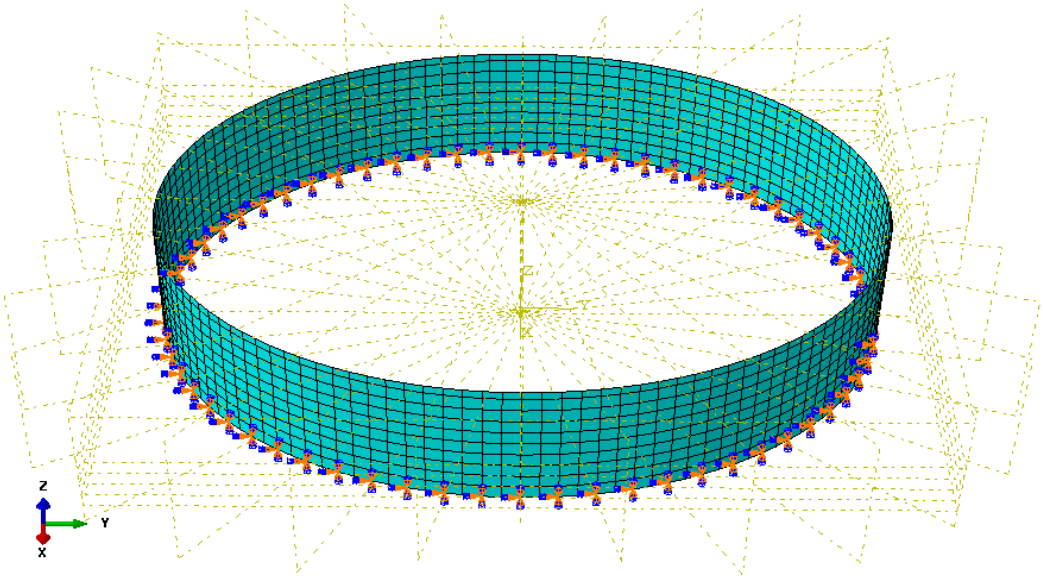

Figure 5.3 – Finite element model for Tank 3F - ABAQUS/CAE

Reinforcement in concrete is provided by means of rebars. Rebars are one-dimensional strain theory elements (rods). The rebars are defined embedded in oriented surfaces. They are typically used with elastic-plastic material behavior and are superposed on a mesh of standard element types used to model the plain concrete. Effects associated with the rebar/concrete interface, such as bond slip and dowel action, are modeled approximately by introducing some “tension stiffening” into the concrete cracking model to simulate load transfer across cracks through the rebar.

5.6.3 Material properties

For linear elastic analysis, the linear elastic material behavior were specified as follows: The specified compression strength of concrete (f'_c) and yield strength of reinforcement (f_y) are considered 30 MPa and 400 MPa respectively, where the modulus of elasticity of concrete (E_c) and reinforcement (E_s) are taken as 26000 MPa and 200000 MPa respectively. The concrete section was considered as uncracked section.

For nonlinear FE analysis, the nonlinear properties of construction materials as described in Chapter 4 are considered in the analysis in order to study the nonlinear response of the tank walls under shrinkage effect. As described in detail in Chapter 4, the stresses in concrete shell of the circular tanks are due to bending and bending plus axial stresses. Therefore, the Modified Hognestad method (MacGregor 1997) is used as an analytical approximation for the compressive stress-strain curve for concrete. A reasonable starting point for relatively heavily reinforced concrete modeled with a fairly detailed mesh is to assume that the strain softening after failure reduces the stress linearly to zero at a total strain of about 10 times the strain at failure. The tensile strain at failure in normal concrete is typically 10^{-4}, which suggests that tension stiffening that reduces the stress to zero at a total strain of about 10^{-3} is reasonable. The analytical approximation to the tension and compression stress-strain curve for reinforcement is modeled using elastic-plastic curve for grade 400 reinforcing bars with yield strength f_y = 400 Mpa, and maximum strain at ultimate load which equals to 0.008.

For both linear and nonlinear FE analysis, the following material proprieties are considered in FE analysis:

Thermal expansion coefficient of concrete (α_c) = $1x10^{-5}$

Thermal expansion coefficient of reinforcement (α_s) = 0.0

Poisson's ratio of concrete (ν_c) = 0.18

Poisson's ratio of reinforcement (ν_s) = 0.0

Shrinkage strain of concrete ($\varepsilon_{shrinkage}$) = - 600 x 10^{-6} mm/mm = - 600 $\mu\varepsilon$

It should be noted that, in RC structures, concrete is expected to shrink and not the reinforcement, therefore, the thermal expansion coefficient of steel is assumed to be zero.

As discussed in Chapters 2 and 4, concrete damaged plasticity (CDP) model is used in this study since it is the most suitable concrete model for dynamic analysis. However, in order to verify the results of the shrinkage effect, Tank 2F is analyzed using both brittle cracking (BC) model and concrete damaged plasticity model. The results of this comparison are discussed later on in this Chapter under "Sensitivity study".

5.6.5 Loads

Typically for concrete structures the shrinkage strain of concrete ($\varepsilon_{shrinkage}$) is equal to 600×10^{-6} mm/mm (600 με) (ACI 224R-01 2008).

Considering that,

$$\varepsilon_{shrinkage} = \alpha_c \Delta T \qquad (5\text{-}34)$$

By knowing that $\varepsilon_{shrinkage} = -600 \times 10^{-6}$ and $\alpha_c = 1 \times 10^{-5}$, then $\Delta T = -60^{o}$ C

Therefore, in order to simulate concrete shrinkage strain, a change of temperature -60^{o} C (contraction) is applied to the tank walls.

5.7 Results of analysis

Tanks 1, 2 and 3 as specified in Section 5.7 are subjected to shrinkage strain by applying thermal contraction to the tank walls. Therefore, the total strain in the wall is caused by shrinkage and restraint of connecting parts such as tank supports. The total strain (ε_{total}) is derived from the analysis, knowing that the shrinkage strain ($\varepsilon_{shrinkage}$) is 600×10^{-6}; hence, the restraint strain ($\varepsilon_{restraint}$), which cause cracking in concrete can be determined from Equation 5-22.

The results of linear and nonlinear FE analysis for Tanks 1, 2 and 3 with different boundary conditions are presented in the following sections.

5.7.1 Free base condition and model verification

Figure 5.4 shows the total strain, restraint strain, stress in reinforcement, and hoop stress in concrete for Tank 2FR. The negative and positive values represent compression and tension stresses, respectively.

As shown in Figure 5.4 (a), the tank wall is contracting. Since no external restraint in the radial direction is provided at the tank base, the wall behavior is the same for both linear and nonlinear material models. However, the wall reinforcement provides a form of restraint to shrinkage movement. Therefore, the horizontal restraint strain is not zero as shown in Figure 5.4(b). The horizontal restraint strain is the difference between the total strain and shrinkage strain of concrete. Also, since the reinforcement is uniformly distributed, the wall response is the same along the height.

As shown in Figure 5.4(c), horizontal reinforcing bars are under compression (σ_{sc} = 114 MPa), and the stress in horizontal reinforcing bars is also proportional to the total horizontal strain.

Figure 5.4(d) shows that the concrete is under tension. Also, the horizontal stress in concrete is proportional to the horizontal restraint strain and the tensile stress in concrete is well below the concrete tensile strength. Accordingly, no cracks developed in concrete as the shrinkage movement is not restrained.

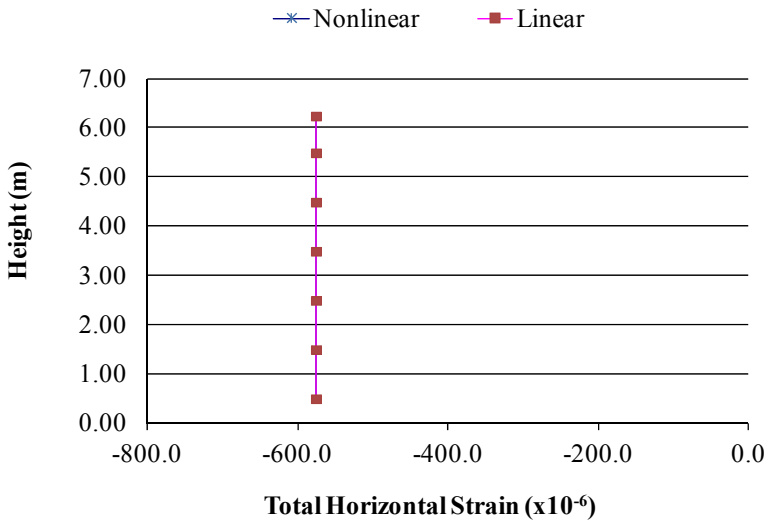

(a)

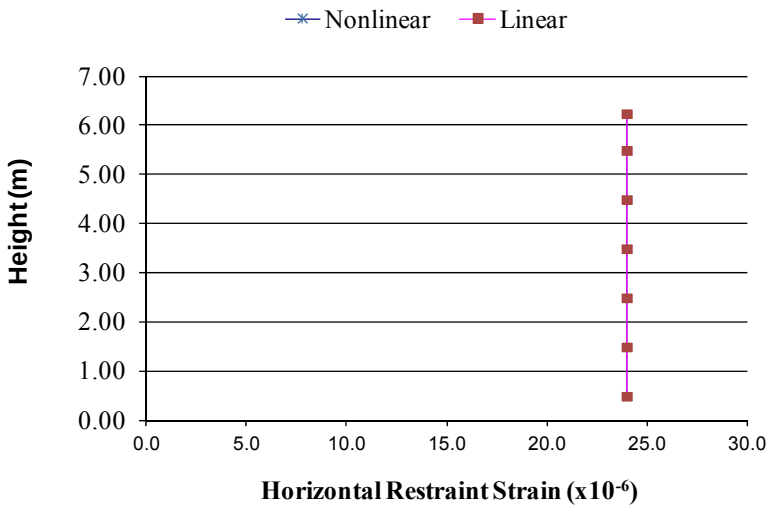
Nonlinear
Linear
7.00
6.00
5.00
4.00
3.00
2.00
1.00
0.00
Height (m)
0.0
5.0
10.0
15.0
20.0
25.0
30.0
Horizontal Restraint Strain (x10-6)

(b)

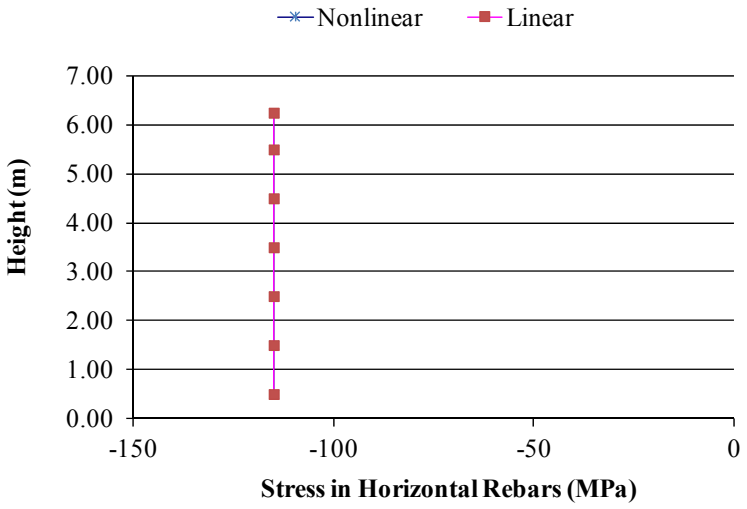
Nonlinear
Linear
7.00
6.00
5.00
4.00
3.00
2.00
1.00
0.00
Height (m)
-150
-100
-50
0
Stress in Horizontal Rebars (MPa)

(c)

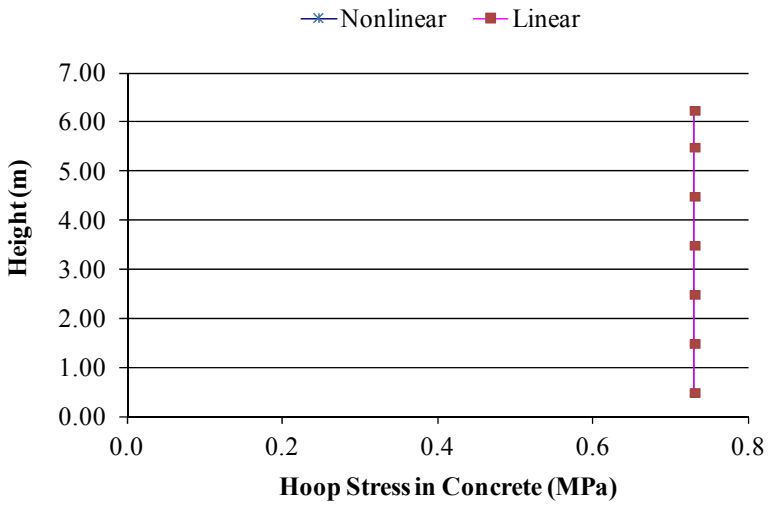

(d)

Figure 5.4 – Strain and stress distribution for Tank 2FR; (a) Total Horizontal strain, (b) Horizontal restraint strain, (c) Stress in horizontal rebars, (d) Hoop stress in concrete

In order to verify the results of the FE model, the stresses in reinforcing steel (σ_{sc}) are calculated, for Tank 2FR, under the effect of shrinkage strain using equations indicated in section 5.5 as follows:

The concrete and steel areas are:

$A_c = 1{,}000 \text{x} 400 = 400{,}000 \text{ mm}^2 / \text{m}$

$A_s = 2{,}727 \text{ mm}^2 / \text{m}$

The reinforcement ratio is

$$\rho = \frac{2{,}727}{400{,}000} = 0.0068$$

From Equation 5-18

$$E_{ce} = \frac{26{,}000}{1 + 2.5} = 7429 \text{ MPa}$$

And then n_e is

$$n_e = \frac{200{,}000}{7429} = 27$$

For comparison, the creep effect is neglected, n and E_c are used instead of n_e and E_{ce}. By applying the same equation, n is equal

$$n = \frac{200{,}000}{26{,}000} = 7.7$$

From Equation 5-4

$$z = \frac{20}{10\text{x}0.0068} = 294 \text{ mm}$$

By considering L equal to tank circumferential = π x D, Equation 5-9 gives

$$C_1 = \frac{2\text{x}294}{(3\text{x}125{,}664 - 2\text{x}294)} = 0.0016$$

Using Equations 5-5 and 5-6, the restraining force and stresses in concrete immediately after first crack are

$N_{cr1} = 1{,}007{,}598$ N / m

$\sigma_{c1} = 2.52$ MPa

Equation 5-19 gives

$\sigma_{av} = 2.56$ MPa

From Equation 5-17

$C_3 = 0.36$

From Equation 5-14 the crack spacing is

$$S = \frac{2x294(1 + 0.36)}{3x0.36} = 546 \text{ mm}$$

From Equation 5-16

$$C_2 = \frac{294}{3x546 - 2x294} = 0.28$$

Using Equations 5-10, 11, and 12, the final compressive stress in horizontal bars is:

$N_{cr} = 977{,}902$ N / m

$$\sigma_{st} = \frac{997{,}902}{2{,}727} = 359 \text{ MPa}$$

$\sigma_{sc} = -0.28x359 = -100.5$ MPa

The σ_{sc} based on FE analysis is equal to 114 MPa as indicated before, which is found to be in agreement with the expressions derived by Gilbert (1992) with only 12% difference in the results. It should be noted that, the expressions derived by Gilbert (1992) are for a concrete member restrained at both ends, which may explain the minor difference in the results. Therefore, the results of the FE analysis are considered to be reliable and accurate.

5.7.2 Hinged base condition

Figures 5.5 (a, b, c) present the maximum hoop stresses in concrete in the vicinity of cracks along the wall height for Tanks 1H, 2H and 3H.

According to the material properties defined in Chapter 4, the cracking failure stress of concrete (f_t) and the modulus of elasticity of concrete (E_c) equal 2.6 MPa and 26,000 MPa, respectively. Therefore, the cracking strain of concrete (ε_{crack}) is:

$$\varepsilon_{crack} = \frac{f_t}{E_c} = \frac{2.6}{26000} = 100x10^{-6} \qquad (5\text{-}35)$$

The cracking failure stress of concrete is shown as dashed line on all figures. As shown in the Figures, cracks develop to nearly the mid height from the base. Also, the hoop stress in the concrete wall decreases from the base to the top. Consequently, cracks are wider near the bottom of the tank walls. The results of this study indicate that the concrete will crack under shrinkage effect, and therefore loses its strength. Hence, it is appropriate to neglect the tensile strength of concrete in the tank design for hinged based walls.

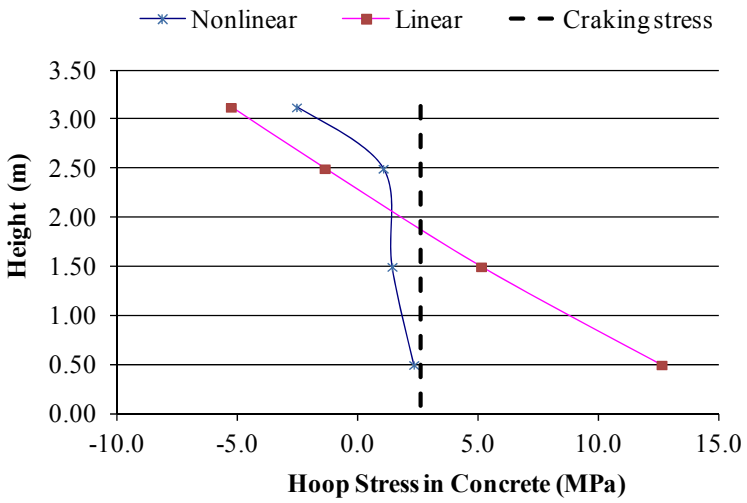

(a)

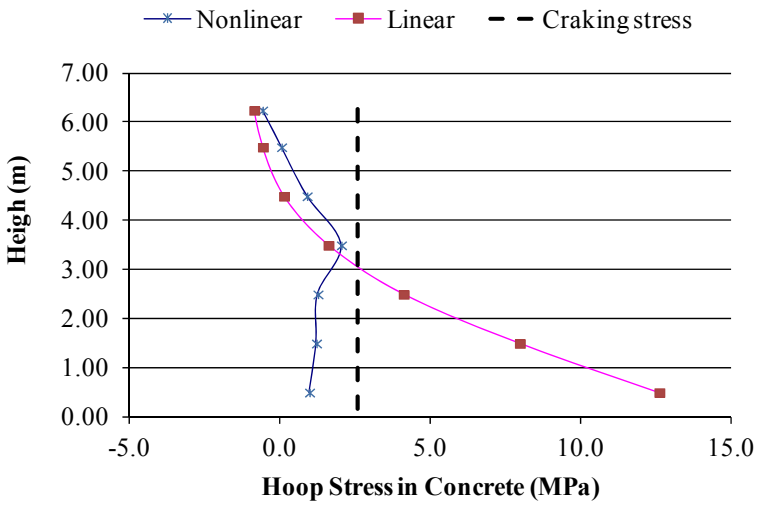

(b)

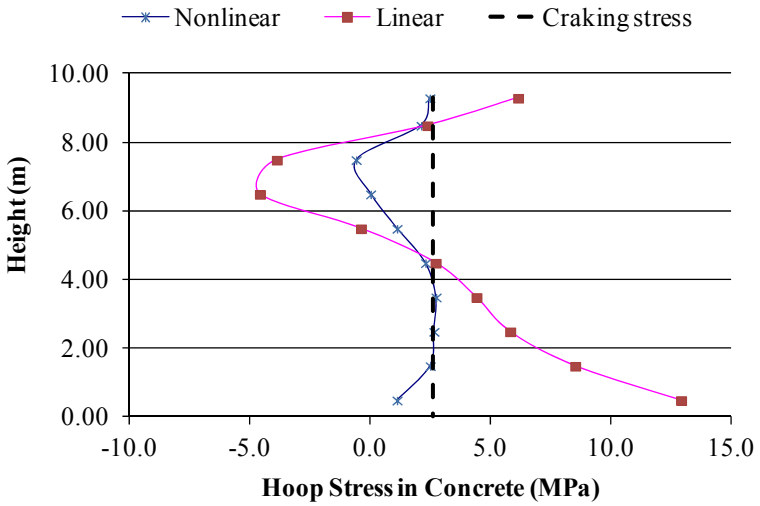

(c)

Figure 5.5 – Maximum hoop stress in concrete; (a) Tank 1H, (b) Tank 2H, (c) Tank 3H

5.7.3 Fixed base condition

Figures 5.6 (a, b, c) present the maximum hoop stresses in concrete in the vicinity of cracks along the wall height for Tanks 1F, 2F and 3F.

As shown in the Figures, cracks develop to nearly the mid height from the base. Also, the hoop stress in concrete wall decreases from the base to the top. Consequently, cracks are wider near the bottom of the tank walls. Similar to hinged base condition, the results of this study also indicate that the concrete will crack under shrinkage effect. Therefore, it is appropriate to neglect the tensile strength of concrete in the tank design for fixed based walls.

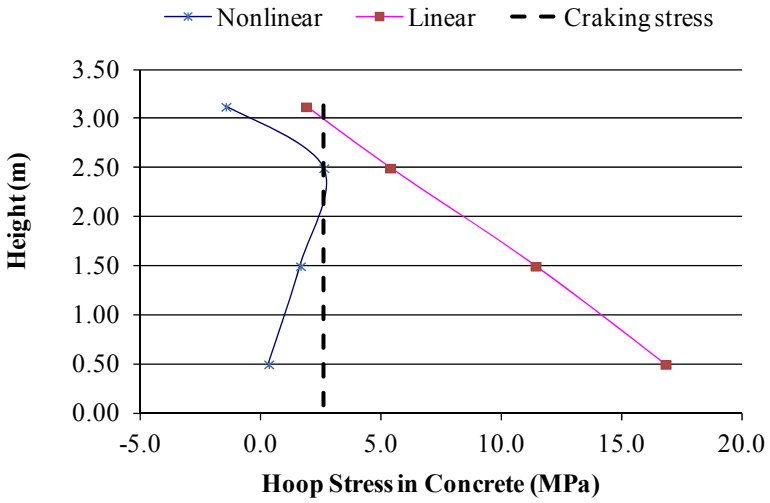

(a)

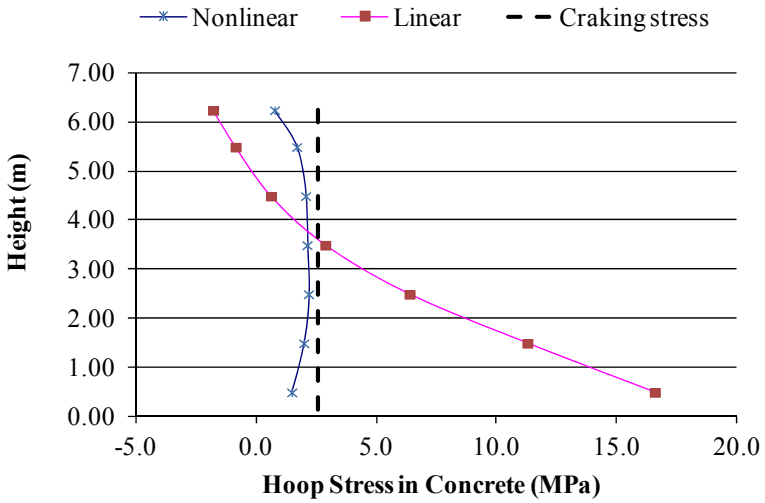

(b)

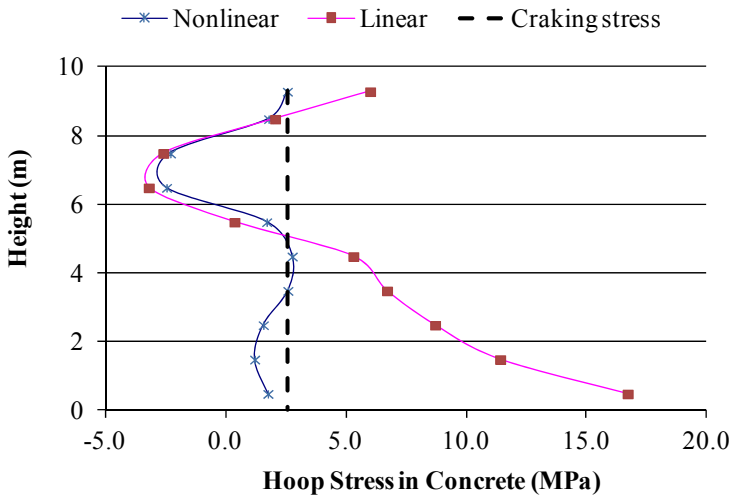

(c)

Figure 5.6 – Maximum hoop stress in concrete; (a) Tank 1F, (b) Tank 2F, (c) Tank 3F

5.7.4 Sensitivity study

A sensitivity study is carried out in order to investigate the effect of the mesh size and the proposed concrete model on the results of the FE analysis. This sensitivity study is performed for Tank 2F, where the elements sizes are taken as 1.0 m x 1.0 m, 0.5 m x 0.5 m, and 0.25 m x 0.25 m. These three different mesh sizes are referred to as Mesh 1 (M1), Mesh 2 (M2), and Mesh 3 (M3), respectively. The length of the element above the water level is taken as 0.5m for models M1 and M2, and 0.25 m for model M3. Therefore, the number of elements along the wall height is considered as seven, thirteen, and twenty six for models M1, M2 and M3, respectively. Furthermore, in order to verify the results of concrete model that is used in the analysis, the concrete is modeled using concrete damaged plasticity (CDP) model and brittle cracking (BC) model.

As shown in Figure 5.7, the results of this study indicate that the selected element size does not have a major effect on the results; therefore, the selected mesh size is considered appropriate. Also, as shown in the same Figure, the results of both concrete models (CDP and BC) are very similar. Therefore, the concrete damaged plasticity model is also considered appropriate.

Furthermore, Tank 2F is analyzed using different values for shrinkage strain (ε_{sh}) in order to study the effect of ε_{sh} on concrete stress. As shown in Figure 5.8, the results of FE analysis indicate that cracks start to develop in concrete at shrinkage strain of -120 x 10^{-6}.

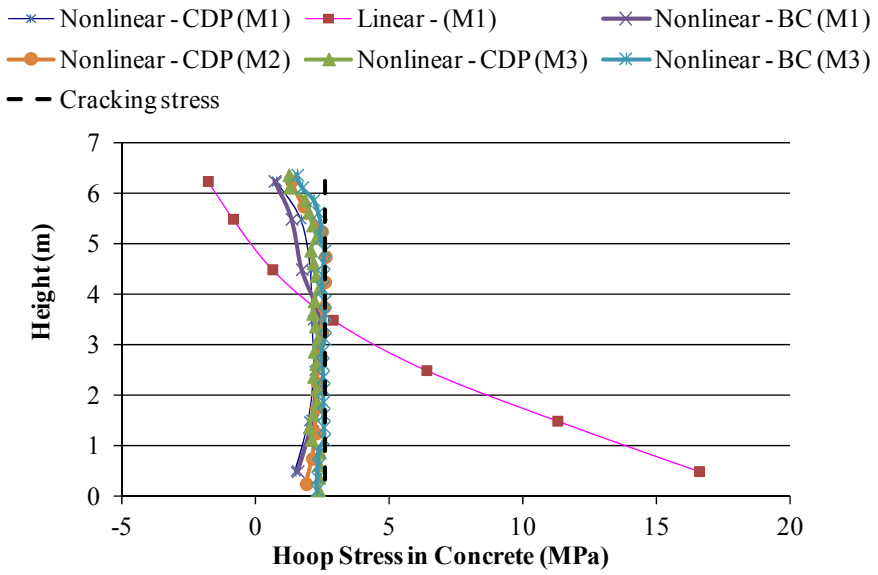

Figure 5.7 – Sensitivity study – Maximum hoop stress in concrete - Tank 2F

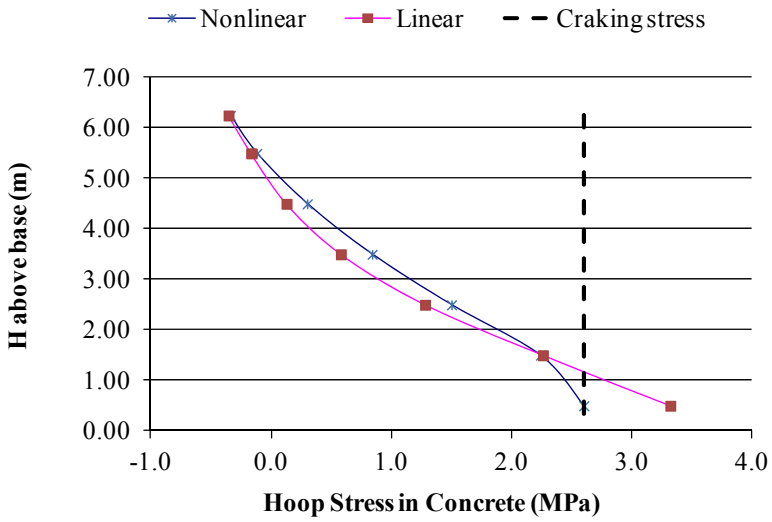

Figure 5.8 – Maximum hoop stress in concrete for ε_{sh} -120 x 10^{-6} - Tank 2F

5.8 Summary

The study included in this Chapter investigates the behavior of circular reinforced concrete tanks with different diameter/height ratios under shrinkage effect considering both linear and nonlinear material Behavior. The variation of the stress in steel reinforcement and concrete section in the vicinity of cracks are investigated.

In this study, both concrete damaged plasticity and brittle cracking models are investigated for nonlinear modeling of concrete. It is found that the results of FE analysis for both concrete models are very similar in simulating the nonlinear Behavior of concrete for circular tanks. Furthermore, the effect of the mesh size on the results of FE analysis is examined in order to determine the suitable element size to be used in the analysis. It is found that one meter by one meter element can be considered as a reasonable element size considering the large size of the circular tanks that are analyzed in this study.

The results of the nonlinear FE analysis of RC circular tanks in this study show that the concrete will crack under shrinkage effect. Once cracks start to develop in concrete, the concrete will lose its tensile strength. Therefore, the tensile strength of concrete is considered in tank design and should be neglected. However, since concrete is weak in tension, cracking is inevitable in concrete structures. Therefore, crack width and spacing can be controlled by providing a sufficient amount of reinforcement to limit tensile stresses in reinforcement in the vicinity of cracks.

CHAPTER 6
NONLINEAR BEHAVIOR OF GROUND-SUPPORTED CIRCULAR TANKS UNDER PUSH-OVER ANALYSIS

6.1 General

This study examines the nonlinear Behavior of the upright circular RC tanks filled with water. Nonlinear FE analysis (push-over analysis) is carried out in order to investigate the behavior of circular tanks under seismic loading. This study also investigates R-values specified in the current practice for fixed and hinged base tanks. In this study, the tank foundations are assumed to be rigid where the effect of soil-structure interaction is not considered.

As discussed in detail in Chapter 3, the results of FE analysis for modeling the entire tank using shell elements are very similar to the results of FE analysis for axi-symmetric model. Accordingly, the FE analysis in this study is carried out using axi-symmetric elements.

This study also investigates the nonlinear Behavior of RC circular tanks for a wide range of tank aspect ratios (D/H) and reinforcement ratios (ρ). The results of nonlinear push-over FE analysis are used to calculate R-values for different cases. The approaches developed by Krawinkler and Nasser (1992) and Miranda and Bertero (1994), as described previously in detail in Chapter 2, have been used to calculate the ductility factor.

Currently, the Canadian design standards do not directly address the structural design of liquid containing concrete structures. Therefore, the standard of American Concrete Institute (ACI 350.3-06 2006), which is one of the most comprehensive and preferred standards in this regard, is used to calculate the hydrodynamic forces in which the design is performed according to ACI 350-06 (2006).

6.2 Tank configuration and design parameters

This study is performed on ground-supported, open top, circular RC tanks. The tank diameter (D) is assumed to be 40m which is considered constant for all cases. Various water depths are used with H_L equals to 3 m, 6 m, and 9 m corresponding to H_w equal to 3.25 m, 6.5 m and 9.6 m,

respectively. Tanks with H_L equals to 3 m, 6 m and 9 m are referred to as Tanks 1, 2 and 3, respectively. Only hinged and fixed base conditions are used in this study which are referred to as H and F, respectively.

It should be noted that due to the presence of seismic cables, the analysis of flexible base condition using axi-symmetric elements is not possible. For this reason, only one tank with free base condition is selected and analyzed for comparison. The free base condition is referred to as FR.

In order to satisfy the code requirements for strength and serviceability, the RC circular tanks are designed to resist the applied hydrostatic and hydrodynamic loads according to ACI 350-06 (2006) and ACI 350.3-06 (2006). The detailed load and design calculations for one of the tanks that are considered in this study are included in Appendix A.1.

The hydrodynamic forces are calculated assuming the tanks are located in a high seismic zone having S_s = 150% and S_1 = 60% with R_i equals to 2.0 for fixed and hinged base conditions and 3.25 for free base condition. For design purpose, linear FE analysis is first performed on the tanks in order to calculate the internal forces in the tank walls due to hydrostatic and seismic loads. The results of this linear FE analysis, for hydrostatic and hydrodynamic loads, are combined to be used in the design of the tank walls. In this study, the wall design is based on maximum design forces along the wall height. Horizontal and vertical reinforcement are considered to be uniform along tank height. The effect of shear forces is also considered in the design. However, the shear stresses are found to be relatively small and do not control the design.

The design of tanks for seismic load depends on R-values specified in the codes. The R-values specified in the codes are empirical in nature, and there is no rationale behind them. One of the main parameters affecting the R-values is the reinforcement ratio (ρ). Therefore, further study is performed using push-over FE analysis in order to investigate the effect of reinforcement ratios on R-values where a wide range of reinforcement ratios is considered.

According to ACI 350-06 (2006), two load combinations are considered in the design of Tanks 1, 2 and 3. They are defined as (1.2HS + EQ) and (1.4HSxS_d), where HS and S_d are the hydrostatic force, and environmental durability factor, respectively, and EQ is the total earthquake force including P_i, P_w, P_c, and P_{VL} as described in detail in Chapter 3. The reinforcement ratios corresponding to load combinations 1 and 2 are referred to as Case 1 and 2, respectively.

In order to cover the entire spectrum of all possible reinforcement ratios, the minimum and maximum reinforcement ratios specified in the code are considered as two additional cases for tanks under considerations. The minimum and maximum reinforcement ratios are referred to as Case 3 and 4, respectively. The minimum reinforcement (As min) is considered based on shrinkage and temperature requirements, where the maximum reinforcement (As max) is considered based on the maximum requirements to eliminate compression (brittle) failure according to ACI 350-06 (2006).

It is worth mentioning that, for Tanks 1, 2 and 3, the impulsive forces are much higher than the convective forces. The ratios of P_i/P_c are 3.6, 4.1, and 5. The ratios of $(P_i+P_w)/P_c$ are 6.2, 5, 6 for Tanks 1, 2 and 3, respectively. Accordingly, the convective component of seismic force is found to have a small effect on the overall seismic behavior for tanks under consideration. The effect of Pc and Pi on the results will be discussed in detail in Chapter 7. Therefore, an additional case study, referred to as Case 5, is considered where Tanks 1, 2 and 3 are designed under the combined effect of P_i and P_w only. In Case 5, the reinforcement ratio is calculated for load combination including the effect of HS, P_i and P_w (1.2HS + P_i + P_w).

The wall thickness (t_w) is calculated to satisfy the design requirements for all considered load combinations. For Cases 1 to 4, the wall thickness (t_w) is assumed to have a constant value of 400 mm for Tanks 1, 2, and 3 in order to exclude the effect of wall thickness on the results.

Also, the results of FE analysis for Case 5 are used to verify the calculated R_i-values based on the results of dynamic time-history FE analysis as discussed in Chapter 7. Therefore, for the

purpose of direct comparison, in Case 5, t_w is considered as 250 mm, 300 mm, and 400 mm for Tanks 1, 2 and 3, respectively.

Hence, for each tank with fixed and hinged base conditions, a total of five cases for tank reinforcement ratios are considered in this study as follows:

Case 1: Load combination including seismic load and hydrostatic load (1.2HS + EQ)

Case 2: Load combination including hydrostatic load ($1.4HSxS_d$)

Case 3: Minimum specified reinforcement ratio, this case may govern the design for lower seismic zones

Case 4: Maximum specified reinforcement ratio

Case 5: Load combination including HS, P_i and P_w ($1.2HS + P_i + P_w$)

Load cases 1 and 2 are the governing load cases for design of LCS based on ACI 350 (2006)

As indicated before, for comparison reasons, FE analysis is also performed for a tank with free base condition, referred to as FR. Only Tank 2 having a wall thickness of 400 mm is used for the comparison. For free base tank, only Case 1 is considered in which the reinforcement ratio is calculated based on load combination including seismic load and hydrostatic load (1.2HS + EQ).

Tank dimensions, support conditions, size and spacing of reinforcement for Tanks 1, 2, and 3 are shown in Table 6.1. In this table, the case numbers are included alongside the tank numbers. For example for Tank 2H-3: 2 refers to tank number 2 where H_L is equal to 6.0m, H refers to hinged base, and 3 refers to Case number 3.

Table 6.1 - Tank dimensions and reinforcement

Tank No.	Base Condition	H_L (m)	H_w (m)	t_w (mm)	Horizontal Bars, EF		Vertical Bars, IF		Vertical Bars, OF	
					Bar Size	S (mm	Bar Size	S (mm)	Bar Size	S (mm)
1H-1, 2, 3*	Hinged	3.0	3.25	400	20M	250	20M	250	20M	250
1F-1, 2, 3*	Fixed	3.0	3.25	400	20M	250	20M	250	20M	250
1H-4	Hinged	3.0	3.25	400	25M	60	25M	60	25M	60
1F-4	Fixed	3.0	3.25	400	25M	60	25M	60	25M	60
1H-5	Hinged	3.0	3.25	250	15M	300	15M	300	15M	300
1F-5	Fixed	3.0	3.25	250	15M	300	15M	250	15M	300
2H-1	Hinged	6.0	6.50	400	20M	220	20M	250	20M	250
2F-1	Fixed	6.0	6.50	400	20M	250	20M	200	20M	250
2H-2	Hinged	6.0	6.50	400	25M	250	20M	250	20M	250
2F-2	Fixed	6.0	6.50	400	20M	230	20M	200	20M	250
2H-3	Hinged	6.0	6.50	400	20M	250	20M	250	20M	250
2F-3	Fixed	6.0	6.50	400	20M	250	20M	250	20M	250
2H-4	Hinged	6.0	6.50	400	25M	60	25M	60	25M	60
2F-4	Fixed	6.0	6.50	400	25M	60	25M	60	25M	60
2H-5	Hinged	6.0	6.50	300	20M	250	15M	225	15M	200
2F-5	Fixed	6.0	6.50	300	15M	225	20M	150	15M	225
3H-1	Hinged	9.0	9.60	400	25M	200	20M	250	20M	250
3F-1	Fixed	9.0	9.60	400	25M	240	25M	170	20M	250
3H-2	Hinged	9.0	9.60	400	25M	135	20M	250	20M	250
3F-2	Fixed	9.0	9.60	400	25M	160	20M	250	20M	250
3H-3	Hinged	9.0	9.60	400	20M	250	20M	250	20M	250
3F-3	Fixed	9.0	9.60	400	20M	250	20M	250	20M	250
3H-4	Hinged	9.0	9.60	400	25M	60	25M	60	25M	60
3F-4	Fixed	9.0	9.60	400	25M	60	25M	60	25M	60
3H-5	Hinged	9.0	9.60	400	25M	200	20M	250	20M	250
3F-5	Fixed	9.0	9.60	400	25M	250	25M	175	20M	250
2FR-1	Free	6.0	6.50	400	25M	85	20M	250	20M	250

* Tank reinforcement is controlled by minimum limit specified by ACI 350-6 (2006); Case Numbers 2 and 3 are identical to Case 1.

H_L: Water depth, H_w: Wall Height, t_w: Wall thickness, S: Spacing, EF: Each face, IF: Inside face, OF: Outside face

6.3 Finite element analysis

As discussed in detail in Chapter 3, the hydrodynamic load distribution around the tank circumference is a cosine distribution. For maximum tank response, it is found to be appropriate to use the approximation of uniformly distributed load instead of the actual cosine distribution. Also, it is found that, axi-symmetric elements can be used in FE analysis instead of modeling the entire tank using shell elements.

In this study, nonlinear FE push-over analysis is carried out on the circular tanks indicated in Table 6.1 in order to investigate the nonlinear behavior of the tank wall. The computer program ABAQUS (ABAQUS/CAE 2008) is used to perform the FE analysis using axi-symmetric elements. The nonlinear behavior of tank materials, as described in detail in Chapter 4, has been considered in the analysis in order to study the nonlinear response of the tank wall. The concrete tensile strength is considered in the nonlinear FE push-over analysis. For push-over FE analysis, the distribution of the applied seismic load along the wall height is determined based on ACI350.3-06 (2006). The number of elements used along the wall height is three, six, and nine for Tanks 1, 2 and 3, respectively. However, a mesh sensitivity study is performed in order to study the effect of element size on the results of FE analysis and verify the size of elements that is used in the FE analysis is appropriate.

As previously indicated, the reinforcement in concrete walls is provided by means of rebars. Rebars are one-dimensional strain theory elements (rods); which are defined as embedded elements in oriented surfaces. The rebars are typically used with elastic-plastic material behavior and are superposed on a mesh of standard element types used to model the plain concrete.

6.4 Results of push-over FE analysis

In this study, the nonlinear load-deflection response, based on the results of push-over FE analysis, of Tanks 1, 2, and 3 is presented. The nonlinear load-displacement response represents the relationship between the maximum deflection of the tank wall in the radial direction (U1) and the corresponding pressure at tank base. The load-deflection response presented in this Chapter illustrates the nonlinear Behavior of tank walls under push-over FE analysis. For each case, the tank response is presented from the initial load condition up to the ultimate lateral pressure and

the corresponding maximum lateral displacement at failure. For all cases considered in this study, the failure occurs when strain in reinforcement reaches the ultimate strain.

Furthermore, the nonlinear force-displacement response (relationship) is used to calculate R-values using the approaches developed by Krawinkler and Nasser (1992), referred to as (K and N), using Equations 2-6 and 2-7, and Miranda and Bertero (1994), referred to as (M and B), using Equations 2-8 and 2-9 for rock sites as described in detail in Chapter 2. The strength (overstrength) factor (R_s) is calculated using Equation 2-7, and the response modification factor (R) is based on Equation 2-6. It should be noted that, the response modification factor for the convective component (R_c) is equal to one as per ACI 350.3-06 (2006). Therefore, the results of push-over FE analysis are used to calculate the response modification factor for the impulsive component (R_i) only. Thus, the symbol R is used instead of R_i throughout this study.

It is worth mentioning that, for ground-supported circular concrete tanks, there is no maximum drift specified in the current practice for the tank walls. Instead, the design of the tank wall is usually dictated by controlling the crack width. Sadjadi (2009) studied the cracking and leakage of LCS and concluded that, leakage occurs soon after the yielding of the reinforcement. Therefore, to calculate the ductility ratio (μ), the maximum displacement considered is the displacement at the first yield in the reinforcement as will be discussed later.

In addition, in order to further assess the nonlinear behavior of tanks, the nonlinear load-deflection response based on push-over analysis is compared with the loads calculated based on ACI350.3-06 (2006) for R = 1.0 and R = 2.0 for fixed and hinged base condition, referred to as (ACI350.3 - R = 1.0) and (ACI350.3 - R = 2.0), respectively. However, for free base condition, the response is compared with the loads calculated based on R = 1.0 and R = 3.25, referred to as (ACI350.3 - R = 1.0) and (ACI350.3 - R = 3.25), respectively. In ACI 350.3-06 (2006), the calculated loads include the hydrostatic water pressure plus pressure resulting from earthquake forces. Based on ACI 350.3 (2006), the value of R is limited to 2.0 for fixed and hinged based tanks. Furthermore, the results presented show the values of pressure at which cracking of concrete is initiated (P_{cr}), pressure at which yield of horizontal bars is initiated (P_{yH}), and

pressure at which yield of vertical bars is initiated (P_{yV}). These values are indicated on the load-deflection response diagrams.

The actual nonlinear force-displacement relationship, referred to as (non-linear), describes the behavior of structural element subjected to monotonically increasing displacement. For the purpose of design, the force-displacement relationship is often approximated by idealized bilinear relationship (ATC-19 1995). In this study, the approximation developed by Pauley and Priestley (1992), referred to as (bilinear approximation), is used. This approximation has been developed for characterizing load-displacement relation for reinforced concrete elements. This approximation assumes prior knowledge of yield strength (V_y) of the structural element, referred to as P_y. The elastic stiffness is based on the secant stiffness of the element calculated from the force-displacement curve at the force corresponding to $0.75V_y$.

6.4.1 Mesh sensitivity study

A sensitivity study is carried out to ensure that the selected element size for the FE analysis is appropriate. This study is performed for tank 1H-1. A total of four FE models are analyzed for the same tank, where the number of elements along the tank wall is taken as three, six, twelve, and twenty four. The results of this study as shown in Figure 6.1 indicate that the selected element size does not have a major effect on the results of the analysis. Therefore, the selected mesh size is appropriate. Accordingly, the numbers of elements along the wall height are considered three, six, and nine elements for Tanks 1, 2 and 3, respectively.

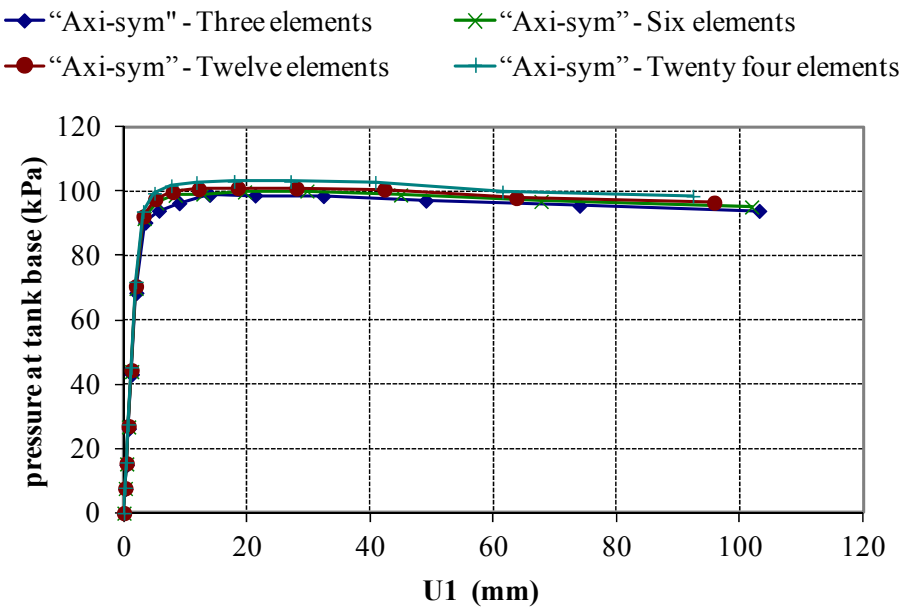

Figure 6.1 – Mesh sensitivity study – Load-deflection response for Tank 1H-1

6.4.2 Hinged base condition

For Tank 1H-1, the tank reinforcement is governed by the minimum limit specified by ACI350-06 (2006) (As min). The load deflection response of Tank 1H-1 is shown in Figure 6.2. The first two consecutive yields in tank reinforcement are developed in horizontal bars. No yielding is developed in vertical bars. The behavior of the tank wall is elastic (linear) under hydrostatic water pressure plus the elastic earthquake pressure (ACI350.3 - R = 1.0). The required strength to resist factored load (V_d or P_d) based on (ACI350.3 - R = 2.0) which is equal to 53 kPa is less than the pressure required for concrete to reach its cracking strength (P_{cr}) which is equal to 90 kPa. The first bar yields at pressure (P_y) equal to 97 kPa. The overstrength factor (R_s) using Equation 2-7 is equal to 1.84. The values of ductility factor (R_μ) based on Krawinkler and Nasser (K and N), using Equations 2-8 and 2-9, and Miranda and Bertero (M and B), using Equations 2-8 and 2-9, is equal to 1.60 and 1.64, respectively. Accordingly, the response modification factor (R) using Equation 2-6 is equal to 2.94 and 3.02 based on (K and N) and (M and B), respectively. The tank reinforcement is controlled by minimum limit specified by ACI 350-06 (2006), therefore, Case numbers 2 and 3 are identical to Case number 1.

For Tank1H-4, as shown in Figure 6.3, the ductility factor (R_μ) based on (K and N) and (M and B) is equal to 1.16 and 1.24, respectively. Also, the section nominal capacity has increased due

to the increase in reinforcement ratio. Therefore, the first reinforcement yielded at pressure of (P_y) equals to 582 kPa, which is much higher than Case numbers 1, 2 and 3.

For Tank 1H-5, as shown in Figure 6.4, the ductility factor (R_μ) based on (K and N) and (M and B) is equal to 1.54 and 1.57, respectively, which is similar to Tank 1H-1. The overstrength factor (R_s) based on Equation 2-7 is equal to 1.18. Accordingly, the R based on Equation 2-6 is equal to 1.82 and 1.85 for (K and N) and (M and B), respectively. The reduction in the overstrength factor (R_s) and response modification factor is due to the smaller wall thickness and reinforcement ratio for Tank 1H-5. Similarly, the first reinforcement yielded at pressure of (P_y) equal to 59 kPa, which is close to the cracking strength (P_{cr}) of 57 kPa. These values are much smaller than those for Tank 1H-1.

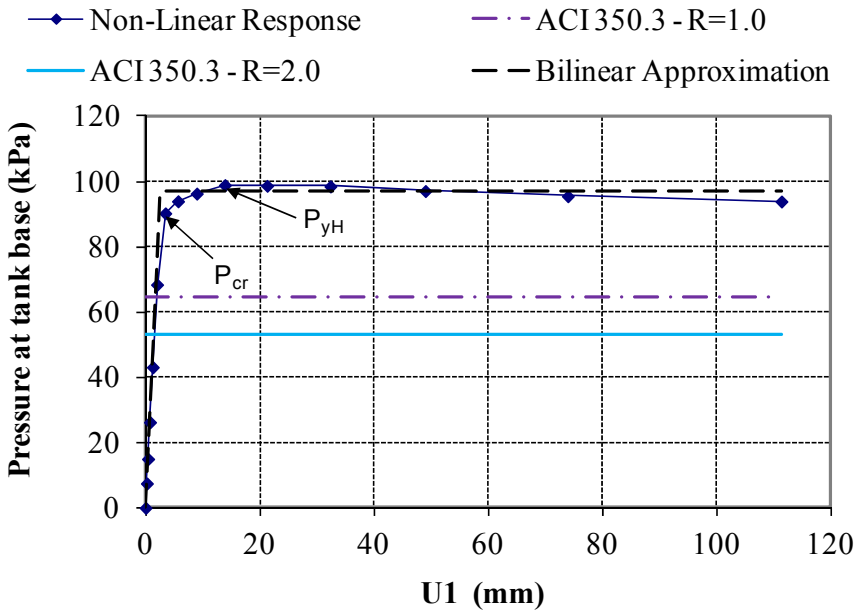

Figure 6.2 - Load-deflection response – Tank 1H-1

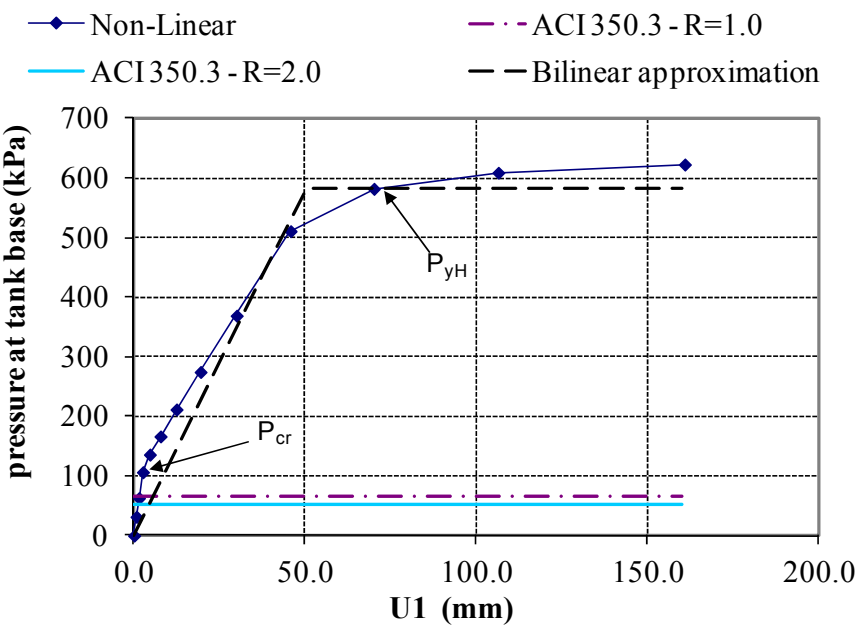

Figure 6.3 - Load-deflection response – Tank 1H-4

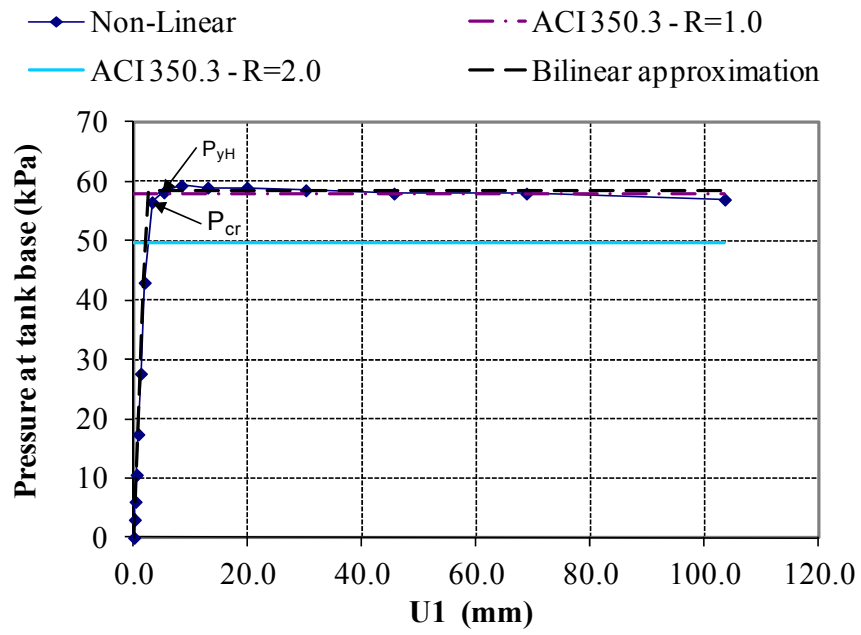

Figure 6.4 - Load-deflection response – Tank 1H-5

For Tank 2H-1, the vertical reinforcement is governed by (As min). Figure 6.5 shows that the first yield is developed in the horizontal bars at a pressure equals to 127 kPa. The behavior of the tank wall is elastic (linear) under (ACI350.3 - R = 1.0) which is equal 119 kPa. The required strength to resist factored load equals 101 kPa, which is less than (P_{cr}) of 117 kPa. The overstrength factor (R_s) is equal to 1.26. The value of R_μ based on (K and N) and (M and B) is equal to 1.94 and 2.0, respectively. Therefore, the response modification factor based on (K and N) and (M and B) is equal to 2.44 and 2.52, respectively.

For Tanks 2H-2, 3 and 4, as shown in Figures 6.6, 6.7 and 6.8, the ductility factor (R_μ) based on (K and N) is equal to 1.42, 1.91 and 1.07 for Case numbers 2, 3 and 4, respectively. The value of R_μ based on (M and B) is equal to 1.44, 1.94 and 1.03 for Case numbers 2, 3 and 4, respectively. The overstrength factor is equal to 1.88, 1.2 and 6.86 for Case numbers 2, 3 and 4, respectively. The first yield of reinforcement is developed at pressure (P_y) equal to 189 kPa, 118 kPa and 690 kPa for Case numbers 2, 3 and 4, respectively.

For Tank 2H-5, as shown in Figure 6.9, the ductility factor (R_μ) based on (K and N) and (M and B) is equal to 1.33 and 1.29, respectively. These values are smaller than those of Tank 2H-1. The overstrength factor (R_s) is equal to 1.23. Accordingly, the response modification factor based on (K and N) and (M and B) is equal 1.64 and 1.58, respectively. Also, the reduction in the R-value is due to the smaller wall thickness and reinforcement ratio for Tank 2H-5. Similarly, cracking strength is equal to 73 KPa and the first reinforcement yields at a pressure of 117 kPa. These values are much smaller than those for Tank 2H-1.

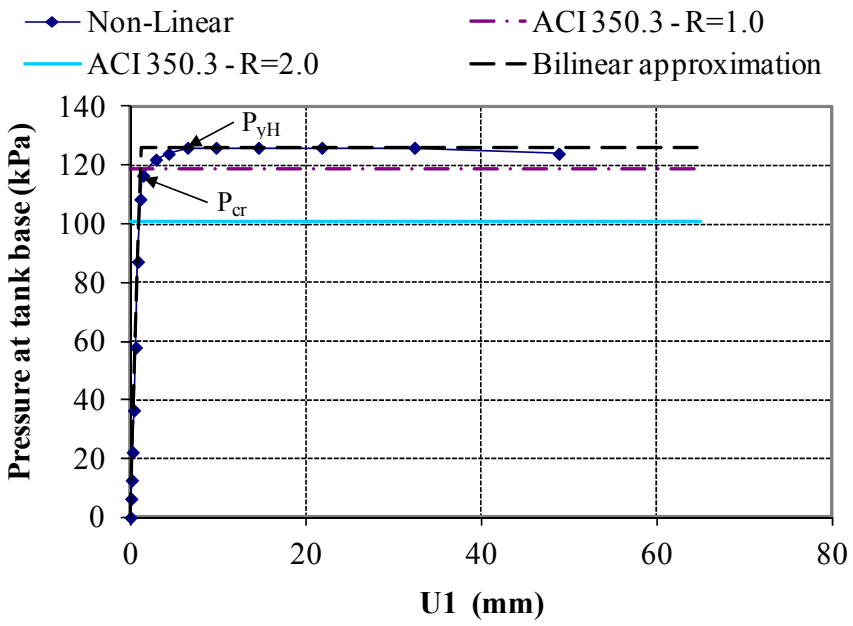

Figure 6.5 - Load-deflection response – Tank 2H-1

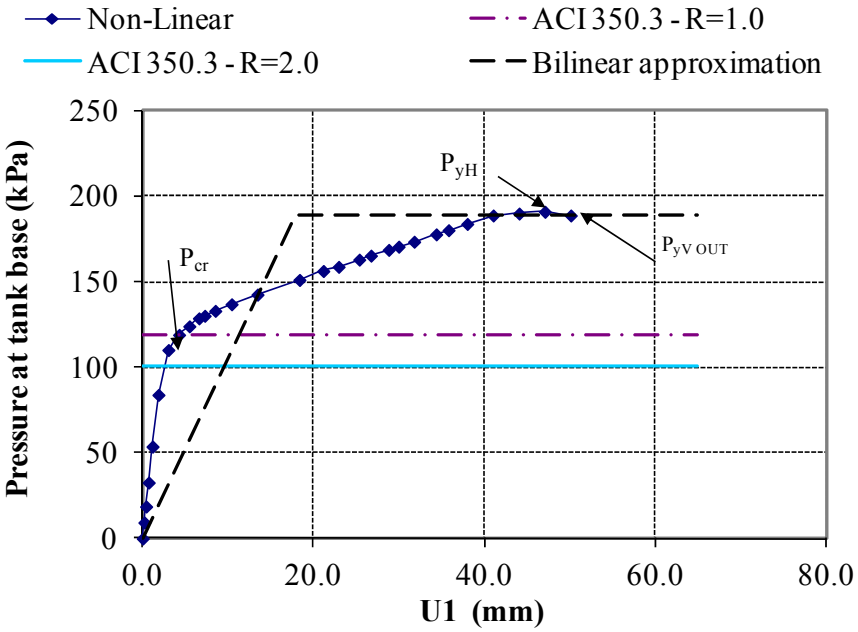

Figure 6.6 - Load-deflection response – Tank 2H-2

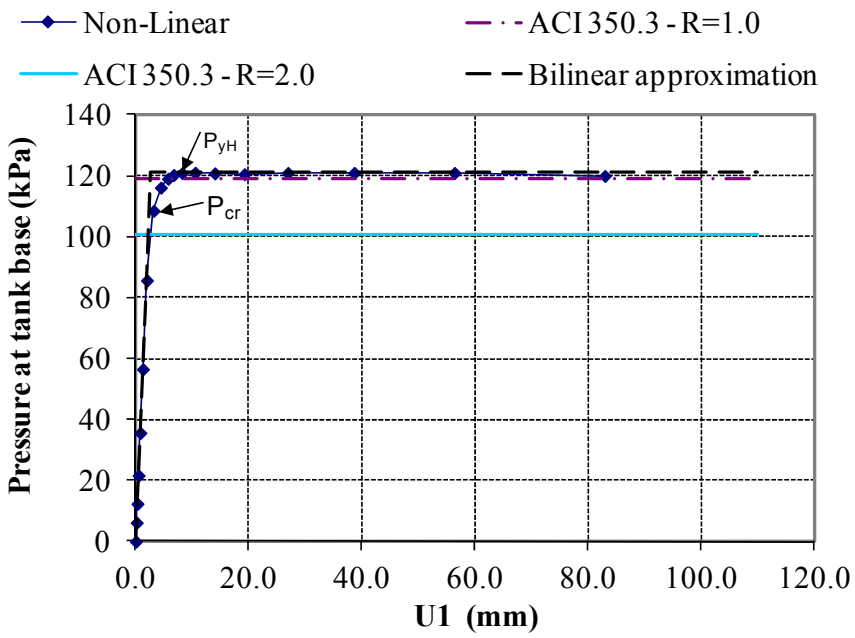

Figure 6.7 - Load-deflection response – Tank 2H-3

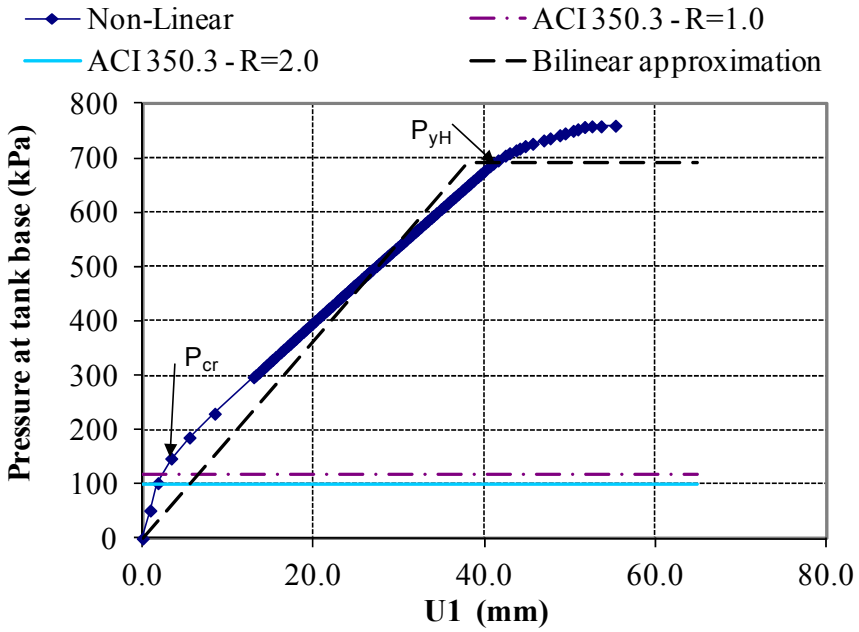

Figure 6.8 - Load-deflection response – Tank 2H-4

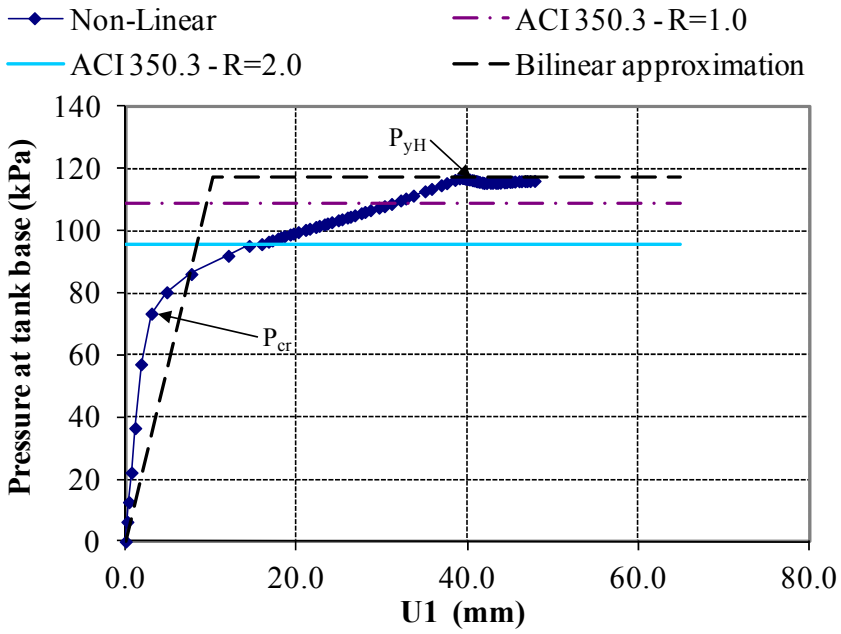

Figure 6.9 - Load-deflection response – Tank 2H-5

For Tank 3H-1, the vertical reinforcement is governed by (As min). Figure 6.10 shows that the exterior vertical reinforcement yielded first at a pressure equal to 168 kPa. The horizontal bars start to yield almost at the same pressure. In this case, the pressure required for concrete to reach its cracking strength is equal to 89 kPa. The pressures based on (ACI350.3 - R = 1.0 and R = 2.0) are 177 kPa, and 150 kPa, respectively. Therefore, overstrength factor is equal to 1.12, and values of R_μ based on (K and N) and (M and B) are equal to 1.43 and 1.39, respectively. Accordingly, the R-values are equal to 1.60 and 1.56 based on (K and N) and (M and B), respectively.

For Tanks 3H-2, 3 and 4, as shown in Figures 6.11, 6.12 and 6.13, the ductility factor (R_μ) based on (K and N) is equal to 1.26, 1.92 and 1.07 for Case numbers 2, 3 and 4 respectively. The ductility factor based on (M and B) is equal to 1.18, 2.2 and 1.04 for Case numbers 2, 3 and 4 respectively. Also, the first yield of reinforcement is developed at pressure (P_y) equal to 214 kPa, 110 kPa, and 533 kPa for Case numbers 2, 3 and 4, respectively.

For Tank 3H-5, as shown in Figure 6.14, the ductility factor (R_μ) based on (K and N) and (M and B) is equal to 1.43 and 1.39, respectively, which is the same as Tank 3H-1. The overstrength factor is equal to 1.18. Accordingly, the response modification factor based on (K and N) and (M and B) is equal to 1.68 and 1.64, respectively, which is very similar to Tank 3H-1. This similarity is due to the use of the same wall thickness for Tank 3H-1 and Tank 3H-5. The exterior vertical reinforcement yields first at pressure of 168 kPa, the horizontal bars start to yield at almost the same pressure. In this case, the pressure required for concrete to reach its cracking strength is 89 kPa. The behaviors of Tank 3H-5 and Tank 3H-1 are almost the same even though the convective force (P_c) is not considered in the design of Tank 3H-5, which indicates that the effect of the P_c on the tank response is relatively small.

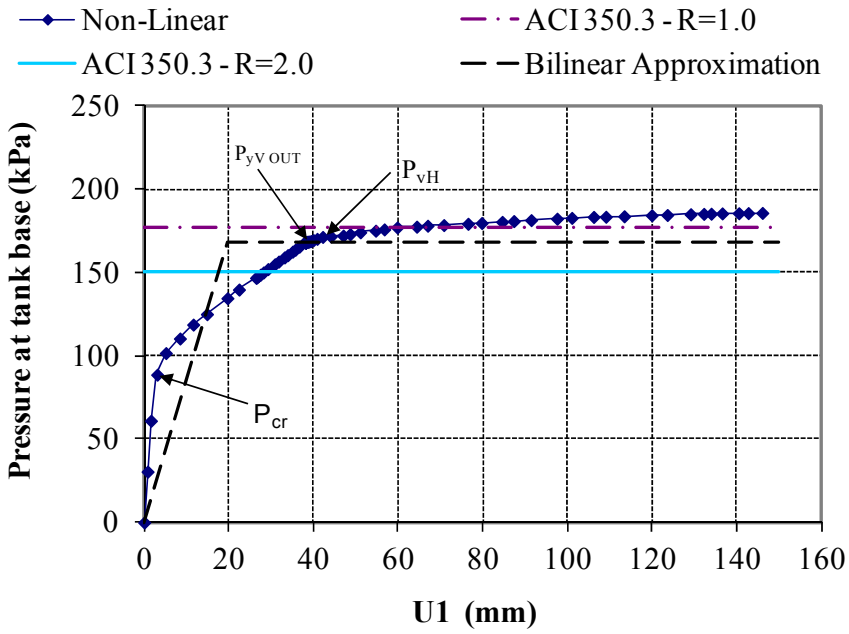

Figure 6.10 - Load-deflection response – Tank 3H-1

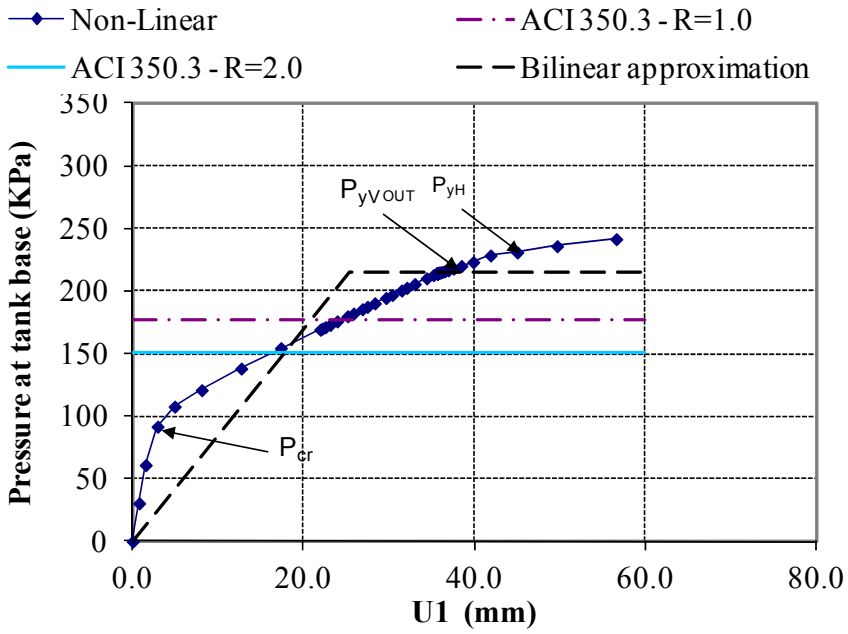

Figure 6.11 - Load-deflection response – Tank 3H-2

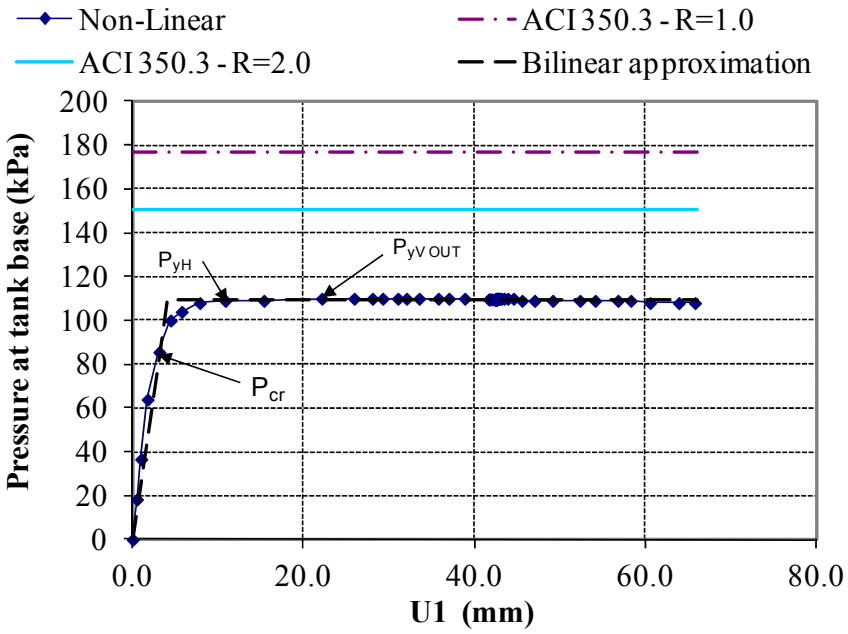

Figure 6.12 - Load-deflection response – Tank 3H-3

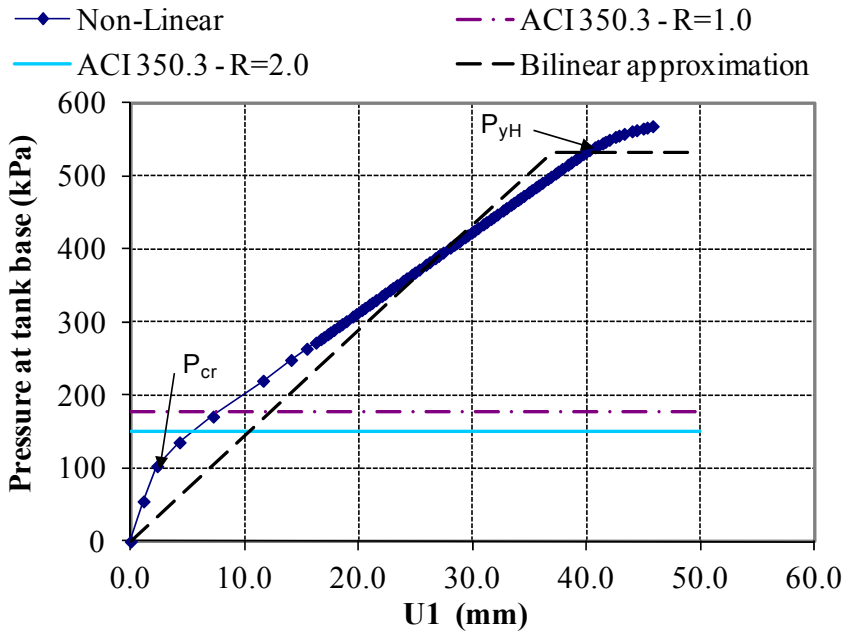

Figure 6.13 - Load-deflection response – Tank 3H-4

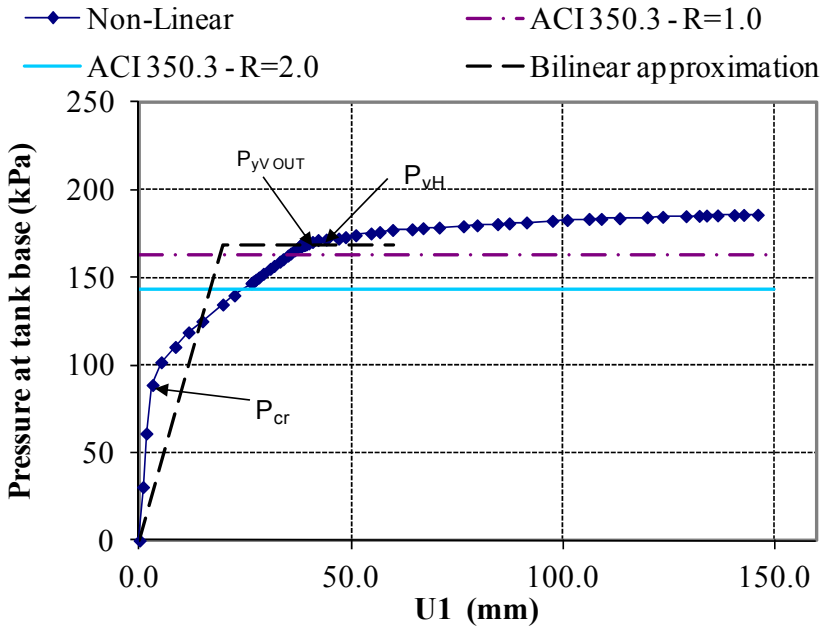

Figure 6.14 - Load-deflection response – Tank 3H-5

6.4.3 Fixed base condition

For Tank 1F-1, similar to hinged base condition, the tank reinforcement is governed by (As min). Figure 6.15 shows that the first yield is developed at a pressure equal to 205 kPa, which is much higher than the design pressure. The behavior of the tank wall is elastic (linear) under (ACI350.3 - R = 1.0). Also, the required strength to resist factored load is less than the pressure required for concrete to reach its cracking strength (P_{cr}) which is equal to 139 kPa. The overstrength factor (R_s) is equal to 3.87. The ductility factor (R_μ) based on (K and N) and (M and B) is equal to 1.39 and 1.59, respectively. Accordingly, the R-value is equal to 5.36 and 6.15 based on (K and N) and (M and B), respectively. It should be noted that tank reinforcement is controlled by minimum limit specified by ACI 350-06 (2006); Case numbers 2 and 3 are identical to Case number1.

For Tank 1F-4, as shown in Figure 6.16, the ductility factor (R_μ) based on (K and N) and (M and B) is equal to 1.06 and 1.02, respectively. Similar to hinge base condition, the section nominal capacity has increased due to the increase in reinforcement ratio. Therefore, the first yield of reinforcement is developed at pressure (P_y) equal to 980 kPa, which is much higher than Case numbers 1, 2 and 3.

For Tank 1F-5, as shown in Figure 6.17, the ductility factor (R_μ) based on (K and N) and (M and B) is equals to 1.51 and 1.53, respectively, which is similar to Tank 1F-1. The overstrength factor (R_s) is equals to 1.76. Accordingly, the R-value based on (K and N) and (M and B) is equal to 2.65 and 2.71, respectively. Similar to hinged base tank, the reduction in the overstrength factor (R_s) and R-values is due to the smaller wall thickness and reinforcement ratio for Tank 1F-5. Similarly, the first reinforcement yielded at pressure of (P_y) equal to 87 kPa, which is relatively similar to the cracking strength (P_{cr}) of 77 kPa. These values are much smaller than those of Tank 1F-1.

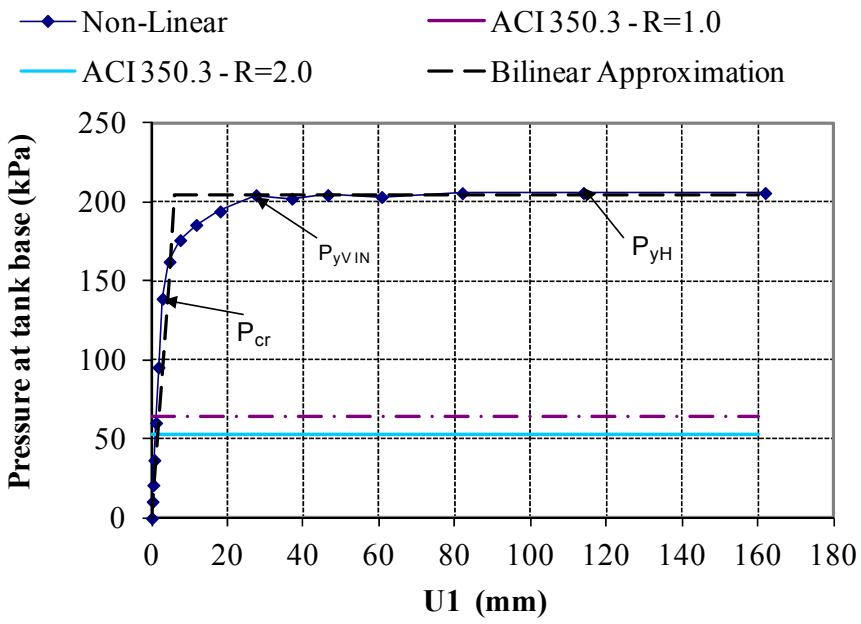

Figure 6.15 - Load-deflection response – Tank 1F-1

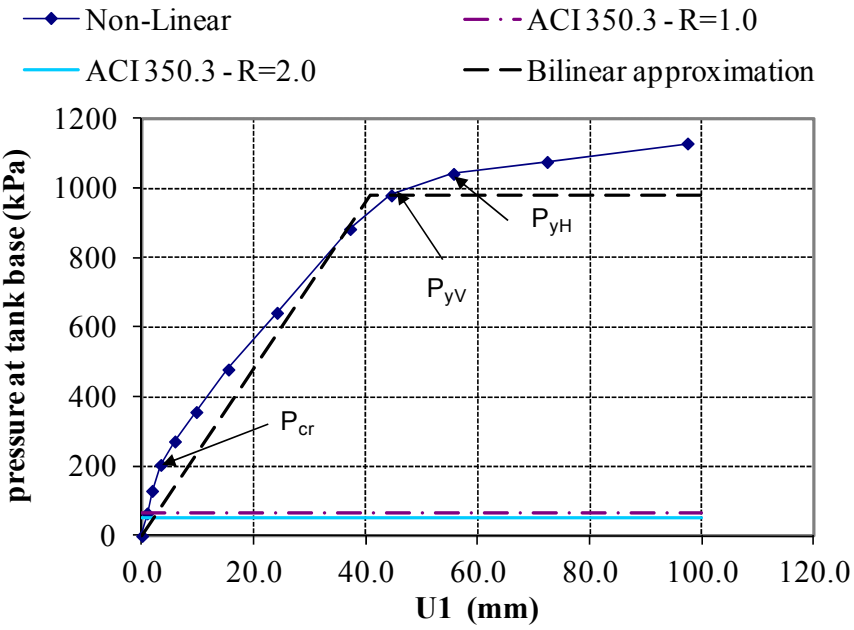

Figure 6.16 - Load-deflection response – Tank 1F-4

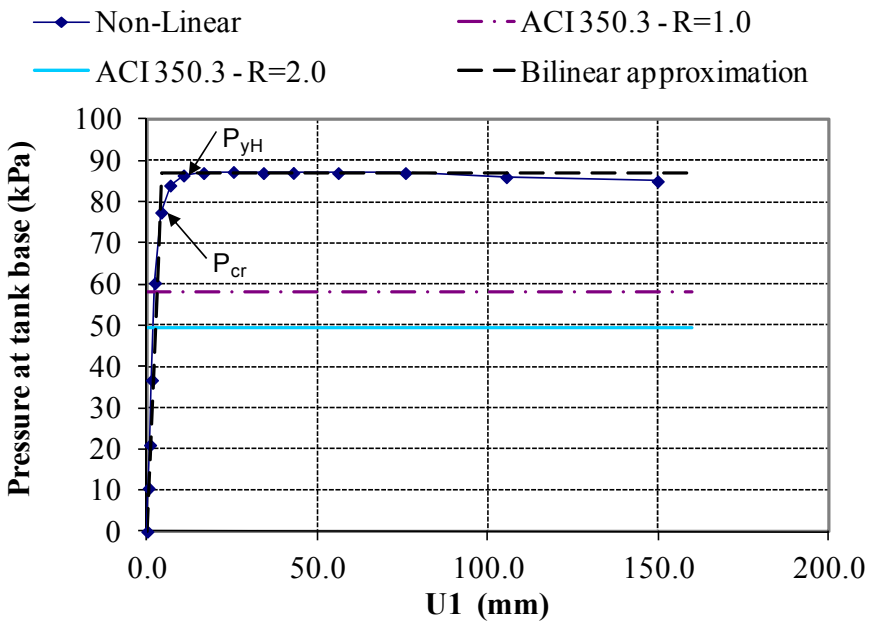

Figure 6.17 - Load-deflection response – Tank 1F-5

For Tank 2F-1, tank reinforcement is governed by (As min) except the interior vertical bars at tank base. Figure 6.18 shows that the first yield is developed in the horizontal bars at a pressure equal to 180 kPa, the vertical bars at the inside face of the fixed base starts to yield shortly after that. The behavior of the tank wall is elastic under (ACI350.3, R = 1.0) which is equal to 119 kPa. The value of R_s is equal to 1.79, and value of R_μ based on (K and N) and (M and B) is equal to 2.19 and 2.24, respectively. Accordingly, the response modification factor based on (K and N) and (M and B) is equal to 3.93 and 4.02, respectively.

For Tanks 2F-2, 3 and 4, as shown in Figures 6.19, 6.20, and 6.21, the ductility factor (R_μ) based on (K and N) is equal to 2.17, 1.89 and 1.06 for Case numbers 2, 3 and 4, respectively. The value of R_μ based on (M and B) is equal to 2.21, 1.92 and 1.03 for Case numbers 2, 3 and 4, respectively. The overstrength factor is equal to 1.87, 1.43 and 8.39 for Case numbers 2, 3 and 4, respectively. Also, the first yield of reinforcement is developed at pressure (P_y) is equal to 188 kPa, 144 kPa and 844 kPa for Case numbers 2, 3 and 4, respectively.

For Tank 2F-5, as shown in Figure 6.22, the ductility factor (R_μ) based on (K and N) and (M and B) is equal to 2.4 and 2.45, respectively. These values are similar to those for Tank 2F-1. The overstrength factor (R_s) equals to 1.1. Accordingly, response modification factor is 2.64 and 2.7, respectively. Also, the reduction in the R-values is due to the smaller wall thickness and reinforcement ratio for Tank 2F-5. Similarly, cracking strength is equal to 103 KPa and the first reinforcement yields at a pressure of 105 kPa. These values are smaller than those for Tank 2F-1.

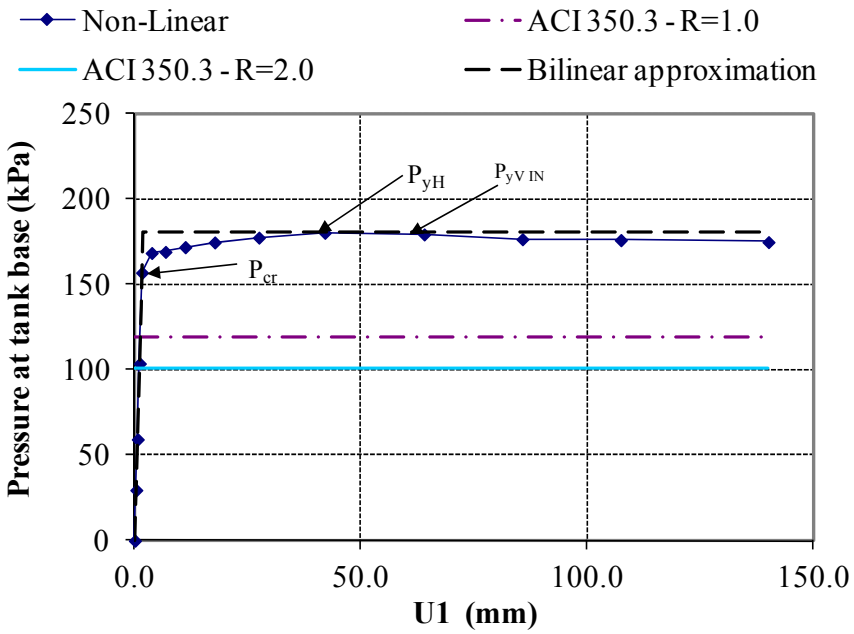

Figure 6.18 - Load-deflection response – Tank 2F-1

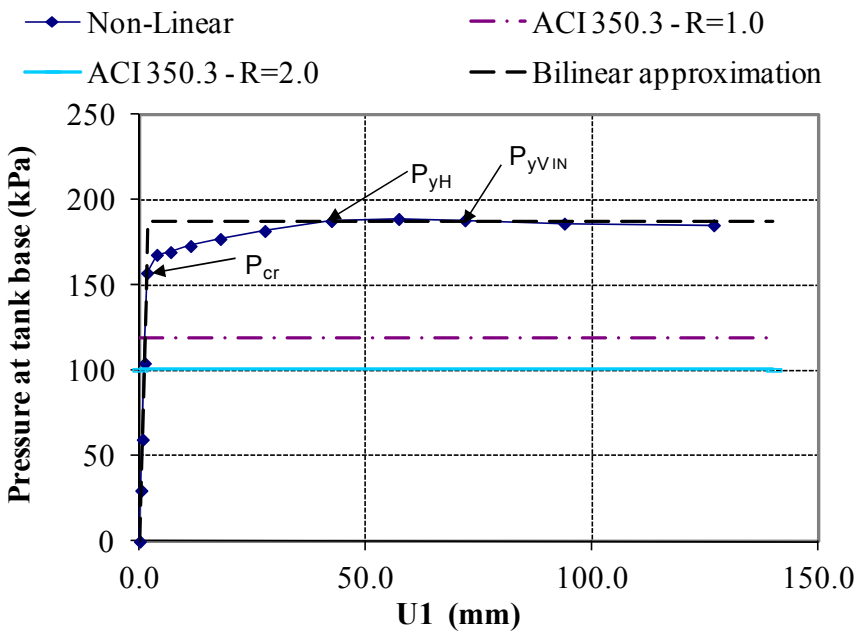

Figure 6.19 - Load-deflection response – Tank 2F-2

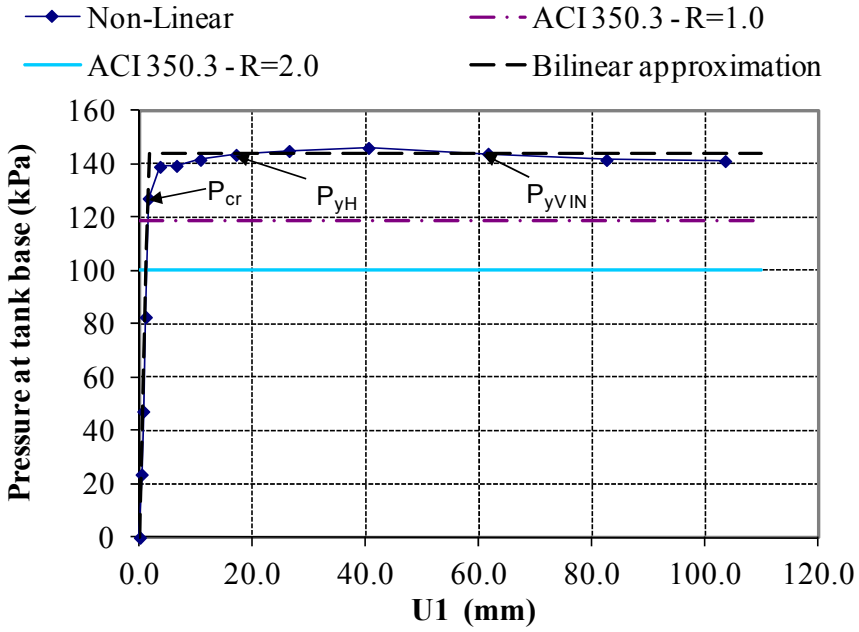

Figure 6.20 - Load-deflection response – Tank 2F-3

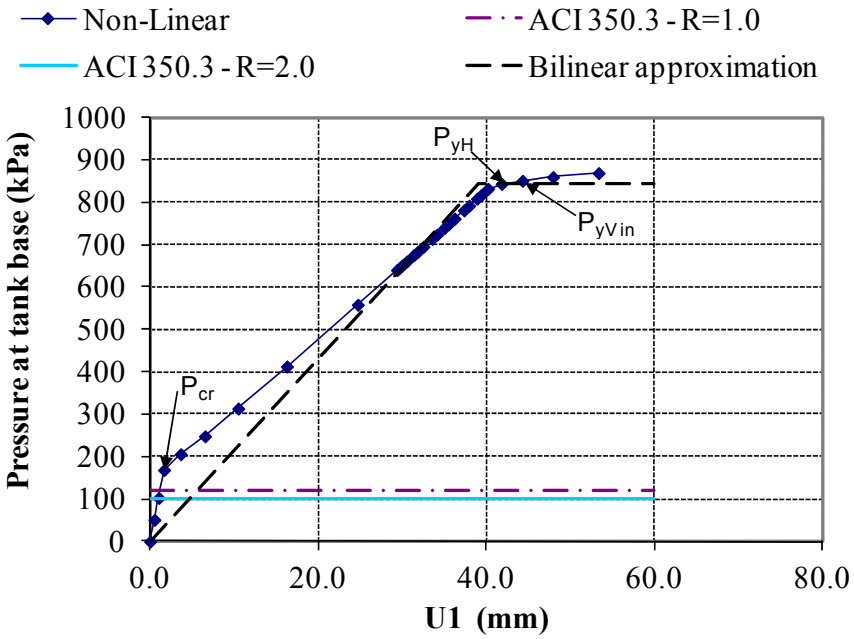

Figure 6.21 - Load-deflection response – Tank 2F-4

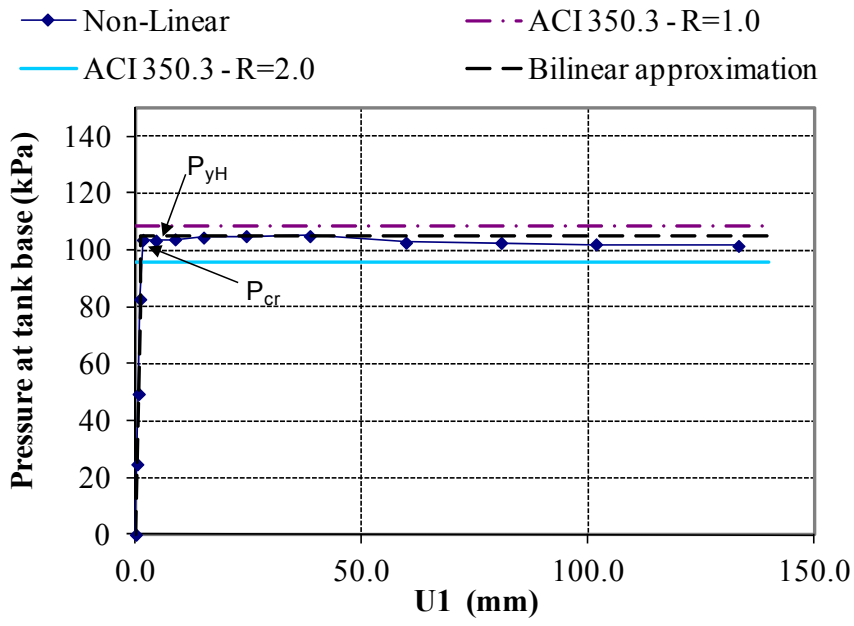

Figure 6.22 - Load-deflection response – Tank 2F-5

For Tank 3F-1, the exterior vertical reinforcement is governed by (As min). Figure 6.23 shows that the first yield is developed in the interior vertical bars at the base at a pressure equal to 198 kPa. The horizontal bars start to yield almost at the same pressure. Also, the pressure required for concrete to reach its cracking strength is equal to 116 kPa, this value is less than the design pressure. The value of R_s is equal to 1.32. The value of R_μ based on (K and N) and (M and B) is equal to 1.46 and 1.44, respectively. Accordingly, the R-values are equal to 1.92 and 1.89 for (K and N) and (M and B), respectively.

For Tanks 3F-2, 3 and 4, as shown in Figures 6.24, 6.25, and 6.26, the ductility factor (R_μ) based (K and N) is equal to 1.25, 1.72 and 1.08 for Case numbers 2, 3 and 4 respectively. The ductility factor based on (M and B) is equal to 1.18, 1.92 and 1.04 for Case numbers 2, 3 and 4 respectively. Also, the first yield of reinforcement is developed at pressure (P_y) equal to 253 kPa, 107 kPa and 668 kPa for Case numbers 2, 3 and 4, respectively.

For Tank 3F-5, as shown in Figure 6.27, the ductility factor (R_μ) based on (K and N) and (M and B) is equal to 1.46 and 1.44, respectively. These values are exactly the same as those for Tank 3F-1. The overstrength factor (R_s) based on Equation 7-5 is equal to 1.38. Accordingly, the response modification factor based on (K and N) and (M and B) is equal to 2.02 and 1.98, respectively, which is very similar to Tank 3F-1. This similarity is due to the use of the same wall thickness for Tank 3H-1 and Tank 3H-5. Also, the exterior vertical reinforcement bars yield first at a pressure equal to 197 kPa. The horizontal bars start to yield at similar pressure. In this case, the pressure required for concrete to reach its cracking strength is equal to 116 kPa. The behaviors of Tank 3F-5 and Tank 3F-1 are very similar even though the effect of convective force (P_c) is excluded from the design of Tank 3F-5, which indicates that the effect of the P_c on the tank response is relatively small and can be neglected.

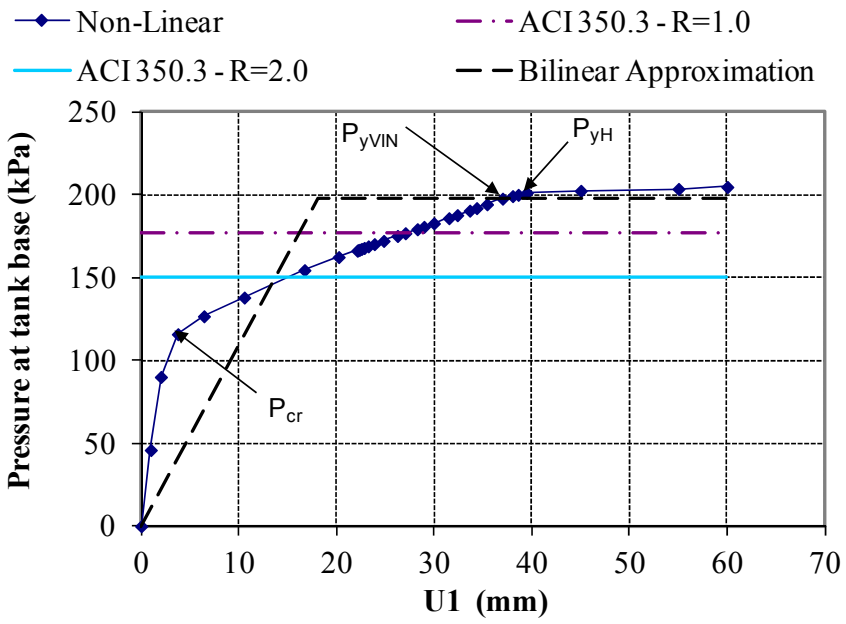

Figure 6.23 - Load-deflection response – Tank 3F-1

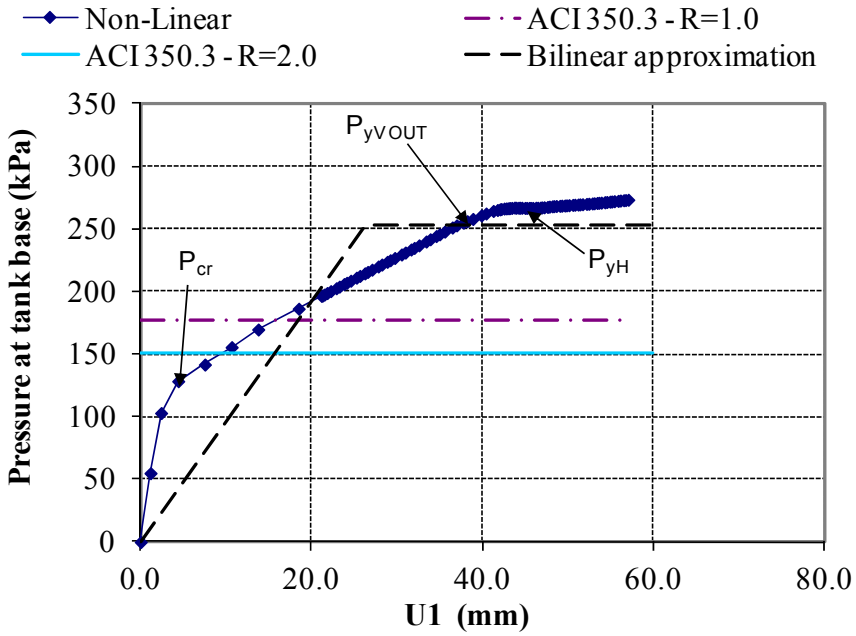

Figure 6.24 - Load-deflection response – Tank 3F-2

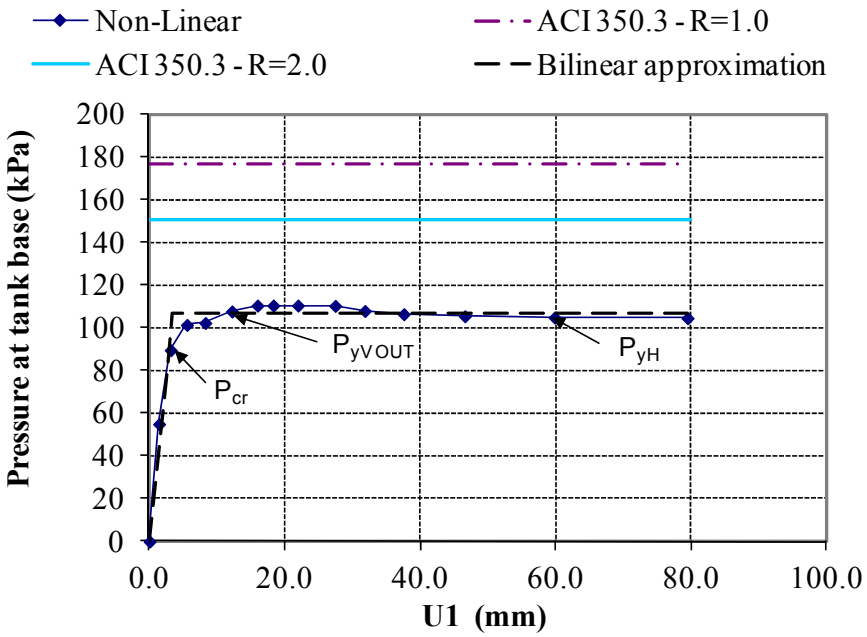

Figure 6.25 - Load-deflection response – Tank 3F-3

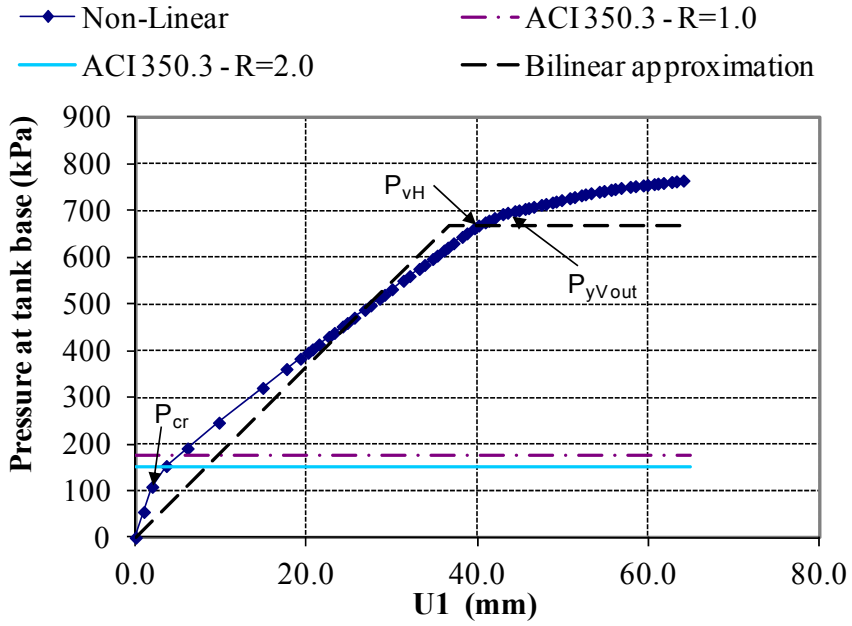

Figure 6.26 - Load-deflection response – Tank 3F-4

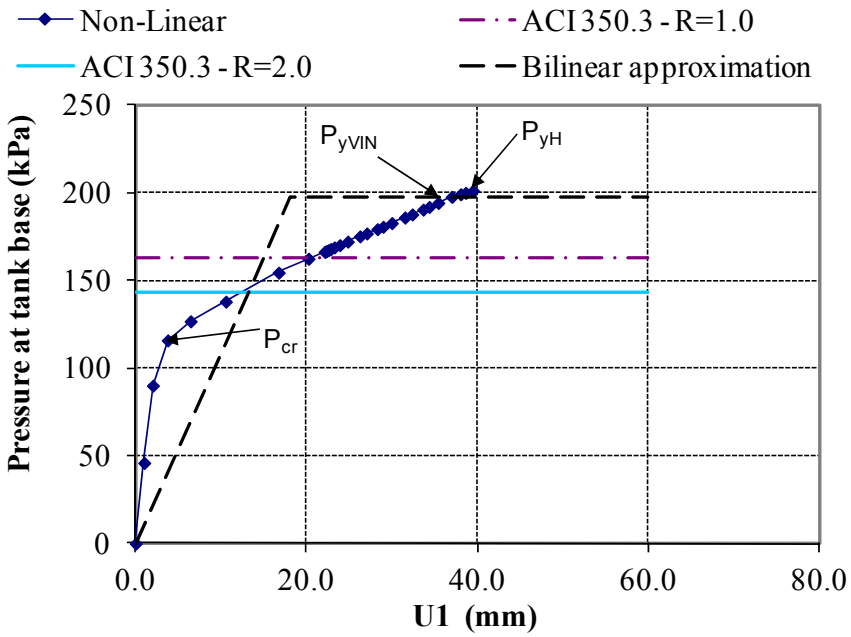

Figure 6.27 - Load-deflection response – Tank 3F-5

6.4.4 Free base condition

For Tank 2FR-1, the vertical reinforcement is governed by (As min) for all possible load cases. Figure 6.28 shows that the first yield is developed in horizontal bars at a pressure equal to 320 kPa. The behavior of the tank wall is elastic (linear) under (ACI350.3 - R = 1.0) which is equal 119 KPa. The required strength to resist factored load (V_d or P_d) is equal to 89 kPa, which is very similar to (P_{cr}). The overstrength factor is 3.59. The values of R_μ based on (K and N) and (M and B) are equal to 1.32 and 1.27, respectively. Accordingly, the response modification factor is equal to 4.73 and 4.55 for (K and N) and (M and B), respectively. It should be noted that the response modification factor for free base condition is more than the values for tanks with fixed and hinged base conditions.

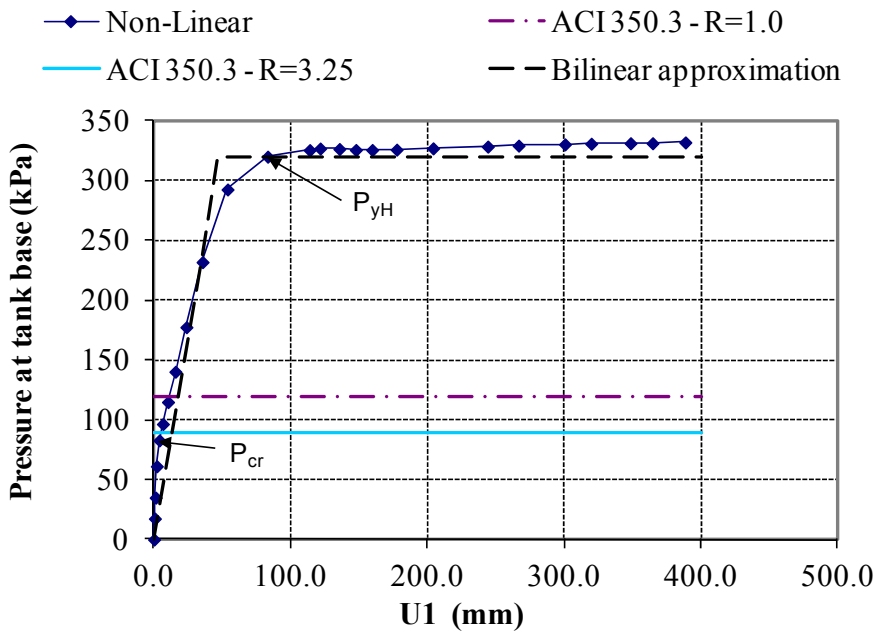

Figure 6.28 - Load-deflection response – Tank 2FR-1

6.4.5 Discussion of the results

The results of nonlinear push-over FE analysis are summarized in this section. The summary of the results for this study is presented in order to investigate the circular tank response under seismic load and to verify R_i-values specified in the current practice.

For all tanks considered in this study, by observing the required reinforcement for different tanks as indicated in Table 6.1, it is found that for load combinations specified in ACI 350-06 (2006), even though the amount of horizontal reinforcement for tanks with hinged base condition is higher than those for fixed base condition, the total amount of reinforcement (vertical and horizontal) is higher for fixed base tanks.

For Case numbers 1 to 5, fixed base tanks develop first yield in reinforcement at higher pressure than hinged base tanks. Similarly, the values of pressure at which cracking of concrete is initiated for fixed base tanks are higher than those for hinged base tanks. Also, for Tanks 1 and 2, for all considered reinforcement ratios, the tank response is elastic (linear) under hydrostatic water pressure plus the elastic earthquake pressure (ACI350.3 - R = 1.0).

Tables 6.2, 6.3, and Figures 6.29 and 6.30 show that, R_i-values depend on tank base conditions and relative tank dimensions (D/H_L ratios). Also, R_i-values for fixed base tanks are higher than those for hinged base tanks. The R_i-values for free base condition (shown in the previous section) are more than the values for fixed and hinged base conditions. Also, R_i-values for shallower tanks (i.e. larger D/H_L ratios) are higher than those for taller tanks.

Figures 6.29 and 6.30 present R_i-values for Case 1 and Case 5, respectively. The tank wall thickness (t_w) for Case 1 is more than that for Case 5 except for Tank 3 where t_w is the same for both cases. These Figures show that the wall thickness and reinforcement ratios have a major effect on the R_i-values due to the overstrength factor (R_s). However, the variation in wall thickness does not have a major effect on ductility factor (R_μ). Also, Tables 6.2 and 6.3 show that, the results of Tank 3 are very similar for Case 1 and Case 5. This similarity indicates that the effect of the P_c on the tank response is very small. The effect of P_c is not included in Case 5 where the wall thickness is maintained the same for Case 1 and Case 5 as indicated earlier.

Figure 6.31 shows that, for fixed and hinged base conditions, R_i-values increase as the tank reinforcement increase due to the increase in the overstrength factor. Tables 6.2 and 6.3 show that the pressure at which yield of reinforcement is initiated (P_y) increases as the reinforcement ratio increases. These Tables also show that, the pressure at which concrete reaches its cracking strength (P_{cr}) increases as the reinforcement ratio increases. In addition, P_y and P_{cr} for fixed base tanks are more than those for hinged base tanks.

As shown in Figure 6.32, for fixed and hinged base tanks, the ductility factor (R_μ) is inversely proportional to the reinforcement ratio. In this case, walls with a high amount of reinforcement yield at much higher loads. Also, the ductility factors for fixed and hinged base tanks are similar. However, overstrength factors for fixed base tanks are larger than those for hinged based tanks. Therefore, the total R_i-value is expected to be larger for fixed base tanks as compared to hinged base tanks.

Table 6.2 – Summary of response modification factor results for Case 1

H_w (m)	H_L (m)	(D/H_L)	Base Condition	R_s	R_μ (K and N) ((M and B))	R_i (K and N) ((M and B))	P_{cr} (kN)	P_y (kN)
3.25	3.0	13.33	Hinged	1.84	1.6 (1.64)	2.94 (3.02)	90	97
3.25	3.0	13.33	Fixed	3.87	1.39 (1.59)	5.35 (6.15)	139	205
6.5	6.0	6.67	Hinged	1.26	1.94 (2.0)	2.44 (2.52)	117	127
6.5	6.0	6.67	Fixed	1.79	2.19 (2.24)	3.93 (4.02)	157	180
9.6	9.0	4.44	Hinged	1.12	1.43 (1.39)	1.6 (1.56)	89	168
9.6	9.0	4.44	Fixed	1.32	1.46 (1.44)	1.92 (1.89)	116	198

(K and N): Krawinkler and Nasser, (M and B): Miranda and Bertero

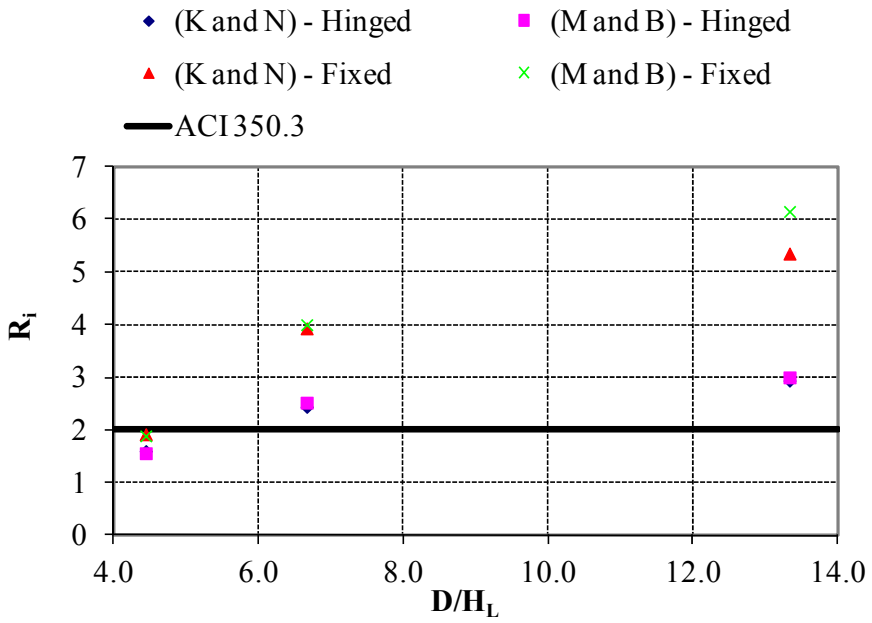

Figure 6.29 – Effect of tank dimensions on response modification factor – Case 1

Table 6.3 – Summary of response modification factor results for Case 5

H_w (m)	H_L (m)	(D/H_L)	Base Condition	R_s	R_μ (K and N) ((M and B))	R_i (K and N) ((M and B))	P_{cr} (kN)	P_y (kN)
3.25	3.0	13.33	Hinged	1.18	1.54 (1.57)	1.82 (1.85)	57	59
3.25	3.0	13.33	Fixed	1.76	1.51 (1.53)	2.65 (2.71)	77	87
6.5	6.0	6.67	Hinged	1.23	1.33 (1.29)	1.64 (1.58)	73	117
6.5	6.0	6.67	Fixed	1.1	2.4 (2.45)	2.64 (2.7)	103	105
9.6	9.0	4.44	Hinged	1.18	1.68 (1.64)	1.68 (1.64)	89	168
9.6	9.0	4.44	Fixed	1.38	1.46 (1.44)	2.02 (1.98)	116	197

(K and N): Krawinkler and Nasser, (M and B): Miranda and Bertero

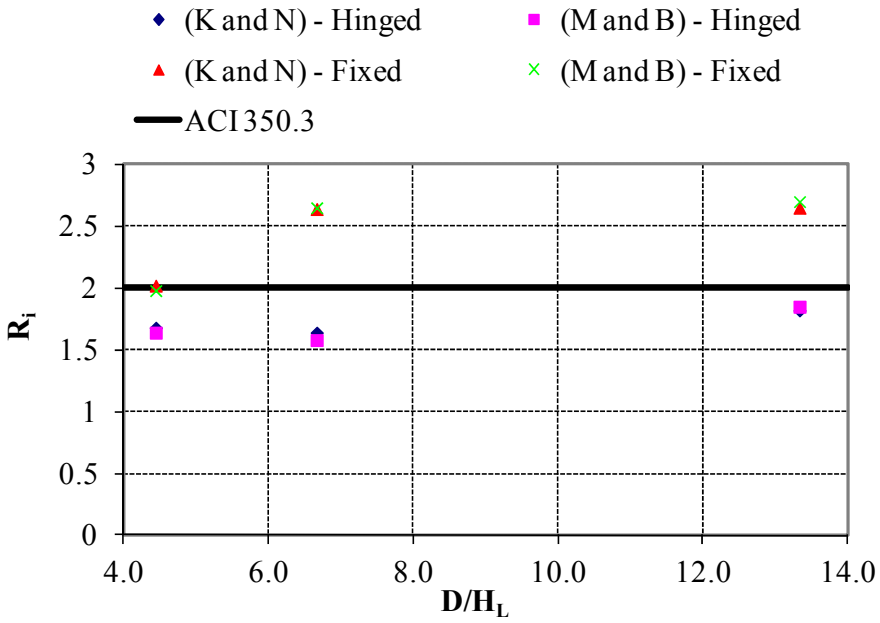

Figure 6.30 – Effect of tank dimensions on response modification factor – Case 5

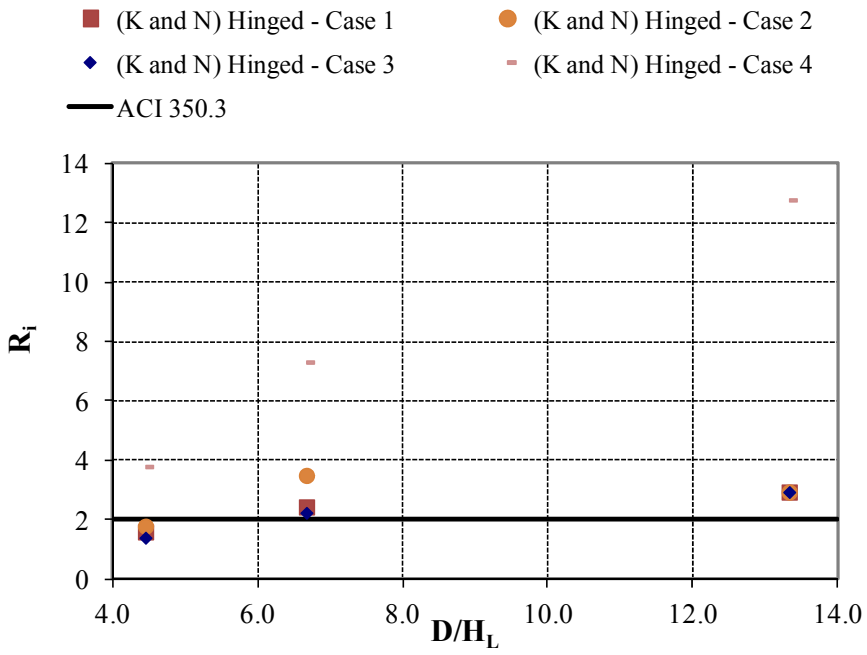

(a)

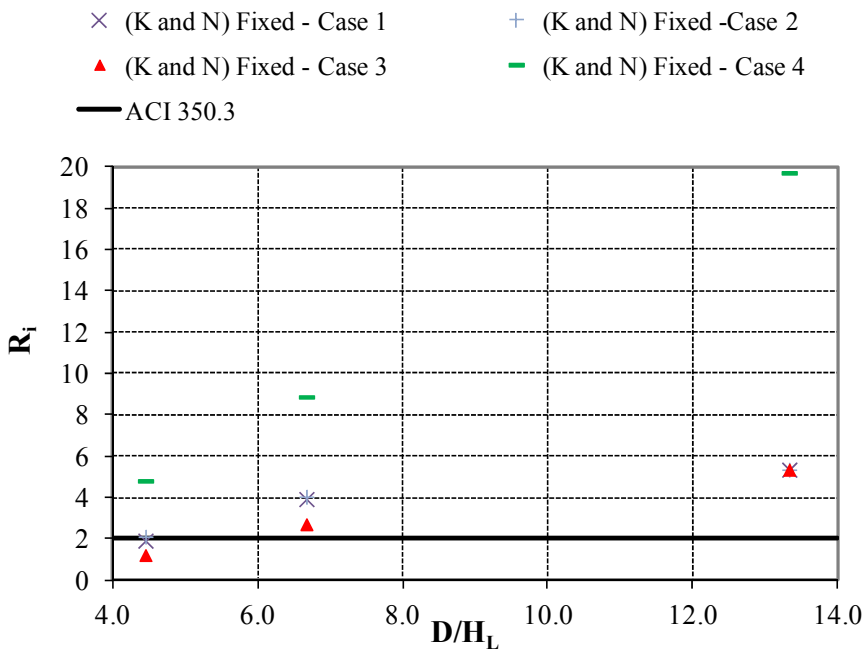

(b)

Figure 6.31 – Effect of tank reinforcement on R_i-values; (a) Hinged, (b) Fixed

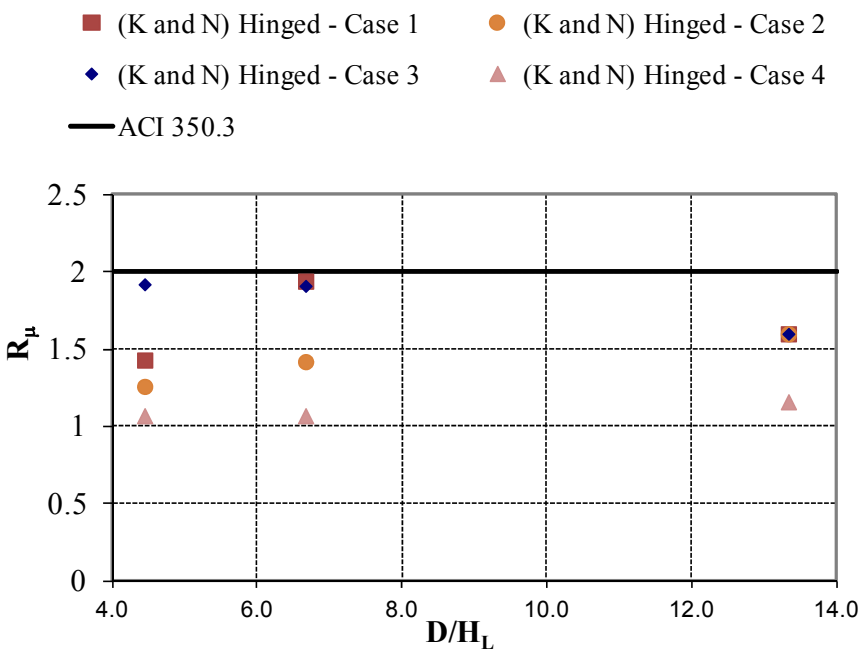

(a)

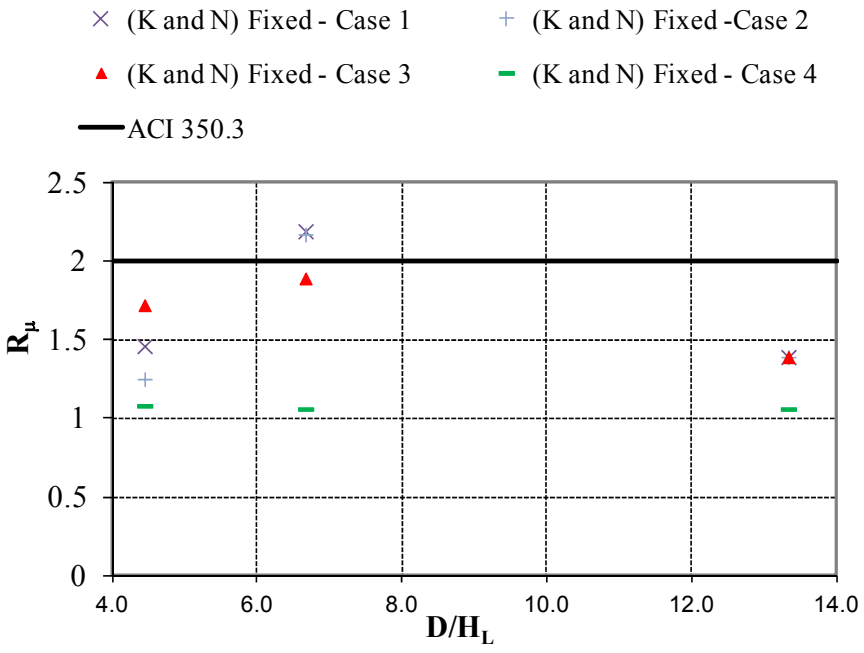

(b)

Figure 6.32 – Effect of tank reinforcement on R_μ-values; (a) Hinged, (b) Fixed

6.5 Summary

In this Chapter, nonlinear push-over FE element analysis is carried out in order to investigate the behavior of ground-supported RC concrete circular tanks under seismic loading. The results of FE analysis are used to verify the R_i-values specified in the current practice. This study is performed for tanks having different D/H_L ratios and for a wide range of reinforcement ratios in order to investigate the effect of such parameters on the results.

The results of this study show that fixed base tanks develop the first yield of reinforcement at higher load compared to hinged base tanks. Also, it is found that higher R_i-values could be assigned to fixed base tanks compared to those with hinged base conditions. It is also found that, shallower tanks can be assigned higher response modification factors. It is concluded that, there is no single Ri-value for all cases; thus, R_i-values depend on support conditions, D/H_L ratios, as well as other parameters.

CHAPTER 7
NONLINEAR BEHAVIOR UNDER TIME-HISTORY ANALYSIS

7.1 General

In this chapter, the nonlinear dynamic behavior of ground-supported circular open top tanks is investigated. Time-history FE analysis is performed to study the nonlinear response of circular tanks under seismic loads. The focus of this study is to determine the main parameters that have major effects on the dynamic response of these types of tanks. In this study, R_i-values specified in the current practice are also evaluated. Furthermore, the results of the FE time-history analysis are used to verify the seismic loads calculated based on current practice and to examine the adequacy of the code provisions in estimating the seismic loads accordingly. Also, the response of hinged, fixed and anchored flexible base tanks is examined. Furthermore, for flexible base tanks, the nonlinear Behavior of reinforced concrete (RC) and prestressed concrete (PC) tanks are also investigated. A wide range of D/H ratios is also considered in order to investigate the effect of tanks dimensions on the response.

The effect of earthquake frequency content on the dynamic response of ground-supported circular tanks is also investigated in this study. For this purpose, four different horizontal ground motions with different frequency contents are used in this study. Time-history FE analysis is carried out in order to investigate the tank response due to each ground motion.

For tanks considered in this study, (P_i) and (P_w) are much higher than (P_c) in which the latter is found to have a small effect on the overall seismic behavior. Also, the convective component of motion generally occurs at a later time than that of the impulsive response. Therefore, similar to push-over FE analysis that was discussed in Chapter 6, the effect of convective component is ignored. Only the effect of impulsive component and wall inertia are considered in the time-history dynamic analysis. Also, the soil-structure interaction and uplift effects are not considered. This study shows that the effect of convective component on dynamic response is small, and therefore it is neglected in the analysis.

7.2 Tank configuration and design parameters

In this study, nonlinear FE time-history analysis is conducted on RC and PC circular tanks in order to investigate the nonlinear behavior of such structures under dynamic seismic loads. Circular RC and PC tanks with a wide range of H_L/D ratios and different support conditions (flexible and nonflexible) are considered in order to verify the effect of these parameters on the tank response, and therefore verify R_i-values specified in the current practice.

In order to satisfy the code requirements for strength and serviceability, the circular tanks are designed to resist the applied hydrostatic and hydrodynamic loads according to ACI 350-06 (2006) and ACI 350.3-06 (2006).

The hydrodynamic forces are calculated based on ACI 350.3-06 (2006), where tank walls are designed based on ACI 350-06 (2006). The tanks are designed representing high seismic zone having S_s= 150% and S_1= 60%, corresponding to 1940 El-Centero earthquake record. S_s is the mapped maximum considered earthquake 5% damped spectral response acceleration parameter at short periods, expressed as a fraction of acceleration due to gravity g. S_1 is the mapped maximum considered earthquake 5% damped spectral response acceleration; parameter at a period of 1 second, expressed as a fraction of acceleration due to gravity g. Furthermore, for time-history FE analysis, the El-Centro record is scaled in such way that its peak ground acceleration (PGA) in the horizontal direction reaches 0.4g from its original value of 0.32g, where (g) is the acceleration due to gravity (9.807 m/s^2).

For all cases, the tank diameter (D) is assumed to be 40 m. Three different water depths, H_L equal to 3 m, 6 m and 9 m are considered, referred to as Tanks 1, 2 and 3, respectively. These water depths are corresponding to wall heights H_w equal to 3.25m, 6.5m and 9.6m, respectively. Three different values of wall thickness (t_w) are considered. These values are 250mm, 300mm, and 400mm for Tanks 1, 2 and 3, respectively. The hinged, fixed, and flexible base are referred to as H, F, and FL, respectively.

In order to verify, whether or not, the effect of P_c can be neglected for tanks under consideration, seismic forces for Tanks 1, 2 and 3 are calculated based on ACI 350.3-06 (2006) including the

effect of (P_i), (P_c), and (P_w). The base shear and bending moment due to these forces are referred to as V and Mb, respectively. In addition, for the same tanks, the seismic forces are calculated based on ACI 350.3-06 (2006) excluding the effect of (P_c), where only (P_i) and (P_c) are included. The results of this case are referred to as (P_i+P_w) and (M_i+M_w), for base shear and bending moment, respectively. Accordingly, a comparison between the results of these two cases (including and excluding P_c) is carried out.

The comparison between the results as shown in Tables 7.1 and 7.2 indicates that, the ratios of (P_i+P_w) to total base shear V are more than 98% and 95% for nonflexible and flexible base conditions, respectively. In addition, the ratios of (M_i+M_w) to M_b are around 97% and 94% for nonflexible and flexible base conditions, respectively. Therefore, the impulsive forces (P_i) and the lateral inertial forces of the accelerating wall (P_w) are much higher than the convective forces (P_c). Since the convective component has a negligible effect on the overall seismic response, it can be ignored in this study.

Moreover, according to ACI350.3-06 (2006), response modification factor for convective component of the accelerating liquid (R_c) is equal to one, and the response modification factor for impulsive component (R_i) is equal to 2.0 and 3.25 for fixed/hinged and anchored flexible base tanks, respectively. Since R_c is equal to 1.0, for all types of tanks, this parameter is not investigated in this study. As noted above, the effect of convective component was not considered in the study. However, this component can have a significant effect on design and should be considered in the design of such structures. Hence, Tanks 1, 2 and 3 are designed under the effect of P_i and P_w combined where only R_i is considered.

The base shear and bending moment are calculated according to the following equations (ACI 350.3-06 2006):

$$V = \sqrt{(P_i + P_w)^2 + P_c{}^2} \quad (7\text{-}1)$$

$$M_b = \sqrt{(M_i + M_w)^2 + M_c{}^2} \quad (7\text{-}2)$$

where,

M_b = Bending moment on the entire tank cross section just above the base of the tank wall

M_c = Bending moment on the entire tank cross section just above the base of the tank wall due to the convective force P_c

M_i = Bending moment on the entire tank cross section just above the base of the tank wall due to the impulsive force P_i

M_w = Bending moment on the entire tank cross section just above the base of the tank wall due to the wall inertia force P_w

The detailed calculations of hydrodynamic forces, bending moments, and tank design for nonflexible and flexible base are included in Appendices A.1 and A.2, respectively.

Table 7.1 – Earthquake hydrodynamic forces

Tank No.	Base cond.	H_L (m)	H_w (m)	t_w (mm)	P_i (kN)	P_w (kN)	P_c (kN)	V (kN)	P_i+P_w (kN)	$\frac{(P_i+P_w)}{V}$ %
1H/ 1F	Hinged/ Fixed	3.00	3.25	250	1281	957	360	2276	2238	98.3
2H/ 2F	Hinged/ Fixed	6.00	6.50	300	5125	974	1253	6227	6099	98
3H/ 3F	Hinged/ Fixed	9.00	9.60	400	11521	2155	2295	13867	13676	98.6
1FL	Flexible	3.00	3.25	250	789	594	360	1429	1383	96.8
2FL	Flexible	6.00	6.50	300	3154	599.5	1253	3957	3753	94.9
3FL	Flexible	9.00	9.60	400	7090	1326	2295	8723	8416	96.4

Table 7.2 – Earthquake hydrodynamic bending moments on the entire tank

Tank No.	Base cond.	H_L (m)	H_w (m)	t_w (mm)	M_i (kN.m)	M_w (kN.m)	M_c (kN.m)	M_b (kN.m)	M_i+M_w (kN.m)	$\frac{(M_i+M_w)}{M_b}$%
1H/ 1F	Hinged/ Fixed	3.00	3.25	250	1441	1569	544	3059	3010	98.4
2H/ 2F	Hinged /Fixed	6.00	6.50	300	11531	3166	3852	15194	14697	96.7
3H/ 3F	Hinged /Fixed	9.00	9.60	400	38884	10343	10880	50414	49227	97.6
1FL	Flexible	3.00	3.25	250	887	966	544	1931	1853	96
2FL	Flexible	6.00	6.50	300	7096	1948	3852	9831	9044	92
3FL	Flexible	9.00	9.60	400	23928	6365	10880	32188	30293	94.1

The effects of impulsive and convective forces on the overall dynamic response are in agreement with those of previous research studies. Using FE method in a three dimensional space, Moslemi (2011) investigated the dynamic effect of seismic force on circular open top ground-supported water tanks having aspect ratios similar to those used in this study. In his study, the effect of a wide range of parameters such as tank wall flexibility, vertical component of earthquake, sloshing of liquid free surface, tank aspect ratio, and base fixity on dynamic behavior of such structures were addressed. The results of his study showed that, the resulting convective forces have less effect on the overall dynamic response of the tanks as compared to the impulsive forces. As a result, the seismic behavior of the tanks was mainly dominated by the impulsive component rather than the convective component.

7.2.1 Nonflexible base tanks

In this study, nonflexible base is referred to as fixed and hinged base conditions. However, the current practice assigns the same value of R for fixed and hinged base tanks ($R_i = 2$). The effect of support condition on R-values for RC hinged and fixed tanks is investigated.

The tank design due to seismic load is affected by the response modification factor (R) which is specified in the current practice. In other words, as previously discussed in Chapter 6, the design

of tanks for seismic load depends on R-values specified in the codes. The R-values specified in the codes are empirical in nature, and do not seem to be rationally derived. One of the main parameters affecting the R-values is the reinforcement ratio (ρ). Therefore, for the Tanks 1, 2 and 3, further study is performed in order to investigate the effect of tank reinforcement on R-values. For this purpose, Tanks 1, 2 and 3 are designed with different values of R_i-factor starting from R_i equals to 1.0. Hence, a total of four cases are considered in this study for each tank, where R_i-values are ranging from one to four. The wall horizontal and vertical reinforcement are considered uniform along tank height (i.e. design is based on maximum forces).

The internal design forces and bending moments of tanks under consideration are calculated based on the results of linear static FE analysis. The tank walls are designed according to ACI 350 (2006). The size and spacing of reinforcement for Tanks 1, 2 and 3 with nonflexible base conditions are shown in Table 7.3.

In order to distinguish between different cases, the value of R is referred to as the case number, where the case number, which is equal to R-value, is included alongside the tank number. For example, for Tank 1H-R2; 1 refers to Tank number 1 with H_L equals 3.0 m, H refers to hinged base, and R2 refers to R equals 2.

7.2.2 Anchored flexible base tanks

For circular tanks with anchored flexible supports, the hydrodynamic forces are calculated based on ACI 350.3-06 (2006) with R = 3.25. For theses tanks, both RC and PC tanks are investigated. For RC tanks, the tank walls are designed according to ACI 350-06 (2006). For PC tanks, the design is according to ACI 373R (1997), AWWA D110 (2004) and Chapter 18 of ACI 350-06 (2006).

ACI 350.3-06 (2006) indicates that the flexible base condition applies to prestressed tanks only. However, RC flexible base tanks are also considered in this study for the purpose of direct comparison with fixed and hinged base conditions.

The design forces and bending moments for tanks with flexible base are calculated based on the results of linear static FE analysis. Moreover, for flexible supports, seismic cables in the tangential directions of the tank wall resist the seismic forces at the tank base. Also, the stiffness of the bearing pads in both tangential and radial directions is considered in the analysis and design of such tanks.

For PC tanks, the crack control and liquid-tightness is achieved by the circumferential prestressing together with non-prestressed vertical reinforcement near each face of the wall. The minimum thickness of the core wall is maintained as 250mm for cast-in-place concrete walls with internal circumferential tendons and vertical conventional reinforcement according to ACI 373R (1997). In addition, the initial the circumferential prestressing force (P_i) is calculated to be of a sufficient magnitude to counteract the axial circumferential tension in the wall due to stored water and seismic force after accounting for the prestress losses. The final effective prestressing force (after long term losses) is referred to as P_e. Furthermore, 1.38 MPa (200 psi) residual compressive stress is provided in the wall, with the combined stresses due to hydrostatic and hydrodynamic forces, after consideration of the prestress losses in order to prevent vertical cracking (ACI 373R 1997). It should be noted that, the circumferential prestressing tendons are bonded according to ACI 350-06 (2006).

The reinforcement, prestressing strands, and seismic cable details for Tanks 1, 2 and 3 with anchored flexible base conditions are shown in Tables 7.4 and 7.5. As indicated before, in LCS, leakage occurs soon after the yielding of the reinforcement (Sadjadi 2009). Therefore, an additional case for RC tanks is investigated where R is calculated at reinforcement yield, referred to as (RCY).

For the case of RCY, in order to calculate R-value at which yield of wall reinforcement is initiated, the following steps are used:

- The hydrostatic and equivalent static seismic loads for R_i equal to 3.25 are calculated based on ACI 350.3 (2006).

- The tank reinforcement is designed accordingly for the combined effect of hydrostatic and seismic loads according to ACI 350 (2006).
- Nonlinear dynamic time-history FE analysis is carried out, and the stress in reinforcing bars is obtained and compared with yield stress.
- If the reinforcement does not yield, the above steps are repeated for different R_i-values until reinforcement starts to yield.
- The R-value for RCY case study is considered based on the value at which yield of bars is initiated.

The designation of each considered case is added alongside the tank number. For example, for Tank 1FL-PC; 1 refers to Tank number 1 with H_L equal to 3.00 m, FL refers to flexible base, and PC refers to prestressed tank.

The detailed design calculations according to ACI 350.3, ACI 350 and ACI 373R for a typical case of the anchored flexible-base tanks are included in Appendix A.2 for reference.

The definitions of symbols in Tables 7.3, 7.4 and 7.5 are as follows:

H_L: Water Depth
H_w: Wall Height
t_w: Wall thickness
EF: Each face
IF: Inside face
OF: Outside face
For prestressing strand size designation 15: Nominal Diameter is equal to 15.24 mm
f_{pu}: Specified tensile strength of prestressing strands = 1860 MPa
P_i: Initial circumferential prestressing force
P_e: Effective (final) circumferential prestressing force (after long term losses)

Table 7.3 - Tank dimensions and reinforcement – Fixed and hinged base

					Horizontal Bars, EF		Vertical Bars, IF		Vertical Bars, OF	
Tank No.	Base condition	H_L (m)	H_w (m)	t_w (mm)	Bar Size	Spacing (mm)	Bar Size	Spacing (mm)	Bar Size	Spacing (mm)
1H-R1	Hinged	3.00	3.25	250	15M	230	15M	300	15M	300
1F-R1	Fixed	3.00	3.25	250	15M	300	15M	180	15M	300
1H-R2	Hinged	3.00	3.25	250	15M	300	15M	300	15M	300
1F-R2	Fixed	3.00	3.25	250	15M	300	15M	250	15M	300
1H-R3	Hinged	3.00	3.25	250	15M	390	15M	300	15M	300
1F-R3	Fixed	3.00	3.25	250	15M	300	15M	300	15M	300
1H-R4	Hinged	3.00	3.25	250	15M	430	15M	300	15M	300
1F-R4	Fixed	3.00	3.25	250	15M	300	15M	325	15M	300
2H-R1	Hinged	6.00	6.50	300	20M	180	15M	225	15M	170
2F-R1	Fixed	6.00	6.50	300	15M	170	20M	120	15M	225
2H-R2	Hinged	6.00	6.50	300	20M	250	15M	225	15M	200
2F-R2	Fixed	6.00	6.50	300	15M	225	20M	150	15M	225
2H-R3	Hinged	6.00	6.50	300	20M	260	15M	225	15M	225
2F-R3	Fixed	6.00	6.50	300	15M	260	20M	175	15M	225
2H-R4	Hinged	6.00	6.50	300	20M	280	15M	225	15M	225
2F-R4	Fixed	6.00	6.50	300	15M	275	20M	185	15M	225
3H-R1	Hinged	9.00	9.60	400	25M	160	20M	250	20M	250
3F-R1	Fixed	9.00	9.60	400	25M	195	25M	140	20M	250
3H-R2	Hinged	9.00	9.60	400	25M	200	20M	250	20M	250
3F-R2	Fixed	9.00	9.60	400	25M	250	25M	175	20M	250
3H-R3	Hinged	9.00	9.60	400	25M	230	20M	250	20M	250
3F-R3	Fixed	9.00	9.60	400	25M	280	25M	195	20M	250
3H-R4	Hinged	9.00	9.60	400	25M	250	20M	250	20M	250
3F-R4	Fixed	9.00	9.60	400	25M	300	25M	205	20M	250

H_L: Water Depth, H_w: Wall Height. t_w: Wall thickness , EF: Each face

Table 7.4 - Tank dimensions and reinforcement – Anchored flexible base

				Horizontal Bars EF		Vertical Bars EF	
Tank No.	H_L (m)	H_w (m)	t_w (mm)	Bar Size	Spacing (mm)	Bar Size	Spacing (m)
1FL-PC	3.00	3.25	250	—	—	15M	300
1FL-RC	3.00	3.25	250	20M	240	15M	300
1FL-RCY	3.00	3.25	250	20M	340	15M	300
2FL-PC	6.00	6.50	300	—	—	15M	225
2FL-RC	6.00	6.50	300	25M	230	15M	225
2FL-RCY	6.00	6.50	300	25M	320	15M	225
3FL-PC	9.00	9.60	400	—	—	20M	250
3FL-RC	9.00	9.60	400	25M	150	20M	250
3FL-RCY	9.00	9.60	400	25M	210	20M	250

Table 7.5 - Tank prestressing and seismic cable details – Anchored flexible base

	Horizontal Prestressing Seven Wire Strands – Size 15				Base seismic cables	
Tank No.	No. of Strands	Spacing (mm)	P_i (kN)	P_e (kN)	Strand Size (mm)	Spacing (m)
1FL-PC	3	400	530	398	15	5.0
1FL-RC	—	—	—	—	15	5.0
1FL-RCY	—	—	—	—	15	5.0
2FL-PC	3	200	530	398	15	2.0
2FL-RC	—	—	—	—	15	2.0
2FL-RCY	—	—	—	—	15	2.0
3FL-PC	5	270	884	663	15	0.9
3FL-RC	—	—	—	—	15	0.9
3FL-RCY	—	—	—	—	15	0.9

7.3 Computer model and finite element analysis

The FE analysis is conducted using ABAQUS/CAE Version 6.8.3 (Dassault Systèmes Simulia Corp. 2008). Using the interactive and graphical technique the computer model is created using ABAQUS/CAE. Material properties, loads and boundary conditions are assigned to the geometry. FE analysis is carried out on the circular tanks described in Section 7.2. In this study, nonlinear time-history dynamic analysis is performed where the nonlinearity of construction material is considered.

7.3.1 Geometry

The entire tank is modeled using four-node quadrilateral shell elements as shown in Figure 7.1 for Tank 2FL. The wall thickness is significantly smaller than the wall height and tank diameter; therefore, shell elements were considered appropriate to be used in modeling the tank walls. In this case, the thickness is defined through the section property definition. The conventional shell elements used in the analysis have three displacement and three rotational degrees of freedom at each joint. The numbers of elements along the wall height are considered four, seven, and ten elements for Tanks 1, 2 and 3 respectively.

Along the water height (H_w), the tank wall is divided equally into one meter long elements, where the number of elements along the wall up to the water height is considered as three, six, and nine elements for Tanks 1, 2 and 3 respectively. The length of the very top element is considered to be equal to the tank freeboard which is equal to 0.25m, 0.5m and 0.6m for Tanks 1, 2 and 3, respectively. In order to maintain the aspect ratio to one, each tank circumference was divided into 128 equal elements where the element size along the circumference is approximately equal to 1 m. Accordingly, the total number of elements for Tanks 1, 2 and 3 are 512, 896 and 1280 respectively. However, mesh sensitivity study is performed in order to investigate the effect of the element size on the results.

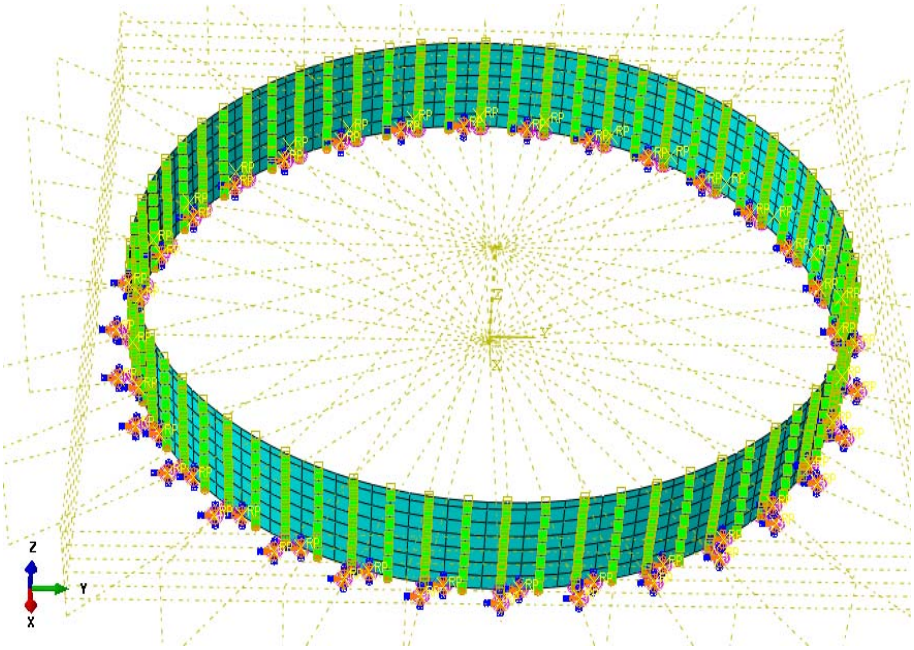

Figure 7.1 – Finite element model for Tank 2FL - ABAQUS/CAE

7.3.2 Material properties

For linear elastic analysis, the material properties are specified as follows; the specified compression strength of concrete (f'_c) and yield strength of reinforcement (f_y) are 30 MPa and 400 MPa, respectively, where the modulus of elasticity of concrete (E_c) and reinforcement (E_s) are taken as 26000 MPa and 200000 MPa respectively. The concrete section is considered as uncracked section.

For nonlinear analysis, the materials properties as described in detail in Chapter 4 are used for this study. Concrete damaged plasticity (CDP) model is used since it is the most suitable concrete model for dynamic analysis.

The prestressing force is applied in the form of thermal contraction that is applied only to the prestressing tendons which are assumed to be fully bonded to concrete. Therefore, the thermal expansion coefficient of concrete and reinforcement is assumed to be zero.

For both linear and nonlinear FE analysis, the following material proprieties are considered:

Thermal expansion coefficient of concrete (α_c) and reinforcement (α_s) = 0.0
Thermal expansion coefficient of prestressing tendons (α_{spt}) = $1x10^{-5}$
Poisson's ratio of concrete (ν_c) = 0.18
Poisson's ratio of reinforcement (ν_s) and prestressing tendons (ν_{pt}) = 0.0

Reinforcement is modeled using the same technique described in Chapter 6. Since the tendons are fully bonded for PC tanks, the prestressing tendons are modeled using the same technique as the reinforcement.

7.3.3 Damping

In this study, five percent damping was considered in the time-history dynamic analysis. General damping was introduced in ABAQUS in the form of "Rayleigh" damping. To define Rayleigh damping, two damping factors are specified: α_R for mass proportional damping and β_R for stiffness proportional damping. In general, damping is a material property specified as part of the material definition. For a given mode *i* the fraction of critical damping (ζ_i) can be expressed in terms of the damping factors α_R and β_R using Equation 7-3:

$$\zeta i = \frac{\alpha_R}{2\omega_i} + \frac{\beta_R w_i}{2} \qquad (7\text{-}3)$$

where ω_i is the natural frequency at i^{th} mode. Generally speaking, this equation implies that the mass proportional Rayleigh damping, α_R, damps out the lower frequencies and the stiffness proportional Rayleigh damping, β_R, damps out the higher frequencies.

Therefore, in this study, free vibration analysis is carried out on the three dimensional models of Tanks 1, 2 and 3. The natural frequencies obtained from modal analysis are used to calculate the Rayleigh damping factors to be included in the time-history analysis.

7.3.4 Boundary conditions and flexible support

For fixed and hinged base tanks, the tank supports were defined by means of applying boundary conditions that would restrain the movements or rotations in the desired direction.

For anchored flexible base tanks, the seismic cables and bearing pads are modeled as spring elements. Hence, in the tangential direction, the stiffness of seismic cables and bearing pads is considered to be linear as described in Chapter 4. The stiffness of the anchored flexible support in the tangential direction (K_t) is calculated using Equations 7-4 and 7-5 (ACI 350.3-06 2006).

K_t = (K of Seismic cables + K of Bearing pads) (7-4)

$$K_t = 1000\left[\left(\frac{A_S\, E_S \cos^2\alpha}{L_C S_c}\right) + \left(\frac{2G_P w_p L_p}{t_p S_p}\right)\right] \quad (7\text{-}5)$$

In the radial direction, the stiffness of the bearing pads is also considered to be linear. The stiffness of the flexible support in the radial direction (K_r) is calculated using Equations 7.6 and 7.7 (ACI 350.3-06 2006).

K_r = (K of Bearing pad) (7.6)

$$K_r = 1000\left(\frac{2G_P w_p L_p}{t_p S_p}\right) \quad (7\text{-}7)$$

where,

A_s is the area of each seismic cable

E_s = 200,000 MPa

Lc = 838mm (the length of the RUBATEX Sleeve plus the embedded length = 35xD_s)

Sc is the spacing between the seismic cables

G_p: shear modules of elastomeric bearing pad

w_p: width of elastomeric bearing pad

L_p: length of elastomeric bearing pad

t_p: thickness of elastomeric bearing pad

S_p: spacing of elastomeric bearing pad

D_s: diameter of seismic cables

K: stiffness

The detailed design and support stiffness calculations of flexible base are included in Appendix A.2.

As shown in Figure 7.2, the flexible base is modeled using two spring elements at each node of the tank base in the tangential and radial directions. Each spring was defined by connecting two points, where one end of each spring was selected to be one of the tank joints at the base, where the other end of the spring was modeled as fixed support.

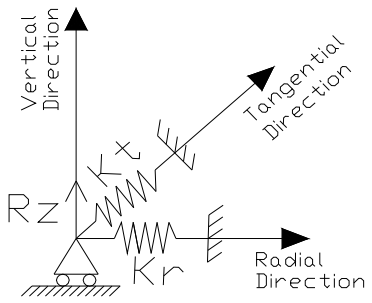

Figure 7.2 – Flexible support model

SPRINGA element in ABAQUS/CAE is used in the analysis to model actual physical springs representing the flexible support. This element acts between two nodes, with its line of action being the line joining the two nodes. The linear spring behavior is defined by specifying constant

spring stiffness (force per relative displacement) where the force in a SPRINGA element is positive in tension.

SPRINGA element introduces stiffness between two degrees of freedom without introducing an associated mass, where the relative displacement was measured along the direction of the SPRINGA element in the reference direction.

7.3.5 Loads

7.3.5.1 Prestressing

The prestressing force is applied as thermal contraction to the prestressing tendons, and therefore the thermal expansion coefficient of concrete and mild reinforcement is assumed to be zero. The required change of temperature (ΔT) to simulate the prestressing force can be calculated using Equations 7-8 and 7-9 as follows:

$$E_s = \frac{\sigma_s}{\varepsilon_s} \tag{7-8}$$

$$\varepsilon_s = \alpha_s \Delta T \tag{7.9}$$

where,

The elastic modulus of prestressing tendons (E_s) = 200,000 MPa

The thermal expansion coefficient of prestressing tendons (α_{spt}) = $1x10^{-5}$

The initial (σ_i) and effective stresses (σ_e) in the prestressing tendons of 1263 MPa and 947 MPa, respectively, are known from the design stage. Accordingly, the strain in prestressing tendons can be calculated from Equation 7-8. By substituting ε_s from Equation 7-8 in Equation 7-9, the change of temperature (ΔT) can be expressed as:

$$\Delta T = \frac{\sigma_s}{E_s \alpha_s} \tag{7-10}$$

Therefore, in order to simulate the initial and effective prestressing forces in tendons, temperature change of −631.5^{o}C (contraction) and −473.6 ^{o}C are applied to the tank walls, respectively.

7.3.5.2 Earthquake ground forces

The earthquake force is applied in the form of time-history ground acceleration based on actual ground motion records. However, in order to investigate the effect of earthquake frequency content on the dynamic response of ground-supported circular tanks, linear FE time-history analysis is performed. In this analysis, only Tank 1H is subjected to four different horizontal ground motions with different frequency content properties.

The longitudinal components of 1940 El-Centro, 1994 Northridge, 1971 San-Fernando, and 1957 San-Francisco earthquakes were considered as horizontal ground excitations for Tank 1H, where only the first ten seconds of the records are used in time-history analyses. The El-Centro horizontal record is scaled in such a way that its peak ground acceleration (PGA) reaches 0.4g, where g is the ground acceleration (g = 9.807 m/sec^2). The other horizontal ground motion records were scaled in such a way to have the same value of Power index (P_a) (Housner 1975) as that of the scaled El-Centro record.

An integration step of 0.02 sec is used to be small enough to characterize the tanks response. Also, a sufficient number of modes are used in order to obtain modal mass participation of at least 90% of the total impulsive and wall combined mass in the direction under consideration.

As indicated by Moslemi (2011), the Power index is the most appropriate indices to be used for scaling of the earthquake motions and as a result, the intensity of motions can be satisfactorily characterized by this parameter. The earthquake motions are usually characterized by parameters related primarily to the amplitude of the shaking, such as peak ground acceleration; however, research studies show that it is not a reliable measure by itself (Housner 1975). The single peak on an accelerogram cannot be considered as an accurate representation of the earthquake record as a whole.

Housner (1975) proposed that a measure of seismic intensity could be defined by the average rate of buildup of the total energy per unit mass input to the structure. Taking into consideration that the integral of the squared ground acceleration is proportional to the total input energy, the Power index was introduced as:

$$Pa = \frac{E(D)}{D} = \frac{1}{D}\int_{t_0}^{t_0+D_0} a^2(t)dt \qquad (7\text{-}11)$$

where,

E(D) is the total energy input during time D
D is the "significant duration" of earthquake
t_0 is the time at the beginning of the strong shaking phase
a(t) is the base acceleration
In other words, the Power index can be considered as a measure of the rate at which energy would be fed into the system.

In Equation 7-11, t_0 and t_0+D_0 are the limits of the strong portion of motion. Equation 7-11 can be interpreted as the average value of the squared acceleration over the significant duration interval D.

The common definition of significant duration of motion (Trifunac and Brady 1975) is used in this study where the significant duration is defined as the interval between instants t_5 and t_{95} at which 5% and 95% of the total integral in Equation 7-12 as follows:

$$AI = \frac{\pi}{2g}\int_0^{t_r} a^2(t)dt \qquad (7\text{-}12)$$

where,
AI is the Arias intensity (Arias 1970)
t_r is the total duration of the ground motion.

It should be noted that, the concept of significant duration has the benefit of considering the properties of the whole accelerogram and defining a continuous time interval during which the shaking may be considered as strong.

By replacing D with $t_{95} - t_5$ in Equation 7.11, the earthquake power can be defined as:

$$Pa = \frac{1}{t_{95} - t_5} \int_{t_5}^{t_{95}} a^2(t)dt \qquad (7\text{-}13)$$

The scaled earthquake records are shown in Figure 7.3, where the proprieties of the scaled records are listed in Table 7.6.

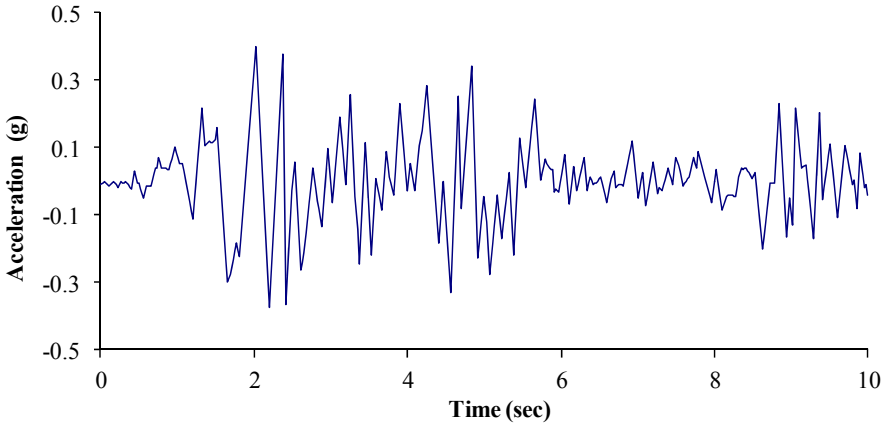

(a)

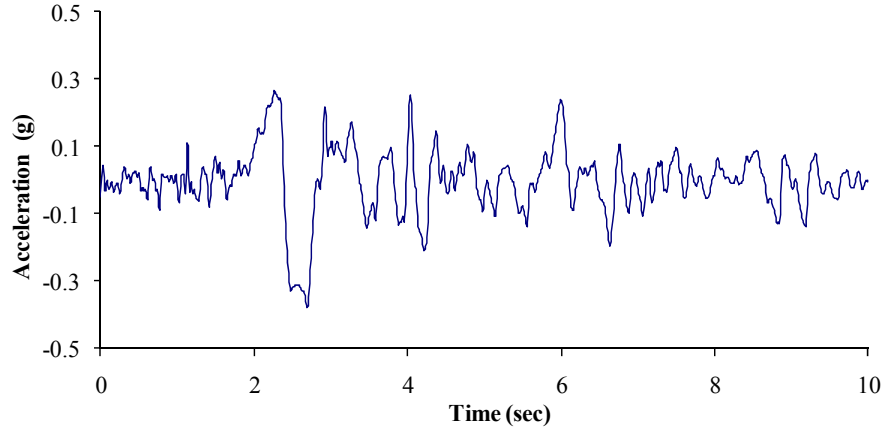

(b)

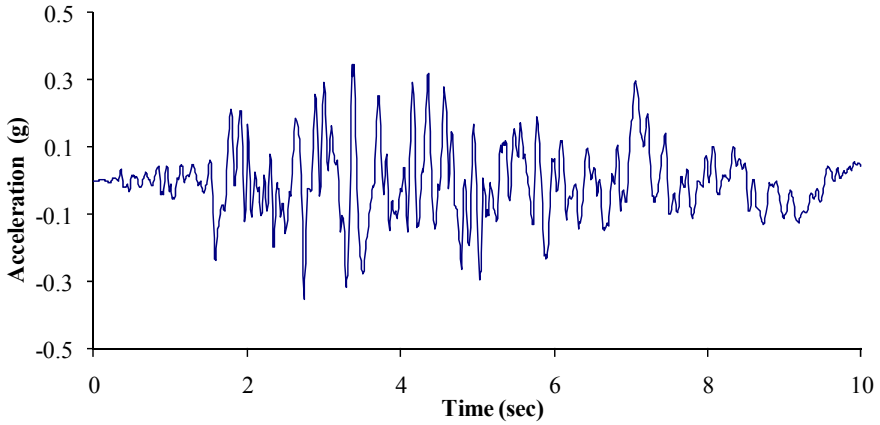

(c)

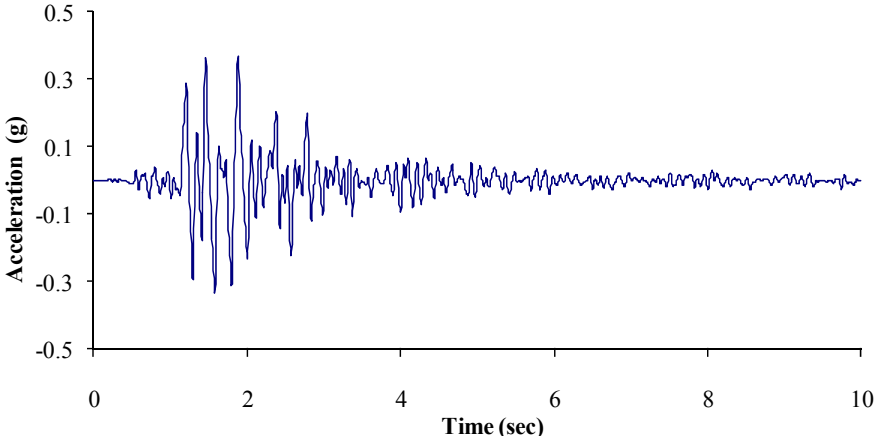

(d)

Figure 7.3 – Scaled earthquake record (horizontal component); (a) El-Centro, (b) Northridge, (c) San-Fernando, (d) San-Francisco

Table7.6 – Ground motions properties

Earthquake	t_5(Sec)	t_{95}(Sec)	D(Sec)	Pa(m^2/s^4)	$\frac{PGA}{PGV}$
El-Centro	1.63	13.25	11.62	1.13	0.88
Northridge	2.12	9.14	7.02	1.12	0.51
San-Fernando	1.75	10.08	8.33	1.12	1.11
San-Francisco	1.18	4.15	2.97	1.13	2.44

Furthermore, the ratio of peak ground acceleration (PGA) in units of g to the peak ground velocity (PGV) in units of m/sec is considered a good indicator of the frequency content of the ground motion. Accordingly, ground motions with PGA/PGV < 0.8 are classified as low frequency content, ground motions with 0.8 < PGA/PGV < 1.2 are classified as intermediate frequency content, and ground motions with PGA/PGV > 1.2 are classified as high frequency content. Therefore, the Northridge earthquake is classified as low frequency content, the El-Centro and San-Fernando earthquakes are classified as intermediate frequency content and the San-Francisco earthquake is classified as high frequency content.

The four ground motions as shown in Figure 7.3 are applied to Tank 1H in order to investigate the effect of frequency content on the seismic response of the ground-supported circular tanks. The time-history base shear responses of the tank subjected to the different ground motions based on linear FE analysis are shown in Figure 7.4.

For comparison, the ratio of peak base shear response of each ground motion with respect to the highest value corresponding to El-Centro ground motion is shown in Figure 7.5. As shown in this figure, the intermediate frequency content earthquake of El-Centro results in the highest response values compared to all other records. Accordingly, the response values due to El-Centro ground motion are highly amplified as a result of the similarity between the frequency characteristics of the tank and the earthquake motion. Therefore, using the horizontal component of El-Centro ground motion is considered appropriate for the time-history analysis that is performed in this study.

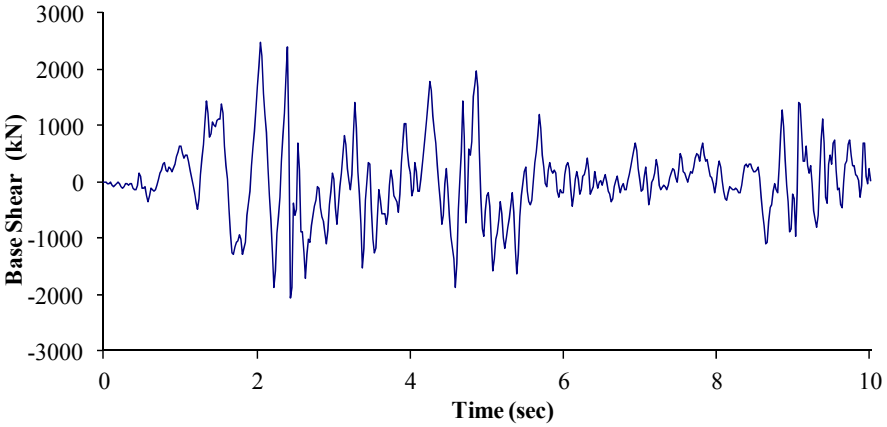
3000
2000
1000
0
-1000
-2000
-3000
Base Shear (kN)
0
2
4
6
8
10
Time (sec)

(a)

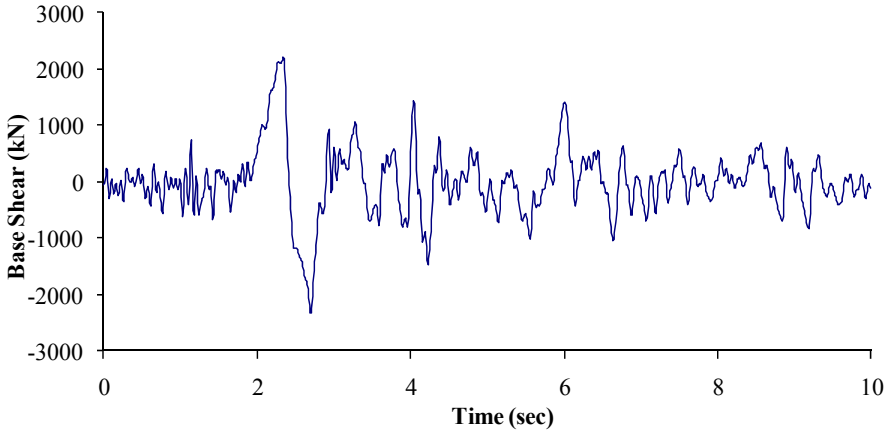
3000
2000
1000
0
-1000
-2000
-3000
Base Shear (kN)
0
2
4
6
8
10
Time (sec)

(b)

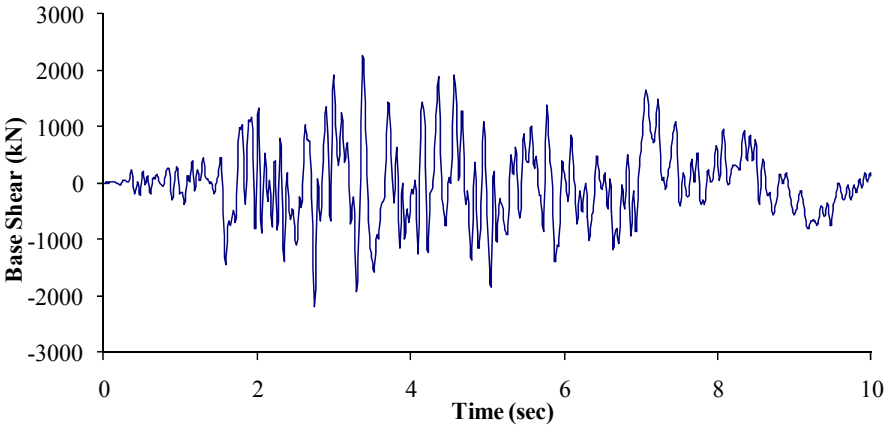
3000
2000
1000
0
-1000
-2000
-3000
Base Shear (kN)
0
2
4
6
8
10
Time (sec)

(c)

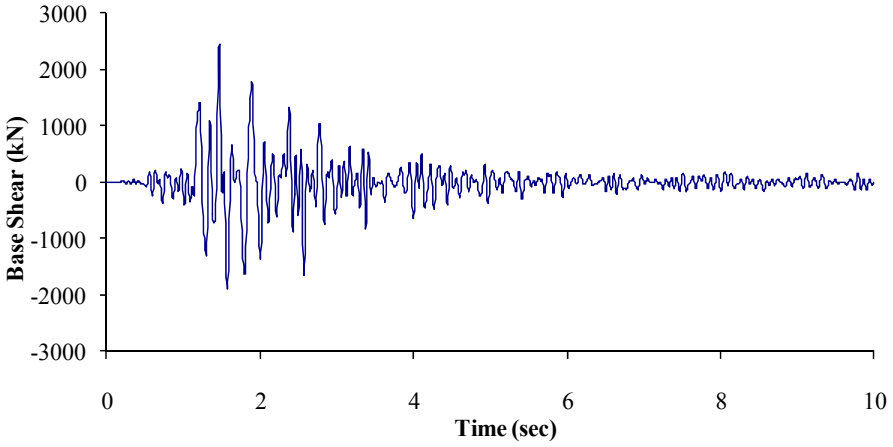

(d)

Figure 7.4 – Time-history of base shear response for Tank 1H; (a) El-Centro, (b) Northridge, (c) San-Fernando, (d) San-Francisco

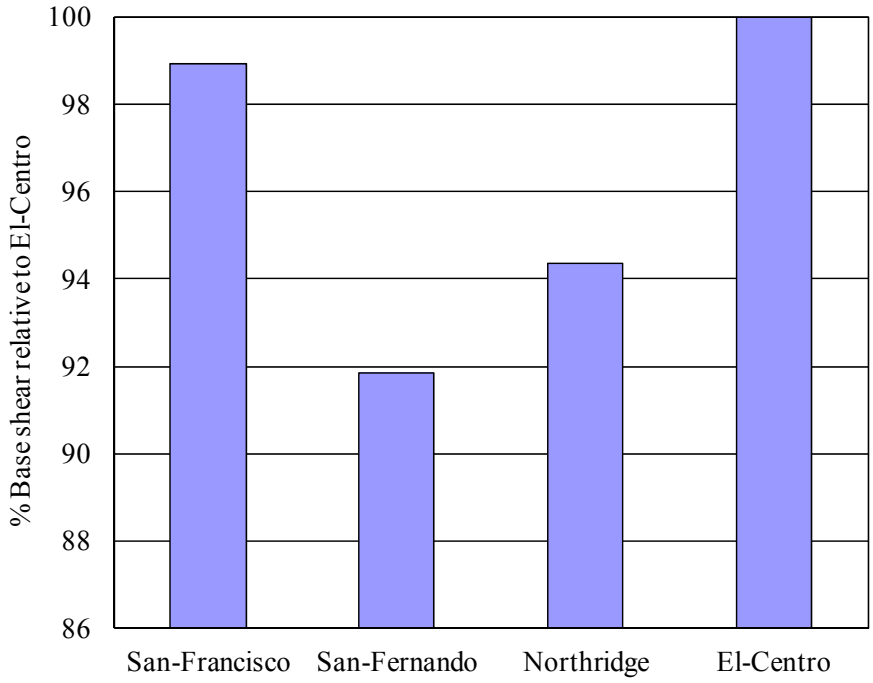

Figure 7.5 – Percentage of peak base shear relative to El-Centro ground motion

The effect of the frequency content of the four considered ground motions on tank response are in agreement with those of previous research studies. Recently, a study by Moslemi (2011) was

conducted in order to investigate the dynamic behavior of circular open top ground-supported water tanks. Moslemi investigated two cylindrical tanks having aspect ratios similar to those used in this study. In his study, same ground motions as used in the current study were used. He concluded that, the response values due to El-Centro record are highly amplified as compared to other ground motions. This was due to the similarity between the frequency characteristics of the tank system and earthquake motion. For this reason, the El-Centro ground motion is used in this study.

7.3.5.3 Gravity load

The gravity load (wall self weight) can be created by defining a uniform acceleration which is the ground acceleration ($g = 9.807$ m/sec^2) in a fixed direction (-Z), where Z is the vertical direction. ABAQUS calculates the loading using the acceleration magnitude, the material density specified in the material definition, and the section thickness from section properties. Therefore, the gravity load is the total weight of the tank walls. However, if nonstructural mass included in the model in a given element, it will accordingly participate in any mass proportional distributed loads, such as gravity loading, defined on that element. Also, the effect of the gravity load on the internal forces is minimal since the main forces that control the tank design are the hoop forces and vertical moments for most cases. The gravity force is included as concentrated loads at element nodes.

7.3.5.4 Hydrostatic load

The hydrostatic load is defined as a pressure over the interior surface of the tank wall around tank circumference and facing outward as shown in Figure 7.6. ABAQUS is capable of defining pressure load that have a hydrostatic pressure distribution; however, the option of defining a hydrostatic pressure applied to the surface is valid only for ABAQUS/Standard analyses. Therefore, the hydrostatic load was applied as load that is uniform over the surface. Accordingly, the hydrostatic load is calculated at a height that is corresponding to the centerline of the shell elements at a certain level, where this value was considered as the uniform pressure at this height. The calculations of the hydrostatic load for Tank 2 are included in Appendix A.1 for reference.

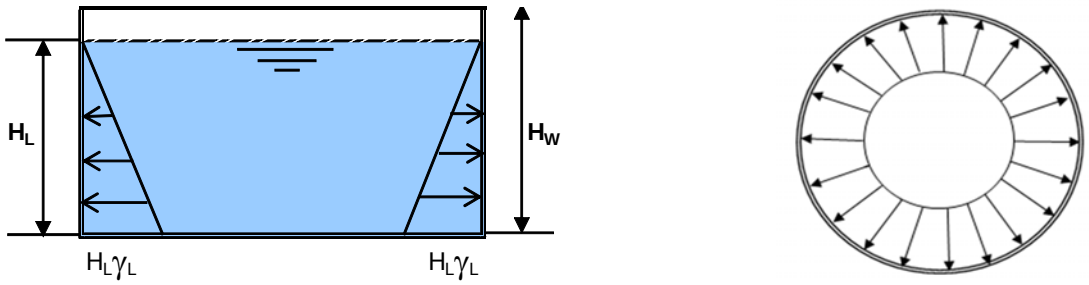

(a) (b)

Figure 7.6 – Hydrostatic pressure; (a) Vertical distribution, (b) Horizontal distribution (tank circumference)

7.3.5.5 Mass

In FE analysis, only the masses associated with impulsive component and the tank wall are included since the effect of the convective component is negligible as described in Section 7.2.

A study was performed on anchored ground supported circular tanks (Virella and Godoy 2006) in order to investigate the validity of modeling the impulsive mass using added mass approach versus modeling with the acoustic elements. This study was performed on a wide range of height/diameter (H/D) of the tanks from 0.4 to 0.95. It was found that the response of the tanks that were examined using both approaches (added mass and acoustic elements) is very similar; in fact, the differences between the fundamental periods obtained using both approaches are smaller than 3%. Thus, it was concluded that the added mass approach can provide a good approximation for calculating the response of tanks filled with liquid, as the results compare very well with the more sophisticated models in which the liquid is represented as acoustic finite elements regardless of the aspect ratio (H/D) of the tank. In addition, in the study performed by Virella and Godoy (2006), the lumped masses obtained from the added mass have the same vertical variation as the impulsive pressure distribution from which they are derived, and they have, however, a uniform distribution around the circumference of the tank. Also, in their study, they introduced a new scheme in order to represent the added mass in the direction normal to the shell elements, where the added liquid mass in lumped form was attached to the shell nodes by means of rigid, massless links with small length. These links were rigid truss elements where the supports permitted the motion of the nodal mass only in the direction normal to the shell. Hence,

the motion of the support was restricted in the global tangential direction (perpendicular to the element axis) and in the vertical direction, but it was free to move in the global radial direction (i.e. the local axial direction). The total impulsive mass M_i was calculated as per Equation 7.14 by first obtaining a mass resultant m_{res} for the tank meridian in the direction of the ground excitation, and then integrating around the circumference to compute the total impulsive mass of the tank. The added mass components in the direction of the excitation are directly proportional to the impulsive pressure which varies with a cosine distribution around the tank circumference as shown in Figure 3.6 (a). Hence, to integrate the radial mass in order to obtain the impulsive mass, the mass m_{res} was projected along the direction of the excitation. Moreover, m_{res} was calculated for the $\theta = 0$ meridian. To calculate m_{res} for $\theta > 0$, it was multiplied by cos θ.

$$M_i = 4Rm_{res}\int_0^{\pi}\cos^2(\theta)d\theta = \pi Rm_{res} \qquad (7\text{-}14)$$

where,

R is the tank radius

m_{res} is the mass resultant calculated as the sum of individual masses m_i at different nodes along the $\theta = 0$ meridian

M_i is the total impulsive mass

Accordingly, the total impulsive mass M_i in a specific direction calculated using Equation 7.14 was twice the impulsive mass computed using Housner's methodology (Housner 1963). However, as the masses can only move in the radial direction, they showed that half of this total impulsive mass is excited in a specific direction.

Hence, the mass of the tank wall was defined as a "structural" mass which is the sum of all the mass contributions to the shell elements of the tank model. The structural mass was calculated from the material and section properties. Accordingly, the structural mass includes the mass due to any material definitions associated with the shell elements such as the mass from any rebars

included in shell elements. In ABAQUS, the nonstructural mass contribution to an element is not allowed if that element has no structural mass.

Since the impulsive mass of the contained liquid acts rigidly with the tank walls; therefore it was defined as added mass in the form of a "non-structural" mass which is the contribution to the model mass from features that are not part of the structural properties. The added non-structural mass is specified in the form of mass per unit area to the shell elements, in which the masses are assigned to all shell elements. The added mass components around the tank circumference were distributed based on cosine distribution similar to the impulsive pressure as shown in Figure 3.6 (a), where mass component in the direction of the ground excitation is equal to the mass at each polar angle (θ) multiplied by cosine (θ). Also, the added mass was modeled in such way to have the same vertical variation as the impulsive pressure distribution as shown in Figure 3.7. The total impulsive mass (M_i) was calculated based on Housner's methodology according to ACI 350.3-06 (2006).

Furthermore, in order to verify using the nonstructural mass approach in modeling the impulsive mass, the mass for Tank 1H is defined using added mass and nonstructural mass approaches. The material nonlinearity was not considered in this verification. The scaled El-Centro is used for time-history FE analysis. Figure 7.7 shows that the time-history responses of base shear for both methods are identical with only 1.5% difference for peak value. Therefore, even though the non-structural mass is exited in the direction of global direction of the ground motion, it will not have any effect on the total base shear. Also, the maximum peak internal forces will not be affected since they are calculated at $\theta = 0$ meridian.

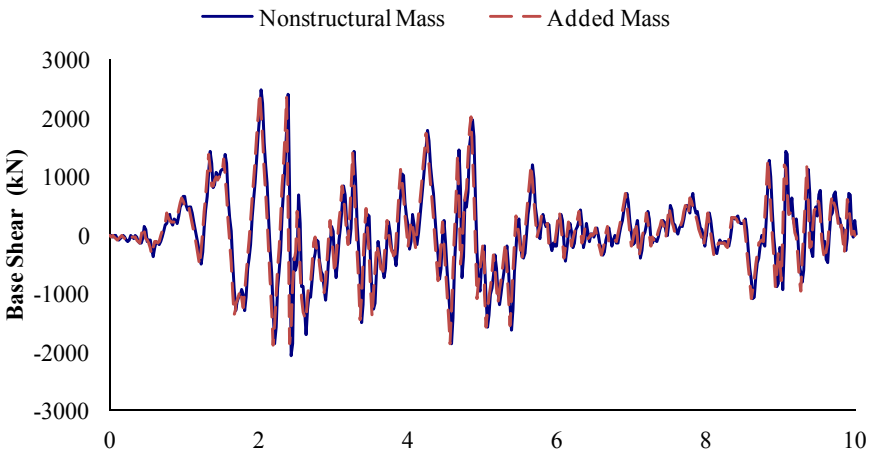

Figure 7.7 – Time-history of base shear response for Tank 1H - El-Centro
Added mass versus Nonstructural mass

7.3.5.6 Shear resistance for anchored flexible base tanks

For anchored flexible base tanks, the main mechanism for transferring the base shear from the wall to the foundation is the tangential resistance offered by a system of seismic cables connecting the wall to the perimeter footing. Typically these cables are 15 mm (0.6") diameter, 7-wire, high-strength strands. Each cable is embedded partially in the footing and partially in the walls, and is inclined to 45 deg. from the horizontal in a direction tangent to the wall.

When an unbalanced horizontal force, such as earthquake, acts on the tank, the seismic cables inclined normal to the direction of the seismic force offers no resistance, while other cables especially those parallel to the force offer the maximum resistance. This resistance is in the form of cable tension that prevents the displacement of the wall relative to the footing. The benefit of this mechanism is that it provides load transfer from the wall to the footing by means of membrane action, and not by vertical bending.

According to AWWA D110 (2004), for tanks with anchored flexible base, the anchorage is achieved by diagonal-strand seismic cables embedded in the wall and footing, which resist tangential movements but permit only limited radial movement of the wall under hydrostatic load. Therefore, under hydrostatic loads, the anchored flexible base is allowed to move in the

radial direction until seismic cables bear against concrete. Accordingly, the tank base will move as a rigid body in the direction of the applied force under seismic force.

It should be noted that the base pads for tanks with unanchored flexible base shall be designed to resist the total seismic base shear, where the maximum total base-pad frictional resistance shall not exceed the gravity load of the wall multiply by the coefficient of friction, unless adequate shear keys or other positive mechanical means of attachments are provided to transfer the shear forces from the concrete to the base pads (AWWA D110 2004). It should be noted that the coefficient of friction or base-joint friction between the concrete and an elastomeric pad can be assumed as 0.5 to compute the maximum allowable base-pad, service-load, frictional resistance unless a more precise method of determining the coefficient of friction between the two surface is used. However, Ramanathan et al. (2010) used a coefficient of friction of 1.0 for elastomeric bearing pad in their study. Moreover, only anchored flexible base tanks are considered in this study where a limited radial movement will take place until seismic cables bear against concrete, as compressible sponge rubber sleeves shall be used over seismic cable through the base joints to allow for the controlled radial wall movement. Furthermore, for Tanks 1FL, 2FL and 3FL the ratio between gravity load of the tank wall multiplied by the coefficient of friction and total base-pad frictional resistance is more than one when the tanks are subjected to prescribed seismic loads as described in this chapter. The sliding factor of safety for Tanks 1FL, 2FL and 3FL are 1.1, 1.07 and 1.03, respectively.

7.4 Results of time-history FE analysis

7.4.1 Model verification

This study is performed for fixed and hinged base conditions. Tanks 2H and 2F are modeled using two different FE computer programs (SAP2000 and ABAQUS) in order to verify the output results of the computer model that is used in the FE analysis. Furthermore, the results of FE analysis are compared with those of current practice in order to evaluate the accuracy of the current practice in predicting the seismic response of the ground-supported circular tanks.

The nonlinear behavior of tank material is not considered in this verification. For the purpose of design and analysis, as indicated in Section 7.3.2, the specified compression strength of concrete

(f'_c) and yield strength of reinforcement (f_y) are considered as 30 MPa and 400 MPa respectively. The modulus of elasticity of concrete (E_c) is taken as 26000 MPa. The El-Centro ground motion horizontal component as shown in Figure 7.3 is used in the time-history analysis. The horizontal component was scaled in such way that its peak ground acceleration (PGA) in the horizontal direction reaches 0.4g (original value 0.32g), where (g) is the acceleration due to gravity (9.807 m/s^2). In addition, in order for the current practice results to be comparable with those obtained from finite element (FE) analyses, the values of the response modification factor for the impulsive component (R_i) is considered as unity for seismic force calculations. Hence, in calculating the design forces using the current practice, the design forces were calculated based on ACI 350.3-06 (2006). The tanks were designed representing high seismic zone having mapped spectral accelerations S_s = 150% and S_1 = 60%.

For current practice, the dynamic properties of the model (natural periods of vibration and associated modal masses corresponding to the impulsive and convective) are calculated based on (Housner 1963) using a two-mass idealization approach, where the wall flexibility is not considered. On the other hand, the FE element analysis is performed using lumped masses along the wall height where the wall flexibility is included in the analysis.
Table 7.7 shows that, the results of finite element analysis using ABAQUS and SAP2000 for fixed and hinged base tanks are very similar. The difference between the base shear is 6% and 3% for hinged and fixed base condition, respectively, where the difference between the fundamental period of oscillation using two computer programs is only around 1%. Therefore, it can be concluded that the finite element model using ABAQUS is reliable.

The base shear and fundamental period of oscillation are also calculated according to the current practice as presented in Table 7.7. Comparing the results of finite element programs and the current practice for the hinged base condition, it is found that the difference between base shear according to current practice and FE element analysis is 13% and 19% for hinged and fixed support condition, respectively. The difference between fundamental period of oscillation is 37% and 26% for hinged and fixed base condition, respectively.

The current practice leads to relatively higher response values as a result of higher seismic coefficient associated with the fundamental impulsive mode due to lower period corresponding to fundamental impulsive mode. Also, the current practice does not consider the effect of the wall flexibility; thus, the contribution of the first oscillation modes is included while the effect of higher modes is ignored.

Furthermore, the material nonlinearity is not considered in FE analysis for this comparison as concrete walls are considered uncracked. Hence, the actual value of the base shear resulted from time-history nonlinear analysis is expected to be of a lesser value due to the reduced stiffness of the tank wall where the fundamental period of oscillation is expected to increase for the same reason.

The definitions of symbols in Tables 7.7 are as follows:

T_i: Fundamental period of oscillation of the tank plus the impulsive component of the contents

V_{max}: Maximum peak base shear due to impulsive and lateral inertia force of accelerating wall from time-history analysis due to El-Centro horizontal record

V_{min}: Minimum peak base shear due to impulsive and lateral inertia force of accelerating wall from time-history analysis due to El-Centro horizontal record

$V_{El\text{-}Centro}$: Absolute maximum value of peak base shear to impulsive and lateral inertia force of accelerating wall from time-history analysis due to El-Centro horizontal record

$V_{ACI350.3}$: Base shear due to impulsive and lateral inertia force of accelerating wall based on ACI 350.3 with $R_i = 1.0$

R_i : Response modification factor for the impulsive component

Table 7.7 – Computer model verification – Tank 2H

	Hinged Base			Fixed Base		
	ACI350.3 ($R_i = 1$)	SAP2000	ABAQUS	ACI350.3 ($R_i = 1$)	SAP2000	ABAQUS
T_i (Sec)	0.0771	0.12373	0.12277	0.0771	0.10722	0.10516
$V_{ACI350.3}$	12198.4	–	–	12198.4	–	–
V_{max} (kN)	–	9957	10625	–	10190	9870
Time step of V_{max} (Sec)	–	2.51	2.51	–	2.5	2.5
V_{min} (kN)	–	-7352	-7911	–	-7503	-7770
Time step of V_{min} (Sec)	–	2.17	2.17	–	2.16	2.16
$V_{El\text{-}Centro}/V_{ACI350.3}$	–	82%	87%	–	84%	81%

The maximum hoop forces and bending moments in the tank wall due to El-Centro time-history analysis and current practice, at polar coordinate angle (θ) = 0^o, for Tank 2H are shown in Figures 7.8 (a) and (b), respectively. The internal forces and bending moments based on the current practice are obtained by applying the calculated seismic forces based on current practice to the tank as equivalent static load. A comparison shows that the difference between the two sets of results is only 4% for hoop forces and bending moments. Therefore, it can be concluded that the estimated responses are in agreement.

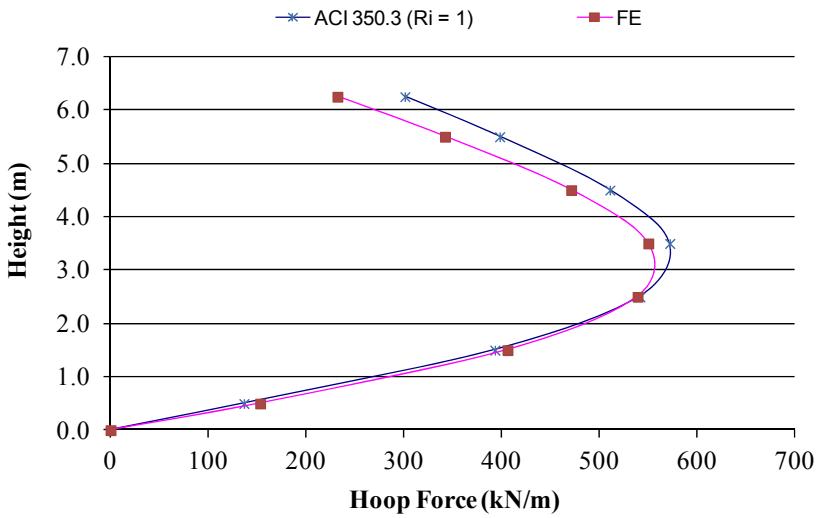

(a)

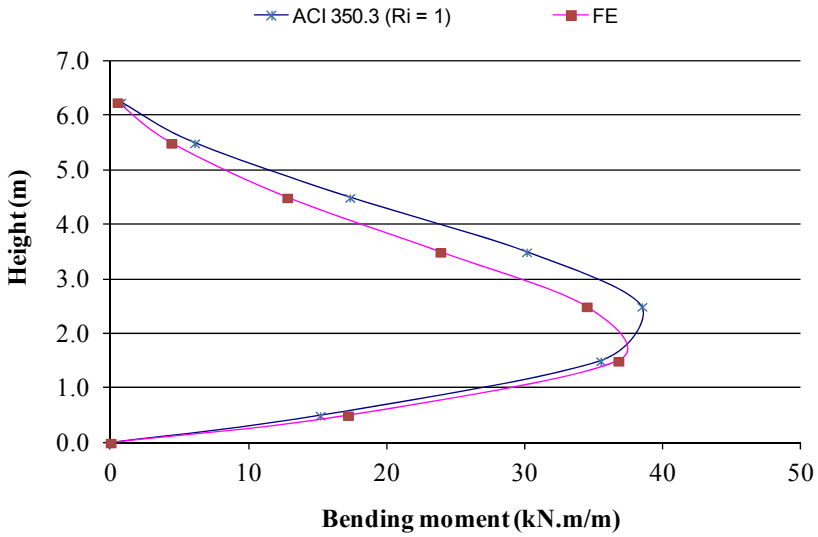

(b)

Figure 7.8 – Comparison between FE time-history and current practice – Tank 2H; (a) Hoop force, (b) Bending moment

7.4.2 Sensitivity study

A sensitivity study is carried out to ensure that the size of the selected elements is appropriate for the performed analysis and to investigate the effect of the mesh size on the results. This study is performed for Tank 1H as shown in Table 7.3. The size of elements is reduced to 0.25 m^2 (from 1.0 m^2) in which two models are analyzed for the same tank having similar properties but with different mesh size. These two models are referred to as Mesh 1 (M1) and Mesh 2 (M2) for mesh size of 1.0 m^2 and 0.25 m^2, respectively. Therefore, the number of elements along the wall height is considered as four, and thirteen for models M1 and M2, respectively. The scaled El-Centro record as shown in Figure 7.3 is used in the time-history FE analysis. Both linear and nonlinear behaviors of tank material are considered in this verification.

As shown in Figure 7.9 (a), the difference between the maximum hoop forces for models M1 and M2 is 8% and 6% for linear and nonlinear analysis, respectively. Similarly for bending moment in the vertical direction, as shown in Figure 7.9 (b), the difference between maximum values of models (M1) and (M2) is 8% and 7% for linear and nonlinear analysis, respectively. It should be noted that the effect of mesh size on the results will be further improved for Tank 2 and Tank 3 since the element size compared to the wall heights is even smaller than the case for Tank 1. Accordingly, the results of this mesh sensitivity study as shown in these Figures indicate that the effect of the selected element size on the results is within an acceptable range.

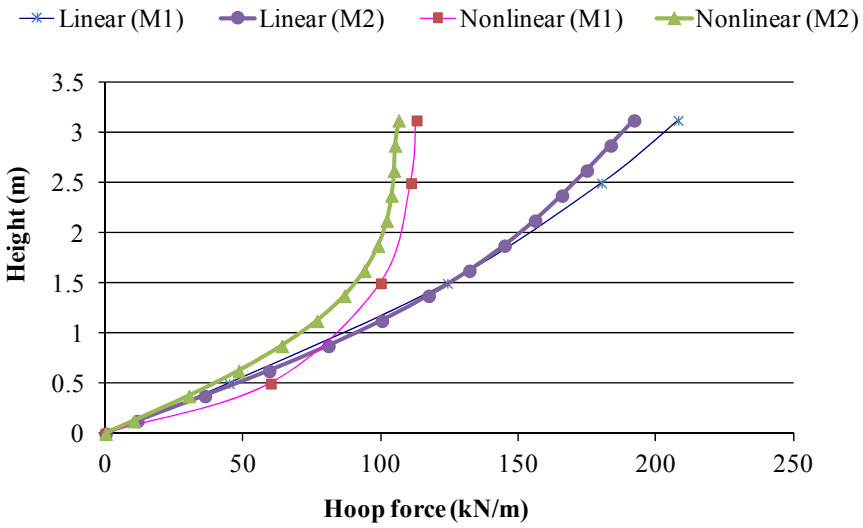

(a)

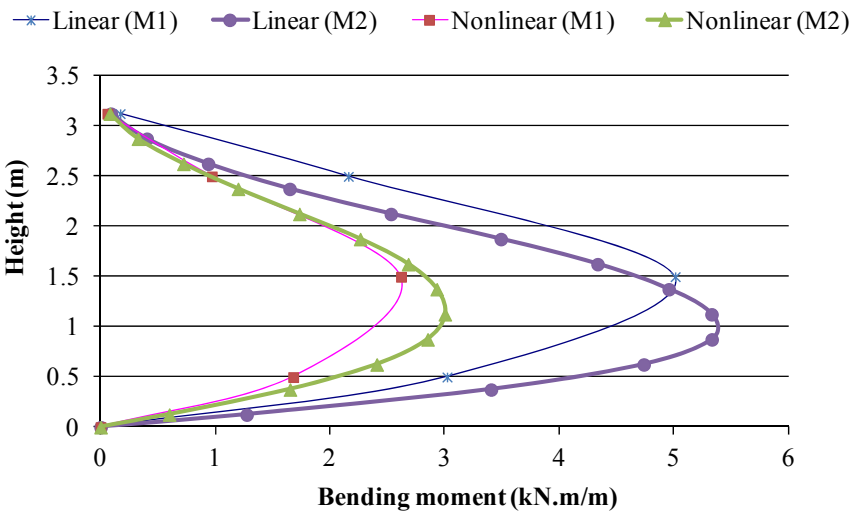

(b)

Figure 7.9 – Mesh sensitivity study - Tank 1H; (a) Hoop forces, (b) Bending moments

7.4.3 Comparison between the results of FE analysis and current practice

In order to evaluate the tank response under the effect of hydrodynamic forces calculated based on current practice, the results of nonlinear FE analysis are compared to those based on current practice for Tanks 1, 2 and 3 with fixed, hinged, and flexible base conditions.

In this study, based on current practice, the hoop forces and bending moments in the tank wall are calculated using linear FE analysis. These forces are obtained based on the equivalent seismic forces applied on the tank wall. The maximum hoop forces and bending moments in tank walls are also obtained from nonlinear dynamic time-history FE analysis. For the purpose of direct comparison between FE analysis and current practice, the tank response under the effect of seismic loads based on current practice is calculated for R_i equals to 1.0.

For fixed and hinged base tanks, the results of total base shear, hoop forces and bending moments in the tank wall are presented in Table 7.8 for Tanks 1, 2 and 3. The results presented in this Table show that, the ratios between current practice and FE are different by a factor of more than 2.35, 2.0 and 2.32 for base shear, hoop forces and bending moments, respectively.

This indicates that the current practice overestimates the tank response for hinged and fixed base tanks.

For RC anchored flexible base tanks, the results of base shear are presented in Table 7.9. As shown in this Table, for base shear, the ratios between current practice and FE are 2.02, 2.23 and 2.15 for Tanks 1FL-RC, 2FL-RC and 3FL-RC, respectively. Similarly for hoop forces, the ratios between current practice and FE are different by a factor of more than 2.0 for all cases. It should be noted that RC anchored flexible base tanks are included for comparison purpose only since flexible base condition can only be used for PC tanks (ACI 350.3-06 2006).

Table 7.8 – Comparison between results of nonlinear time-history FE analysis and current practice – Nonflexible base conditions

	Total base shear (kN)			Maximum hoop force (kN/m)			Maximum bending moment (kN.m/m)		
Tank No.	ACI 350.3 ($R_i = 1$)	FE	$\frac{\text{ACI350.3}}{\text{FE}}$	ACI 350.3 ($R_i = 1$)	FE	$\frac{\text{ACI350.3}}{\text{FE}}$	ACI 350.3 ($R_i = 1$)	FE	$\frac{\text{ACI350.3}}{\text{FE}}$
1H	4476	1901	2.35	228	113	2.02	5	2.1	2.38
1F	4476	1905	2.35	64	23	2.78	22.6	8.1	2.79
2H	12198	4389	2.78	330	123	2.68	21	7.8	2.69
2F	12198	4396	2.77	250	97	2.57	47.7	19.2	2.48
3H	27352	10526	2.60	576	286	2.01	30	12.9	2.32
3F	27352	10617	2.58	484	195	2.48	81	32	2.53

FE: Maximum value of response from time-history FE analysis due to scaled El-Centro horizontal record

Table 7.9 – Comparison between results of nonlinear time-history FE analysis and current practice – Anchored flexible base condition

	Base shear (kN)			Maximum hoop force (kN/m)		
Tank No.	ACI 350.3 ($R_i = 1$)	FE	$\frac{\text{ACI350.3}}{\text{FE}}$	ACI 350.3 ($R_i = 1$)	FE	$\frac{\text{ACI350.3}}{\text{FE}}$
1FL-RC	4476	2220	2.02	570	260	2.19
2FL-RC	12198	5480	2.23	999	476	2.1
3FL-RC	27352	12736	2.15	1497	745	2.01

FE: Maximum value of peak base shear from time-history FE analysis due to scaled El-Centro horizontal record

The results of the comparison between FE analysis and current practice are in agreement with those of previous research studies. A procedure to solve the storage tanks problem in three-dimensional space has been introduced by Kianoush et al. (2006). A case study was used to determine the validity of the code procedure based on lumped mass approach. For this purpose, a rectangular tank having dimensions of water depth (H_L) = 6.0 m, wall depth (H_w) = 6.5 m, and wall thickness (t_w) = 500 mm were used. The length of the container in the direction of the earthquake was assumed to be 20m. It was found that the absolute maximum values of base shear and base moment using staggered displacement method are 119 kN/m and 403 kNm/m, respectively. It was very clear that the response values using the proposed method are much less than those obtained using the code procedure which are 270 kN/m for the base shear and 658 kNm/m for the base moment. In this case, the maximum base shear and base moment are less than those obtained based on the code procedure by factors of 2.26 and 1.63, respectively.

Another study by Chen and Kianoush (2005) was conducted to investigate the response of rectangular tanks. A case study was used to evaluate the validity of using the lumped mass approach. In this study, both a shallow tank and a tall tank were used. The dimensions of the shallow tank were H_L = 5.5 m, H_w = 6.0 m, and t_w = 600 mm and those of tall tank were H_L = 11.2 m, H_w = 12.3 m, and t_w = 1200 mm. The study showed that the maximum base shears are less than those obtained based on the code procedure for both tall and shallow tanks by factors of

2.34 and 1.93 respectively. The results of the present study show similar differences in values between the FE analysis and current practice.

Recently, another study by Moslemi (2011) was conducted in order to investigate the dynamic behavior of circular open top ground-supported water tanks. In this study, the dynamic results obtained from FE method were compared with those recommended by current practice and thereby the adequacy of the current code provisions in estimating the dynamic response of liquid-filled cylindrical was investigated. For this purpose, two cylindrical tanks having aspect ratios of (H_L/D) = 0.115 and 0.324, referred to as shallow tank and tall tank, respectively, were used. The dimensions of the shallow tank were H_L = 5.5 m, H_w = 6.0 m, and t_w = 300 mm and those of tall tank were H_L = 11.0 m, H_w = 12.0 m, and t_w = 500 mm. It was found that, ACI 350.3-06 standard does not appropriately account for the effect of wall flexibility and base fixity. In other words, it gives the same hydrodynamic pressure values for rigid and flexible as well as for hinged and fixed tanks. As a result, it was concluded that in general code provisions yield a conservative estimation of results. This was observed for "Shallow" as well as "Tall" tanks.

7.4.4 R-values based on the results of time-history FE analysis

The results of nonlinear time-history FE analysis for flexible and nonflexible base conditions are presented in this section and compared. Also, the results of FE analysis in this study are used to verify the R-values included in the current practice.

As discussed in Chapter 6, the design of the tank walls is usually dictated by controlling the crack width. Sadjadi (2009) studied the cracking and leakage of LCS under seismic loads and concluded that leakage occurs soon after the yielding of the reinforcement. Also, considering that the earthquake load is a transient load for a very short period of time, the stress in reinforcement can reach the yield stress at a certain location without compromising the structural integrity of the tank. Therefore, for transient loads, such as an earthquake, it is considered appropriate to estimate R-value at the first yield in the reinforcement.

As discussed before in this chapter, Tanks 1, 2 and 3 are designed under the effect hydrostatic and hydrodynamic loads for different R-value. The tanks are subjected to hydrostatic and time-

history earthquake horizontal ground motion. The maximum stress in tank reinforcement is observed for each case in order to determine the R-value at which yielding of reinforcement is initiated.

The relationships between R-values assumed in tank design and corresponding maximum stresses in tank reinforcement for Tanks 1, 2 and 3 are shown in Figures 7.10 (a), (b) and (c), respectively. In these figures, the results based on FE analysis are presented for fixed, hinged and RC flexible base tanks. The summary of R-values at which first reinforcement yield is initiated is presented in Table 7.10 for nonflexible and RC flexible base tanks.

In Figures 7.10 (a), (b) and (c), each point represents the results of FE analysis for one of the tanks used in this study. For example, for Tank 1 with hinged base, the maximum stresses in tank reinforcement at R_i equal to 2.0 represents the results obtained from FE analysis for Tank 1H-R2.

Furthermore, as discussed previously for the case of RCY, in order to calculate R-value at which yield of tanks reinforcement is initiated similar steps are taken.

The results of this study show that, the tank reinforcement for fixed base tanks yields at higher assigned R-values than those for hinged base tanks. For flexible base RC tanks, tank reinforcement yields at higher assigned R-values than those for nonflexible base tanks. R-values based on FE analysis for fixed, hinged and RC flexible base tanks are higher than the values specified in the current practice. The R-value indicated in current practice for flexible base condition is for PC tanks only (ACI 350.3-06 2006). For all cases, the results of FE analysis also indicate that, there is no single value for R, where R-values depend on tank relative dimensions and support conditions.

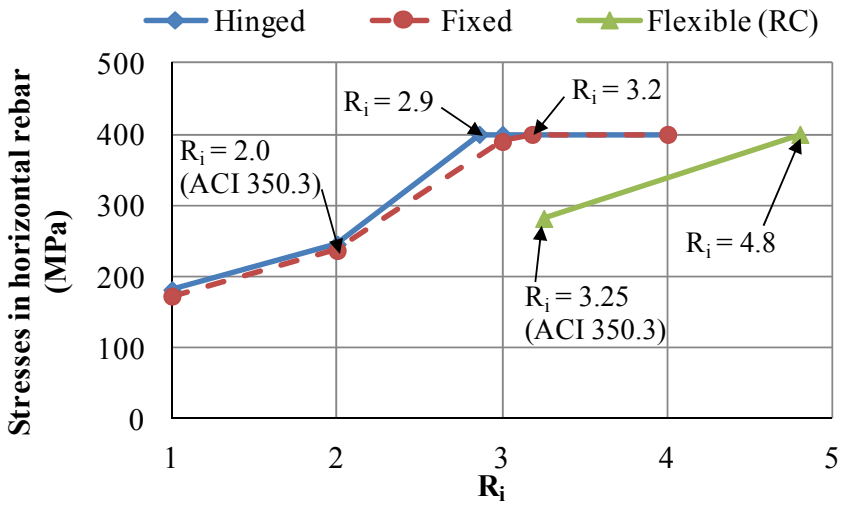
Hinged
Fixed
Flexible (RC)
Stresses in horizontal rebar (MPa)
500
400
300
200
100
0
1
2
3
4
5
Ri
Ri = 2.9
Ri = 3.2
Ri = 2.0 (ACI 350.3)
Ri = 4.8
Ri = 3.25 (ACI 350.3)

(a)

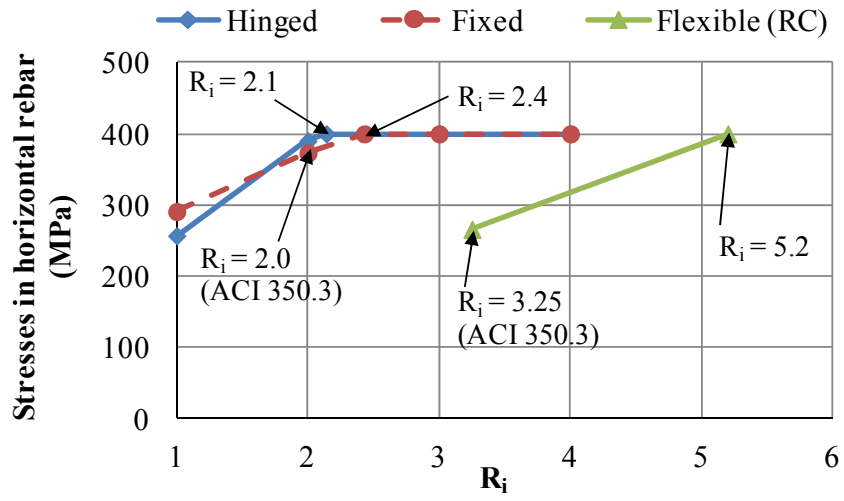
Hinged
Fixed
Flexible (RC)
Stresses in horizontal rebar (MPa)
500
400
300
200
100
0
1
2
3
4
5
6
Ri
Ri = 2.1
Ri = 2.4
Ri = 2.0 (ACI 350.3)
Ri = 5.2
Ri = 3.25 (ACI 350.3)

(b)

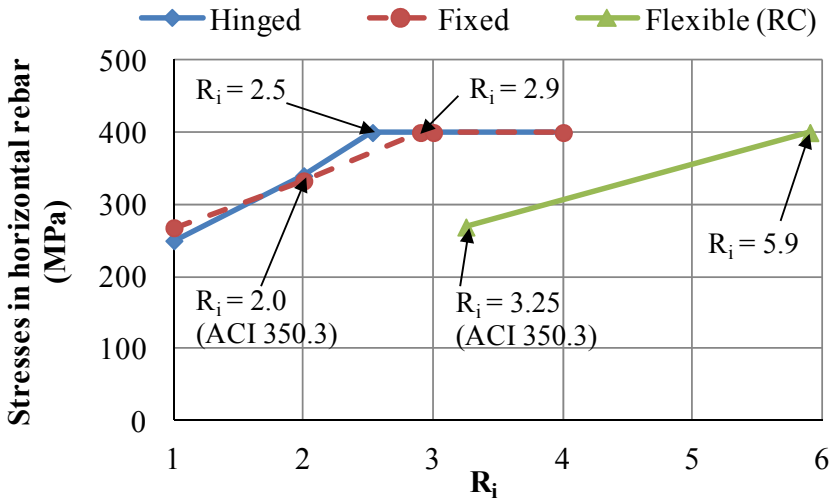

(c)

Figure 7.10 – Effect of R_i-values on stress in reinforcement; (a) Tank 1, (b) Tank 2, (c) Tank 3

Table 7.10 – Summary of R_i-values based on results of FE analysis

Tank No.	H_L (m)	Base Condition	t_w (mm)	Ri
1H	3.0	Hinged	250	2.9
1F	3.0	Fixed	250	3.2
1FL	3.0	Flexible	250	4.8
2H	6.0	Hinged	300	2.1
2F	6.0	Fixed	300	2.4
1FL	3.0	Flexible	300	5.2
3H	9.0	Hinged	400	2.5
3F	9.0	Fixed	400	2.9
1FL	9.0	Flexible	400	5.9

FE refers to the value of R_i when the reinforcement yielded under the effect of scaled El-Centro time-history FE analysis.

For PC flexible base tanks, the increase in stresses in prestressing tendons under the effect of hydrostatic and dynamic earthquake loads is relatively small for all tanks. A typical PC tank response under time history analysis is shown in Figure 7.11 which represents Tank 1FL-PC.

This Figure shows load stages including initial prestressing, hydrostatic load, presstressing losses (assumed 25%) and seismic load. Therefore, to determine the R-values at which yield of prestressing tendons is initiated may not be practical for PC tanks. In this case, the ratio between linear and nonlinear base shear based on time-history FE analysis is used to determine the value of ductility reduction factor (Newmark and Hall 1982). The R-values calculated based on this approach for PC tanks are presented and discussed in detail in the next Section of this Chapter.

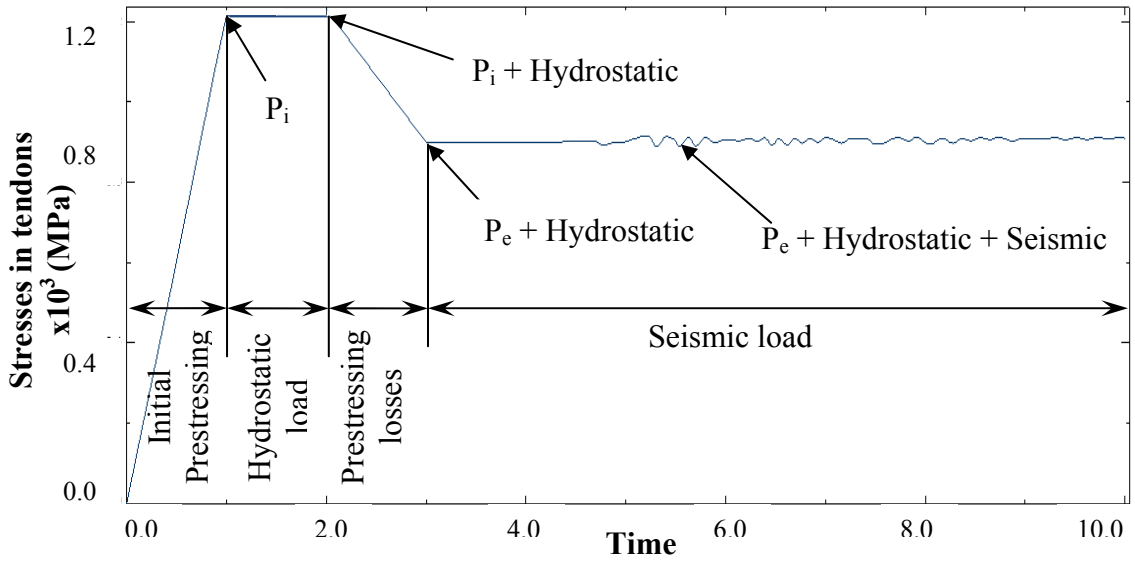

Figure 7.11 – Tank response under time-history analysis – Tank 1FL-PC

Furthermore, for concrete tanks, functional requirements such as controlling the crack width is needed. Therefore, the results of FE time-history analysis are used to calculate the crack width. In this study, crack width is calculated according to ACI224.2R-92 (1992), which is discussed in detail in Chapter 2.

Ziari and Kianoush (2009b) carried out a study on cracking and leakage behavior of reinforced concrete elements under combinations of stresses. It is found that the compression zone developed in the section as a result of flexural stresses can effectively prevent leakage through the crack regardless of the crack width. This means that flexural cracks are not of concern with regard to leakage, because the liquid passage through the depth of the section is obstructed by the presence of uncracked concrete in compression. Therefore, the cracks in the tank walls due to bending moment in the vertical direction are not investigated in this study.

Ziari and Kianoush (2009) also investigated the direct tension induced cracking of reinforced concrete and the resulting leakage. In their study, it is observed that direct tension cracks are full depth cracks which can cause liquid leakage. It is also observed that a tension crack as wide as 0.25 mm can partially remediate itself through aself-healing process. Therefore, the vertical cracks in tanks wall due to hoop forces are investigated in this study. It should be noted that most of the current codes limit the crack width to about 0.4 mm in ordinary structures and 0.25 mm in liquid containing structures under hydrostatic loads.

However, since crack width is related to tensile stress in reinforcement, cracks attributed to transit loads, such as earthquake, applied for short periods may not be as serious as cracks due to sustained load, since the cracks due to transient load may be expected to close or at least decrease in width upon removal of the load ACI224.2R-92 (1992).

The relationships between the assumed R-values in tanks design and corresponding maximum horizontal crack width for Tanks 1, 2 and 3 are shown in Figures 7.12 (a), (b) and (c), respectively. The maximum crack width is calculated based on ACI224.2R-92 (1992) using the model developed by Broms and Lutz (1965). As shown in these Figures, the maximum crack widths are more than 0.1mm. However, the tanks are expected to leak during an earthquake event. However, the reinforcing steel strain used to calculate the maximum crack width represents longitudinal strain that is taken from most highly strained element from the results of FE analysis. Therefore, the crack widths presented in these Figures are considered as local and do not represent the cracking pattern for the entire tank. Also, as indicated previously, when designing for a rare event such as earthquake, the cracks attributed to earthquake loads applied for short periods may not be as serious as cracks due to sustained loads since these cracks may be expected to close or at least reduce in width upon removal of the load. Therefore, the crack widths as shown in these Figures are considered acceptable during an earthquake event.

For PC flexible base tanks, Nawy (2001) indicated that in considering decompression and cracking, it has to be assumed that no cracking is allowed. If probability of cracking exists due to a possible overload, an additional prestressing force and the addition of nonprestressed reinforcement become necessary to control cracking. Also, it should be noted that any averload

beyond the prestressing force is expected to cause a dynamic increase in cracking such that all the applied loads start to be carried by the prestressing steel alone, with a consequent failure of the structural member. Therefore, provision of an adequate level of residual compressive stress in the concrete becomes necessary. As shown previously in Figure 7.11 for a typical PC flexible base tank, the tensile stresses in prestressing tendons under the effects of hydrostatic and dynamic earthquake loads have exceeded by around 5%. The maximum crack width (w_{max}) for bonded pretensioned prestressed concrete can be calculated using Equation 7-15 (Nawy and Chiang 1980) as follows:

$$w_{max} = 5.85x10^{-5} \left(\frac{A_t}{\sum O}\right) x \left(\frac{\Delta f_s}{6.895}\right) \qquad (7\text{-}15)$$

where,

Δf_s is the net stress in prestressing tendons (MPa), which is the difference between the stress in the prestressing steel at any load level beyond the decompression load and the stress in the prestressing steel corresponding to the decompression load

A_t is the effective concrete area in uniform tension (mm^2)

$\sum O$ is the sum of perimeters of all effective bars crossing section on tension side (mm)

A_t = 1,000x250 = 250,000 mm^2 / m

$\Delta f_s = 49$ MPa

$\sum O = 75$ mm^2 / m

Using Equation 7-15 the maximum crack width for Tank 1FL-PC is

$$w_{max} = 5.85x10^{-5} \left(\frac{250{,}000}{75}\right) x \left(\frac{49}{6.895}\right) = 1.4 \text{ mm}$$

It should be noted that, even though 1.38 MPa (200 psi) residual compressive stress is provided in the wall, with the combined stresses due to hydrostatic and hydrodynamic forces, after

consideration of the prestress losses in order to prevent vertical cracking, yet a relatively large crack width of 1.4 mm has been developed in the concrete which is considered as unacceptable. Therefore, R_i–value of 3.25 for PC flexible base tanks is relatively high and may not be appropriate.

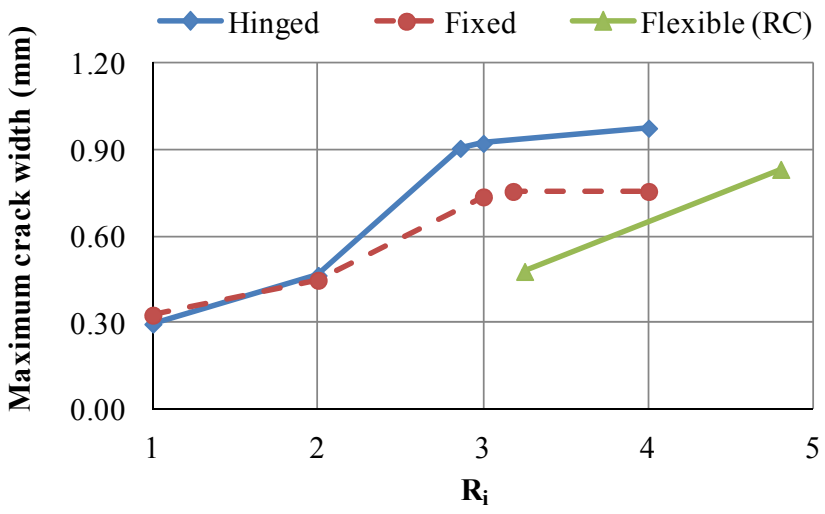

(a)

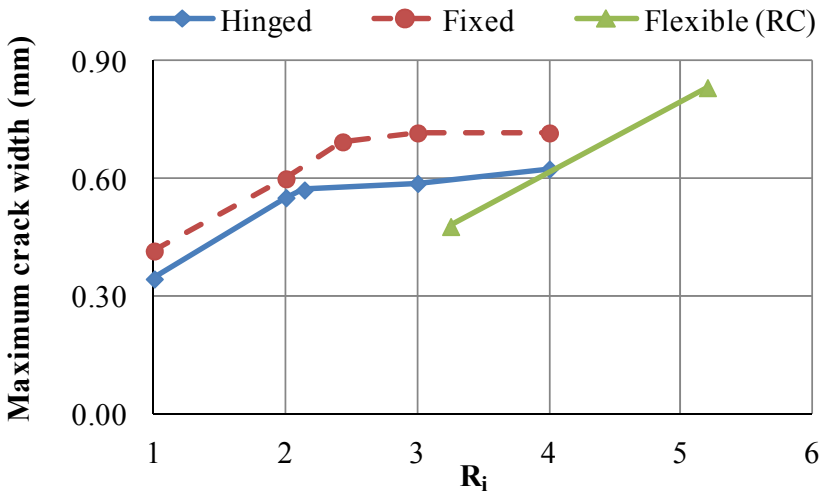

(b)

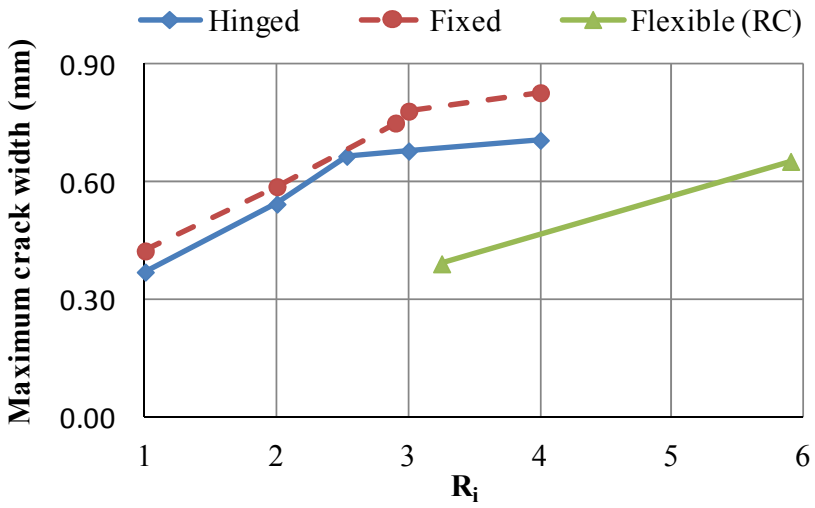

(c)

Figure 7.12 – Effect of R-values on crack width; (a) Tank 1, (b) Tank 2, (c) Tank 3

7.4.5 Discussion of the results

For fixed, hinged and RC anchored flexible tank supports, the R_i-values at which yield of reinforcement is initiated are presented in Figure 7.13 for different (D/H_L) ratios. As shown in this Figure, the R-values for fixed base tanks are higher than those for hinged base tanks. Also, the R_i-values depend on (D/H_L) ratios, as indicated earlier. However, R_i-values indicated in the current practice are slightly less than those based on time-history FE analysis. The R_i-values for RC flexible base tanks are considerably higher than those for hinged and fixed base tanks.

For the purpose of direct comparison between FE analysis and current practice, the tank base shear based on current practice is calculated for R_i equals to 1.0. The ratios between base shear of nonlinear FE analysis and current practice are presented in Figure 7.14 for different (D/H_L) ratios and support conditions. As shown in this Figure, the values of base shear based on nonlinear time-history FE analysis for fixed and hinged base tanks are almost identical. The values of base shear for RC flexible base tanks are of a lesser value for all considered (D/H_L) ratios. Also, the ratios between base shear of nonlinear FE analysis and current practice are on average around 250% and 210% for nonflexible and flexible base tanks, respectively. This may indicate that the dynamic base shear for flexible base tanks is around 20% more than the base shear for fixed and hinged base tanks.

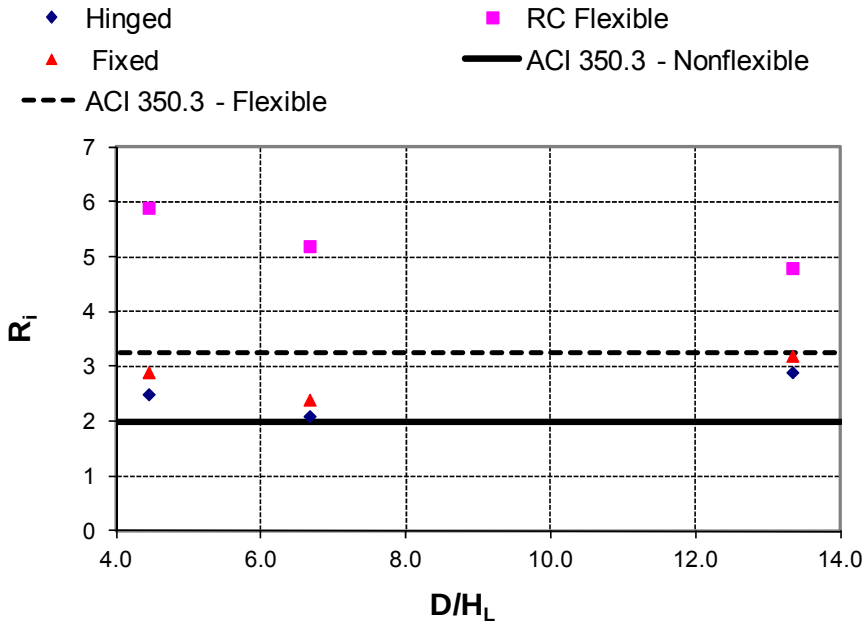

Figure 7.13 – Effect of tank dimensions and support conditions on R-values

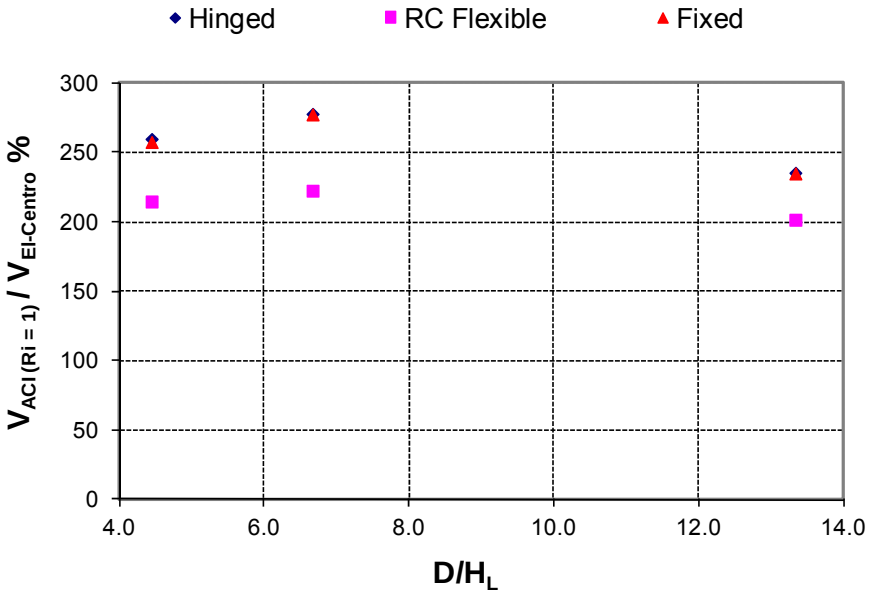

Figure 7.14 – Effect of tank dimensions and support conditions on dynamic base shear

For comparison, an additional case for PC anchored flexible base tanks with horizontal and vertical prestressing is investigated. In this study, linear and nonlinear time-history FE analysis is performed on Tanks 1FL-PC, 2FL-PC and 3FL-PC under the effect the scaled record of El-Centro earthquake (PGA = 0.4g). In order to distinguish between the results of FE analysis for PC tanks with and without vertical prestressing, the results for tanks with horizontal prestressing and vertical conventional reinforcement are referred to as Flexible H-PC, and the results for tanks with horizontal and vertical prestressing are referred to as Flexible HV-PC. The values of maximum base shear based on linear and nonlinear FE analysis are referred to as V_{Linear} and $V_{Nonlinear}$, respectively.

Figure 7.15 shows the percentage of $V_{Linear}/V_{Nonlinear}$ for the different support conditions and D/H_L ratios. As shown in this Figure, for tanks with horizontal and vertical prestressing, the percentages of $V_{Linear}/V_{Nonlinear}$ are close to 100% for all D/H_L ratios. In this case, the tank wall is initially under compression due to the prestressing force. Therefore, the effective (cracked) section properties are similar to the gross (uncracked) section properties since no cracks are developed in concrete under hydrostatic and seismic loads. According to Newmark and Hall (1981), $V_{Linear}/V_{Nonlinear}$ ratios define the system ductility factor (FEMA 450 2003). Thus, tanks with horizontal and vertical prestressing may not sustain the required level of ductility, and therefore, may not dissipate energy.

The results presented in Figure 7.15 also show that, $V_{Linear}/ V_{Nonlinear}$ ratios for Flexible - RC are similar to those for Flexible – H PC. Also, the $V_{Linear}/ V_{Nonlinear}$ ratios for Fixed and Hinged base conditions are higher than those for flexible base tanks. Therefore, the flexible base tanks with seismic cables may not dissipate the seismic forces as expected. As mentioned previously, the main reason is due to the linear behavior of the seismic cables as these cables are made of high yield strength material. The results of the nonlinear time-history FE analysis show that cracks develop in concrete near tank supports for fixed and hinged tanks. Vertical reinforcement may yield at the base for fixed base tanks. Therefore, the nonflexible tank supports may have more ductility and dissipate more energy than the flexible tank supports.

As mentioned previously, for PC anchored flexible base tanks, it may not be appropriate to determine R-values bases on yielding of prestressing tendons. For this case, the overstrength factor is considered to be equal to 1.4 (FEMA 450 2003). The R-values for PC flexible base tank are calculated as the product of the ductility factor and the overstrength factor. Accordingly, the R-values are calculated based on the results of the time-history FE analysis that are performed on tanks with different support conditions and various D/H ratios as presented in Figure 7.16. As shown in this Figure, the R_i-values for PC anchored flexible base tanks that are considered in this study are less than the R_i-value specified in current practice. Therefore, it can be concluded that the anchored flexible supports should be designed with smaller R_i-values or other mechanism that can dissipate the seismic energy should be used. Also, Ri-values for PC flexible base tanks are less than those for fixed and hinged base tanks.

While using prestressing tendons improves the tank serviceability by controlling crack width and reducing tensile stress in concrete, yet, this method may reduce the level of ductility and reduces R-values assigned to PC tanks.

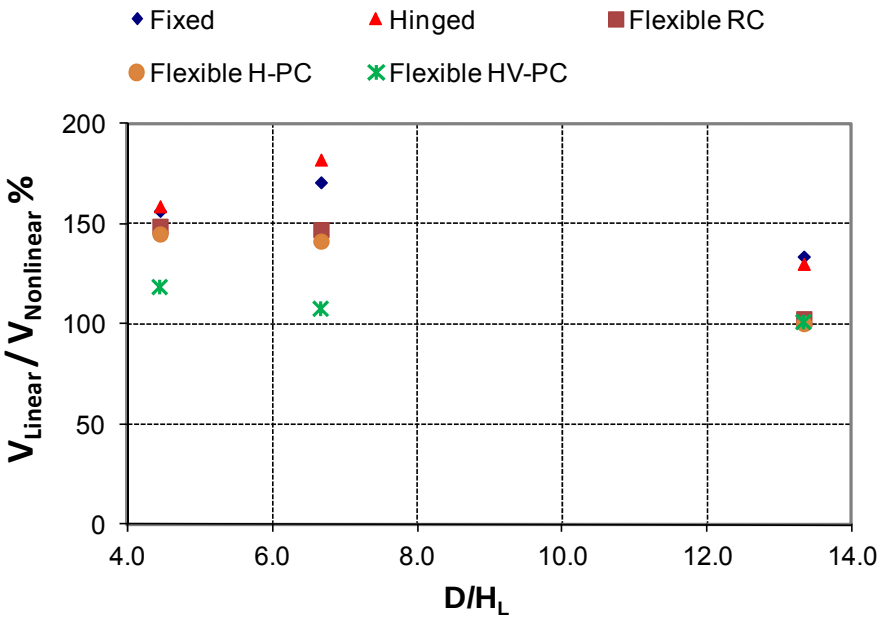

Figure 7.15 – Effect of tank dimensions and support conditions on the ratio between nonlinear and linear dynamic base shear

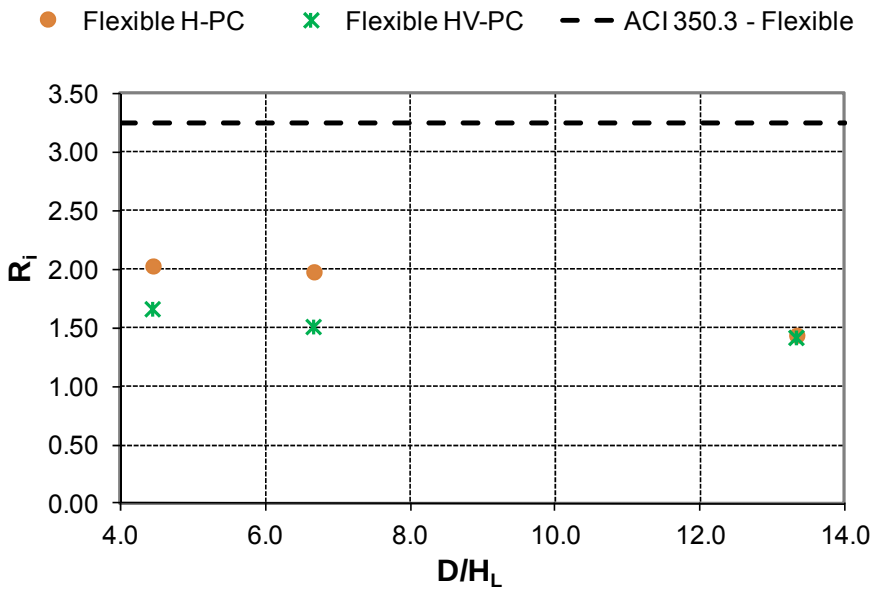

Figure 7.16 – Effect of tank dimensions and support conditions on R-values - PC flexible base

7.4.6 Comparison between results of push-over and time-history FE analysis

The results of nonlinear push-over FE analysis for Case 5, as discussed in Chapter 6, are compared with the results of nonlinear time-history FE analysis for fixed and hinged based tanks. For push-over FE analysis, the R_i-values are calculated based on the approach developed by Krawinkler and Nasser (1992) as described in detail in Chapter 6. For time-history FE analysis, R_i-values are calculated as addressed previously in Section 7.4.4.

As shown in Figure 7.17, the results of time-history and push-over FE analysis are in general agreement. For both types of analysis, R-values for fixed base tanks are more than those for hinged base tanks for all considered (D/H_L) ratios. Also, both types of the analyses indicate that there is no single value for R_i; thus, R_i-values depend on support conditions and (D/H_L) ratios. R_i-values calculated based on time-history analysis are slightly higher than those calculated based on push-over analysis.

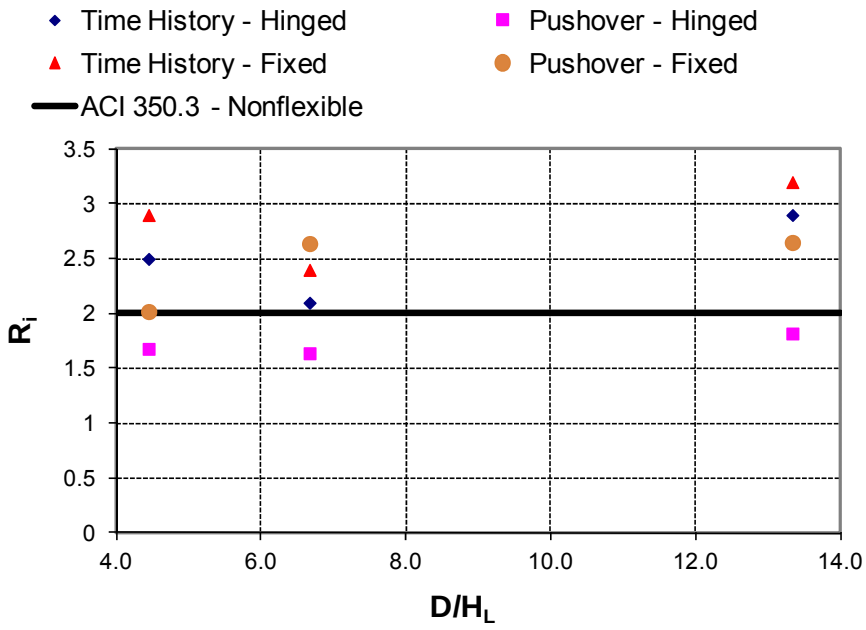

Figure 7.17 – Comparison between R-values based on push-over and time-history analysis

7.5 Summary

In this study, a detailed FE method is employed to study the nonlinear behavior of open top ground-supported circular concrete tanks with different base conditions and D/H_L ratios under horizontal dynamic time-history seismic loads. Both of RC and PC tanks are considered in this study.

It is found that the impulsive force and the lateral inertial forces of the accelerating wall have a much bigger contribution to the total response than the convective term. Therefore, for the specific model and ground motion considered in this study, it is considered that, for practical purposes, an accurate estimation of the response can be obtained by including the effect of impulsive and wall terms and neglecting the sloshing component. Also, modeling the liquid inside the tank using added mass approach versus modeling with the acoustic elements has been investigated previously (Virella and Godoy 2006). It is found that added mass model is very comparable to the acoustic elements model with only 3% difference. It is also found that modeling the impulsive mass using the nonstructural mass/added mass is a reliable approach as this approach has a minor effect on the results.

In this study, the results based on current practice are compared with the results of the FE element time-history analysis of the tank model subjected to the scaled El-Centro horizontal ground motion record. This comparison shows that the results are in very good agreement with only 4% and 13% difference for internal forces and base shear, respectively. This study shows that the results of the proposed finite element technique are acceptable where the FE model is also capable of calculating tank responses under hydrodynamic loads. Furthermore, the results of this study compare very well with analytical method based on current practice, which is derived from on Housner's formulations.

The effect of earthquake frequency content on the dynamic behavior of ground-supported tanks is also investigated by performing time-history FE analysis on one of the tanks using four different ground motions having different frequency contents. The chosen earthquake records had low to high frequency contents. It is observed that the values of tank response due to the intermediate frequency content record of the scaled El-Centro records are amplified as a result of the similarity between the frequency characteristics of the tank and the earthquake record. The results of this study also show that the current practice does not consider the effect of earthquake frequency content on tank response.

Also, a parametric study is carried out to determine the effect of tank relative dimensions and support conditions on response. It is found that the current practice provides reasonably accurate results compared to extensively detailed and timely consumed nonlinear time-history FE for fixed and hinged base tanks. However, the current practice provides more conservative results for fixed and hinged base tank.

It was also found that the flexible base tanks with seismic cables are not capable of dissipating the seismic forces as expected due to the linear behavior of the seismic cables. Also, as the seismic cables are made of tendons with very high yield strength, the flexible supports do not sustain the required level of ductility. In addition, for nonflexible base support, cracks develop in concrete, and reinforcement may yield at the base under higher load for fixed supports. Therefore, the nonflexible tank supports may possess more ductility and dissipating energy

capacity than the anchored flexible base supports. It is also found that the R-values for flexible base condition are less than those specified in current practice.

It should be also noted that, using prestressing method of construction affect the tank ductility, accordingly, if horizontal and vertical prestressing are used the behavior of the tank wall will be almost linear as the cracks may not develop in concrete.

The results of time-history FE analysis in this study are compared with the results of push-over FE analysis, discussed in detail in the previous chapter. The comparison between push-over and time-history FE analysis indicate that the results of both approaches to calculate R-values are in good agreement.

CHAPTER 8
APPLICATION OF PASSIVE ENERGY DISSIPATION SYSTEM

8.1 General

In this chapter, a new design technique is presented to reduce the dynamic response of anchored flexible base tanks to the desired level. The design approach involves the use of external fluid viscous dampers (FVD) in the radial direction around the tank circumferential in order to dissipate the seismic loads. In flexible base tanks, the movement is controlled primarily by seismic cables and to some degree by bearing pads. The results of the nonlinear FE analysis of circular tanks under dynamic time-history analysis, discussed in Chapter 7, show that the flexible base tanks with seismic cables are not capable of dissipating the seismic forces as expected. This is due to linear Behavior of seismic cables. The seismic cables are made of prestressing cables with high yield strength; therefore, the flexible supports are unable to yield. Also, the restraints provided by seismic cables in the tangential direction restrict the wall movement to dissipate the seismic energy.

The main focus of this chapter is to investigate the effect of using fluid viscous dampers in flexible base tanks subjected to ground accelerations. For this purpose, FE technique is used to study the linear and nonlinear response of the tanks under seismic loads using time-history analysis. The results of the FE dynamic analysis are also compared with current practice. In this study, the effect of damping constant (C) on the tank response is also investigated. Furthermore, for the sake of comparison, the effect of FVD on the tank response for flexible supports without seismic cables is also investigated.

8.2 Application of passive energy dissipation system

As the flexible base supports with seismic cables do not dissipate the earthquake energy, a passive energy dissipation system is introduced in the form of fluid viscous dampers (FVD). This device can be placed in the radial direction outside perimeter of the tank wall. In this study, by including FVD in the tanks, the linear and nonlinear behaviors of circular tanks are investigated using earthquake time-history analysis. Furthermore, this study focuses on the behavior of tanks with horizontal prestressing only. The response of tanks with horizontal and vertical prestressing

is linear because no cracks develop in concrete as discussed in Chapter 7. A study is also performed in order to investigate the effect of damping constant on the results of FE analysis.

8.2.1 Fluid viscous dampers

As discussed in detail in Chapter 2, FVD consists of a hollow cylinder filled with a fluid. As the damper piston rod and piston head are stroked, fluid is forced to flow through orifices either around or through the piston head. The fluid flows at high velocities, resulting in the development of friction and thus heat. The heat is dissipated harmlessly to the environment. Although the damper is called a viscous fluid damper, the fluid typically has a relatively low viscosity. The term viscous fluid damper comes from the macroscopic behavior of the damper which is essentially the same as an ideal viscous dashpot (i.e., the force output is directly related to the velocity).

It is expected that by using FVD at the tanks base in the radial direction, the seismic behavior will improve in terms of stress and deflection. However, in order for the FVD to satisfy the design requirements, the required amount of damping constant, the velocity exponent, and the maximum translational velocity of the damper should be calculated.

As indicated before, in a viscous damping model, the output of the damper is calculated using Equation 8-1 as:

$$F_{damper} = CV^{\alpha} \qquad (8\text{-}.1)$$

Generally, the velocity exponent should be: $0.3 \leq \alpha \leq 1.0$. Once performance requirements have been satisfied using linear damping ($\alpha = 1.0$), further refinement can be evaluated with lower velocity exponents.

However, for the purpose of this study, only first iteration for linear dampers with α equal to one is investigated, considering that, the tank behavior can be further improved by using nonlinear dampers. Hence, a simple dashpot is used to model dampers in which the force is proportional to

the velocity, where the proportionality constant is the damping coefficient. Also, the effect of the ambient temperature on damping constant coefficient is not included in this study.

Moreover, the forces in the dampers are calculated from the time-history analyses for different damping constants, and then, the suitable dampers are selected from the manufacturer datasheets. The FVD detail and dimensions are shown in Figure 8.1 where the product datasheet included in Appendix A.4 for reference.

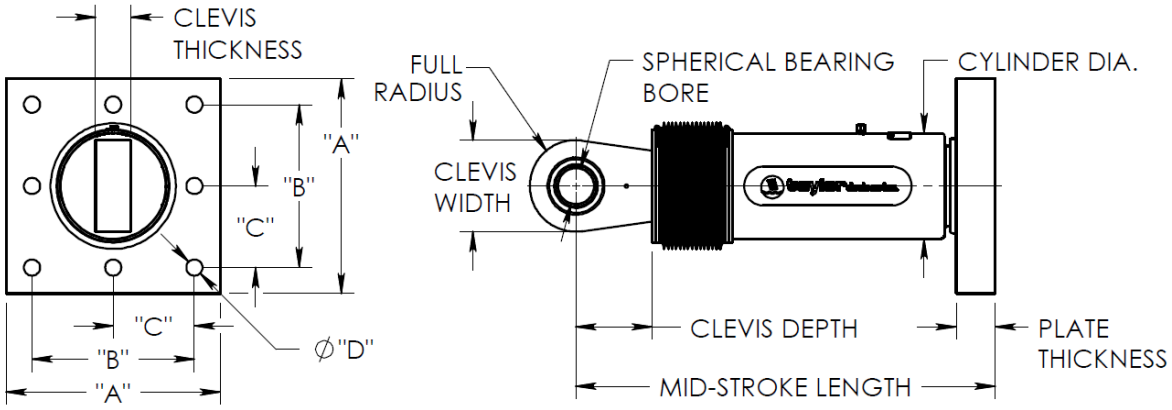

(a) (b)

Figure 8.1 – Fluid viscous damper detail and dimensions; (a) Front view, (b) Side view

The fluid viscous damper connection detail is shown in Figure 8.2. The dampers are connected to the bottom of the tank wall in the radial direction. Embedded steel plates are anchored to concrete wall using steel anchors at damper locations. These steel plates, accordingly, can be welded or bolted to damper end plates on the side of the damper near the tank wall. On the other side of the damper, the damper clevis is connected to fixed steel or concrete bracket that is connected to the tank foundation. As indicated before, the dampers are introduced in the radial direction near the tank base as shown in Figure 8.2 (a), in which the tank base is extended locally at damper locations as shown in Figures 8.2 (b) and 8.3.

The damper supporting brackets are considered to be rigid similar to the tank foundation. For the purpose of this study, a total of thirty two dampers are used for each tank; thus, the polar angle θ between every consecutive dampers is 11.25^{o} as shown in Figure 8.3. The total number of FVC (32 dampers) is found to be reasonable since the damper maximum reaction (245 kN) is found appropriate for designing the end plates and anchoring system.

The dampers are installed horizontally for anchored flexible-base tanks in order to compensate for the lack of ductility and to dissipate the seismic energy especially for prestressed tanks.

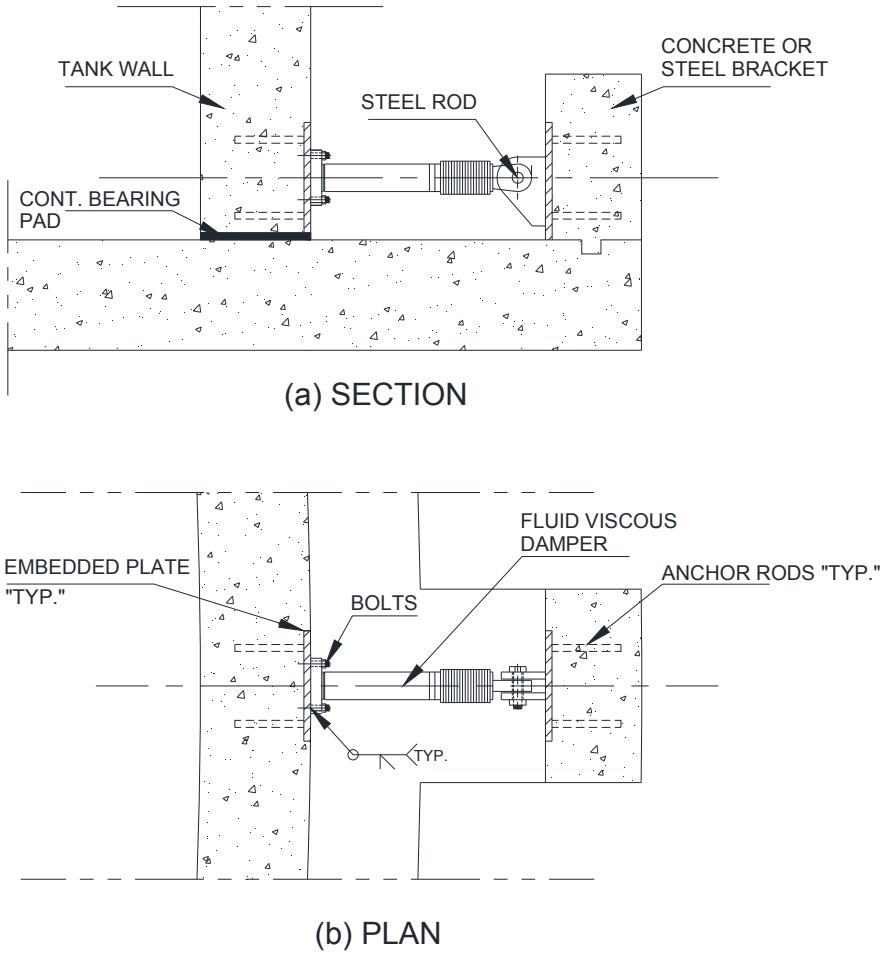

Figure 8.2 – Fluid viscous damper connection detail; (a) Section, (b) Plan

*Note: Tank reinforcement, strands, water stop, and seismic cables are not shown for clarity

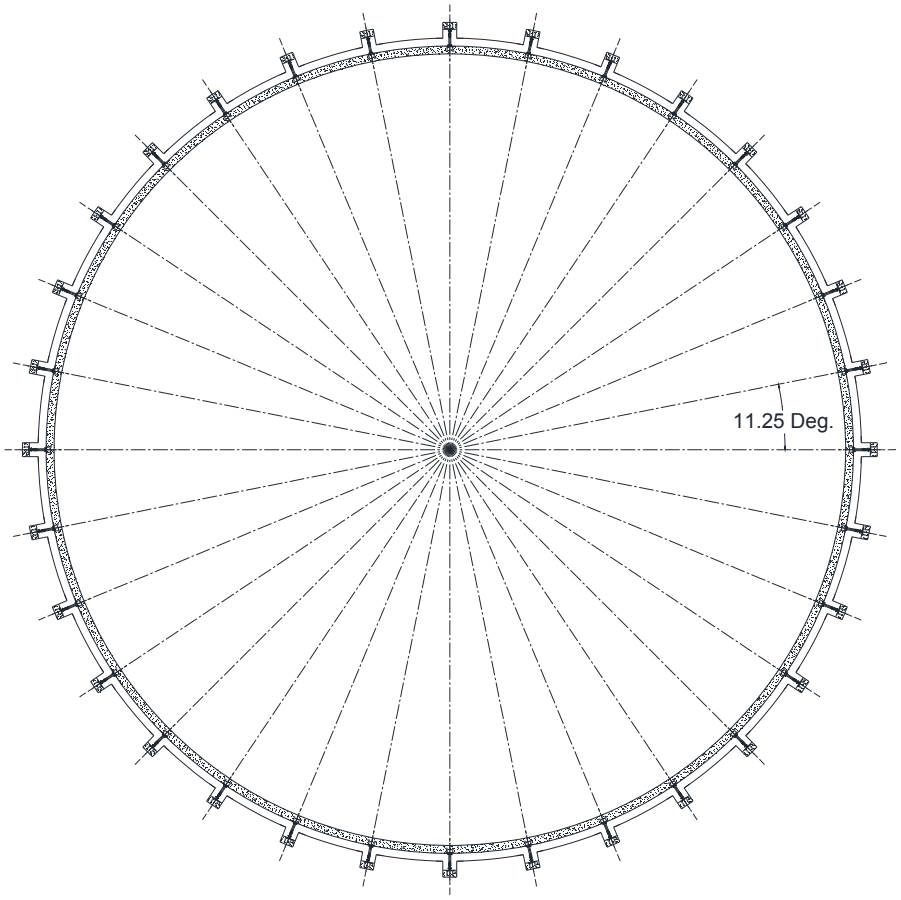

Figure 8.3 – Fluid viscous dampers layout – Plan view

8.2.2 Tank configuration and design parameters

Tanks 1FL-PC, 2FL-PC and 3FL-PC with anchored flexible base condition and horizontal prestressing, as described in detail in Chapter 7, are used in this study. These Tanks are corresponding to D/H_L ratios of 13.33, 6.67 and 4.44, respectively. Tank configurations and design parameters of these tanks are maintained the same as the previous chapter. Wall reinforcement, prestressing strands, and seismic cable details for Tanks 1FL-PC, 2FL-PC and 3FL-PC with anchored flexible base conditions are shown in Table 7.5 included in Chapter 7.

In summary, the tank diameter (D) is equal to 40m, water depths, H_L equal to 3 m, 6 m and 9 m corresponding to wall heights H_w equal to 3.25m, 6.5m and 9.6m, which are referred to as Tanks 1, 2 and 3, respectively. FL refers to flexible base condition and PC refers to prestressed

concrete. The wall thickness t_w is equal to 250mm, 300mm, and 400mm for Tanks 1, 2 and 3, respectively. Only P_i and P_w combined are considered with R_i equal to 3.25.

8.3 Computer model and FE analysis

In this study, the FE analysis is conducted using ABAQUS/CAE Version 6.8.3 using the interactive and graphical technique. Linear and nonlinear FE time-history analyses are carried out on the circular tanks in order to investigate the effect of using FVD on the results.

In summary, the entire tank is modeled using four-node quadrilateral shell element to model the wall where the number of elements along the wall height is four, seven, and ten elements for Tanks 1, 2 and 3 respectively. Both material linear and nonlinear time-history analyses are performed. The FE model including linear and nonlinear material properties, geometry, masses, prestressing force, earthquake time-history accelerations, gravity load, and hydrostatic load are described in detail in Chapter 7. The scaled El-Centro record is also used for time-history FE analysis in this study. The El-Centro record is scaled in such way that its peak ground acceleration (PGA) in the horizontal direction reaches 0.4g from its original value of 0.32g. Also, the concrete tensile strength is not considered in the FE analysis.

The seismic cables and bearing pads are modeled as spring elements as described in Chapter 7. For the case without seismic cables, referred to as W/O SC, only bearing pads are modeled as spring elements where the stiffness of seismic cables are not included in the FE model. The viscous dampers are modeled as dashpots in the radial direction as shown in Figure 8.4. The dashpots are used to model relative velocity-dependent force resistance. The DASHPOTA element (ABAQUS/CAE 2008) is also used to connect two nodes with its line of action being the line joining the two nodes. Each dashpot element is defined by connecting two nodes, in which one end of each dashpot is selected to be one of the tank nodes at the base, where the other end of the dashpot is modeled as fixed support.

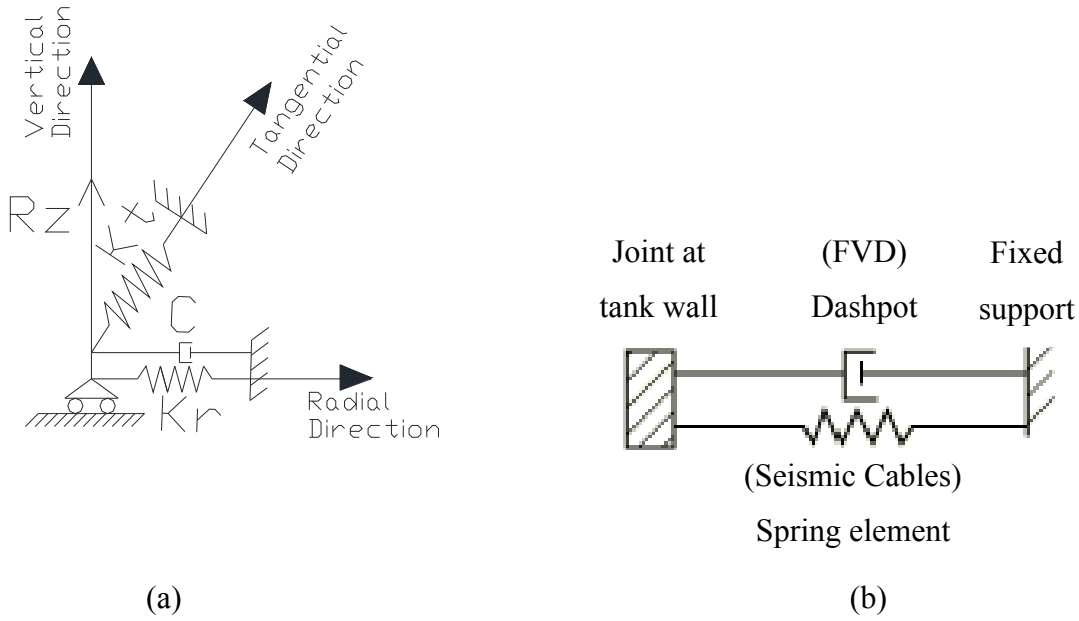

Figure 8.4 – Flexible support and damper model; (a) 3-D view, (b) Radial direction

For comparison, time-history FE analysis is conducted on an equivalent linear single degree of freedom (SDOF) system. The properties of SDOF system, such as mass and stiffness, are calculated to represent the total properties of the tank based on ACI 350.3-06 (2006). Therefore, the mass of equivalent SDOF system (M_{SDOF}) is taken as the total of impulsive and wall inertia masses. The equivalent damping constant (C_{SDOF}) is considered as the summation of the damping constant components of the used dampers in the direction of seismic force. The scaled El-Centro horizontal component of ground motion, as discussed in Chapter 7, is also used in time-history FE analysis of SDOF system.

8.4 Results of time-history FE analysis

The results of time-history FE analysis for Tanks 1FL, 2FL and 3FL with FVD are presented in this section. In this study, a wide range of damping constant (C) values are considered in FE analysis in order to determine the optimal value for C.

In this study, values of damping constant in units of kN.sec/m are included alongside the letter C, where C refers to damping constant for each FVD. For example, C100 refers to damping constant equals to 100 kN.sec/m and C0 indicates that dampers are not used.

The following abbreviations are used in this study:

ACI 350.3 (R_i =1): Tank response for seismic force calculated based on ACI 350.3 with R_i = 1.0
FE: Tank response from FE time-history analysis due to scaled El-Centro horizontal record
$V_{El\text{-}Centro}$: Absolute maximum value of peak base shear from time-history analysis due to scaled El-Centro horizontal record
$V_{ACI\ (Ri=1)}$: Base shear based on ACI 350.3 with R_i = 1.0
R_i: Response modification factor for the impulsive component
FL: Flexible base
W/O SC: Without seismic cables
SDOF: Results of equivalent single degree of freedom system

8.4.1 Internal forces

In order to investigate the effect of damping constant on the internal forces, FE time-history analysis is conducted on Tank 2FL. In this analysis, the material nonlinearity is not considered. The maximum values of the results based on FE analysis for hoop forces are shown in Figure 8.5. As shown in this Figure, the maximum hoop force based on FE time-history analysis for C0 (no FVD) and C1000 are 18% and 40% less than the seismic hoop forces calculated based on ACI 350.3-06 (2006) with R_i equal to one (elastic response), respectively. Therefore, the results indicate that the seismic forces calculated based on the current practice may be overestimated, where the tank response can be further improved by using FVD. The results also show that, values of damping constant affect the hoop forces; hence, the design forces can be reduced by using a higher value of damping constant.

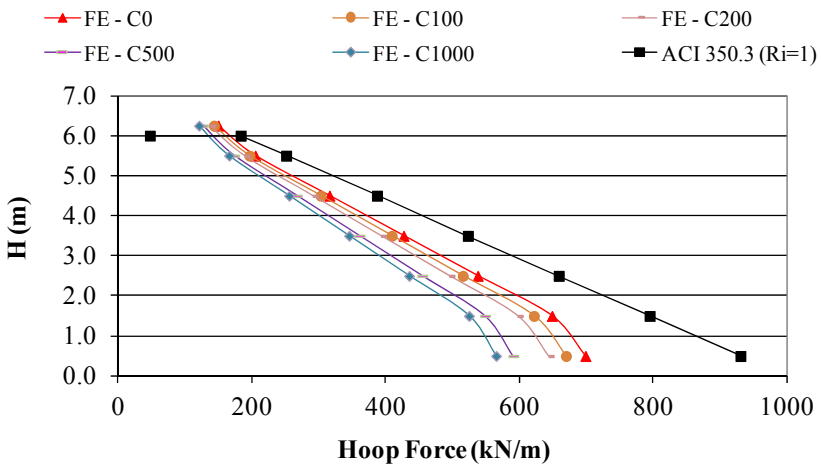

Figure 8.5 – Effect of damping coefficient on hoop forces - Tank 2FL

8.4.2 Base shear and deflection

Figure 8.6 shows the ratios between the maximum dynamic base shear ($V_{El\text{-}Centro}$) and the equivalent static elastic base shear based on ACI 350.3 ($V_{ACI\ (Ri\ =\ 1)}$) for various D/H_L ratios. In this study, the tank models without FVD are compared with tank models including FVD using damping constant of 100 kN.sec/m (C100), in which, both nonlinear and linear material properties are investigated. Also, the results of FE models for tanks with FVD and without seismic cables (W/O SC) are presented.

It can be seen from Figure 8.6 that the dynamic base shear is further reduced due to introducing FVD. However, the reduction in base shear is much greater when nonlinear material properties are included in the FE model. It is also noted that, for C100, the dynamic base shear using nonlinear material properties is 35% less than the case for linear material properties, which indicates that, nonlinear analysis may be required in order to predict a reasonable estimation of force reduction factor. It should be noted that, the nonlinear dynamic base shear using FVD with C100 is less than 45% of the required elastic base shear (R_i =1.0) based on current practice for all considered D/H_L ratios and can be reduced to less than 33% for shallower tanks as shown in the same Figure. In addition, the dynamic response of the tanks can be further improved by increasing the damping constant or using nonlinear FVD.

Also, the results presented in this Figure show that the values of dynamic base shear for supports with FVD and without seismic cables are similar to those for supports with FVD and seismic cables.

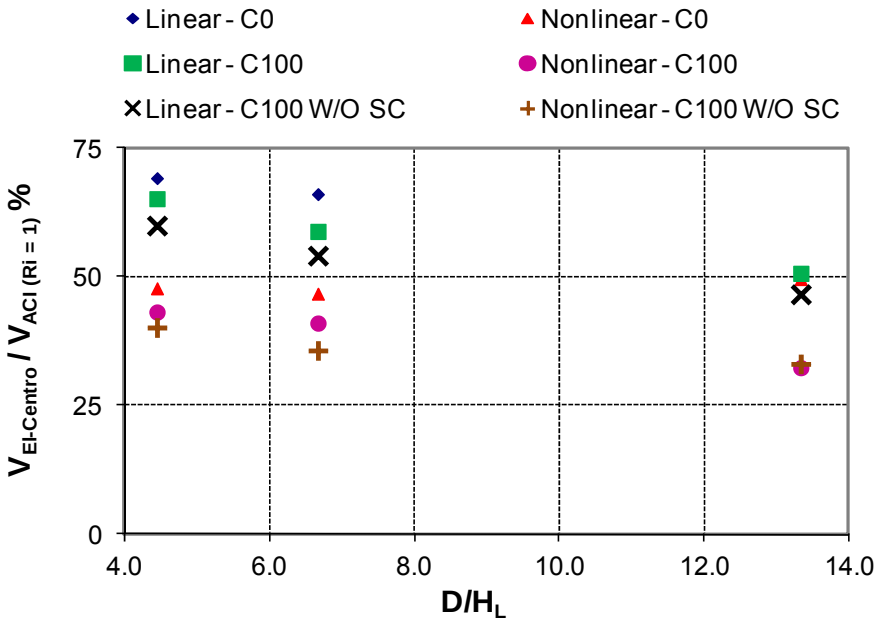

Figure 8.6 – Effect of tank dimensions and damping coefficient on base shear

Furthermore, a sensitivity study is performed on Tank 2Fl in order to further investigate the effect of damping on the tank response. In this study, the damping constant is increased from C0 to C1000, in which linear and nonlinear material models are investigated, separately. In addition, an equivalent single degree of freedom system (SDOF) was analyzed for the purpose of comparison.

As shown in Figure 8.7, the difference between the results for linear and nonlinear models decreases as the damping constant increase due to the significant reduction in the tank response. The results also show that the dynamic base shear significantly decreases as the damping constant increases. The results also show that response of SDOF model without FVD (C0) are in agreement with the elastic base shear (R_i =1.0) recommended by the current practice with only 19% difference. The effect of damping constant on the response of SDOF is relatively small.

In this study, the ductility factor is considered as a ratio of V_{Linear} and $V_{Nonlinear}$ (ATC-19 1995a), the overstrength factor is considered to be equal to 1.4 (FEMA 450 2003). The R_i-values are calculated as the product of the ductility factor and the overstrength factor. Therefore, R_i-values are calculated for tanks with different D/H_L ratios and, also, for various values of damping constant. It should be noted that, for the purpose of comparison, V_{Linear} is always considered for C0.

As shown in Figures 8.8 and 8.9, R_i is directly proportional with damping constant, thus, the tank behavior under seismic loads can be improved by using FVD system. Figure 8.8 also shows that, in order to achieve R_i value recommended by current practice ($R_i = 3.25$), a damping constant of 490 kN.sec/m (interpolated from Ri-values for C100 and C500) should be provided for the used FVD configuration. Figure 8.9 also shows that, for FVD system, the effect of D/H_L ratios on the response modification is relatively small. R_i-values are less than 1.5 for tanks without FVD for all D/H_L ratios, thus, using R_i-value recommended by current practice ($R_i = 3.25$) may underestimate the seismic load.

Figure 8.10 shows the deflection at tank base for Tank 2FL. As shown in this Figure, using FVD system with seismic cables reduces the tank deflection. However, the deflection for supports with FVD and W/O SC is around 85% more than the case for those with FVD and seismic cables. It should be also noted that, the deflection at tank base decreases as the damping constant increases.

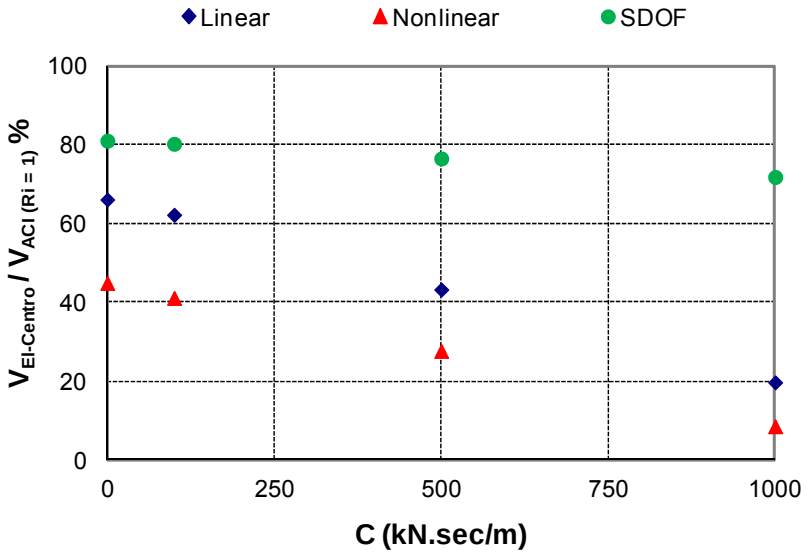

Figure 8.7 – Effect of damping coefficient on base shear –Tank 2FL

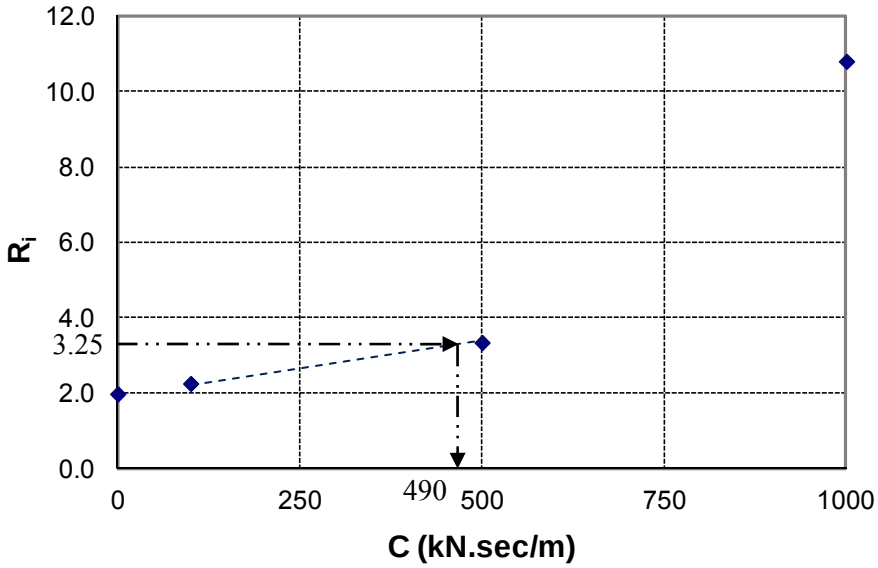

Figure 8.8 – Effect of damping constant on response modification factor – Tank 2FL

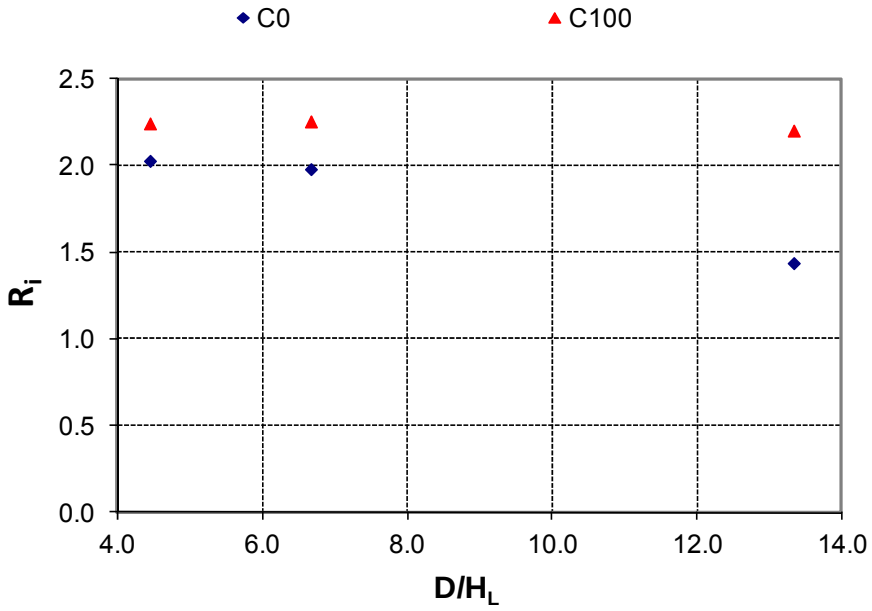

Figure 8.9 – Effect of tank dimensions and damping constant on response modification factor

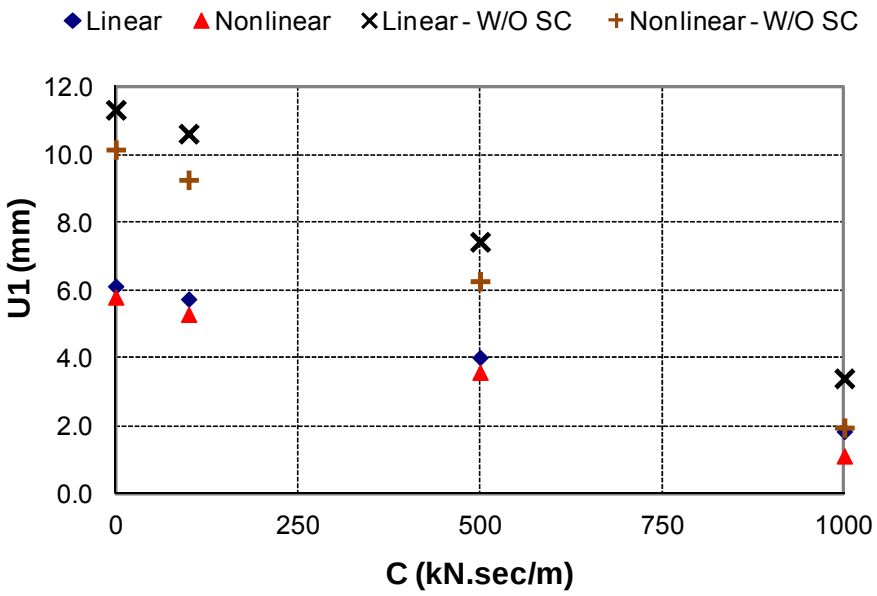

Figure 8.10 – Effect of damping coefficient on base deflection –Tank 2FL

8.5 Summary

In this study, a new design proposal for anchored flexible base tanks, using FVD, is introduced in order to improve the tank response under seismic loads. A detailed FE element method is employed to study the effect of using FVD, in the radial direction, on tank response under dynamic time-history horizontal earthquake ground excitation. The linear and nonlinear behaviors of open top ground-supported flexible base circular tanks are considered in this study for various H/D ratios. Furthermore, the effect of the FVD damping constant on the results is also investigated. In this study, the results based on current practice are also compared with the results of the FE time-history analysis of tank models subjected to the scaled El-Centro horizontal ground motion record including the effect of FVD system.

Based on the results of the FE analysis, it is found that, the behavior of flexible base tanks under seismic loads can be improved by adding FVD. Accordingly, using FVD can improve the tank serviceability by reducing the concrete cracking. Also, FVD can be used as a replacement for seismic cable as the values of base shear are similar for supports with and without seismic cables. However, deflections for supports with FVD and W/O SC are much higher than those for supports with FVD and seismic cables.

However, there are many advantages for using FVDs; these include a high reliability, high force and displacement capacity, market availability, no added stiffness, damping force (possibly) being out of phase with structure elastic forces, moderate temperature dependency, and use of linear analysis for some specific cases. There are also disadvantages in using FVDs, such as, an additional cost associated with installing the FVD, and nonlinear analysis may be required in some cases. Therefore, design optimization is recommended in order to have a better understanding of the design requirements and the overall project cost. The FVD system can be recommended for high seismic zones where the cost of adding FVD is less than the saving in wall thickness, reinforcement, and prestressing. However, the suitable damping constant and dampers layout should be selected for each specific case.

CHAPTER 9
SUMMARY, CONCLUSIONS, AND RECOMMENDATIONS

9.1 Summary

Concrete LCS are designed to withstand the applied hydrostatic and hydrodynamic loads. The design of such structures is based on strength and serviceability criteria in order to resist the applied loads without any extensive cracking that causes leakage. The concrete tanks are designed for seismic forces smaller than the elastic response. They are expected to safely survive the ground motion excitations by taking into account the effect of the R-values.

This study is conducted to examine the nonlinear behavior of ground-supported, open top, circular concrete tanks under push-over and dynamic seismic time-history FE analysis. Also, R-values for such structures are investigated in this study.

In this study, the response of circular tanks subjected to horizontal ground motions is investigated. The sensitivity of tank response to variations in the governing parameters is presented. The computer program ABAQUS/CAE is used for FE analysis. Circular tanks are analyzed using both shell and axisymmetric elements.

The behavior of concrete circular tanks with different diameter/height ratios under shrinkage effect considering both linear and nonlinear material behavior is investigated. In addition, the effect of concrete tensile stress on stresses in reinforcement is also investigated.

In this study, push-over FE analysis is carried out to investigate the nonlinear behavior of ground-supported fixed and hinged based circular tanks under seismic loading. Three different tanks having liquid heights of 3m, 6m, and 9m with a tank diameter of 40m are investigated.

A detailed FE method is also employed to study the nonlinear behavior of open top ground-supported circular tanks with different base conditions under dynamic time-history seismic analysis. Both flexible and nonflexible tank supports are considered in this study. For flexible base tanks, both RC and PC tanks are considered. A comparison between the response of RC and

PC tanks is also presented. Only the impulsive (P_i) and the inertial mass of wall (P_w) are considered in this study. This study shows that the effect of the convective component is small and can be neglected in the analysis. The liquid inside the tank is modeled using added mass approach. In this study, the results based on current practice are compared with the results of the FE time-history analysis for tank models subjected to the scaled El-Centro horizontal ground motion record. The effect of earthquake frequency content on the dynamic behavior of ground-supported tanks is also investigated by performing time-history FE analysis on the tanks using four different ground motions having different frequency contents. The selected earthquake records used in this study have low to high frequency contents. It is observed that the response values due to the intermediate frequency content record of the scaled El-Centro records are amplified as a result of the similarity between the frequency characteristics of the tank and the earthquake record. Also, a parametric study is carried out to determine the effect of tank dimensions and support conditions on tank response.

In this study, a new design approach, in the form of using fluid viscous dampers in the radial direction, is introduced in order to improve the tank response to seismic loads. A detailed FE method is employed to study the effect of using FVD on the tank response under dynamic time-history horizontal earthquake loads. The linear and nonlinear Behaviors of open top ground-supported flexible base circular tanks are considered in this study for various D/H_L ratios. Furthermore, the effect of the FVD damping constant on the results is also investigated. In this study, the results based on current practice are also compared with the results of the FE time-history analysis of tank models subjected to the scaled El-Centro horizontal ground motion record including the effect of FVD system.

9.2 Conclusions

Based on the results of this research study, the following conclusions are made:

1) The code procedure overestimates the response in terms of base shear and base moment. This difference in results is due to the lumping effects of impulsive and convective masses and other simplified assumptions used in the code procedure.

2) The effect of the flexibility of the tank wall should be considered in the calculation of hydrodynamic pressures in concrete LCS.

3) It is appropriate to use the approximation of uniform distributed load and axisymmetric elements instead of the actual cosine distribution by modeling the entire tank to obtain the maximum response of circular tanks.

4) The reinforced concrete walls of circular tanks crack under the effect of temperature and shrinkage. Therefore, the tensile strength of concrete should be neglected in tank analysis and design.

5) Based on the results of nonlinear push-over FE analysis, the fixed based tanks develop the first yield of reinforcement at higher loads compared to hinged base tanks.

6) Based on the results of nonlinear push-over FE analysis, higher response modification factors (R_i-values) could be assigned to fixed base tanks. Also, shallower concrete tanks can be assigned higher response modification factors.

7) Based on the results of the nonlinear time-history FE analysis, it is found that the current practice provides reasonably accurate results in terms of R_i-values compared to extensively detailed and timely consumed nonlinear time-history FE analysis for fixed and hinged base tanks. However, R_i-values specified in current practice for anchored flexible base tanks are more than those based on the results of FE analysis.

8) The recommended R_i-values for RC tanks with fixed and hinged base and PC tanks with anchored flexible support are 2.5, 2.0, and 1.5, respectively.

9) The impulsive force and the lateral inertial force of the accelerating wall have a much bigger contribution to the total response than the convective term for the tanks considered in this study. Therefore, for the specific tank models and ground motions that are considered in this study, for practical purposes, an accurate estimation of the actual

response may be obtained by including the effect of impulsive and wall terms and neglecting the convective component.

10) Modeling the impulsive mass using the nonstructural mass/added mass is a reliable approach since the results based on this approach are very similar to those of modeling the fluid inside the tank using acoustic elements.

11) The use of prestressing affects the tanks ductility. The case of combined horizontal and vertical prestressing result in linear response of the tank wall as cracks may not develop in concrete.

12) The flexible base tanks with seismic cables do not dissipate the seismic forces as expected due to the linear behavior of the seismic cables. Also, the flexible supports do not dissipate energy since the seismic cables are made of tendons with high yield strength.

13) The nonflexible base tanks show more ductility and dissipate more energy than the flexible base tanks. This due to development of cracks in concrete walls in fixed and hinged base tanks.

14) Based on the results of the FE analysis, using FVD reduces the tank response under the seismic loads, which improves the tank serviceability by reducing the concrete cracking.

15) The fluid viscous damper system can be recommended for tanks located in high seismic zones. Adding fluid viscous dampers may result in economical design by reducing wall thickness, reinforcement and prestressing.

9.3 Recommendations for future research

Based on the results of this research study, the following recommendations are suggested for further research:

1) More case studies with various tank capacities, relative dimensions, tank roof configuration, ground excitation properties, construction methods and construction materials such as prestressed composite steel-shotcrete and wire-wound precast concrete tanks can be carried out in order to investigate the effect of theses parameters on the response of LCS.

2) An experimental investigation would be helpful to further understand and verify the behavior of ground-supported circular tanks with and without the effect of passive energy dissipation systems.

3) Study the effect of using passive energy dissipation systems on the linear and nonlinear behavior of rectangular LCS under dynamic loads.

4) Investigate the effect of energy dissipation systems, for flexible supports without seismic cables, on the response of ground-supported circular and rectangular liquid tanks.

5) Investigate the effect of using passive control bearings on the response of ground-supported rectangular LCS.

6) Investigate the effect of soil-structure interaction on the nonlinear behavior of ground-supported rectangular and circular tanks.

7) The convective response modification factor (R_c) under sloshing behavior of LCS can be further investigated in order to verify the R_c-values indicated in the current practice.

8) Develop design tables and design charts to provide guidelines for recommended wall thickness, reinforcement, and prestressing for ground-supported LCS.

APPENDIX A.1
DESIGN OF GROUND-SUPPORTED NONFLEXIBLE-BASE CIRCULAR TANK

Design of Circular Tank

Earthquake Design Loads and Load Distribution

Reference:
Seismic Design of Liquid-Containing Concrete Structures (ACI 350.3R-06 Reference) and Commentary (350.3R-06)

Design Data

Circular Tank Type 2.1 or 2.2
Above Grade

Input
Input Data in the blue cells only

Design in EW Direction

N

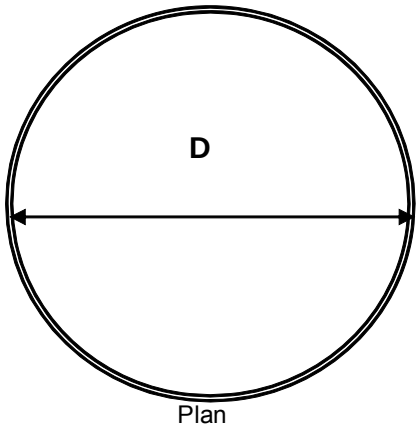

Plan

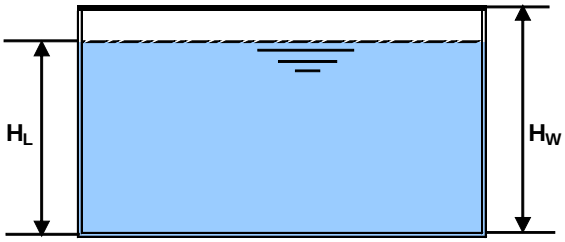

Section

D =	40.0	m
t_w =	400	mm
t_r =	0.0	mm
H_L =	6.0	m
H_W =	6.50	m
H_W(min) =	6.44	m

Freeboard > Free board allawance [okay]

γ_L =	9.8	kN/m^3
γ_C =	23.6	kN/m^3
ρ_L =	1	kN.S^2/m^4
ρ_C =	2.4	kN.S^2/m^4
f'_c =	30	Mpa
E_c =	25927.0	Mpa

S_s =	150.0%	g	ASCE 7-05
S_1 =	60.0%	g	ASCE 7-05
F_a =	0.8		Table 9.7(a)
F_v =	0.8		Table 9.7(b)

I	1		Table 4(c)
Type of Structure	Fixed or hinged-base tanks		
R_i =	2		Table 4(d)
R_c =	1		

A- Dynamic Model

1- Calculation of freedoard

S_{DS} = 2/3x$S_S F_a$ =	0.80	g			9-35/9.4.1
S_{D1} = 2/3x$S_1 F_v$ =	0.32	g			9-36/9.4.1
Ts = S_{D1}/S_{DS} =	0.40				9-34/9.4.1
λ =	(3.68xgxtanh(3.68(HL/D))^½ =			7.71	9-29/9.3.4
T_c =	$(2\pi/\lambda)$x(D)^½ =	9.34	s		9-30/9.3.4
C_c =	2.4SDS/Tc^2 =	0.022			9-38/9.4.2
d_{max} =	(D/2)x(lxC_c) =	0.44	m		R7.1
W_W =	γ_Cxt_wxH_wx(π(D+t_w/2)) =	7739.3	kN		
W_r =	γ_Cxt_rxπx(D/2+t_w)^2	0.0	kN		
W_L =	γ_LxH_Lxπx(D/2)^2	73972.8	kN		
W_i/W_L =	tanh[0.866(D/H $_L$)]/[0.866(D/H_L)]			0.17	9-15/9.3
W_i =	12812.6	kN			
W_c/W_L =	0.230(D/H_L)tanh[3.68(H_L/D)]			0.77	9-16/9.3
W_c	56941.3	kN			
h_i/H_L =	0.375				9-18
h_i =	2.25	m			
h_c/H_L =	0.51				9-19
h_c =	3.07	m			
h_i'/H_L =	2.76				9-21
h_i' =	16.57	m			
h_c'/H_L =	3.66				9-22
h_c' =	21.99	m			
C_w =	0.122				Fig. 9.10
C_l =	Cwx(tw/(10xR)^½ =			0.172	9-24/9.4
T_i =	2πx/((C_l/H_L)x(1000xE_c/ρ_C)^½) =		0.07	s	9-23&25/9.3.4
C_i =	SDS =	0.80			9-32/9.4.1
ε =	[0.151x(D/HL)^2-0.1908(D/HL)+1.021]<=1.0			0.42	9-35/9.5

B- Earthquake Design Loads

1- Dynamic lateral forces

P_W =	$IC_i x \varepsilon W_w/R_i$ =	1300.5 kN		4-1/4.1
P_r =	$IC_i x Wr/R_i$ =	0.0 kN		4-2/4.1
P_i =	$IC_i x W_i/R_i$ =	5125.0 kN		4-3/4.1
P_C =	$ICcx Wc/R_c$ =	1253.1 kN		4-4/4.1

2- Total base shear

V =	$((P_i+P_w+P_r)^{\wedge 2}+P_c^{\wedge 2})^{\wedge ½}$ =	6546.6 kN		4-5/4.1

3- Bending moment on the entire tank cross section (EBP)

M_w =	$P_w x h_w$ =	4226.8 kN.m		4-6/4.1.3
M_r =	$P_r x h_r$ =	0.0 kN.m		4-7/4.1.3
M_i =	$P_i x h_i$ =	11531.3 kN.m		4-8/4.1.3
M_c =	$P_c x h_c$ =	3852.0 kN.m		4-9/4.1.3
M_b =	$((M_i+M_w+M_r)^{\wedge 2}+M_c^{\wedge 2})^{\wedge ½}$ =	16222.1 KM.m		4-10/4.1.3

4- Overturning moment at the base of the tank (IBP)

M_i' =	$P_i x h_i'$ =	84923.6 kN.m		4-11/4.1.3
M_c' =	$P_c x h_c'$ =	27552.2 kN.m		4-12/4.1.3
M_o =	$((M_i+M_w+M_r)^{\wedge 2}+M_c^{\wedge 2})^{\wedge ½}$ =	93310.8 kN.m		4-13/4.1.3

5- Vertical acceleration

T_v =	$2\pi((\gamma_L x D^* H_L^{\wedge 2})/(2xgxt_w xEc))^{\wedge ½}$ =	0.05 S		9-31/9.3.4
C_t =	Ct=SDS =	0.8		4-16/4.1.4.2
b =	0.67			4.1.4.1
Ü =	$C_t Ixb/R_i >= 0.2S_{DS}$	0.267		4-15/4.1.4
P_{hy} =	$Üxq_{hy}$			4-14/4.1.4
P_{HL} =	$Üxq_{HL}$ =	15.69 kPa		

C- Earthquake Load Distrbution

1.a- Hydrostatic force		P_h	7061.0	kN	y(m) =	2.00
2.a-Vertical acceleration effect		$\ddot{U}xP_h$ =	1882.9	kN	y(m) =	2.00
3.a- Impulsive force		$P_i/2$ =	2562.5	kN	y(m) =	2.25
4.a- Convectve force		$P_c/2$ =	626.6	kN	y(m) =	3.07
5.a- Wall inertia force		$p_w/2$ =	650.3	kN	y(m) =	3.25
Max. static shear force in wall		7061.0 kN/m				
Max. seismic shear force in wall		3776.2 kN/m		5-1/5.3.2	V_{EQ}/V_S =	0.53
Max. static bending moment in wall		14122.08 kN.m/m				
Max. seismic bending moment in wall		8942.6 kN.m/m			M_{EQ}/M_S =	0.63
1.b- Hydrostatic pressures		p_h =	176.5	KN/m	y(m) =	2.00
2.b-Vertical acceleration effect		$\ddot{U}xp_h$ =	47.1	KN/m	y(m) =	2.00
3.b- Impulsive pressures	Max-θ = 0	$p_i = 2(P_i/2)/(\pi R)$	81.5	KN/m	y(m) =	2.25
4.b- Convectve pressures	Max-θ = 0	$p_c = 16(P_c/2)/(9\pi R)$	17.7	KN/m	y(m) =	3.07
5.b- Wall inertia force		$p_w = (P_w/2)/(\pi R)$	10.3	KN/m	y(m) =	3.25

Table A.1.1 – Design hydrodynamic and hydrostatic pressures at (θ) = 0 deg – Hinged and Fixed Base

y	P_{hy}	$Üxq_{hy}$	Pi_y	P_{cy}	P_{wy}	P_{EQy}
m	(kPa)	(kPa)	(kPa)	(kPa)	(kPa)	(kPa)
6.50	0	0	0	0	1.59	1.59
6.00	0	0	0	0	1.59	1.59
6.0	0	0	3.40	3.17	1.59	5.91
5.00	9.81	2.62	6.79	3.10	1.59	9.32
4.00	19.61	5.23	10.19	3.03	1.59	13.24
3.00	29.42	7.85	13.59	2.95	1.59	17.34
2.00	39.23	10.46	16.99	2.88	1.59	21.51
1.00	49.04	13.08	20.38	2.81	1.59	25.73
0.00	58.84	15.69	23.78	2.74	1.59	29.96

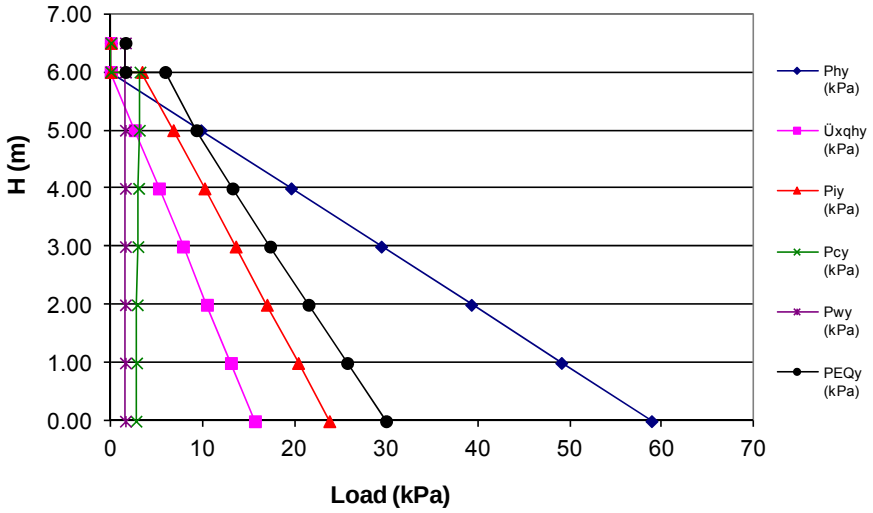

Figure A.1.1 – Design hydrodynamic and hydrostatic pressures at (θ) = 0 deg – Hinged and Fixed Base

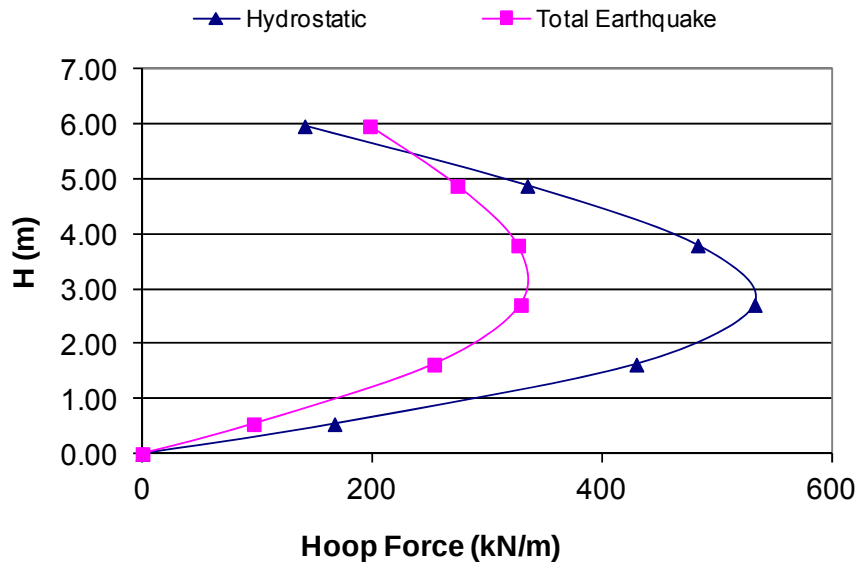

Figure A.1.2 – Design hydrodynamic and hydrostatic hoop forces at (θ) = 0 deg – Hinged Base

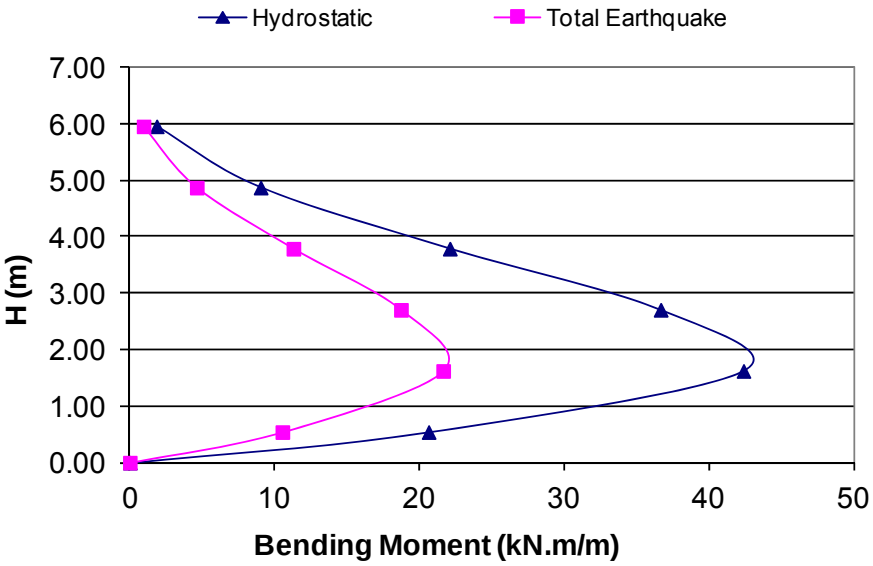

Figure A.1.3 – Design hydrodynamic and hydrostatic bending moment at (θ) = 0 deg – Hinged Base

Design of Concrete Section - Bending Moment

Reference:
Code Requirements for Environmental Engineering Concrete Structures (ACI 350-06)
and Commentary (ACI 350R-06) – 2006.

A- Vertical Bars

Load due to fluid

M_f = 42.4 kN.m/m

V_f = 53.3 kN/m

P_{HS} = 58.8 kPa

Load due to earthquake

M_E = 21.6 kN.m/m

V_E = 27.5 kN/m

P_{EQ} = 30 kPa

f'_c = 30 MPa
E_c = 25927 MPa

f_y = 400 MPa

ϕ = 0.9 for flexure & axial tension 9.3.2

Concrete Cover = 50 mm 7.7.1

Bar sizes = 20 mm

Spacing between bars S = 250 mm

t_w = 400 mm

d = 340 mm

b = 1000 mm

d_c = 60 mm

β_1 = 0.832 10.2.7

$a = \beta 1\ c$

$A_{s,\ min}$ = $3\ (f'_c)^{½}/f_y$ x bd For tensile reinforcement "Imperial Units" 10-3/10.5

$A_{s,\,min}$ =	0.25 $(f'_c)^{\wedge ½}/f_y$ x bd =	1164	mm^2/m	"Metric Units"	
$A_{s,\,min}$ =>	200 $b_w d/f_y$			"Imperial Units"	10-3/10.5
$A_{s,\,min}$ =>	1172	mm^2/m			
Ratio of $A_{s,\,min}$ for shrinkage =		0.005	Both sides		7.12.2.1
$A_{s,\,min}$ =	1172	$mm^{\wedge 2}/m$			

Strength Design Method

Bending

$C_c = T_s$ 10.2.7

S_d x $M_u = C_c$ (d-a/2) 10.2.7

$C_c = \phi\, 0.85\, f'_c\, 0.85\, c\, b$ 10.2.7.1

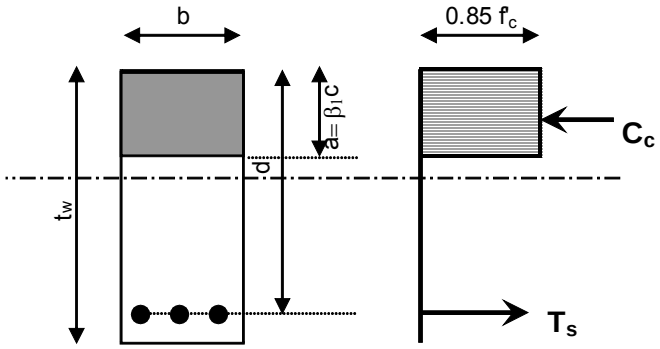

M_{u1} =1.4 (M_D + M_f) =	59.4 kN.m/m		9-1/9.2.1
M_{u2} =1.2 M_D + 1.2 M_f + 1.0M_E =	72.5 kN.m/m		9-5/9.2.1

M_u = Max (M_{u1} & M_{u2}) = 72.5 kN.m/m

Environmental exposure normal

β = 1.35

Aspect ratio = 3.0

f_s = 148 Mpa 9.2.6.1 & 10.6.4

$$\gamma = \frac{Factored\_Load}{Unfactored\_Load} = 1.13$$ 9-8/9.2.6

$$S_d = \frac{\phi f_y}{\gamma f_s} \geq 1.0 = 2.15$$ 9-8/9.2.6

M_u = Max (S_dxM_{u1} & M_{u2}) = 127.4 kN.m/m

$\phi M_n = \phi$ [As fy(d-a/2)] 9.3

$\phi M_n / S_d$ x M_u 9.2.6

c = 22.3 mm a = 18.6 mm

$C_c = T_{s=}$ 426.9 kN

As = $Ts/(\phi f_y)$ = 1186 mm^2/m R9.1.1

$A_{s\ req'd}$ = 1186 mm^2/m

Shear

V_{u1} =1.4 (V_D + V_f) = 74.6 kN/m 9-1/9.2.1

V_{u2} = 1.2 V_D + 1.2 V_f + 1.0V_E = 91.5 kN/m 9-5/9.2.1

Max(V_{u1} & V_{u2}) = 91.5

fs 166 MPa 9.2.6.4 & 5

$$\gamma = \frac{Factored\_Load}{Unfactored\_Load} = 1.13$$

$$S_d = \frac{\phi f_y}{\gamma f_s} \geq 1.0 = 1.92$$

Shear stress carried by shear reinforcement no

S_d = 1

V_u = Max (S_dxV_{u1} & V_{u2}) = 91.5 kN/m

$\phi V_n / S_d$ x V_u 11-1/11.1

$V_n = V_c + V_s$

$V_s = 0$

V_c = $V_c = 2\left(1.9\sqrt{f'_c} + 2500\rho_w \frac{V_u d}{M_u}\right) b_w d$ lb "Imperial Units" 11-5/11.3.2.1

$V_u d/M_u$ >= 1.0 $V_c <$ $= 3.5\sqrt{f'_c}\, b_w\, d$

Vc = 314.3 kN/m "Metric Units"

SAFE

Theoretical Ultimate Load Capacity

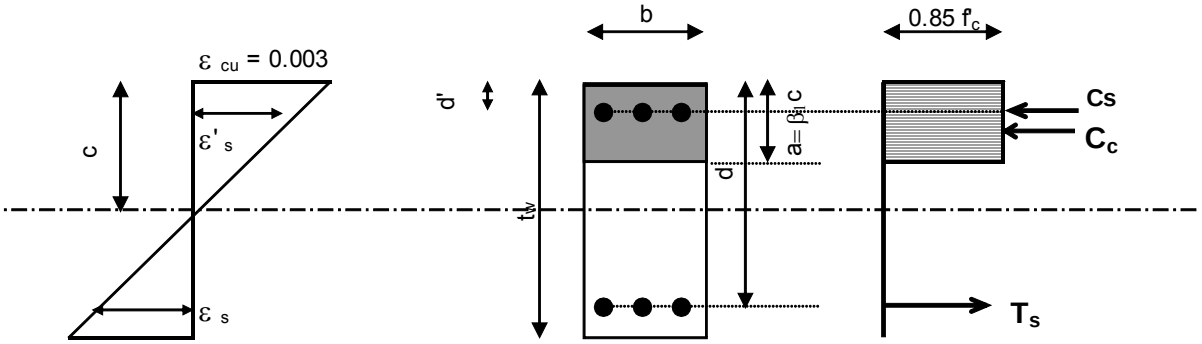

$A_{s\ Provided}$ 1200 mm^2/m $A'_{s\ Provided}$ = 1200 mm^2/m $A_s = A'_s$

ϕ = 0.9

d' = 60 mm

$C_c = \phi\, 0.85\, f'_c\, \beta_1 c\, b$

$C_s = \phi\, A'_s\, f_s$

$T_s = \phi\, A_s\, f_y$

Assume Top Bars in Tension

$\varepsilon'/(d'-c) = \varepsilon_{cu}/c$ $\varepsilon' = \varepsilon_{cu} x (d'-c)/c$

$C_s = A_s' x \varepsilon' x E_s$ $= A_s' x (c-d')/c x \varepsilon_{cu} x E_s$

$C_s + T_s = C_c$

a	b	c
21227.57	240000	-43200000

c = 39.8 mm a = 33.1 mm

ε' = 0.00152 OK e' < 0.002 Top bars in tension

ε_s = 0.02262 OK es > 0.002

$f_s = \varepsilon' x E_s$ = 304.3 MPa $C_s = \phi\, A_s x \varepsilon' x E_s$ = 328.6 kN/m

$T_s = \phi\, A_s\, f_y$ = 432.0 kN/m

$C_c = \phi\, 0.85\, f'_c \beta_1 c\, b$ = 760.6 kN/m

$M_r = \phi\, C_c x (d-a/2) - C_s x (d-d')$ = 138.6 kN.m/m

Design of Concrete Section (Hoop Forces)

Reference:

Code Requirements for Environmental Engineering Concrete Structures (ACI 350-06) and Commentary (ACI 350R-06) – 2006.

B- Horizontal Bars

Load due to fluid

N_f = 533 kN/m

P_{HS} = 58.84 kPa

Load due to earthquake

N_E = 329.5 kN/m

P_{EQ} = 30 kPa

f'_c = 30 MPa

f_y = 400 MPa

ϕ = 0.9 for flexure & axial tension 9.3.4.2

Concrete Cover = 50 mm 7.7.1

Bar sizes = 20 mm

Spacing between bars S = 220 mm

t_w = 400 mm

d = 340.00 mm

b = 1000 mm

d_c = 60 mm

$A_{s,\,min}$ = $3\,(f'_c)^{\frac{1}{2}}/f_y$ x bd For tensile reinforcement "Imperial Units" 10-3/10.5

$A_{s,\,min}$ = $0.25\,(f'_c)^{\frac{1}{2}}/f_y$ x bd = 1164 mm^2/m "Metric Units"

$A_{s,\,min}$ => $200\,b_w\,d/f_y$ "Imperial Units" 10-3/10.5

$A_{s,\,min}$ => 1172 mm^2/m

Ratio of $A_{s,\,min}$ for shrinkage = 0.005 Both sides 7.12.2.1

$A_{s,\,min}$ = 1172 mm^2/m

Strength Design Method

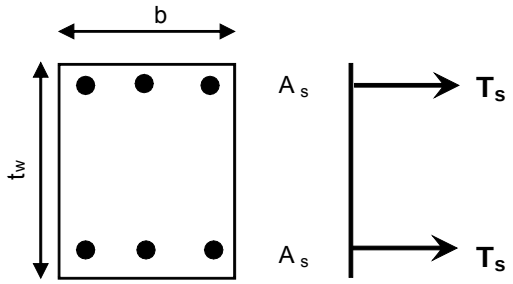

N_{u1} =1.4 (N_D + N_f) = 746.2 kN/m R9.2.8.1

N_{u2} =1.2 N_D + 1.2 N_f + 1.0 N_E = 969.1 kN/m (21.2.1.7) R9.2.3

N_u = Max (N_{u1} & N_{u2}) = 969.1 kN/m

Environmental exposure normal

f_s = 138 Mpa 9.2.6.2 & 3

$$\gamma = \frac{Factored\_Load}{Unfactored\_Load} = 1.12$$

$$S_d = \frac{\phi f_y}{\gamma f_s} \geq 1.0 = 2.32$$

S_d x N_u = 2251.1 kN/m

$\phi N_n = \phi$[As fy] 9.3

ϕN_n / S_d x N_u 9.2.6

T_s = 1125.6 kN

$A_{s\ req'd}$ = $Ts/(\phi f_y)$ = 3127 mm^2/m R9.1.1

Theoretical Ultimate Load Capacity

& = 1

$A_{s\ Provided}$ 3333 mm^2

T_r = 1333.2 kN.m/m

N_r = 2666.4 kN.m/m

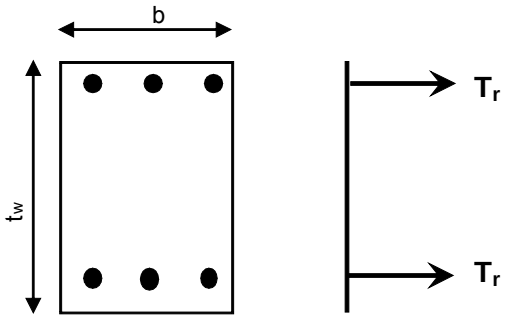

APPENDIX A.2
DESIGN OF GROUND-SUPPORTED ANCHORED FLEXIBLE-BASE CIRCULAR TANK

Design of Circular Tank

Earthquake Design Loads and Load Distribution

Reference:
Seismic Design of Liquid-Containing Concrete Structures (ACI 350.3R-06 Reference) and Commentary (350.3R-06)

Design Data

Circular Tank Type 2.1 or 2.2
Above Grade

Input
Input Data in the blue cells only

Design in EW Direction

N

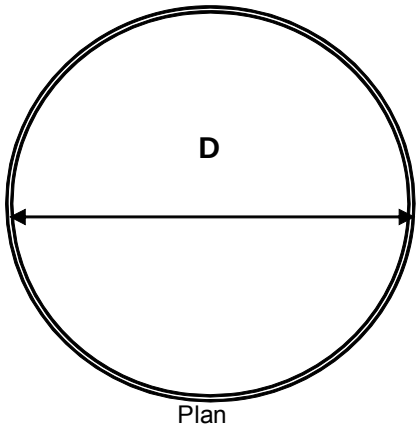

Plan

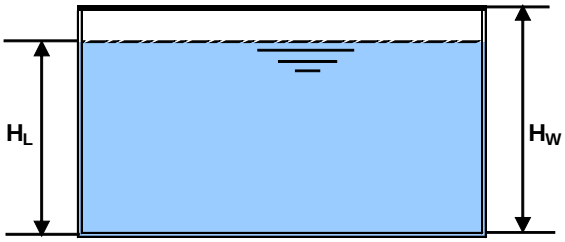

Section

D =	40.0	m
t_w =	300	mm
t_r =	0.0	mm
H_L =	6.0	m
H_W =	6.50	m
H_W(min) =	6.44	m

Freeboard > Free board allawance [okay]

γ_L =	9.8	kN/m^3
γ_C =	23.6	kN/m^3
ρ_L =	1	kN.S^2/m^4
ρ_C =	2.4	kN.S^2/m^4
f'_c =	30	MPa
E_c =	25927.0	MPa

S_s =	150.0%	g	ASCE 7-05
S_1 =	60.0%	g	ASCE 7-05
F_a =	0.8		Table 9.7(a)
F_v =	0.8		Table 9.7(b)
I	1		Table 4(c)

Type of Structure Anchored, flexible-base tanks

R_i =	3.25	Table 4(d)
R_c =	1	

Calculation of spring constant of the tank wall support system

For tank type 2.3

A_s = 140 mm2
E_s = 200000 MPa
α = 45 Deg.
L_c = 838 mm
S_c = 1980 mm

G_p = 0.345 MPa
w_p = 250 mm
L_p = 1000 mm
t_p = 25.4 mm
S_p = 1000 mm

K_a (Radial) = $1000x(2G_pxw_pxL_p)/(t_pxS_p)$ = 6787.9 N/m per m

K_a (Tangential)= $1000x[(A_sxE_sxcos\alpha\text{^}2)/(L_cxS_c) + (2GpxwpxLp)/(tpxSp)]$ = 15228.0 N/m per m 9-27/9.3.4

A- Dynamic Model

1- Calculation of freedoard

S_{DS} = 2/3x$S_S F_a$ =	0.80	g			9-35/9.4.1
S_{D1} = 2/3x$S_1 F_v$ =	0.32	g			9-36/9.4.1
Ts = S_{D1}/S_{DS} =	0.40				9-34/9.4.1
λ =	(3.68xgxtanh(3.68(HL/D))^½ =			7.71	9-29/9.3.4
T_c =	$(2\pi/\lambda)$x(D)^½ =	9.34	s		9-30/9.3.4
C_c =	2.4SDS/Tc^2 =	0.022			9-38/9.4.2
d_{max} =	(D/2)x(IxC$_c$) =	0.44	m		R7.1
W_W =	γ_Cxt_wxH_wx(π(D+t_w/2)) =	5797.2	kN		
W_r =	γ_Cxt_rxπx(D/2+t_w)^2	0.0	kN		
W_L =	γ_LxH_Lxπx(D/2)^2	73972.8	kN		
W_i/W_L =	tanh[0.866(D/H $_L$)]/[0.866(D/H_L)]			0.17	9-15/9.3
W_i =	12812.6	kN			
W_c/W_L =	0.230(D/H_L)tanh[3.68(H_L/D)]			0.77	9-16/9.3
W_c	56941.3	kN			
h_i/H_L =	0.375				9-18
h_i =	2.25	m			
h_c/H_L =	0.51				9-19
h_c =	3.07	m			
h_i'/H_L =	2.76				9-21
h_i' =	16.57	m			
h_c'/H_L =	3.66				9-22
h_c' =	21.99	m			
C_w =	0.122				Fig. 9.10
C_l =	Cwx(tw/(10xR)^½ =			0.149	9-24/9.4
T_i =	$(8\pi$x(W_w+W_r+W_i)/(gDK_a))^{½} =	0.280	s		9-26/9.3.4
C_i =	SDS =	0.80			9-32/9.4.1
ε =	[0.151x(D/HL)^2-0.1908(D/HL)+1.021]<=1.0			0.42	9-35/9.5

B- Earthquake Design Loads

1- Dynamic lateral forces

P_W =	$IC_i x \varepsilon W_w/R_i$ =	599.5 kN	4-1/4.1
P_r =	$IC_i x Wr/R_i$ =	0.0 kN	4-2/4.1
P_i =	$IC_i x W_i/R_i$ =	3153.9 kN	4-3/4.1
P_C =	$ICcx Wc/R_c$ =	1253.1 kN	4-4/4.1

2- Total base shear

V =	$((P_i+P_w+P_r)^{\wedge 2}+P_c^{\wedge 2})^{\wedge ½}$ =	3957.0 kN	4-5/4.1

3- Bending moment on the entire tank cross section (EBP)

M_w =	$P_w x h_w$ =	1948.4 kN.m	4-6/4.1.3
M_r =	$P_r x h_r$ =	0.0 kN.m	4-7/4.1.3
M_i =	$P_i x h_i$ =	7096.2 kN.m	4-8/4.1.3
M_c =	$P_c x h_c$ =	3852.0 kN.m	4-9/4.1.3
M_b =	$((M_i+M_w+M_r)^{\wedge 2}+M_c^{\wedge 2})^{\wedge ½}$ =	9830.7 kN.m	4-10/4.1.3

4- Overturning moment at the base of the tank (IBP)

M_i' =	$P_i x h_i'$ =	52260.7 kN.m	4-11/4.1.3
M_c' =	$P_c x h_c'$ =	27552.2 kN.m	4-12/4.1.3
M_o =	$((M_i+M_w+M_r)^{\wedge 2}+M_c^{\wedge 2})^{\wedge ½}$ =	60809.1 kN.m	4-13/4.1.3

5- Vertical acceleration

T_v =	$2\pi((\gamma_L x D^* H_L^{\wedge 2})/(2xgxt_w xEc))^{\wedge ½}$ =	0.06 S	9-31/9.3.4
C_t =	Ct=SDS =	0.8	4-16/4.1.4.2
b =	0.67		4.1.4.1
Ü =	$C_t Ixb/R_i >= 0.2S_{DS}$	0.164	4-15/4.1.4
P_{hy} =	$Üxq_{hy}$		4-14/4.1.4
P_{HL} =	$Üxq_{HL}$ =	9.66 kPa	

C- Earthquake Load Distrbution

1.a- Hydrostatic force		P_h	7061.0 kN		y(m) =	2.00
2.a-Vertical acceleration effect		$\ddot{U}xP_h$ =	1158.7 kN		y(m) =	2.00
3.a- Impulsive force		$P_i/2$ =	1576.9 kN		y(m) =	2.25
4.a- Convectve force		$P_c/2$ =	626.6 kN		y(m) =	3.07
5.a- Wall inertia force		$p_w/2$ =	299.8 kN		y(m) =	3.25
Max. static shear force in wall		7061.0 kN/m				
Max. seismic shear force in wall		2292.9 kN/m		5-1/5.3.2	V_{EQ}/V_S =	0.32
Max. static bending moment in wall		14122.08 kN.m/m				
Max. seismic bending moment in wall		5434.3 kN.m/m			M_{EQ}/M_S =	0.38
1.b- Hydrostatic pressures		p_h =	176.5 kN/m		y(m) =	2.00
2.b-Vertical acceleration effect		$\ddot{U}xp_h$ =	29.0 kN/m		y(m) =	2.00
3.b- Impulsive pressures	Max-θ = 0	p_i = $2(P_i/2)/(\pi R)$	50.2 kN/m		y(m) =	2.25
4.b- Convectve pressures	Max-θ = 0	p_c = $16(P_c/2)/(9\pi R)$	17.7 kN/m		y(m) =	3.07
5.b- Wall inertia force		p_w = $(P_w/2)/(\pi R)$	4.8 kN/m		y(m) =	3.25

Table A.2.1 – Design hydrodynamic and hydrostatic pressures at (θ) = 0 deg – Anchored, Flexible-Base

y	P_{hy}	$Üxq_{hy}$	Pi_y	P_{cy}	P_{wy}	P_{EQy}
m	(kPa)	(kPa)	(kPa)	(kPa)	(kPa)	(kPa)
6.50	0	0	0	0	0.73	0.73
6.00	0	0	0	0	0.73	0.73
6.0	0	0	2.09	3.17	0.73	4.25
5.00	9.81	1.61	4.18	3.10	0.73	6.03
4.00	19.61	3.22	6.27	3.03	0.73	8.28
3.00	29.42	4.83	8.36	2.95	0.73	10.71
2.00	39.23	6.44	10.45	2.88	0.73	13.22
1.00	49.04	8.05	12.54	2.81	0.73	15.78
0.00	58.84	9.66	14.63	2.74	0.73	18.35

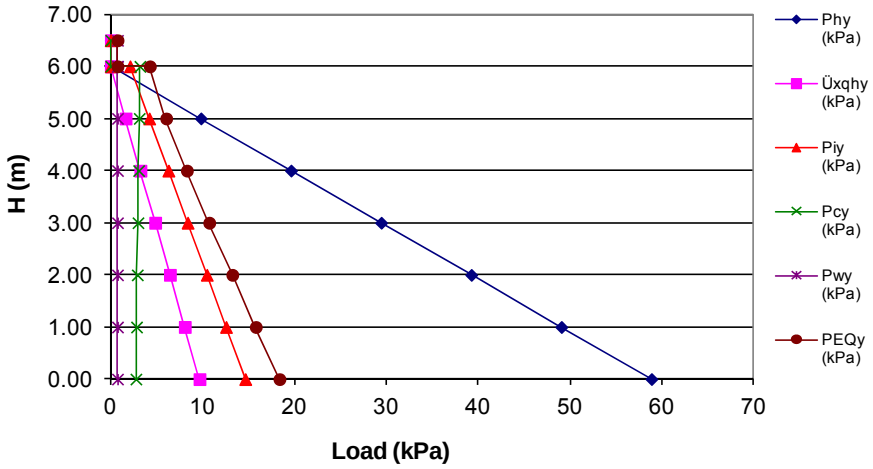

Figure A.2.1 – Design hydrodynamic and hydrostatic pressures at (θ) = 0 deg – Anchored, Flexible-Base

Design of Reinforced Concrete Section (Hoop Forces)

Reference:

Code Requirements for Environmental Engineering Concrete Structures (ACI 350-06) and Commentary (ACI 350R-06) – 2006.

B- Horizontal Bars

Load due to fluid

N_f = 1076 kN/m

P_{HS} = 58.84 kPa

Load due to earthquake

N_E = 281 kN/m

P_{EQ} = 15.36 kPa

f'_c = 30 MPa

f_y = 400 MPa

ϕ =	0.9	for flexure & axial tension			9.3.4.2
Concrete Cover =	50	mm			7.7.1
Bar sizes =	25	mm			
Spacing between bars S =	230	mm			
t_w =	300	mm			
d =	237.50	mm			
b =	1000	mm			
d_c =	62.5	mm			
$A_{s,\,min}$ =	$3 (f'_c)^{½}/f_y$ x bd	For tensile reinforcement		"Imperial Units"	10-3/10.5
$A_{s,\,min}$ =	$0.25 (f'_c)^{½}/f_y$ x bd =	813	mm^2/m	"Metric Units"	
$A_{s,\,min}$ =>	$200\, b_w d/f_y$			"Imperial Units"	10-3/10.5
$A_{s,\,min}$ =>	819	mm^2/m			
Ratio of $A_{s,\,min}$ for shrinkage =	0.005	Both sides			7.12.2.1
$A_{s,\,min}$ =	819	mm^2/m			

Strength Design Method

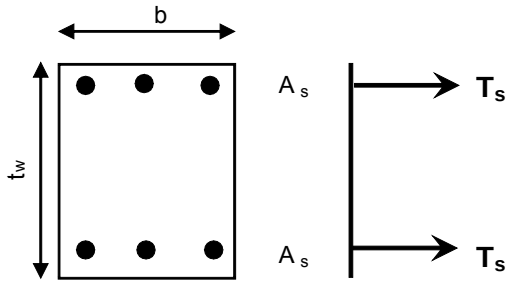

N_{u1} =1.4 (N_D + N_f) = 1505.8 kN/m R9.2.8.1

N_{u2} =1.2 N_D + 1.2 N_f + 1.0 N_E = 1571.7 kN/m (21.2.1.7) R9.2.3

N_u = Max (N_{u1} & N_{u2}) = 1571.7 kN/m

Environmental exposure normal

f_s = 138 Mpa 9.2.6.2 & 3

$$\gamma = \frac{Factored\_Load}{Unfactored\_Load} = 1.40$$

$$S_d = \frac{\phi f_y}{\gamma f_s} \geq 1.0 = 1.86$$

S_d x N_u = 1571.7 KN/m

ϕN_n = & [As fy] 9.3

ϕN_n / S_d x N_u 9.2.6

T_s = 785.8 kN

$A_{s\ req'd}$ = Ts/(& f_y) = 2183 mm^2/m R9.1.1

Design of Prestressed Concrete Section - Circumferential Prestressing

Reference:

Code Requirements for Environmental Engineering Concrete Structures (ACI 350-06) and Commentary (ACI 350R-06) – 2006.

B- Horizontal Bars

Load due to fluid

N_f =	1076	kN/m
P_{HS} =	58.8	kPa

Load due to earthquake

N_E =	281.0	kN/m
P_{EQ} =	15.36	kPa

f'_c =	30	MPa		
f_y =	400	MPa		
f_{pu} =	1860	MPa		
f_{py} =	1581	MPa		
ϕ =	0.85	Prestressing		9.3.2.5
Concrete Cover =	37.5	mm		7.7.3.1

Vertical bar sizes =	15	mm	
Spacing between bars S =	225	mm	
Spacing Tendons =	200	mm	
Number of Strands =	3		
Area of Strand =	140	mm^2	
Residual compressive stress =	1.38	MPa	
t_w =	300	mm	
d =	255.00	mm	
b =	1000	mm	
ϕ Duct =	50	mm	
d_c =	77.5	mm	

$A_{s,\,min}$ =	$3\,(f'_c)^{\frac{1}{2}}/f_y$ x bd	For tensile reinforcement		"Imperial Units"	10-3/10.5
$A_{s,\,min}$ =	$0.25\,(f'_c)^{\frac{1}{2}}/f_y$ x bd =	873	mm^2/m	"Metric Units"	
$A_{s,\,min}$ =>	$200\,b_w\,d/f_y$			"Imperial Units"	10-3/10.5
$A_{s,\,min}$ =>	879	mm^2/m			
Ratio of $A_{s,\,min}$ for bonded reinforcement =		0.004	Vertical both sides		18.9.2
$A_{s,\,min}$ =	879	mm^2/m			

Strength Design Method - Circumferential Prestressing

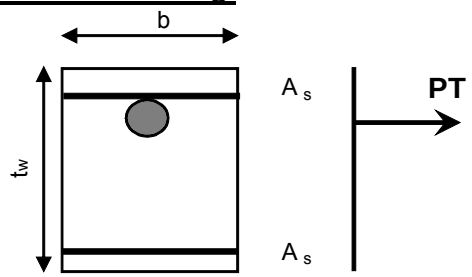

N_{u1} =1.4 (N_D + N_f) = 1505.8 kN/m R9.2.8.1

N_{u2} =1.2 N_D + 1.2 N_f + 1.0 N_E = 1571.7 kN/m (21.2.1.7) R9.2.3

N_u = Max (N_{u1} & N_{u2}) = 1571.7 kN/m

Environmental exposure normal

Pt_e => Nu + Residual stress = 1986 kN/m

Pt_i => 2648 kN/m

σ_i <= MIN(0.94f_{py},0.80f_{pu}) = 1486.1 MPa 18.5.1

Pt_i = 2653 kN/m

Pt_i = 531 kN/Tendon

Pt_e = 1990 kN/m

Pt_e = 398 kN/Tendon

APPENDIX A.3
EFFECT OF RECTANGULAR TANK DIMENSIONS ON HYDRODYNAMIC FORCES

For rectangular tanks three different water heights, H_L, of 3m, 6m and 9m are used. The length of the tank, L, in the direction of the earthquake force is assumed as either 20m or 40m. The widths of the tanks perpendicular to the direction of the earthquake force are assumed as 20m and 40m. The thicknesses of the tank walls are assumed to be 500mm.

Figure A.3.1 shows the effect of the tank length (L) on the hydrodynamic forces for different tank heights. The hydrodynamic forces are divided by the tank height for a better comparison. For the same depth of stored liquid, the effect of the length of the tank in the direction of earthquake on the impulsive force is very small, because by increasing the total mass of the stored liquid W_L, the rate of the ratio between the equivalent mass of the impulsive component to the total mass of the stored liquid W_i/W_L decreases which equalizes the total effect. At the same time for the same depth of stored liquid, the length of the tank in the direction of the earthquake has a major effect on the convective force. As the rate of the ratio between the equivalent mass of the convective component to the total mass of the stored liquid W_c/W_L and the total mass of the stored liquid W_L increase, as the length of the tank perpendicular to the earthquake increases, the total dynamic forces and moments linearly increase, but the length L has no effect on dynamic pressures.

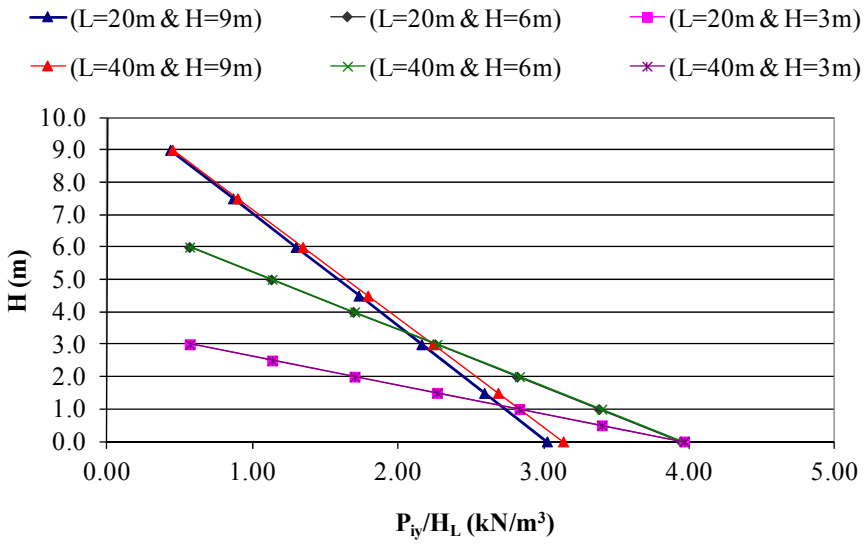

(a)

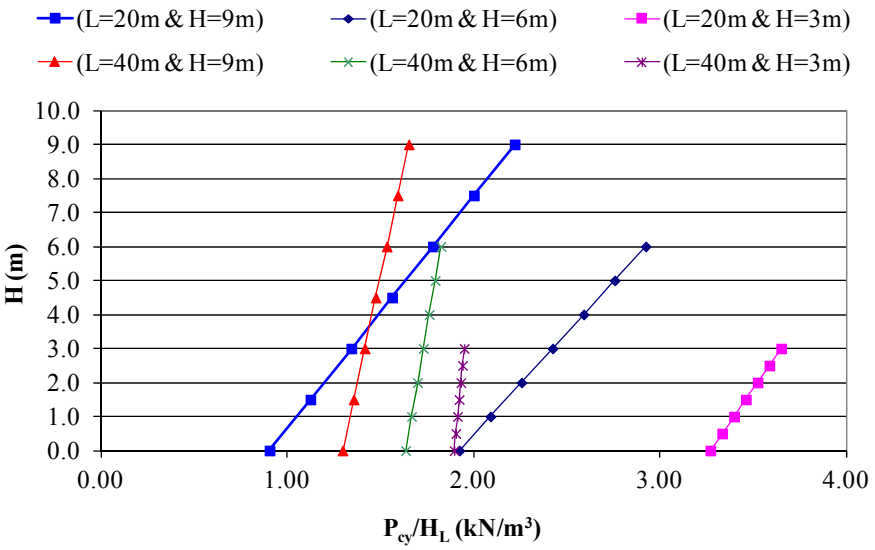

(b)

Figure A.3.1 - Effect of rectangular tank dimensions on hydrodynamic forces B = 40 m and Zone 4, (a) Impulsive force, (b) Convective force

Figure A.3.2 shows the effect of tank height on earthquake/hydrostatic (V_{EQ}/V_S) force and bending moment (M_{EQ}/M_S) ratios for different seismic zones. Figures A.3.2 (a) and (b) show the effect on base shear and base moment ratios, respectively. The figures show that the earthquake/static force ratios are linearly proportion to the seismic zone factor. As the tank height increases, the ratios decrease

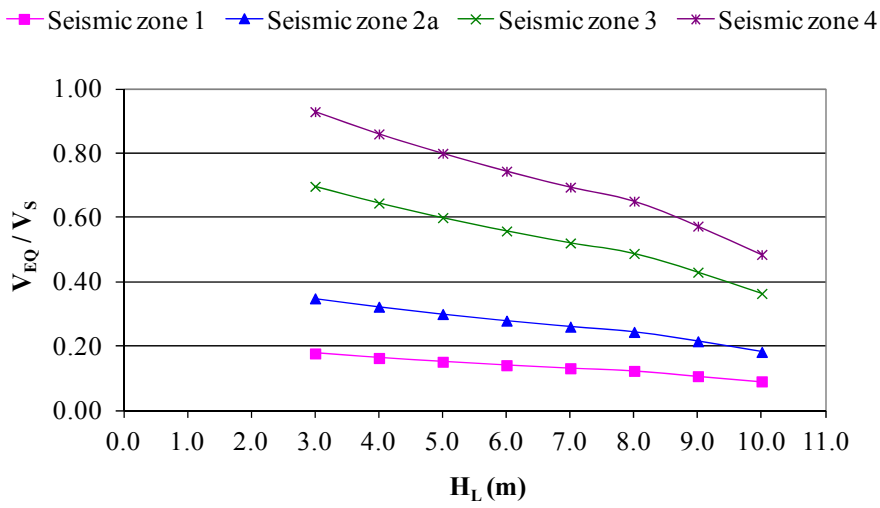

(a)

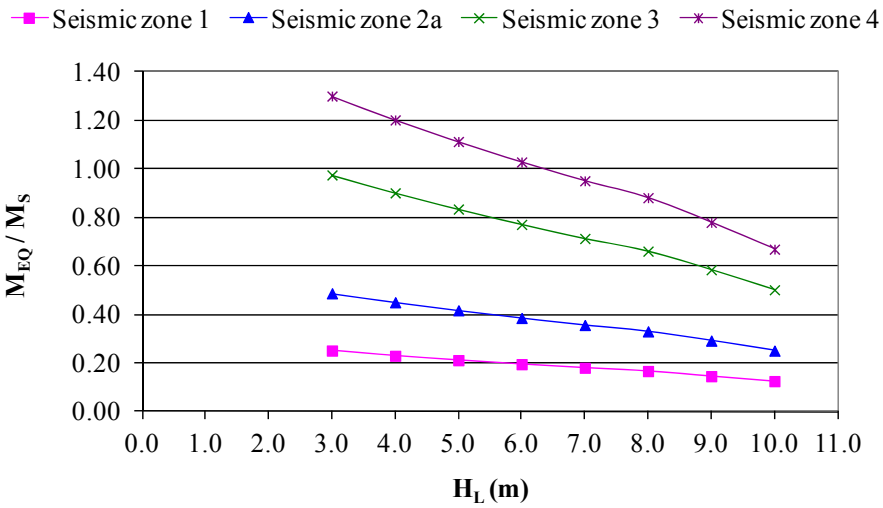

(b)

Figure A.3.2 - Effect of rectangular tank height on Earthquake/Hydrostatic force ratio B=20m, L=20m, (a) Base shear, (b) Base moments

Figure A.3.3 shows that the freeboard (sloshing height) is directly proportional to the seismic zone factor and to the depth of stored liquid. The freeboard is inversely proportional to the length of the tank parallel to the direction of the earthquake force.

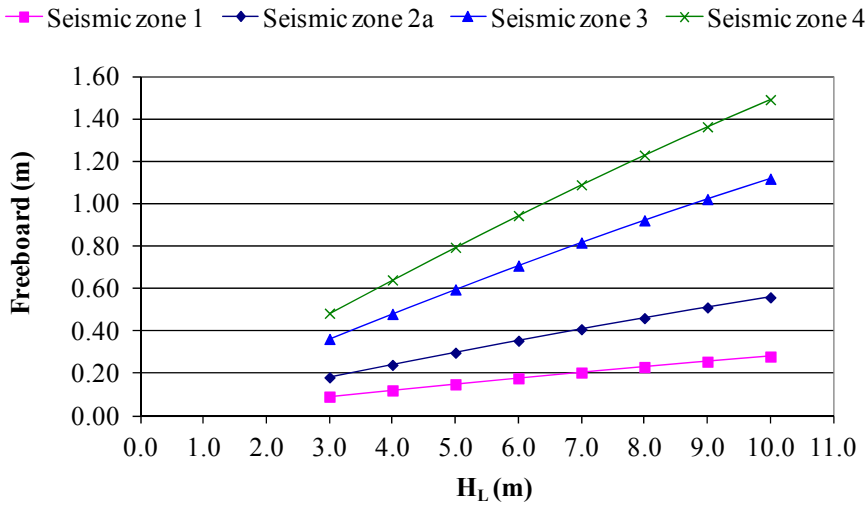

(a)

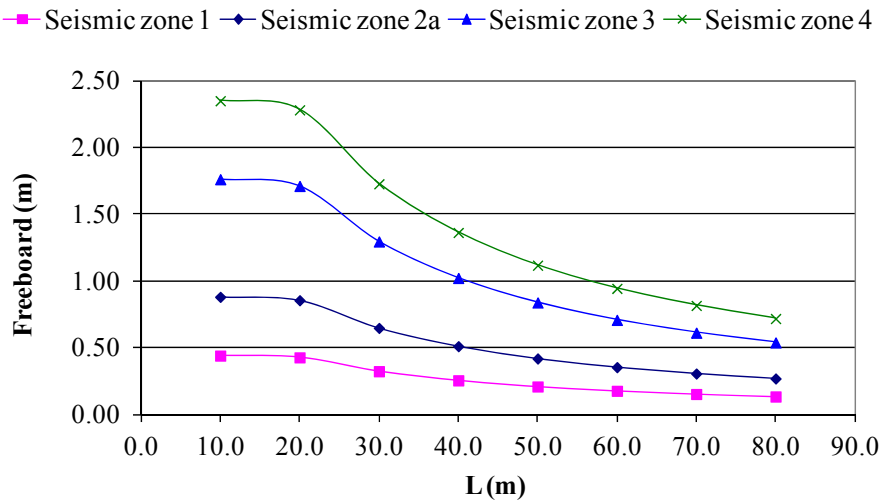

(b)

Figure A.3.3- Effect of rectangular tank dimensions on sloshing height, (a) Water depth B=20m, L=60m, (b) Tank length parallel to the earthquake force B=20m, HL=6m

Figure A.3.4 shows the effect of tank length on seismic forces. It was found that for the same depth of stored liquid, the length of the tank parallel to the direction of the earthquake force almost has no effect on the impulsive force Pi, because the rate of increasing the total mass of the stored liquid W_L equalizes the decreasing rate of the ratio between the equivalent mass of the impulsive component to the total mass of the stored liquid W_i/W_L. For the same depth of stored liquid, the lateral convective force Pc is inversely proportional to the length parallel to the direction of the earthquake force because decreasing the rate of the spectral amplification factor C_c, is more significant than by increasing the rate of the length parallel to the direction of the earthquake force.

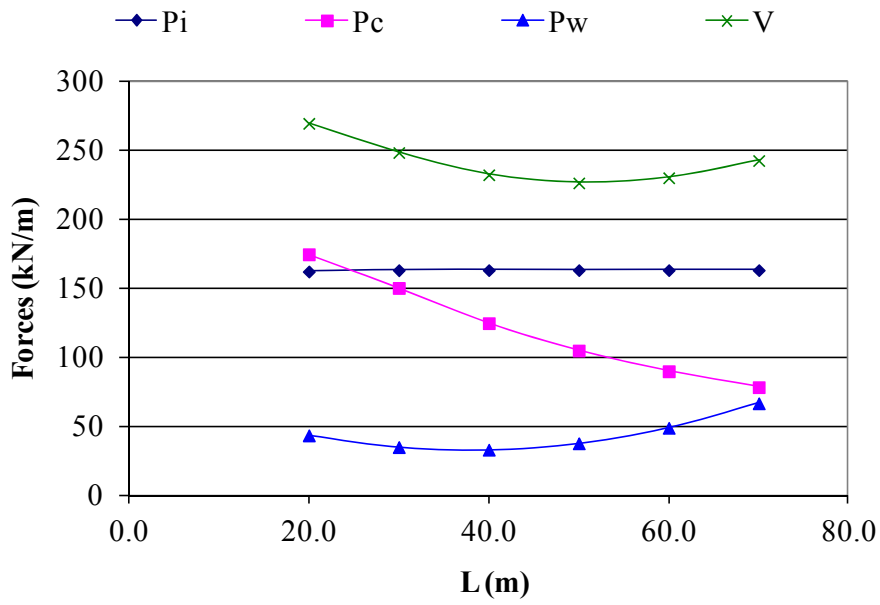

(a)

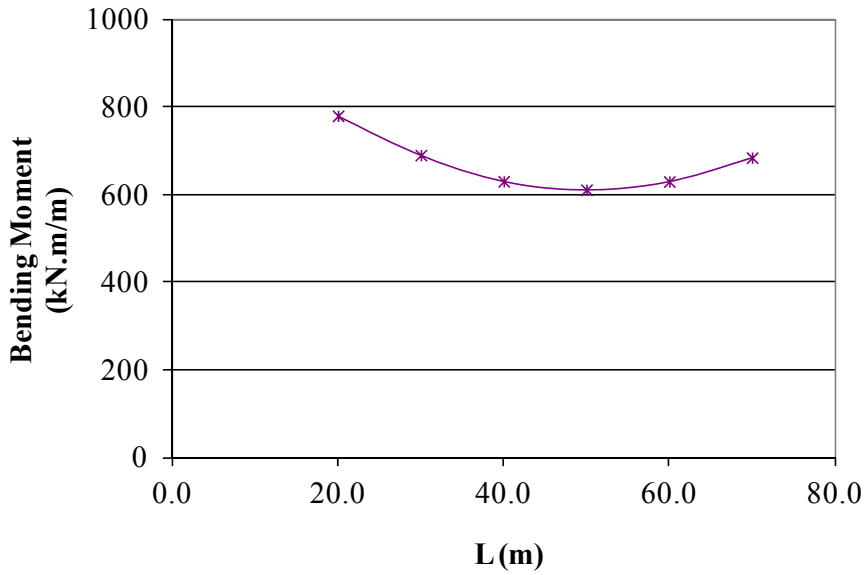

(b)

Figure A.3.4 - Effect of rectangular tank dimensions on seismic forces B=40m, H_L=6.0m, Zone 4, (a) Hydrodynamic forces, (b) Bending moments

APPENDIX A.4
TAYLOR DEVICES INC. FLUID VISCOUS DAMPERS DATASHEET

taylor devices inc.

FLUID VISCOUS DAMPERS & LOCK-UP DEVICES

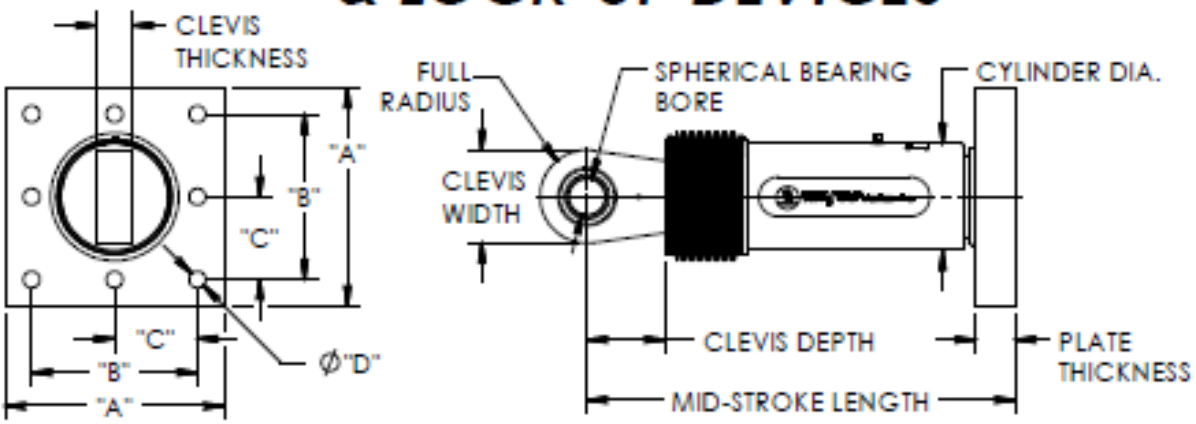

FORCE	SPHERICAL BEARING BORE DIA. (INCHES)	MID-STROKE LENGTH (INCHES)	STROKE (INCHES)	CLEVIS THICKNESS (INCHES)	CLEVIS WIDTH (INCHES)	CLEVIS DEPTH (INCHES)	CYLINDER DIA. (INCHES)	WEIGHT (lbs.)
55 KIP	1.50	31.00	±3	1.63	4 MAX.	3.25	4-1/2 MAX.	98
110 KIP	2.00	38.25	±4	2.13	5 MAX.	4.00	6-3/4 MAX.	215
186 KIP	2.25	40.00	±4	2.25	6 MAX.	5.10	7-1/4 MAX.	400
220 KIP	2.75	41.25	±4	2.75	7-1/2 MAX.	5.88	8-1/4 MAX.	560
330 KIP	3.00	43.50	±4	3.00	8 MAX.	6.38	8-1/2 MAX.	675
440 KIP	3.50	53.00	±5	3.50	9 MAX.	7.50	11-1/4 MAX.	1000
675 KIP	4.00	56.75	±5	4.50	11-1/4 MAX.	8.00	13-3/4 MAX.	1750
900 KIP	5.00	64.00	±5	5.50	12-3/4 MAX.	10.75	16-3/4 MAX.	2400
1450 KIP	†	†	†	†	†	†	†	†
1800 KIP	†	†	†	†	†	†	†	†

FORCE	"A"	"B"	"C"	"D"	PLATE THICKNESS (INCHES)
55 KIP	7.00±.12	5.00±.01	*	0.81±.01	1.50±.03
110 KIP	11.12±.12	8.00±.01	*	1.25±.01	1.50±.03
186 KIP	13.50±.12	10.00±.01	5.00±.01	1.12±.01	2.40±.03
220 KIP	16.50±.12	12.50±.01	6.25±.01	1.25±.01	3.00±.06
330 KIP	17.00±.12	13.00±.01	6.50±.01	1.375±.010	3.00±.06
440 KIP	18.00±.12	13.50±.01	6.75±.01	1.500±.010	4.00±.06
675 KIP	20.00±.12	16.00±.01	8.00±.01	1.63±.01	4.00±.06
900 KIP	†	†	†	†	†
1450 KIP	†	†	†	†	†
1800 KIP	†	†	†	†	†

NOTE:
VARIOUS STROKES ARE AVAILABLE, FROM ±2 TO ±36 INCHES. FORCE CAPACITY MAY BE REDUCED FOR STROKE LONGER THAN STROKE LISTED IN TABLE. ANY STROKE CHANGE FROM THE STANDARD STROKE VERSION DEPICTED CHANGES MID-STROKE LENGTH BY FIVE INCHES PER ±1 INCH OF STROKE.

EXAMPLE: 220 KIP ±4 INCHES STROKE, MID-STROKE LENGTH IS 41.25 INCHES
220 KIP ±6 INCHES STROKE,
6-4 = 2 TIMES FIVE = 10
41.25+10 = 51.25 INCHES MID-STROKE LENGTH

BELLOWS MAY BE REPLACED WITH A STEEL SLEEVE AS DESIRED STROKE LENGTHS INCREASE. CONSULT TAYLOR DEVICES FOR STROKE OVER ± 12 INCHES AND/OR FOR FORCE CAPACITIES FOR STROKE LONGER THAN LISTED IN TABLE.
* DENOTES 4-BOLT MOUNTING PATTERN
† DENOTES CUSTOM PATTERN. CONSULT FACTORY.

APPENDIX B.1
INPUT FILES OF COMPUTER MODELS – PUSH-OVER ANALYSIS

```
*Heading
** Job name: H6-Hinge-Axi Model name: Model-1
** Generated by: ABAQUS/CAE Student Edition 6.9-2
*Preprint, echo=NO, model=NO, history=NO, contact=NO
**
** PARTS
**
*Part, name=AXI
*End Part
**
**
** ASSEMBLY
**
*Assembly, name=Assembly
**
*Instance, name=Part-1-1, part=AXI
*Node
      1,          20.,           0.
      2,          20.,   1.08333337
      3,          20.,   2.16666675
      4,          20.,         3.25
      5,          20.,   4.33333349
      6,          20.,   5.41666651
      7,          20.,          6.5
*Element, type=SAX1
1, 1, 2
2, 2, 3
3, 3, 4
4, 4, 5
5, 5, 6
6, 6, 7
```

```
*Nset, nset=_PickedSet9, internal, generate
 1,  7,  1
*Elset, elset=_PickedSet9, internal, generate
 1,  6,  1
** Section: W300
*Shell Section, elset=_PickedSet9, material=Concrete, controls=EC-1
0.3, 9
*Rebar Layer
R1, 0.0003, 0.225, 0.09, Steel, 90., 1
R2, 0.0003, 0.225, -0.09, Steel, 90., 1
R3, 0.0002, 0.2, 0.0725, Steel, 0., 1
R4, 0.0002, 0.225, -0.0725, Steel, 0., 1
*End Instance
**
*Nset, nset=_PickedSet7, internal, instance=Part-1-1
 1,
*Nset, nset=Set-2, instance=Part-1-1, generate
 1,  7,  1
*Elset, elset=Set-2, instance=Part-1-1, generate
 1,  6,  1
*Nset, nset="Bottom point", instance=Part-1-1
 1,
*Nset, nset="Top Point", instance=Part-1-1
 7,
*Elset, elset=__PickedSurf6_SPOS, internal, instance=Part-1-1, generate
 1,  6,  1
*Surface, type=ELEMENT, name=_PickedSurf6, internal
__PickedSurf6_SPOS, SPOS
*Elset, elset=__PickedSurf20_SPOS, internal, instance=Part-1-1, generate
 1,  6,  1
*Surface, type=ELEMENT, name=_PickedSurf20, internal
```

```
__PickedSurf20_SPOS, SPOS
*End Assembly
**
** ELEMENT CONTROLS
**
*Section Controls, name=EC-1, DISTORTION CONTROL=NO, hourglass=STIFFNESS
1., 1., 1.
**
** MATERIALS
**
*Material, name=Concrete
*Concrete
   1.2e+07,         0.
  1.67e+07, 0.00073928
  2.25e+07, 0.00110892
 2.667e+07, 0.00147856
 2.917e+07,  0.0018482
     3e+07, 0.00221784
  2.55e+07,     0.0038
*Failure Ratios
 1.16, 0.0836,   1.28, 0.3333
*Tension Stiffening
1.,    0.
0., 0.002
*Density
2400.,
*Elastic
 2.46e+10, 0.18
*Material, name=Steel
*Density
7800.,
```

```
*Elastic
 2e+11,0.
*Plastic
 4e+08,0.
**
** BOUNDARY CONDITIONS
**
** Name: BC-1 Type: Displacement/Rotation
*Boundary
_PickedSet7, 1, 1
_PickedSet7, 2, 2
** ----------------------------------------------------------------
**
** STEP: Step-1
**
*Step, name=Step-1
*Static, riks
0.05, 1., 1e-09, , 1.,
**
** LOADS
**
** Name: Pi2   Type: Pressure
*Dsload
_PickedSurf6, HP, 100000., 6., 0.
** Name: pi1   Type: Pressure
*Dsload
_PickedSurf20, P, 27000.
**
** OUTPUT REQUESTS
**
*Restart, write, frequency=0
```

```
**
** FIELD OUTPUT: F-Output-1
**
*Output, field
*Node Output
RF, UT
*Element Output, directions=YES
DAMAGEC, DAMAGET, E, EE, ER, IE, LE, NE, PE, PEEQ, PEEQT, PEMAG, PEQC,
S, SALPHA, SDEG
SE, SEE, SEP, SEPE, SPE, THE, VE, VEEQ
*Element Output, rebar, directions=YES
DAMAGEC, DAMAGET, E, EE, ER, IE, LE, NE, PE, PEEQ, PEEQT, PEMAG, PEQC,
S, SALPHA, SDEG
SE, SEE, SEP, SEPE, SPE, THE, VE, VEEQ
**
** HISTORY OUTPUT: H-Output-2
**
*Output, history
*Node Output, nset="Bottom point"
U1, U2, U3, UR1, UR2, UR3
**
** HISTORY OUTPUT: H-Output-4
**
*Element Output, elset=Set-2
E11, E22, E33, PE11, PE22, PE33, PEP, PRESS, S11, S22, S33
**
** HISTORY OUTPUT: H-Output-3
**
*Element Output, elset=Set-2, rebar
E, S
**
```

** HISTORY OUTPUT: H-Output-1

**

*Node Output, nset=Set-2

U1, U2, U3, UR1, UR2, UR3

*End Step

APPENDIX B.2

INPUT FILES OF COMPUTER MODELS – TIME-HISTORY ANALYSIS

Joint numbers, joint coordinates, element numbers, and earthquake data are removed from the text file due to the very large size of the data.

```
** Shell elements
*Heading
** Job name: H6-Flex-PT-PI Model name: H6+Flex-PT-PI
** Generated by: ABAQUS/CAE 6.10-EF1
*Preprint, echo=NO, model=NO, history=NO, contact=NO
**
** PARTS
**
*Part, name=Point
*End Part
**
*Part, name=Shell-Full
*End Part
**
**
** ASSEMBLY
**
*Assembly, name=Assembly
**
*Instance, name=Shell-Full-1, part=Shell-Full
*Element, type=S4R
** Section: W300
*Shell Section, elset=_PickedSet154, material=Concrete30mpa
0.3, 9
*Rebar Layer
TENDON, 0.00042, 0.2, 0.0725, Strand, 90., 1
R3, 0.0002, 0.24, 0.105, Steel, 0., 1
R4, 0.0002, 0.24, -0.105, Steel, 0., 1
*Nonstructural Mass, elset=_PickedSet105, units=MASS PER AREA
5584.,
*Nonstructural Mass, elset=_PickedSet111, units=MASS PER AREA
```

5163.,
*Nonstructural Mass, elset=_PickedSet118, units=MASS PER AREA
4385.7,
*Nonstructural Mass, elset=_PickedSet124, units=MASS PER AREA
3369.8,
*Nonstructural Mass, elset=_PickedSet130, units=MASS PER AREA
2270.,
*Nonstructural Mass, elset=_PickedSet136, units=MASS PER AREA
1253.8,
*Nonstructural Mass, elset=_PickedSet142, units=MASS PER AREA
475.9,
*Nonstructural Mass, elset=_PickedSet148, units=MASS PER AREA
54.5,
*Nonstructural Mass, elset=_PickedSet106, units=MASS PER AREA
4725.1,
*Nonstructural Mass, elset=_PickedSet113, units=MASS PER AREA
4369.1,
*Nonstructural Mass, elset=_PickedSet119, units=MASS PER AREA
3711.1,
*Nonstructural Mass, elset=_PickedSet125, units=MASS PER AREA
2851.4,
*Nonstructural Mass, elset=_PickedSet131, units=MASS PER AREA
1920.9,
*Nonstructural Mass, elset=_PickedSet137, units=MASS PER AREA
1061.,
*Nonstructural Mass, elset=_PickedSet143, units=MASS PER AREA
402.7,
*Nonstructural Mass, elset=_PickedSet149, units=MASS PER AREA
46.1,
*Nonstructural Mass, elset=_PickedSet107, units=MASS PER AREA
3866.2,

*Nonstructural Mass, elset=_PickedSet114, units=MASS PER AREA
3574.9,
*Nonstructural Mass, elset=_PickedSet120, units=MASS PER AREA
3036.5,
*Nonstructural Mass, elset=_PickedSet126, units=MASS PER AREA
2333.1,
*Nonstructural Mass, elset=_PickedSet132, units=MASS PER AREA
1571.7,
*Nonstructural Mass, elset=_PickedSet138, units=MASS PER AREA
868.1,
*Nonstructural Mass, elset=_PickedSet144, units=MASS PER AREA
329.5,
*Nonstructural Mass, elset=_PickedSet150, units=MASS PER AREA
37.7,
*Nonstructural Mass, elset=_PickedSet108, units=MASS PER AREA
3007.3,
*Nonstructural Mass, elset=_PickedSet115, units=MASS PER AREA
2780.6,
*Nonstructural Mass, elset=_PickedSet121, units=MASS PER AREA
2361.9,
*Nonstructural Mass, elset=_PickedSet127, units=MASS PER AREA
1814.8,
*Nonstructural Mass, elset=_PickedSet133, units=MASS PER AREA
1222.5,
*Nonstructural Mass, elset=_PickedSet139, units=MASS PER AREA
675.2,
*Nonstructural Mass, elset=_PickedSet145, units=MASS PER AREA
256.3,
*Nonstructural Mass, elset=_PickedSet151, units=MASS PER AREA
29.3,
*Nonstructural Mass, elset=_PickedSet109, units=MASS PER AREA

2148.3,
*Nonstructural Mass, elset=_PickedSet116, units=MASS PER AREA
1986.4,
*Nonstructural Mass, elset=_PickedSet122, units=MASS PER AREA
1687.3,
*Nonstructural Mass, elset=_PickedSet128, units=MASS PER AREA
1296.5,
*Nonstructural Mass, elset=_PickedSet134, units=MASS PER AREA
873.3,
*Nonstructural Mass, elset=_PickedSet140, units=MASS PER AREA
482.4,
*Nonstructural Mass, elset=_PickedSet146, units=MASS PER AREA
183.1,
*Nonstructural Mass, elset=_PickedSet152, units=MASS PER AREA
21.,
*Nonstructural Mass, elset=_PickedSet110, units=MASS PER AREA
1289.4,
*Nonstructural Mass, elset=_PickedSet117, units=MASS PER AREA
1192.2,
*Nonstructural Mass, elset=_PickedSet123, units=MASS PER AREA
1012.7,
*Nonstructural Mass, elset=_PickedSet129, units=MASS PER AREA
778.1,
*Nonstructural Mass, elset=_PickedSet135, units=MASS PER AREA
524.2,
*Nonstructural Mass, elset=_PickedSet141, units=MASS PER AREA
289.5,
*Nonstructural Mass, elset=_PickedSet147, units=MASS PER AREA
109.9,
*Nonstructural Mass, elset=_PickedSet153, units=MASS PER AREA
12.6,

*End Instance
**
*Element, type=SpringA, elset=K1-spring
1, Shell-Full-1.255, Point-1.1
*Spring, elset=K3-spring

69744.
*Element, type=SpringA, elset=K3-spring
2, Shell-Full-1.249, Point-1-rad-3.1
*Spring, elset=K4-spring

69744.
*Element, type=SpringA, elset=K4-spring
3, Shell-Full-1.246, Point-1-rad-4.1
*Spring, elset=K5-spring

69744.
*Element, type=SpringA, elset=K5-spring
4, Shell-Full-1.243, Point-1-rad-5.1
*Spring, elset=K6-spring

69744.
*Element, type=SpringA, elset=K6-spring
5, Shell-Full-1.240, Point-1-rad-6.1
*Spring, elset=K7-spring

69744.
*Element, type=SpringA, elset=K7-spring
6, Shell-Full-1.209, Point-1-rad-7.1
*Spring, elset=K8-spring

69744.
*Element, type=SpringA, elset=K8-spring
7, Shell-Full-1.207, Point-1-rad-8.1
*Spring, elset=K9-spring

69744.
*Element, type=SpringA, elset=K9-spring
8, Shell-Full-1.204, Point-1-rad-9.1
*Spring, elset=K10-spring

69744.
*Element, type=SpringA, elset=K10-spring
9, Shell-Full-1.201, Point-1-rad-10.1
*Spring, elset=K11-spring

69744.
*Element, type=SpringA, elset=K11-spring
10, Shell-Full-1.198, Point-1-rad-11.1
*Spring, elset=K12-spring

69744.
*Element, type=SpringA, elset=K12-spring
11, Shell-Full-1.195, Point-1-rad-12.1
*Spring, elset=K13-spring

69744.
*Element, type=SpringA, elset=K13-spring
12, Shell-Full-1.192, Point-1-rad-13.1
*Spring, elset=K14-spring

69744.

*Element, type=SpringA, elset=K14-spring
13, Shell-Full-1.189, Point-1-rad-14.1
*Spring, elset=K15-spring

69744.
*Element, type=SpringA, elset=K15-spring
14, Shell-Full-1.186, Point-1-rad-15.1
*Spring, elset=K16-spring

69744.
*Element, type=SpringA, elset=K16-spring
15, Shell-Full-1.185, Point-1-rad-16.1
*Spring, elset=K17-spring

69744.
*Element, type=SpringA, elset=K17-spring
16, Shell-Full-1.184, Point-1-rad-17.1
*Spring, elset=K18-spring

69744.
*Element, type=SpringA, elset=K18-spring
17, Shell-Full-1.183, Point-1-rad-18.1
*Spring, elset=K19-spring

69744.
*Element, type=SpringA, elset=K19-spring
18, Shell-Full-1.182, Point-1-rad-19.1
*Spring, elset=K20-spring

69744.
*Element, type=SpringA, elset=K20-spring

19, Shell-Full-1.181, Point-1-rad-20.1
*Spring, elset=K21-spring

69744.
*Element, type=SpringA, elset=K21-spring
20, Shell-Full-1.180, Point-1-rad-21.1
*Spring, elset=K22-spring

69744.
*Element, type=SpringA, elset=K22-spring
21, Shell-Full-1.178, Point-1-rad-22.1
*Spring, elset=K23-spring

69744.
*Element, type=SpringA, elset=K23-spring
22, Shell-Full-1.179, Point-1-rad-23.1
*Spring, elset=K24-spring

69744.
*Element, type=SpringA, elset=K24-spring
23, Shell-Full-1.234, Point-1-rad-24.1
*Spring, elset=K25-spring

69744.
*Element, type=SpringA, elset=K25-spring
24, Shell-Full-1.233, Point-1-rad-25.1
*Spring, elset=K26-spring

69744.
*Element, type=SpringA, elset=K26-spring
25, Shell-Full-1.229, Point-1-rad-26.1

*Spring, elset=K27-spring

69744.
*Element, type=SpringA, elset=K27-spring
26, Shell-Full-1.226, Point-1-rad-27.1
*Spring, elset=K28-spring

69744.
*Element, type=SpringA, elset=K28-spring
27, Shell-Full-1.223, Point-1-rad-28.1
*Spring, elset=K29-spring

69744.
*Element, type=SpringA, elset=K29-spring
28, Shell-Full-1.220, Point-1-rad-29.1
*Spring, elset=K30-spring

69744.
*Element, type=SpringA, elset=K30-spring
29, Shell-Full-1.217, Point-1-rad-30.1
*Spring, elset=K31-spring

69744.
*Element, type=SpringA, elset=K31-spring
30, Shell-Full-1.212, Point-1-rad-31.1
*Spring, elset=K32-spring

69744.
*Element, type=SpringA, elset=K32-spring
31, Shell-Full-1.213, Point-1-rad-32.1
*Spring, elset=R1-spring

26656.
*Element, type=SpringA, elset=R1-spring
32, Point-2-rad-32.1, Shell-Full-1.207
*Spring, elset=R2-spring

26656.
*Element, type=SpringA, elset=R2-spring
33, Point-2.1, Shell-Full-1.204
*Spring, elset=R3-spring

26656.
*Element, type=SpringA, elset=R3-spring
34, Point-2-rad-2.1, Shell-Full-1.201
*Spring, elset=R4-spring

26656.
*Element, type=SpringA, elset=R4-spring
35, Point-2-rad-3.1, Shell-Full-1.198
*Spring, elset=R5-spring

26656.
*Element, type=SpringA, elset=R5-spring
36, Point-2-rad-4.1, Shell-Full-1.195
*Spring, elset=R6-spring

26656.
*Element, type=SpringA, elset=R6-spring
37, Point-2-rad-5.1, Shell-Full-1.192
*Spring, elset=R7-spring

26656.
*Element, type=SpringA, elset=R7-spring
38, Point-2-rad-6.1, Shell-Full-1.189
*Spring, elset=R8-spring

26656.
*Element, type=SpringA, elset=R8-spring
39, Point-2-rad-7.1, Shell-Full-1.186
*Spring, elset=R9-spring

26656.
*Element, type=SpringA, elset=R9-spring
40, Point-2-rad-8.1, Shell-Full-1.185
*Spring, elset=R10-spring

26656.
*Element, type=SpringA, elset=R10-spring
41, Point-2-rad-9.1, Shell-Full-1.184
*Spring, elset=R11-spring

26656.
*Element, type=SpringA, elset=R11-spring
42, Point-2-rad-10.1, Shell-Full-1.183
*Spring, elset=R12-spring

26656.
*Element, type=SpringA, elset=R12-spring
43, Point-2-rad-11.1, Shell-Full-1.182
*Spring, elset=R13-spring

26656.

*Element, type=SpringA, elset=R13-spring
44, Point-2-rad-12.1, Shell-Full-1.181
*Spring, elset=R14-spring

26656.
*Element, type=SpringA, elset=R14-spring
45, Point-2-rad-13.1, Shell-Full-1.180
*Spring, elset=R15-spring

26656.
*Element, type=SpringA, elset=R15-spring
46, Point-2-rad-14.1, Shell-Full-1.178
*Spring, elset=R16-spring

26656.
*Element, type=SpringA, elset=R16-spring
47, Point-2-rad-15.1, Shell-Full-1.179
*Spring, elset=R17-spring

26656.
*Element, type=SpringA, elset=R17-spring
48, Point-2-rad-16.1, Shell-Full-1.234
*Spring, elset=R18-spring

26656.
*Element, type=SpringA, elset=R18-spring
49, Point-2-rad-17.1, Shell-Full-1.233
*Spring, elset=R19-spring

26656.
*Element, type=SpringA, elset=R19-spring

50, Point-2-rad-18.1, Shell-Full-1.229
*Spring, elset=R20-spring

26656.
*Element, type=SpringA, elset=R20-spring
51, Point-2-rad-19.1, Shell-Full-1.226
*Spring, elset=R21-spring

26656.
*Element, type=SpringA, elset=R21-spring
52, Point-2-rad-20.1, Shell-Full-1.223
*Spring, elset=R22-spring

26656.
*Element, type=SpringA, elset=R22-spring
53, Point-2-rad-21.1, Shell-Full-1.220
*Spring, elset=R23-spring

26656.
*Element, type=SpringA, elset=R23-spring
54, Point-2-rad-22.1, Shell-Full-1.217
*Spring, elset=R24-spring

26656.
*Element, type=SpringA, elset=R24-spring
55, Point-2-rad-23.1, Shell-Full-1.212
*Spring, elset=R25-spring

26656.
*Element, type=SpringA, elset=R25-spring
56, Point-2-rad-24.1, Shell-Full-1.213

*Spring, elset=R26-spring

26656.
*Element, type=SpringA, elset=R26-spring
57, Point-2-rad-25.1, Shell-Full-1.255
*Spring, elset=R27-spring

26656.
*Element, type=SpringA, elset=R27-spring
58, Point-2-rad-26.1, Shell-Full-1.252
*Spring, elset=R28-spring

26656.
*Element, type=SpringA, elset=R28-spring
59, Point-2-rad-27.1, Shell-Full-1.249
*Spring, elset=R29-spring

26656.
*Element, type=SpringA, elset=R29-spring
60, Point-2-rad-28.1, Shell-Full-1.246
*Spring, elset=R30-spring

26656.
*Element, type=SpringA, elset=R30-spring
61, Point-2-rad-29.1, Shell-Full-1.243
*Spring, elset=R31-spring

26656.
*Element, type=SpringA, elset=R31-spring
62, Point-2-rad-30.1, Shell-Full-1.240
*Spring, elset=R32-spring

```
26656.
*Element, type=SpringA, elset=R32-spring
63, Point-2-rad-31.1, Shell-Full-1.209
*Spring, elset=k2-spring

69744.
*Element, type=SpringA, elset=k2-spring
64, Shell-Full-1.252, Point-1-rad-2.1
*End Assembly
*Amplitude, name=HY, definition=SMOOTH STEP
        0.,          0.,          1.,          1.
*Amplitude, name="Imperial Valley"
**
** MATERIALS
**
*Material, name=Concrete30mpa
*Damping, alpha=0.687736, beta=0.003635
*Density
2400.,
*Elastic
 2.5727e+10, 0.18
*Expansion
0.,
*Concrete Damaged Plasticity
30.,   0.1,  1.16, 0.666,    0.
*Concrete Compression Hardening
 2.2224e+07,     0.
 2.7036e+07, 0.0006
 2.9352e+07, 0.0012
     3e+07, 0.0018
```

2.9442e+07, 0.0024
2.8146e+07, 0.003
2.6388e+07, 0.0036
2.028e+07, 0.0054
1.3794e+07, 0.0075
2.688e+06, 0.015
*Concrete Tension Stiffening
500000., 0.
409270., 0.0001
312640., 0.0003
269663., 0.0004
224719., 0.0005
150562., 0.0008
100843., 0.001
45224.7, 0.002
20505.6, 0.003
11236., 0.005
*Concrete Compression Damage
0., 0.
0.13, 0.0006
0.24, 0.0012
0.34, 0.0018
0.43, 0.0024
0.5, 0.003
0.57, 0.0036
0.71, 0.0054
0.82, 0.0075
0.97, 0.015
*Concrete Tension Damage
0., 0.
0.3, 0.0001

```
 0.55, 0.0003
  0.7, 0.0004
  0.8, 0.0005
  0.9, 0.0008
 0.93,  0.001
 0.95,  0.002
 0.97,  0.003
 0.99,  0.005
*Material, name=Steel
*Density
7800.,
*Elastic
 2e+11,0.
*Expansion
0.,
*Plastic
 4e+08,  0.
 4e+08, 0.1
*Material, name=Strand
*Density
7800.,
*Elastic
 2e+11,0.
*Expansion
 1e-05,
*Plastic
 1.581e+09,     0.
  1.86e+09, 0.0575
**
** BOUNDARY CONDITIONS
**
```

** Name: BC-1 Type: Displacement/Rotation
*Boundary
_PickedSet75, 3, 3
** Name: Poiints Type: Displacement/Rotation
*Boundary
_PickedSet359, 1, 1
_PickedSet359, 2, 2
_PickedSet359, 3, 3
_PickedSet359, 4, 4
_PickedSet359, 5, 5
_PickedSet359, 6, 6
**
** PREDEFINED FIELDS
**
** Name: PT1   Type: Temperature
*Initial Conditions, type=TEMPERATURE
_PickedSet360, 631.5
** --
**
** STEP: PT
**
*Step, name=PT
*Dynamic, Explicit
, 1.
*Bulk Viscosity
0.06, 1.2
**
** PREDEFINED FIELDS
**
** Name: PT2   Type: Temperature
*Temperature

_PickedSet361, 0.
**
** OUTPUT REQUESTS
**
*Restart, write, number interval=1, time marks=NO
**
** FIELD OUTPUT: F-Output-1
**
*Output, field, time interval=0.01, time marks=YES
*Node Output
A, U, V
*Element Output, directions=YES
LE, PE, PEEQ, S
*Contact Output
CSTRESS,
**
** HISTORY OUTPUT: Reactions
**
*Output, history, time interval=0.01
*Node Output, nset=R
RF1, RF2, RF3
**
** HISTORY OUTPUT: Stresses
**
*Element Output, elset=Stresses
E11, E22, E33, S11, S22, S33
*Element Output, elset=Stresses, rebar
E, S
**
** HISTORY OUTPUT: Forces
**

```
*Element Output, elset=Stresses
SF1, SF2, SF3, SM1, SM2, SM3
*End Step
** ----------------------------------------------------------------
**
** STEP: HY
**
*Step, name=HY
*Dynamic, Explicit
, 1.
*Bulk Viscosity
0.06, 1.2
**
** LOADS
**
** Name: HY1   Type: Pressure
*Dsload, amplitude=HY
_PickedSurf85, P, 53900.
** Name: HY2   Type: Pressure
*Dsload, amplitude=HY
_PickedSurf86, P, 44100.
** Name: HY3   Type: Pressure
*Dsload, amplitude=HY
_PickedSurf87, P, 34300.
** Name: HY4   Type: Pressure
*Dsload, amplitude=HY
_PickedSurf88, P, 24500.
** Name: HY5   Type: Pressure
*Dsload, amplitude=HY
_PickedSurf89, P, 14700.
** Name: HY6   Type: Pressure
```

```
*Dsload, amplitude=HY
_PickedSurf90, P, 4900.
**
** PREDEFINED FIELDS
**
** Name: PT1   Type: Temperature
*Temperature, op=NEW
** Name: PT2   Type: Temperature
*Temperature, op=NEW
_PickedSet361, 0.
**
** OUTPUT REQUESTS
**
*Restart, write, number interval=1, time marks=NO
**
** FIELD OUTPUT: F-Output-1
**
*Output, field, time interval=0.01, time marks=YES
*Node Output
A, U, V
*Element Output, directions=YES
LE, PE, PEEQ, S
*Contact Output
CSTRESS,
**
** HISTORY OUTPUT: Reactions
**
*Output, history, time interval=0.01
*Node Output, nset=R
RF1, RF2, RF3
**
```

```
** HISTORY OUTPUT: Stresses
**
*Element Output, elset=Stresses
E11, E22, E33, S11, S22, S33
*Element Output, elset=Stresses, rebar
E, S
**
** HISTORY OUTPUT: Forces
**
*Element Output, elset=Stresses
SF1, SF2, SF3, SM1, SM2, SM3
*End Step
** ----------------------------------------------------------------
**
** STEP: PTLoss
**
*Step, name=PTLoss
*Dynamic, Explicit
, 1.
*Bulk Viscosity
0.06, 1.2
**
** PREDEFINED FIELDS
**
** Name: PT3   Type: Temperature
*Temperature
_PickedSet362, 157.9
**
** OUTPUT REQUESTS
**
*Restart, write, number interval=1, time marks=NO
```

```
**
** FIELD OUTPUT: F-Output-1
**
*Output, field, time interval=0.01, time marks=YES
*Node Output
A, U, V
*Element Output, directions=YES
LE, PE, PEEQ, S
*Contact Output
CSTRESS,
**
** HISTORY OUTPUT: Reactions
**
*Output, history, time interval=0.01
*Node Output, nset=R
RF1, RF2, RF3
**
** HISTORY OUTPUT: Stresses
**
*Element Output, elset=Stresses
E11, E22, E33, S11, S22, S33
*Element Output, elset=Stresses, rebar
E, S
**
** HISTORY OUTPUT: Forces
**
*Element Output, elset=Stresses
SF1, SF2, SF3, SM1, SM2, SM3
*End Step
** ----------------------------------------------------------------
**
```

```
** STEP: EQ
**
*Step, name=EQ
*Dynamic, Explicit
, 7.
*Bulk Viscosity
0.06, 1.2
**
** BOUNDARY CONDITIONS
**
** Name: EQ Type: Acceleration/Angular acceleration
*Boundary, amplitude="Imperiial Valley", type=ACCELERATION
_PickedSet76, 1, 1, 1.
**
** OUTPUT REQUESTS
**
*Restart, write, number interval=1, time marks=NO
**
** FIELD OUTPUT: F-Output-1
**
*Output, field, time interval=0.01, time marks=YES
*Node Output
A, U, V
*Element Output, directions=YES
LE, PE, PEEQ, S
*Contact Output
CSTRESS,
**
** HISTORY OUTPUT: Reactions
**
*Output, history, time interval=0.01
```

```
*Node Output, nset=R
RF1, RF2, RF3
**
** HISTORY OUTPUT: Stresses
**
*Element Output, elset=Stresses
E11, E22, E33, S11, S22, S33
*Element Output, elset=Stresses, rebar
E, S
**
** HISTORY OUTPUT: Forces
**
*Element Output, elset=Stresses
SF1, SF2, SF3, SM1, SM2, SM3
*End Step
```

REFERENCES

- ACI committee 207, 2007, “Report on Thermal and Volume Change Effects on Cracking of Mass Concrete (ACI 207.2R-07)”, American Concrete institute, Farmington Hills, Mich. USA.

- ACI committee 224, 2004, “Cracking of Concrete Members in Direct Tension (ACI 224.2R-92)”, American Concrete institute, Farmington Hills, Mich. USA.

- ACI committee 224, 2008, “Control of Cracking in Concrete Structures (ACI 224R-01)”, American Concrete institute, Farmington Hills, Mich.USA.

- ACI Committee 318, 2008, “Building Code Requirements for Structural Concrete (ACI 318–08) and Commentary,” American Concrete Institute, Farmington Hills, MI, 465 pp.

- ACI Committee 350.3-06, 2006, "Seismic design of liquid-containing concrete structures (ACI 350.3-06) and commentary (ACI 350.3R-06)", American Concrete Institute, Farmington Hills, MI, U.S.A.

- ACI Committee 350-01, 2001, "Code requirements for environmental engineering concrete structures (ACI 350-01) and commentary (ACI 350R-01)", American Concrete Institute, Farmington Hills, MI, U.S.A.

- ACI Committee 350-06, 2006, “Code Requirements for Environmental Engineering Concrete Structures (ACI 350-06) and Commentary (ACI 350R-06)” , American Concrete Institute, Farmington Hills, MI, U.S.A.

- ACI Committee 371, 2008, "Guide for the analysis, design and construction of elevated concrete and composite steel-concrete water storage tanks (ACI 371R-08)", American Concrete Institute, Farmington Hills, MI, U.S.A.

- ACI Committee 373R, 1997, "Design and Construction of Circular Prestressed Concrete Structures with Circumferential Tendons (ACI 373R-97)", American Concrete Institute, Farmington Hills, MI, U.S.A.

- American Petroleum Institute, API 620, 1998, "Design and construction of large, welded, lowpressure storage tanks", American Petroleum Institute Standard, Washington D.C., U.S.A.
- American Petroleum Institute, API 650, 1998, "Welded steel tanks for oil storage", American Petroleum Institute Standard, Washington D.C., U.S.A.

- American Society of Civil Engineers (ASCE), 1980, "Structural analysis and design of nuclear plant facilities", ASCE Manuals and Reports on Engineering Practice No. 58, New York, New York.

- American Society of Civil Engineers (ASCE), 1998, "Seismic analysis of safety-related nuclear structures and commentary", ASCE 4-98, Reston, VA.

- American Society of Civil Engineers (ASCE), Structural Engineering Institute, 2005, "Minimum design loads for buildings and other structures", ASCE/SEI 7-05, Reston, VA.

- American Society of Civil Engineers (ASCE), Structural Engineering Institute, 2010, "Minimum design loads for buildings and other structures", ASCE/SEI 7-10, Reston, VA.

- American Water Works Association (AWWA), 1984 and 2005, "Welded steel tanks for water storage", AWWA D100, CO.

- American Water Works Association (AWWA), 1995, "Circular prestressed concrete tanks with circumferential tendons", AWWA Dl15, Denver, CO.

- American Water Works Association (AWWA), 1995, "Wire and strand-wounded circular prestressed concrete water tanks", AWWA D110, Denver, CO.

- American Water Works Association (AWWA), 2004, "Wire and strand-wounded circular prestressed concrete water tanks", AWWA D110-04, Denver, CO.

- Anshel, J.S., 1999, "Kobe earthquake of January 17, 1995. Lifeline performance. 1995", ASCE Publication.

- Applied Technology Council (ATC), 1997a, "NEHRP commentary on the guidelines for the seismic rehabilitation of buildings", 1997 Ed., Rep. No. FEMA-274, Prepared for the Building Seismic Safety Council (BSSC) by the Applied Technology Council (ATC), Federal Emergency Management Agency (FEMA), Washington, D.C.

- Applied Technology Council (ATC), 1997b, "NEHRP guidelines for the seismic rehabilitation of buildings", 1997 Ed., Rep. No. FEMA-273, Prepared for the Building Seismic Safety Council (BSSC) by the Applied Technology Council (ATC), Federal Emergency Management Agency (FEMA), Washington, D.C.

- Arias, A., 1970, "A measure of earthquake intensity", Seismic Design for Nuclear Power Plants, MIT Press, Cambridge.

- Arya, A. S., Thakkar, S. K., and Goyal, A. C., 1971, "Vibration analysis of thin cylindrical containers", Journal of the Engineering Mechanics Division, ASCE, Vol. 97, pp. 317-331.

- ATC, 1978, "Tentative Recommended Provisions for Seismic Regulation of Buildings, Report No. ATC-3.06, Applied Technology Council, Redwood City, CA.

- ATC, 1995a, "Structural Response Modification Factors", ATC-19 Report, Applied Technology Council, Redwood City, California.

- ATC, 1995b, “A Critical Review of Current Approaches to Earthquake Resistant Design”, ATC-34 Report, Applied Technology Council, Redwood City, California.

- Balendra, T., 1979, “Earthquake finite element analysis of an annular cylindrical liquid storage tank”, In: Proc. 3rd Int. Conference on Finite Element Methods, Australia.

- Balendra, T., Ang, K.K., Paramasivan, P., and Lee, S.L., 1982, "Seismic design of flexible cylindrical liquid storage tanks", Earthquake Engineering and Structural Dynamics, 10, 477-496.

- Brooms, Bengt B., and Lutz Leroy A., 1965, “Effect of Arrangement of Reinforcement on Crack Width and Spacing of Reinforced Concrete Members”, ACI Jurnal, Proceedings V. 62, pp. 1395-1410.

- BS 8007, 1987, “Code of practice for design of concrete structures for retaining aqueous liquids”, British Standard Institution.

- BSSC, 2003, NEHRP (National Earthquake Hazards Reduction Program) Recommended Provisions for Seismic Regulations for New Buildings and Other Structures (FEMA 450). Part 2: Commentary. Building Seismic Safety Council, Washington, D.C, USA.

- Charney, F. A, and Bertero, V. V., 1982, “An Evaluation of the Design and Analytical Response of a Seven-Story Reinforced Concrete Fram-Wall Structure”, UBC/EERC-82/08, University of California at Berkeley

- Chen, J.Z. and Kianoush, M.R., 2004, “Response of concrete rectangular liquid storage tanks in different seismic zones. Proceedings of the 13th World Conference on Earthquake Engineering, Vancouver, B.C., 15 p.

- Chen, J.Z., and Kianoush, M.R., 2005, "Seismic response of concrete rectangular tanks for liquid containing structures", Canadian Journal of Civil Engineering, 32, 739-752.

- Clough, D. P., 1977, "Experimental evaluation of seismic design methods for broad cylindrical tanks", Report No. UCB/EERC-77/10, Earthquake Engineering Research Center, University of California, Berkeley.

- Clough, R. W., Niwa, A., and Clough, D. P., 1979, "Experimental Seismic Study of Cylindrical Tanks," Journal of the Structural Division, ASCE, Vol. 105, No. 12, pp. 2565-2590.

- Clough, R.W., and Clough, D.P., 1977, "Seismic response of flexible cylindrical tanks", Paper K 5/1 Trans. 4t h International Conference on Structural Mechanics in Reactor Technology, San Francisco, CA.

- Clough, R.W., Niwa, A., and Clough, D.P., 1979, "Experimental seismic study of cylindrical tanks", Journal of the Structural Division, ASCE, Vol. 105, No. 12, pp. 2565-2590.

- Constantinou, M. C., and Symans, M. D., 1993b, "Seismic response of structures with supplemental damping." Struct. Des. Tall Build, 2(2),77–92.

- Constantinou, M.C. and Symans, M.D., 1992, "Experimental and analytical investigation of seismic response of structures with supplemental fluid viscous dampers," Report No. NCEER-92-0032, National Center for Earthquake Engineering Research, State University of New York at Buffalo, New York.

- CSA-A23.3, 2010, "Design of concrete structures," Canadian Standards Association, Mississauga, Ontario, Canada.

- Dassault Systèmes Simulia Corp., 2008, "ABAQUS/CAE Documentation, Version 6.8–3", Providence, RI, USA.

- Driver, R.G.; Kulak, G.L.; Elwi, A.E. and Kennedy, D.J.L., 1998, "Cyclic Test of Four-Story Steel Plate Shear Wall," Journal of Structural Engineering, ASCE, Vol. 124, No. 2, pp. 112–120.

- Eduardo Miranda, M.ERRI, and Vitelmo V. Bertero, 1994, "Evaluation of strength Reduction Factors for Earthquake-Resistance Design, Earthquake Spectra", Vol. 10, No. 2.

- Edvardsen C., 1999, "Water Permeability and Autogenous healing of Cracks in Concrete", ACI Material Journal, Vol. 96, No. 4, pp. 448-454.

- El Damatty, A. A., Korol, R.M., and Mirza, F.A., 1997, "Stability of elevated liquid-filled conical tanks under seismic loading, Part I—Theory", Earthquake Eng. And Struct. Dyn., 26, 1191-1208.

- Epstein, H.I., 1976, "Seismic design of liquid storage tanks", Journal of the Structural Division, ASCE, 102(9): 1659-1673.

- Eurocode 8, 1998, "Design provisions for earthquake resistance of structures, Part 1-General rules and Part 4 − Silos, tanks and pipelines", European committee for Standardization, Brussels.

- European Committee for Standardization (ECS), 1998 and 2006, "Design provisions for earthquake resistance of structures, Part 1- General rules and Part 4 - Silos, tanks and pipelines", Eurocode 8, Brussels, Belgium.

- Favre, R., 1983, "Fissuration et Deformations", Manual du Comite Ewo-International du Beton (CEB), Ecole Polytechnique Federale de Lausanne. Switzerland. 249.

- Freeman, S.A., 1990. Proceedings of the 4th U.S.-Japan Workshop on Improvement of Building Structural Design and Construction Practices. ATC-15-3 Report. Applied Technology Council. Redwood City, California, USA.

- Frosch, R.J., 1999, “Another look at Cracking and Crack Control in reinforced Concrete”, ACI Structural Jornal, V. 96, No. 3, pp. 437-442.

- Ghaemmaghami, A.R., Moslemi, M., and Kianoush, M.R., 2010, "Dynamic behavior of concrete liquid tanks under horizontal and vertical ground motions using finite element method", 9th US National and 10th Canadian Conf. on Earthquake Eng., Toronto, Canada.

- Gilbert, R.I, 1992, “Shrinkage Cracking in Fully Restrained Concrete Members”, ACI Structural Journal, V.89, No. 2, American Concrete Institute, 141-149.

- Goodyear Tire and Rubber Company, 1959, “Handbook of Molded and Extruded Rubber”, second edition, S-5138.

- Gordon, D. W., Bennett, T. J., Herrmann, R. B., and Rogers, A. M., 1970, “The south central Illinois earthquake of November 9, 1968”, Macroseismic studies, Bull. Seism. Soc. Am. 60, 953-971.

- Haroun, M. A., and Housner, G. W., 1981, “Seismic design of liquid-storage tanks”, Journal of Technical Councils, ASCE, New York, Vol. 107, No. 1, pp. 191−207.

- Haroun, M.A., 1984, "Stress analysis of rectangular walls under seismically induced hydrodynamic loads", Bulletin of the Seismological Society of America, 74(3), 1031-1041.

- Haroun, M.A., and Ellaithy, H.M., 1985, "Seismically induced fluid forces on elevated tanks", J. Tech. Topics Civil Eng., 1, 1-15.

- Haroun, M.A., and Housner, G.W., 1981, "Earthquake response of deformable liquid storage tanks", Journal of Applied Mechanics, ASME, 48, 411-418.

- Haroun, M.A., and Tayel, M.A., 1985, "Response of tanks to vertical seismic excitations", Earthquake Engng. And Struct. Dyn., 13, 583-595.

- Housner G.W., Haroun M. A., 1979, "Vibration tests of full-scaled liquid storage tanks", Proceedings of US National Conference on Earthquake Engineering. Stanford University, pp. 137-145.

- Housner, G.W., 1963, "The dynamic behavior of water tanks", Bulletin of the Seismological Society of America 53(2), 381-389.

- Housner, G.W., 1963, "The dynamic pressures on Fluid Containers" Technical Information Document (TID) 7024, Chapter 6 Appendix F, U.S Atomic Energy Commission.

- Housner, G.W., 1975, "Measures of severity of earthquake ground shaking", Proceedings of the U.S. National Conference on Earthquake Engineering, EERI, Ann Arbor, MI, 25-33.

- Hunt, B., and Priestley, N., 1978, "Seismic water waves in a storage tank". Bulletin of the Seismological Society of America, 68(2), 487-499.

- Hwang, J.-S., Huang, Y.-N., and Hung, Y.-H., 2005, "Analytical and experimental study of toggle-brace-damper systems", J. Struct. Eng., 131_7_, 1035–1043.

- IBC, 2011, "International Building Code", International Code Council, Inc., USA: ICC.
- International Code Council (ICC), 2006, International building code, 2006 Ed., Delmar Cengage Learning, Clifton Park, N.Y.

- Jacobsen, L. S., 1949, "Impulsive hydrodynamics of fluid inside a cylindrical tank and of fluid surrounding a cylindrical pier", Bulletin of the Seismological Society of America, Vol. 39, No. 3, pp. 189−203.

- Jacobsen, L. S., and Ayre, R. S., 1951, "Hydrodynamic experiments with rigid cylindrical tanks subjected to transient motions", Bulletin of the Seismological Society of America, 41(4): 313 - 346.

- Jankowiak, T. and Odygowski, T. (2005), "Identification of Parameters of Concrete Damage Plasticity Constitutive Model," Foundations of Civil and Environmental Engineering, pp. 53–69.

- Jennings, P. C., 1971, "Engineering features of the San Fernando earthquake of February 9, 1971. Technical Report", CaltechEERL:1971.EERL-71-02. California Institute of Technology.

- Joshi, S.P., 2000, "Equivalent mechanical model for horizontal vibration of rigid Intze tanks", ISET Journal of Earthquake Technology, 37, 39-47.

- Kianoush MR., Acarcan M., and Ziari A., 2008, "Behavior of base restrained reinforced concrete walls under volumetric changes", Journal of Engineering Structure, vol 30, 1526-1534.

- Kianoush, M.R., Acarcan, M., and Dullerud, E, 2006. "Cracking in Liquid-Containing Structures". Concrete international, Vol. 28 No. 4, pp. 62-66.\

- Kianoush, M.R., and Chen, J.Z., 2006, "Effect of vertical acceleration on response of concrete rectangular liquid storage tanks", Engineering Structures, 28(5), 704-715.

- Kianoush, M.R., Mirzabozorg, H., and Ghaemian, M., 2006, "Dynamic analysis of rectangular liquid containers in three-dimensional space", Canadian Journal of Civil Engineering, 33, 501-507.

- Kianoush, M.R., Hafez, A., Mirzabozorg, H., 2005, "A parametric study on the seismic behavior of liquid containing structures based on ACI 350 Code", presented in 1st Canadian Conference on Effective Design of Structures McMaster University, Hamilton, Ontario, Canada.

- Kim, J. K., Koh, H. M., and Kwahk, I. J., 1996, "Dynamic response of rectangular flexible fluid containers", ASCE Journal of Engineering Mechanics, 122(9): 807−817.

- Kircher, C. A., 1999, "Seismic regulations for passive structural control systems-Overview of United States codes", Proc., 2nd World Conf. on Structural Control, Wiley, Chichester, U.K.

- Koh, H. M., Kim, J. K., and Park, J. H., 1998, "Fluid-structure interaction analysis of 3D rectangular tanks by a variationally coupled BEM-FEM and comparison with test results", Earthquake Engineering and Structural Dynamics, 27: 109-124.

- Kono, 1980, "Facts about failures and instability of plant structure (mainly for flat bottom cylindrical storage tanks)", the 31st Nat. Cong, of Theoretical & Applied Mechanics, pp. 7-12.

- Krawinkler, H. and Nassar, A., 1990, "Strength and Ductility Demands for SDOF and MDOF Systems Subjected To Whittier Narrows Earthquake Ground", SMIP 1990

Seminar on Seismological and Engineering Implications of Recent Strong-Motion Data, p. 3-1 - 3-10.

- Krawinkler, H. K., and Nassar, A. A., 1992. "Seismic design based on ductility and cumulative damage demands and capacities", Nonlinear seismic analysis and design of reinforced concrete buildings. P. Fajfar and H. Krawinkler, eds., Elsevier Science, New York.

- Lee, J. and Fenves, G.L., 1998, "Plastic-Damage Model for Cyclic Loading of Concrete Structures," Journal of Engineering Mechanics, ASCE, Vol. 124, No. 8, pp. 892–900.

- Li, Z. J., Balendra, T., Tan, K. H., and Kong, K. H., 2005, "Finite Element Modeling of Cyclic Behavior of Shear Wall Structure Retrofitted using GFRP", 7th International Symposium on Fiber-Reinforced (FRP) Polymer Reinforcement for Concrete Structures. SP-230−74.

- Lubliner, J.; Oliver, J.; Oller, S. and Onate, E., 1989, "A Plastic-Damage Model for Concrete," International Journal of Solids and Structures, Vol. 25, No. 3, pp. 299–326.

- Lund, L. V., 1996, "Lifeline Utilities Performance in the 17 January 1994 Northridge, California, Earthquake", Bulletin of the Seismological Society of America, Vol. 86, No.1B.

- Ma, D. C., Liu, W. K., Gvildys, J., and Chang, Y. W., 1982, "Seismic Behavior of Liquid-Filled Shells", Nuclear Engineering and Design, Vol. 70, pp. 437-455.

- MacGregor, J. G., 1997, "Reinforced Concrete: Mechanics and Design", 3rd ed., 939 pp. Prentice-Hall, Inc., Englewood Cliffs, New Jersey, USA.

- MacGregor, J. G., and Bartlett F. M., 2000, "Reinforced Concrete: Mechanics and Design", 1st Canadian Edition, Ed., Prentice Hall Canada Inc.

- Malhotra, P.K., 1995, "Base uplifting analysis of flexibly supported liquid-storage tanks", Journal of Earthquake Engineering and Structural Dynamics, Vol. 24, No. 12, pp. 1591-1607.

- Malhotra, P.K., 1997, "Seismic response of soil-supported unanchored liquid-storage tanks", Journal of Structural Engineering, ASCE, New York, Vol. 123, No. 4, pp. 440-450.

- Malhotra, P.K., Wenk, T., and Wieland, M., 2000, "Simple procedure for seismic analysis of liquid-storage tanks", Structural Engineering International, International Association for Bridge and Structural Engineering (IABSE), Zurich, Switzerland, 10(3), pp. 197-201.

- Manos, G. C., and Clough, R. W., 1982, "Response of a Cylindrical Liquid Storage Tank to Static and Dynamic Lateral Loads", AMD-Vol. 53, American Society of Mechanical Engineers, New York, New York, Earthquake Ground Motion and Its Effect on Structures, presented at the Winter Annual Meeting, ASME, Phoenix, pages 77-90, 1982.

- Masoudi, M., Eshghi, S., and Ghafory-Ashtiany, M., 2006, "Recommendation for Response Modification Factor (R) of Elevated Concrete Tank". First European Conference on Earthquake Engineering and Seismology, Geneva, Switzerland, 1899.

- Miranda, E., 1993a, "Site-Dependent Strength Reduction Factors", Journal of Structural Engineering ASCE, Vol. 119, No. 12, pp, 3505-3519.

- Miranda, E., 1993b, "Evaluation of Site-Dependent Inelastic Seismic Design Spectra", Journal of Structural Engineering, American Society of Civil Engineering, 119(5), 1319−1338.

- Miranda, E., and Bertero, V. V., 1994, "Evaluation of strength reduction factors for earthquake resistant design", Earthquake Spectra, EERI, 10 (2), pp. 357-379.

- Moslemi, M., 2011, "Dynamic Response of Circular and Conical Elevated Tanks", Doctor of Philosophy thesis, Ryerson University.

- Moslemi, M., Kianoush, M.R., and Pogorzelski, W., 2011, "Seismic response of liquid-filled elevated tanks", Journal of Engineering Structures, 33(6), 2074-2084.

- Mostafa Masoudi, Sassan Eshghi, and Mohsen Ghafory-Ashtiany, 2006, "Recommendation for Response Modification Factor (R) of Elevated Concrete Tank", Presented in First European Conference on Earthquake Engineering and Seismology, Geneva, Switzerland.

- Nassar, A. and Krawinkler, H., 1991, "Seismic Demands for SDOF and MDOF Systems", John A. Blume Earthquake Engineering Center, Report 95, Dept. of Civil Engineering, Stanford University.

- National Fire Protection Association (NFPA), 2006, NFPA 5000: Building construction and safety code, Quincy, Mass.

- Newmark, N. M., and Hall, W. J., 1982, Earthquake spectra and design. Earthquake Engineering Research Institute. Berkeley, California, USA.

- Nawy, Edward G., and Chiang, Jim Y., 1980, "Serviceability Behavior of Post-Tensioned Beams," PCI Journal, V. 25, No. 1, pp. 74-95.

- Nawy, Edward G., 2001, "Prestressed Concrete: A Fundamental Approach", 3rd ed., 07458, Prentice-Hall, Inc., Upper Saddle River, New Jersey, USA.

- Niwa, A., 1978, "Seismic behavior of tall liquid storage tanks", UCB/EERC-78/04, Earthquake Engineering Research Center, University of California, Berkeley, 1978-02.

- NZS 3106, 1986 and 2010, "Code of practice for concrete structures for the storage of liquids", Standards Association of New Zealand, Wellington.

- Park, J. H., Koh, H. M., and Kim, J., 1992, "Liquid-structure interaction analysis by coupled boundary element-finite element method in time domain", Proceedings of the 7th International Conference on Boundary Element Technology, BE-TECH/92, Computational Mechanics Publication, Southampton, England. 89−92.

- Paulay, T. And M.J.N. Priestley, 1992, "Seismic Design of Reinforced Concrete and Masonry Building", John Wiley and Sons. New York, USA.

- PCA, 1992, "Circular Concrete Tanks without Prestressing", IS072.01D, Portland Cement Association, Skokie, IL.

- Puleo, Stephen, 2003, "Dark Tide: The Great Boston Molasses Flood of 1919", Boston, Massachusetts: Beacon Press.

- Ramanathan, K., DesRoches, R. and Padgett, J., 2010, "Analytical Fragility Curves for Multispan Continuous Steel Girder Bridges in Moderate Seismic Zones", Journal of the Transportation Research Board, Volume 3, pp 173-182.

- Rai, D.C., "Seismic Retrofitting of R/C Shaft Support of Elevated Tanks", Earthquake Spectra, 18, 745-760.

- Rinne, J.E., 1967, "Oil storage tanks", The Prince William Sound, Alaska Earthquake of 1964 and Aftershocks, Vol II, Part A, U.S. Coast and Geodetic Survey, Washington D.C., 245-252.

- Sadjadi, R., 2009, “Response of Reinforced Concrete Rectangular Liquid Containing Structures under Cyclic Loading”, Doctor of Philosophy dissertation, Ryerson University, Toronto, Canada.

- SAP2000 Version 11, 2008, Integrated Software for Structural Analysis & Design, Computer and Structures Inc, Berkeley, CA, USA.

- Sezen, H., and Whittaker, A.S., 2006, "Seismic performance of industrial facilities affected by the 1999 Turkey earthquake", ASCE Journal of Performance of Constructed Facilities, 20(1), 28-36.

- Shenton III, H.W., and Hampton, F.P., 1999, "Seismic response of isolated elevated water tanks", ASCE Journal of Structural Engineering, 125(9), 965-976.

- Shibata, 1974, "Report of earthquake damages in overseas industrial facilities - Spherical tank and cylindrical tank", Seisan Kenkyu, 26(7), 259-264.

- Shih, C. F., and Babcock, C. D., 1980, “Scale Model Buckling Test of a Fluid Filled Tank under Harmonic Excitation”, American Society of Mechanical Engineers, Paper 80-C2/PVP-66.

- Soong, T. T., and Spencer, Jr. B. F., 2002, “Supplemental energy dissipation: State-of-the-art and state-of-the-practice.” Eng. Struct., 24-3-, 243–259.

- Steinberg, L. J., and Cruz, A.M., 2004, “When Natural and Technological Disasters Collide: Lessons from the Turkey Earthquake of August 17, 1999”, Natural Hazards Rev. Volume 5, Issue 3, pp. 121-130.

- Symans, et al., 2008, “Energy Dissipation Systems for Seismic Applications: Current Practice and Recent Developments”, Journal of Structural Engineering, ASCE, Vol. 134, No. 1, 0733-9445.

- Symans, M. D., and Constantinou, M. C., 1998, “Passive fluid viscous damping systems for seismic energy dissipation.” J. of Earthquake Technology, 35(4), 185–206.

- Taucer, F. F., Spacone, E., and Filippou, F. C., 1991, “A Fiber Beam-Column Element for Seismic Response Analysis of Reinforced Concrete Structures”, Report to the National Science Foundation and the California Department of Transportation, Earthquake Engineering Research Center, University of California, Berkeley, California.

- Trifunac, M.D., and Brady, A.G., 1975, "A study on the duration of strong earthquake ground motion", Bulletin of the Seismological Society of America, 65(3), 581-626.

- Veletsos, A. S., 1974, “Seismic Effects in Flexible liquid storage tanks”, Proceedings of the 5th World Conference on Earthquake Engineering, Rome, Italy, Vol. 1, pp. 630-639.

- Veletsos, A. S., 1984, “Seismic response and design of liquid storage tanks”, In Guidelines for the seismic design of oil and gas pipeline systems, Albuquerque, N. Mex. Tech, Council on Lifeline Earthquake Engineering, ASCE, New York, N.Y.

- Veletsos, A.S., and Kumar, A., 1984, "Dynamic response of vertically excited liquid storage tanks", Proceedings of the Eighth World Conference on Earthquake Engineering, Vol. I, California, USA, pp. 453-459.

- Veletsos, A.S., and Tang, Y., 1990, "Soil-structure interaction effects for laterally excited liquid-storage tanks", Journal of Earthquake Engineering and Structural Dynamics, Vol. 19, No. 4, pp. 473-496.

- Veletsos, A.S., and Yang, J.Y., 1977, "Earthquake response of liquid storage thanks", Proc. 2nd Adv. Civil. Eng. through Eng. Mech. Conf., ASCE, North Carolina, 1-24.

- Virella, J.C., Godoy, L.A., and Suarez, L.E., 2006, "Fundamental modes of tank-liquid systems under horizontal motions", Journal of Engineering Structures, 28, 1450-1461.

- Watanabe, T., 1966, "Damage to Oil Refinery Plants and a Building on Compacted Ground by the Niigata Earthquake and Their Restoration", Soil and Foundation, Vol. VI No. 2, The Japanese Society of Soil Mechanics and Foundation Engineering, March, 86-99.

- Whittaker, A. S., Aiken, I. D., Bergman, D., Clark, P. W., Cohen, J., Kelly, J. M., and choll, R. E., 1993, "Code requirements for design and implementation of passive energy dissipation systems." Proc., ATC-17–1 Seminar on Seismic Isolation, Passive Energy Dissipation, and Active Control, Vol. 2, ATC, Redwood City, Calif., 497–508.

- Yang, J. Y., 1976, "Dynamic behavior of fluid tank system", Ph.D. thesis, Civil Engineering, Rice University, Houston, Tex.

- Ziaolhagh, N., 2008, "Shrinkage and Temperature Reinforcement in Concrete Liquid-Containing Structures", Master of Applied Science, Ryerson University.

- Ziari, A., and Kianoush, M.R., 2009b, "Investigation of direct tension cracking and leakage in RC elements", Journal of Engineering Structures, 31:466-474.

- Ziari A., and Kianoush M.R., 2009a, "investigation of flexural cracking and leakage in RC elements", Journal of Engineering Structures, 31(5), pp 1056-1067.